Pontifícia Universidade Católica
do Rio de Janeiro

Florian Alain Yannick Pradelle

Use of biofuels in compression ignition engines – Potential of diesel-biodiesel-ethanol blends

PUC-Rio - Certificação Digital Nº 1312923/CA

Tese de Doutorado

Thesis presented to the Programa de Pós-graduação em Engenharia Mecânica of PUC-Rio in partial fulfilment of the requirements for the degree of Doutor em Ciências - Engenharia Mecânica.

Advisor: Prof. Sergio Leal Braga

Rio de Janeiro

March 2017

PONTIFÍCIA UNIVERSIDADE CATÓLICA
DO RIO DE JANEIRO

Florian Alain Yannick Pradelle

Use of biofuels in compression ignition engines – Potential of diesel-biodiesel-ethanol blends

Thesis presented to the Programa de Pós-graduação em Engenharia Mecânica of PUC-Rio in partial fulfillment of the requirements for the degree of Doutor em Ciências – Engenharia Mecânica. Approved by the undersigned Examination Committee.

Prof. Sergio Leal Braga
Advisor
Departamento de Engenharia Mecânica – PUC-Rio

Prof. Carlos Valois Maciel Braga
Departamento de Engenharia Mecânica – PUC-Rio

Prof. José Alberto dos Reis Parise
Departamento de Engenharia Mecânica – PUC-Rio

Profa. Ana Rosa Fonseca de Aguiar Martins
Departamento de Engenharia Química e de Materiais – PUC-Rio

Prof. Carlos Andre Vaz Junior
Universidade Federal do Rio de Janeiro

Dra. Marcelle Alves Farias
Lubrizol do Brasil Ltda.

Dr. Tadeu Cavalcante Cordeiro de Melo
Petrobras

Prof. Márcio da Silveira Carvalho
Vice Dean of Graduate Studies
Centro Técnico Científico – PUC-Rio

Rio de Janeiro, March 10th, 2017

PUC-Rio - Certificação Digital Nº 1312923/CA

All rights reserved.

Florian Alain Yannick Pradelle

Florian Pradelle graduated in chemical engineering in 2012 from École Nationale Supérieure de Chimie de Paris – Chimie ParisTech (Paris, France), and he got his master degree in 2012 from Université Pierre et Marie Curie – Paris 6 (Paris, France). Currently, he is working as researcher in the ITUC / PUC-Rio in the field of energy, dealing especially with problematic involving biofuels in internal combustion engines.

Ficha Catalográfica

Pradelle, Florian Alain Yannick

Use of biofuels in compression ignition engines : potential of diesel-biodiesel-ethanol blends / Florian Alain Yannick Pradelle ; advisor: Sergio Leal Braga. – 2017.
302 f. : il. color. ; 30 cm

Tese (doutorado)–Pontifícia Universidade Católica do Rio de Janeiro, Departamento de Engenharia Mecânica, 2017.
Inclui bibliografia

1. Engenharia Mecânica – Teses. 2. Motor de ignição por compressão. 3. Misturas diesel-biodiesel-etanol. 4. Miscibilidade. 5. Propriedades físico-químicas. 6. Combustão. I. Braga, Sergio Leal. II. Pontifícia Universidade Católica do Rio de Janeiro. Departamento de Engenharia Mecânica. III. Título.

CDD: 621

PUC-Rio - Certificação Digital Nº 1312923/CA

PUC-Rio - Certificação Digital Nº 1312923/CA

I dedicate this work to my beloved wife, Renata, and my parents, Annick and Alain.

« S'il n'y a pas eu de question, il ne peut y avoir connaissance scientifique. Rien ne va de soi. Rien n'est donné. Tout est construit. »
Gaston Bachelard ; *La Formation de l'esprit scientifique* (1938).

Acknowledgments

To my wife, Renata, and her family for their incentive and support to complete this present work and their patience during the busy days. I particularly thank my beloved wife for her affection, her inspiration and for her unconditional support (including for the sacrifices she did).

To my parents, Annick and Alain, and my brother, Sylvain, for their everlasting incentive and support, even with an ocean between us.

To my adviser professor Sergio Leal Braga, for his friendship, confidence, dedication, attention and teaching during all the phase of this work.

To Peugeot Citroën do Brasil Automóveis Ltda, in particular Franck Turkovics, for their financial support to part of this work and their contribution leading to the formulation of the additive.

To the financial support of the Brazilian agencies CAPES, FAPERJ and of the *Departamento de Engenharia Mecânica* of PUC-Rio, for the provided grants, without which this work could not have been done.

To the *Instituto Tecnológico*, ITUC / PUC-Rio, in particular professor Ana Rosa Fonseca de Aguiar Martins, Marcos Thomé de Almeida, Luciano Medeiros Pires and Renato Gomes, for the support and their help to solve logistic issues.

To Leonardo Costa Braga, Severino A. Wanderley, Nestor Corrêa Cotelo, Fernando Zegarra Sanchez, Gerson Silvério, Gilson Coutinho Pradanoff, Jorge Ricardo Moura and Bruno Maia from the *Laboratório de Engenharia Veicular*, LEV / PUC-Rio, for their contribution to the success of engine tests, from the installation and instrumentation of the engine to the realization of the tests.

PUC-Rio - Certificação Digital Nº 1312923/CA

To professor Paulo Roberto de Souza Mendes to allow me to use the resources of the *Laboratório de Caracterização de Fluidos* and to Gisllane Oliveira, quality manager, for her attention and support.

To professor Márcio da Silveira Carvalho to allow me to use the resources of the *Laboratório de Micro Hidrodinâmica e Meios Porosos*, LMMP / PUC-Rio, and to Felicle Lopez and Ranena Ponce for sharing their experiences.

To Marcileny Porto, coordinator of the *Centro de Pesquisas e Caracterização de Petróleo e Combustíveis*, COPPEComb / UFRJ, and Renato, Monica and Luis Otávio, for their unconditional support to my research.

To the *Laboratório de Motores e Combustíveis* of the *Instituto Nacional de Metrologia, Qualidade e Tecnologia*, LAMOC / INMETRO, and the *Laboratório de Combustíveis e Lubrificantes* of the *Instituto Nacional de Tecnologia*, LACOL / INT, to their contributions to this work.

To all people (and they are great in number) who contribute directly and indirectly to this work, in particular the members of the examination committee for their precious advice that led to the final version of this document.

PUC-Rio - Certificação Digital Nº 1312923/CA

Abstract

Pradelle, Florian Alain Yannick; Braga, Sergio Leal (advisor). **Use of biofuels in compression ignition engines - Potential of diesel-biodiesel-ethanol blends.** Rio de Janeiro, 2017. 302p. Tese de Doutorado - Departamento de Engenharia Mecânica, Pontifícia Universidade Católica do Rio de Janeiro.

In order to partially replace the demand of fossil diesel fuels, to reduce high import costs and to comply with environmental standards, sustainable policies have led to partially replace diesel fuel by biodiesel. However, other technologies, such as diesel-biodiesel-ethanol mixtures, are being investigated. The major challenge of these mixtures is to improve the miscibility and the stability of alcohol in diesel fuel. In this study, an original additive, from renewable compounds, improved the miscibility of anhydrous ethanol in diesel fuel with 15% by volume of biodiesel and temperature in which stable mixtures were observed. Several physicochemical properties of the additivated mixtures were measured in a large range of ethanol concentration to evaluate aspects of consumption, combustion quality, behavior at low temperature, interaction between the fluid and the surface, and safety. The results showed that blends with, at least 1.0%, by volume of additive and 20% by volume of anhydrous ethanol are stable at temperatures above 10°C and respected most of the current Brazilian specifications for diesel fuel. Experimental tests on a compression ignition engine MWM 4.10 TCA (Euro III) were performed with these mixtures. The results showed that the diesel fuel substitution alters the characteristics of combustion: the increased ethanol content implied an increase of the ignition delay, a faster heat release and a decrease of maximum pressure. Despite these non-optimized conditions for injection and combustion, results showed a better conversion of ethanol chemical energy into brake power, in comparison to the values found in flex fuel spark ignition engine, in addition to a small increase in the indicated efficiency of the engine.

Keywords

Ignition compression engine; Diesel-biodiesel-ethanol blends; Miscibility; Physicochemical properties; Performance; Combustion.

PUC-Rio - Certificação Digital Nº 1312923/CA

Resumo

Pradelle, Florian Alain Yannick; Braga, Sergio Leal. **Utilização de biocombustíveis em motores de ignição por compressão - Potencial das misturas diesel-biodiesel-etanol.** Rio de Janeiro, 2017. 302p. Tese de Doutorado - Departamento de Engenharia Mecânica, Pontifícia Universidade Católica do Rio de Janeiro.

Para substituir parcialmente a demanda em óleo diesel de origem fóssil, reduzir os elevados custos de importação e respeitar as normas ambientais, políticas sustentáveis já levaram a substituir parcialmente óleo diesel por biodiesel. Entretanto, outras tecnologias, como as misturas diesel-biodiesel-etanol, estão sendo investigadas. O principal desafio dessas misturas consiste em melhorar a miscibilidade e a estabilidade do álcool no óleo diesel. No presente trabalho, formulou-se um aditivo original, a partir de compostos renováveis, que permitiu melhorar a faixa de concentração de etanol anidro dentro de óleo diesel com 15 % em volume de biodiesel e de temperatura onde observa-se misturas estáveis. Diversas propriedades físico-químicas das misturas aditivadas foram medidas em uma larga faixa de concentração de etanol para avaliar os aspetos de consumo, qualidade da combustão, comportamento a baixa temperatura, interação entre fluido e superfície, e segurança. Os resultados obtidos mostraram que misturas com, pelo menos, 1,0 % em volume de aditivo e até 20% em volume de etanol anidro são estáveis para temperaturas superiores a 10°C e respeitam a maioria das especificações brasileiras atuais para óleo diesel. Ensaios experimentais em um motor de ignição por compressão MWM 4.10 TCA (Euro III) foram realizados com estas misturas. Os resultados obtidos mostraram que a substituição do óleo diesel altera as características da combustão: o crescente teor de etanol leva ao aumento do atraso de ignição, à liberação de calor mais rápida e à diminuição da pressão máxima. Mesmo nessas condições não otimizadas de injeção e de combustão, os resultados mostraram uma melhor conversão da energia química no etanol para produzir potência efetiva, comparado com os valores encontrados nos motores flex fuel de ciclo Otto, além de um pequeno aumento no rendimento térmico do motor.

Palavras-chave

Motor de ignição por compressão; Misturas diesel-biodiesel-etanol; Miscibilidade; Propriedades físico-químicas; Desempenho; Combustão.

PUC-Rio - Certificação Digital Nº 1312923/CA

Table of contents

1 Introduction 29
1.1. Brazilian Energy Matrix 29
1.2. Biofuels in Compression Ignition (CI) Engines 35
1.3. Potential of Ethanol-Diesel Blends (E-Diesel) 37
1.4. Potential of Diesel-Biodiesel-Ethanol (DBE) Blends 38
1.5. Brazilian Experience 40
1.6. Objectives 42
1.7. Performed Activities and Organization of the Thesis 43

2 Literature Review 47
2.1. Blend Stability Issue 47
2.1.1. Miscibility of Ethanol in Diesel Fuel 47
2.1.2. Additive-Based Strategies 54
2.1.3. Commercial Additives for E-Diesel 64
2.2. Blend Properties Issues 66
2.2.1. Viscosity 66
2.2.2. Lubricity 68
2.2.3. Cetane Number 72
2.2.4. Specific Gravity 75
2.2.5. Heating value 76
2.2.6. Wetting Properties: Surface Tension and Contact Angle 76
2.2.7. Fuel Oxygen Content 77
2.2.8. Flammability Limits, Flash Point and Auto-ignition Temperature 78
2.2.9. Cold Properties: Cloud Point, Cold Filter Plugging Point (CFPP) and Pour Point 81
2.2.10. Materials Compatibility Issue 83
2.3. Combustion Characteristics 83
2.4. Pollutants Emission 88
2.5. Partial Conclusion 90

PUC-Rio - Certificação Digital Nº 1312923/CA

3 Experimental Section 91
3.1. Formulation of an Additive to Blend Commercial Additivated Diesel B7 Fuel with Hydrous and Anhydrous Ethanol 91
3.1.1. Materials 91
3.1.2. Methodology 95
3.2. Formulation of an Additive to Blend Diesel B0 fuel with Variable Anhydrous Ethanol and Biodiesel's Content 98
3.2.1. Materials 98
3.2.2. Methodology 100
3.3. Assessment of Some Physicochemical Properties for Anhydrous Ethanol – Diesel B15 Blends 103
3.3.1. Materials 103
3.3.2. Methodology 103
3.4. Evaluation of the Engine Efficiency Running on Diesel B15 Fuel Blended with up to 20 vol% of Anhydrous Ethanol and 1.0 vol% of Additive. 117
3.4.1. Materials 117
3.4.2. Methodology 127

4 Calculation Procedure 130
4.1. Design of Experiments: Doehlert design 130
4.2. Engine and Combustion Parameters 134
4.2.1. Geometrical Properties 135
4.2.2. Fuel and Air Consumption 135
4.2.3. Brake Power (P_b), Brake Mean Effective Pressure (BMEP) and Indicated Mean Effective Pressure (IMEP) 137
4.2.4. Combustion Characteristics 138
4.2.5. Efficiency Calculation: Fuel Conversion Efficiency (η_f), Volumetric Efficiency (η_v), Indicated Efficiency (η_i) and Mechanical Efficiency (η_m) 140
4.3. Uncertainties 141
4.3.1. Experimental Uncertainties 141
4.3.2. Propagated Uncertainties 141

PUC-Rio - Certificação Digital Nº 1312923/CA

5 Results and Discussion 142
5.1. Formulation of an Additive to Blend Commercial Additivated Diesel B7 Fuel with Anhydrous and Hydrous Ethanol 143
5.1.1. Stability Study of Ethanol-Diesel-Additive Blends (48:50:2) at Ambient Temperature 143
5.1.2. Influence of Additive Concentration in Ethanol-Diesel (49:51) Blends at Ambient Temperature 144
5.1.3. Maximum Addition of Hydrous Ethanol in Diesel Fuel with 4 vol% of Additive until Phase Separation at Ambient Temperature 146
5.1.4. Influence of Temperature in the Stability of Anhydrous Ethanol – Diesel Blends with 2 vol% of Additive 150
5.1.5. Partial Conclusion 153
5.2. Formulation of an Additive to Blend Diesel B0 Fuel with Variable Anhydrous Ethanol and Biodiesel's Content 154
5.2.1. Stability Study of the Additives in DBE Blends at Different Temperatures and Different Biodiesel Concentration 154
5.2.2. Impact of the Best Additive in Anhydrous Ethanol-Diesel B15 Blends at Different Ethanol Concentration in Function of Temperature and Additive Content 159
5.2.3. Partial Conclusion 165
5.3. Assessment of Some Physicochemical Properties for Anhydrous Ethanol – Diesel B15 Blends 165
5.3.1. Specific Gravity at 25°C and 20°C 166
5.3.2. Kinematic Viscosity at 40°C 169
5.3.3. Surface Tension at 25°C 170
5.3.4. Contact Angle at 21°C 171
5.3.5. Flash Point 173
5.3.6. Cold Filter Plugging Point (CFPP) 174
5.3.7. Corrosiveness to Copper at 50°C 175
5.3.8. Cetane Number (CN) 176
5.3.9. Lubricity at 25°C and 60°C 178
5.3.10. Lower Heating Value (LHV) 181

PUC-Rio - Certificação Digital Nº 1312923/CA

5.3.11. Partial Conclusion 184
5.4. Evaluation of the Engine Efficiency Running on Diesel B15 Blended with up to 20 vol% of Anhydrous Ethanol and 1.0 vol% of Additive. 185
5.4.1. Experimental Conditions: Limitation of Maximum Torque 185
5.4.2. Fuel and Air Consumption 199
5.4.3. Brake Mean Effective Pressure (BMEP) and Indicated Mean Effective Pressure (IMEP) 207
5.4.4. Combustion Characteristics 210
5.4.5. Engine Efficiency 225
5.4.6. Partial Conclusion 233

6 Conclusion 235
6.1. Conclusion of the Present Work 235
6.2. Perspectives 238
6.3. Publications 240

References 242

Appendixes 263
Appendix A: Comparative Study of Stability and Physicochemical Properties of Different DBE Blends 263
Appendix B: Comparative Study of Emissions Tendencies of Different DBE Blends during Engine Tests 266
Appendix C: Mass Flow Rate of Moist Air 269
Appendix D: Air-Fuel Equivalence Ratios 272
Appendix E: Results of the Doehlert Design of Experiments 275
Appendix F: Physicochemical Properties of the Blends 277
Appendix G: Matlab Code to Analyze the Experimental Data 283
Appendix H: Experimental Results of the Engine Tests 294

PUC-Rio - Certificação Digital Nº 1312923/CA

List of figures

Figure 1: Domestic energy supply in 2015 [EPE, 2016]. 30
Figure 2: Oil products consumption by sector over the period 1970-2015 [EPE, 2016]. 30
Figure 3: Transportation sector energy consumption over the period 1975-2015 [EPE, 2016]. 31
Figure 4: Profile of light vehicles (passenger cars and light-weight commercial vehicles) fueled with diesel fuel for the period 2015-2024 [MME-EPE, 2015]. 32
Figure 5: Temperature of phase separation for ethanol blends with paraffinic and olefinic blends (top), aromatic and naphthenic blends (middle) and ester blends (bottom) [Caetano, 2003]. 48
Figure 6: Miscibility of diesel fuel in function of alcohol content [Caetano, 2003; Da Silva, 2005]. 50
Figure 7: Level curves for SR_{max} in the map temperature/ethanol content [Lapuerta, 2007]. 51
Figure 8: Effect of water and additive on the mean solubility at different temperatures [Lapuerta, 2007]. 52
Figure 9: Effect of ethanol on the phase behavior of the ternary system for various quality of ethanol: fuel ethanol (top) and SD-1 denatured ethanol (bottom) [Fernando, 2004]. 53
Figure 10: Isotherms of solubility of diesel – ethanol – RME (left) diesel – ethanol – REE (right) system using different concentration of ethanol [Makareviciene, 2005]. 55
Figure 11: Polytherm of solubility of diesel – ethanol – RME system [Makareviciene, 2005]. 56
Figure 12: Stability results at different temperatures [Lapuerta, 2009]. 57
Figure 13: Ternary diagram of regular DBE blends [Lin, 2013]. 59

PUC-Rio - Certificação Digital Nº 1312923/CA

Figure 14: Stability performance of ethanol–diesel blends with emulsifier ‘‘CLZ’’ for addition (a) 0.4%, (b) 0.6%, (c) 0.8% and (d) 1.0% of CLZ [Lei, 2012]. 64
Figure 15: Effect of ethanol content on fuel viscosity [Shahir, 2014]. 67
Figure 16: Variation of kinematic viscosity in E-diesel blends (20 vol% of ethanol) in function of biodiesel content at 15°C [Park, 2012]. 68
Figure 17: Typical Stribeck curve showing the variation in frictional drag (expressed as the friction coefficient) with the Gumbel number for a lubricated contact [Andablo-Reyes, 2011]. 69
Figure 18: Variation of cetane number in ethanol-diesel blends in function of biodiesel content (top) and ethanol content (bottom). 73
Figure 19: Effect of fuel oxygen content on HC and CO emissions [Rahimi, 2009]. 78
Figure 20: Difference between Cloud Point, CFPP and Pour Point. 81
Figure 21: Indicated pressure diagram at 1,200 rpm for different blends and BMEP [Hulwan, 2011]. 84
Figure 22: Indicated pressure diagram at 1,600 rpm for different blends and BMEP [Hulwan, 2011]. 85
Figure 23: Spray behavior characteristics in the constant volume chamber (P_{inj} = 100 MPa, m_{fuel} = 10 mg, time after the start of energizing = 0.8 ms (about 5.76° of crank angle)) [Park, 2012]. 87
Figure 24: Gay-Lussac pycnometer, water bath model TV 4000 (Tamson) and a Ohaus Explorer E02140 Balance (from left to right). 103
Figure 25: Ubbelohde glass capillary viscometer (Cannon) and experimental equipment in the Fluids’ Characterization Laboratory (LCF) at PUC-Rio. 105
Figure 26: Lauda TE 1C tensiometer (left) and zoom on the platinum ring (right) in the Fluids’ Characterization Laboratory (LCF) at PUC-Rio. 106
Figure 27: Tracker S (Teclis Scientific) automated drop tensiometer in the Laboratory of Microhydrodynamics and Flow in Porous Media (LMMP) at PUC-Rio. 107

PUC-Rio - Certificação Digital Nº 1312923/CA

Figure 28: Image of a drop given by the software. 108
Figure 29: Schematic view of a manual tag closed cup tester [ATSM D56, 2010]. 109
Figure 30: Tracker S (Teclis Scientific) automated drop tensiometer in the *Centro de Pesquisas e Caracterização de Petróleo e Combustíveis* (CoppeComb) at UFRJ. 110
Figure 31: CFPP equipment, model NTL 450 from Normalab (left) and zoom on the wire mesh filter in the *Centro de Pesquisas e Caracterização de Petróleo e Combustíveis* (COPPEComb) at UFRJ. 111
Figure 32: Ecoline immersion thermostat from Lauda, model E 100 used for corrosion test in the *Centro de Pesquisas e Caracterização de Petróleo e Combustíveis* (COPPEComb) at UFRJ. 112
Figure 33: Cetane Method Test Engine Assembly [ASTM D613, 2013]. 113
Figure 34: PCS Instruments HFRR system in the *Laboratório de Combustíveis e Lubrificantes* (LACOL) at the *Instituto Nacional de Tecnologia* (INT). 115
Figure 35: Schematic Diagram of HFRR [ASTM D6079, 2011]. 115
Figure 36: Laboratory air conditions [adapted from the ISO 12156-1, 2006]. 116
Figure 37: View of the tested engine – model MWM 4.10 TCA. 122
Figure 38: The subassemblies of the Bosch VE distributor pump [Bosch, 1999]. 122
Figure 39: Adjustment of the static injection advance. 123
Figure 40: Views of the dynamometer bench for testing. 123
Figure 41: Laminar flowmeter used in the measurement of intake air. 124
Figure 42: Coriolis flowmeter used in the measurement of DBE blends. 125
Figure 43: Scheme of the measurement of pressure and crank angle. 126

PUC-Rio - Certificação Digital Nº 1312923/CA

Figure 44: Instrumentation used for the measurement of pressure and crank angle. 126
Figure 45: Spatial representation of the Doehlert matrix design [CNAM, 2011]. 130
Figure 46: Sequential properties in relation to the experimental domain: translation of the domain for 2 and 3 factors and reduction of the domain (from left to right) [CNAM, 2011]. 131
Figure 47: Sequential properties in relation to the number of factors for 1, 2 and 3 factors (from left to right) [CNAM, 2011]. 132
Figure 48: Chemical structure of the main compound of both vegetal oils: linoleic acid in soybean oil (left) and ricinoleic acid in castor oil (right). 144
Figure 49: Volumetric ratio between the ethanol phase and diesel fuel phase after decantation for different additive's content. 145
Figure 50: Maximum volumetric fraction (%) of ethanol in 100 mL of diesel fuel with 4 vol% until phase separation after 15 min of decantation (Part 1 of 2). 147
Figure 51: Separation ratio (SR) after 3 days of decantation in function of temperature of anhydrous ethanol-diesel fuel without additive at 10, 20 and 30°C. 151
Figure 52: Multiple phases system for blends with 40 vol% of ethanol (left) and crystals observed in blends with 90 and 80 vol% of anhydrous ethanol (right), after 3 days of decantation at 10°C. 151
Figure 53: Separation ratio (SR) after 3 days of decantation in function of anhydrous ethanol content at 20°C (top) and 10°C (bottom) in ethanol – diesel fuel. 152
Figure 54: Separation ratio (SR) after 2 hours of decantation for diesel B7 fuel at 30°C (top) and 25°C (bottom) for all tested additives. 155
Figure 55: Separation ratio (SR) after 2 hours of decantation for diesel B15 fuel at 15°C (top) and 10°C (bottom) for all tested additives. 156

PUC-Rio - Certificação Digital Nº 1312923/CA

Figure 56: Separation ratio (SR) after 2 hours of decantation and volumetric ratio for ethanol and both biofuels for diesel B7 and B15 fuels in function of the investigated temperature (°C). 158
Figure 57: Separation ratio (SR) for E-diesel (B15) unstable blends in function of the ethanol content and temperature for a) 0.0, b) 0.5, c) 1.0 and d) 2.0 vol% of additive. 160
Figure 58: Separation ratio (SR) for E-diesel (B15) unstable blends in function of the ethanol content and additive content at a) 20, b) 15 and c) 10°C. 161
Figure 59: Kinetics of decantation measuring separation ratio (SR) up to 3 weeks of decantation for E-diesel (B15) blends for different ethanol content at a) 15 and b) 10°C. 162
Figure 60: Separation ratio (SR) after 3 weeks of decantation of E-diesel (B15) blends for different ethanol content and temperature a) without additive and b) with 2.0 vol% of additive. 164
Figure 61: Specific gravity (kg/m^3) at 25°C of DBE blends, in function of additive and ethanol content. 166
Figure 62: Specific gravity (kg/m^3) at 20°C of E-diesel blends a) without and b) with 2 vol% additive, in function of ethanol content. 167
Figure 63: Kinematic viscosity (mm²/s) at 40°C of DBE blends, in function of additive and ethanol content. 169
Figure 64: Surface tension (mN/m) at 25°C of DBE blends, in function of additive and ethanol content. 170
Figure 65: Contact angle (°) at 21°C of DBE blends, in function of additive and ethanol content. 171
Figure 66: Drop volume (mm^3) of DBE blends, in function of additive and ethanol content. 172
Figure 67: Flash point (°C) of DBE blends, in function of additive and ethanol content. 173
Figure 68: Cold Filter Plugging Point (°C) of DBE blends, in function of additive and ethanol content. 174
Figure 69: Brazilian maximum value of CFPP (°C) according to the month [Brasil, 2013]. 175

PUC-Rio - Certificação Digital Nº 1312923/CA

Figure 70: ASTM Copper Strip Corrosion Standard. 176
Figure 71: a) Cetane Number of DBE blends and b) Relative impact of additive on CN, in function of additive and ethanol content. 177
Figure 72: Mean wear scar diameter (μm), b) film percentage (%) and c) friction coefficient of DBE blends at 25°C and 60°C, in function of additive and ethanol content (up to 20 vol%). 179
Figure 73: Values of the lower heating value (LHV) of the DBE blends, in function of additive content. 183
Figure 74: Observed maximum torque for each DBE blend and engine speed: a) absolute values (N.m) and b) fraction of B7 maximum torque (%). 186
Figure 75: Position of the accelerator (%) for each DBE blend and value of torque at a) 1,500 rpm, b) 1,800 rpm and c) 2,100 rpm. 188
Figure 76: Injected energy (kJ) for each DBE blend and value of torque at a) 1,500 rpm, b) 1,800 rpm and c) 2,100 rpm. 190
Figure 77: Injected volume (μL) for each DBE blend and value of torque at a) 1,500 rpm, b) 1,800 rpm and c) 2,100 rpm. 191
Figure 78: Lubricating oil temperature (°C) for each DBE blend and value of torque at a) 1,500 rpm, b) 1,800 rpm and c) 2,100 rpm. 193
Figure 79: Water temperature (°C) for each DBE blend and value of torque at a) 1,500 rpm, b) 1,800 rpm and c) 2,100 rpm. 194
Figure 80: Inlet air temperature (°C) for each DBE blend and value of torque at a) 1,500 rpm, b) 1,800 rpm and c) 2,100 rpm. 195
Figure 81: Relative humidity (%) for each DBE blend and value of torque at a) 1,500 rpm, b) 1,800 rpm and c) 2,100 rpm. 196
Figure 82: Exhaust gas temperature (°C) for each DBE blend and value of torque at a) 1,500 rpm, b) 1,800 rpm and c) 2,100 rpm. 197
Figure 83: Exhaust gas pressure (bar) for each DBE blend and value of torque at a) 1,500 rpm, b) 1,800 rpm and c) 2,100 rpm. 198
Figure 84: Fuel consumption (kg/h) for each DBE blend and value of torque at a) 1,500 rpm, b) 1,800 rpm and c) 2,100 rpm. 200
Figure 85: Air / fuel ratio (kg/kg) for each DBE blend and value of torque at a) 1,500 rpm, b) 1,800 rpm and c) 2,100 rpm. 201

PUC-Rio - Certificação Digital Nº 1312923/CA

Figure 86: Lambda (-) for each DBE blend and value of torque at a) 1,500 rpm, b) 1,800 rpm and c) 2,100 rpm. 202
Figure 87: Specific fuel consumption (kg/(kW.h)) for each DBE blend and value of torque at a) 1,500 rpm, b) 1,800 rpm and c) 2,100 rpm. 203
Figure 88: Specific fuel consumption due to ethanol (kg/(kW.h)) for each DBE blend and value of torque at a) 1,500 rpm, b) 1,800 rpm and c) 2,100 rpm. References of diesel B7 and B15 fuels are also given for each engine speed. 204
Figure 89: Conversion of ethanol (MJ/(kW.h)) for each DBE blend and value of torque at a) 1,500 rpm, b) 1,800 rpm and c) 2,100 rpm. References of diesel B7 and B15 fuels are also given for each engine speed. 206
Figure 90: Brake Mean Effective Pressure (BMEP, bar) for each DBE blend and value of torque at a) 1,500 rpm, b) 1,800 rpm and c) 2,100 rpm. 208
Figure 91: Indicated Mean Effective Pressure (IMEP, bar) for each DBE blend and value of torque at a) 1,500 rpm, b) 1,800 rpm and c) 2,100 rpm. 209
Figure 92: Ignition delay (°) for each DBE blend and value of torque at a) 1,500 rpm, b) 1,800 rpm and c) 2,100 rpm. 210
Figure 93: Indicated pressure (bar) for each DBE blend at 2,100 rpm and 25% of the maximum diesel B7 fuel maximum torque. 212
Figure 94: CA10 (°) for each DBE blend and value of torque at a) 1,500 rpm, b) 1,800 rpm and c) 2,100 rpm. 213
Figure 95: CA50 (°) for each DBE blend and value of torque at a) 1,500 rpm, b) 1,800 rpm and c) 2,100 rpm. 214
Figure 96: CA90 (°) for each DBE blend and value of torque at a) 1,500 rpm, b) 1,800 rpm and c) 2,100 rpm. 215
Figure 97: CA90 – CA10 (°) for each DBE blend and value of torque at a) 1,500 rpm, b) 1,800 rpm and c) 2,100 rpm. 216

PUC-Rio - Certificação Digital Nº 1312923/CA

Figure 98: Maximum gross heat release rate (J/°) for each DBE blend and value of torque at a) 1,500 rpm, b) 1,800 rpm and c) 2,100 rpm. 217
Figure 99: Maximum pressure increase rate (bar/°) for each DBE blend and value of torque at a) 1,500 rpm, b) 1,800 rpm and c) 2,100 rpm. 218
Figure 100: Crank angle of maximum pressure increase rate (°) for each DBE blend and value of torque at a) 1,500 rpm, b) 1,800 rpm and c) 2,100 rpm. 219
Figure 101: Maximum pressure (bar) for each DBE blend and value of torque at a) 1,500 rpm, b) 1,800 rpm and c) 2,100 rpm. 220
Figure 102: Percentage of recovered chemical energy (%) for each DBE blend at 1,800 rpm and 25% of the maximum diesel B7 fuel maximum torque. 221
Figure 103: Crank angle of maximum pressure (°) for each DBE blend and value of torque at a) 1,500 rpm, b) 1,800 rpm and c) 2,100 rpm. 222
Figure 104: Polytropic coefficient during compression (-) for each DBE blend and value of torque at a) 1,500 rpm, b) 1,800 rpm and c) 2,100 rpm. 223
Figure 105: Polytropic coefficient during expansion (-) for each DBE blend and value of torque at a) 1,500 rpm, b) 1,800 rpm and c) 2,100 rpm. 224
Figure 106: Maximum percentage of recovered chemical energy (%) for each DBE blend and value of torque at a) 1,500 rpm, b) 1,800 rpm and c) 2,100 rpm. 226
Figure 107: Fuel Conversion Efficiency η_f (%) for each DBE blend and value of torque at a) 1,500 rpm, b) 1,800 rpm and c) 2,100 rpm. 228
Figure 108: Indicated Efficiency η_i (%) for each DBE blend and value of torque at a) 1,500 rpm, b) 1,800 rpm and c) 2,100 rpm. 229
Figure 109: Volumetric Efficiency η_v (%) for each DBE blend and value of torque at a) 1,500 rpm, b) 1,800 rpm and c) 2,100 rpm. 230

PUC-Rio - Certificação Digital Nº 1312923/CA

Figure 110: Mechanical Efficiency η_m (%) for each DBE blend and value of torque at a) 1,500 rpm, b) 1,800 rpm and c) 2,100 rpm. 232

PUC-Rio - Certificação Digital Nº 1312923/CA

List of tables

Table 1: Fossil diesel fuel in Brazil over the period 2006-2015 [EPE, 2016]. 32
Table 2: Biodiesel in Brazil over the period 2006-2015 [EPE, 2016]. 33
Table 3: Biodiesel plants in Brazil over the period 2005-2014 [EPE, 2016]. 34
Table 4: Surface tension for the investigated DBE blends at 20°C [Barabás, 2009]. 77
Table 5: Approximate fuel characteristics related to flammability of neat diesel fuel, ethanol and gasoline (Battelle apud [Hansen, 2005] and [Shahir, 2014]). 79
Table 6: Measured flash point for the investigated DBE blends [Barabás, 2009]. 80
Table 7: Measured CFPP for the investigated DBE blends [Barabás, 2009]. 82
Table 8: Physicochemical properties of the Brazilian additivated S10 diesel B7 fuel studied. 92
Table 9: Physicochemical properties of the studied hydrous and anhydrous ethanol. 92
Table 10: Physicochemical properties of the soybean and castor oil biodiesel. 93
Table 11: Physicochemical properties of the soybean oil and castor oil. 94
Table 12: Physicochemical properties of the *n*-butanol. 94
Table 13: Doehlert matrix in term of real coordinates for each biodiesel-oil combination. 96
Table 14: Summary of the performed tests conditions described in Section 3.1.2. 96
Table 15: Physicochemical properties of the studied Brazilian S10 diesel B0 fuel. 99

PUC-Rio - Certificação Digital Nº 1312923/CA

Table 16: Physicochemical properties of the biodiesel (85% soybean and 15% beef tallow). 100
Table 17: Doehlert matrix in term of real coordinates for each biomass source. 101
Table 18: Summary of the performed tests conditions described in Section 3.2.2. 101
Table 19: Added volume of each compound of the blends. 102
Table 20: Copper Strip Classifications [ASTM D130, 2012]. 112
Table 21: Physicochemical properties of the studied Brazilian S10 diesel B0 fuel. 118
Table 22: Physicochemical properties of the different biodiesel blends used in this section. 119
Table 23: Physicochemical properties of the castor oil. 120
Table 24: Physicochemical properties of the commercial Brazilian S10 diesel B7 fuel. 120
Table 25: Main characteristics of the engine model MWM 4.10 TCA [MWM International, 2007]. 121
Table 26: Doehlert matrix design in term of reduced variables. 131
Table 27: Summary of the performed tests conditions, given in chronological order. 142
Table 28: Separation ratio (SR) for each biodiesel (B) – vegetal oil (O) sources after 3 hours of decantation. 143
Table 29: Separation ratio (SR) for each biodiesel – vegetal oil sources. 149
Table 30: Best additive's composition for each biodiesel – vegetal oil sources. 150
Table 31: Separation ratio (SR) and stability range for E-diesel (B15) blends in function of the ethanol content, additive content and temperature. 159
Table 32: Specific gravity (kg/m^3) for the DBE blends with 20 vol% of anhydrous ethanol at 20 and 25°C. 168
Table 33: Water drop properties used to control the cleanness of the glass lamella. 171

PUC-Rio - Certificação Digital Nº 1312923/CA

Table 34: Values available in literature of the LHV of the different compounds. 181
Table 35: Values available in literature of the specific gravity at 20°C of the different compounds. 182
Table 36: Values of the lower heating value (LHV) of the different fuel. 182

PUC-Rio - Certificação Digital Nº 1312923/CA

Nomenclature

a	Crank radius (m)
A/F	Air / Fuel ratio (-)
ANP	*Agência Nacional do Petróleo, Gás Natural e Biocombustíveis*
ATDC	After Top Dead Centre
B	Bore (m)
BDC	Bottom Dead Centre
BHT	Butylated hydroxytoluene
$BMEP$	Brake Mean Effective Pressure
BTDC	Before Top Dead Centre
BX	Diesel fuel blended with X vol% of biodiesel
c_p	Specific heat at constant pressure (kJ/(kg.K))
c_v	Specific heat at constant volume (kJ/(kg.K))
CA	Crank Angle (°)
CA10	Value of crank angle where 10% of the energy due to combustion has been released (°)
CA50	Value of crank angle where 50% of the energy due to combustion has been released (°)
CA90	Value of crank angle where 90% of the energy due to combustion has been released (°)
CFPP	Cold Filter Plugging Point (°C)
CI	Compression Ignition engine
CN	Cetane Number (-)
CO	Carbon Monoxide
CO_2	Carbon Dioxide
DBE	Diesel-Biodiesel-Ethanol blends
DOE	Design of Experiments
DR	Dragging Ratio (-)
E-diesel	Ethanol-diesel blends
EX	Diesel fuel blended with X vol% of ethanol
FAME	Fatty Acid Methyl Ester
HC	Unburned Hydrocarbons

PUC-Rio - Certificação Digital Nº 1312923/CA

HFRR	High Frequency Reciprocating Rig
$IMEP$	Indicated Mean Effective Pressure
INPM	*Instituto Nacional de Pesos e Medidas*
L	Stroke (m)
l	Connecting Rod Length (m)
LHV	Lower Heating Value (kJ/kg)
LSD	Low Sulphur Diesel fuel
M	Molecular mass (g/mol)
m	Mass (kg)
$\dot{m}$	Mass flow (kg/h)
MWSD	Mean Wear Scar Diameter (μm)
N	Engine speed (rpm)
N_0	Number of experiments in the center of the experimental domain
NO_x	Nitrogen Oxides
P	Power (kW)
p	Pressure (Pa or bar or atm)
PM	Particulate Matter
R	Gas Constant (J/(kg.K) or m^3.atm/(mol.K)).
RCM	Rapid Compression Machine
REE	Rapeseed Ethyl Ester
RME	Rapeseed Methyl Ester
r_c	Compression ratio (-)
rpm	Rotation per min (min^{-1})
s	Distance between the crank axis and the piston pin axis (m)
SD	Specially Denatured alcohol
sfc	Specific fuel consumption (kg/(kW.h))
S10	Diesel fuel with a maximum sulfur limit of 10 mg/kg
SO_2	Sulphur Dioxide
SR	Separation Ratio (-)
T	Temperature (K or °C)
TDC	Top Dead Centre
To	Torque (N.m)
ULSD	Ultra-Low Sulphur Diesel fuel
U_r	Relative moisture content (-)
V	Volume (m^3)

PUC-Rio - Certificação Digital Nº 1312923/CA

V_c.	Clearance Volume (m^3)
V_d	Displaced Volume (m^3)
vol	Volume basis
$\dot{V}$	Volumetric flow (kg/m^3)
v	Velocity (m/s)
W	Work (J)
wt	Weight basis
X_1	Reduced variable associated to biodiesel concentration (in sections 3.1 and 5.1) and vegetal oil concentration (in sections 3.2 and 5.2)
X_2	Reduced variable associated to vegetal oil concentration (in sections 3.1 and 5.1) and m-butanol concentration (in sections 3.2 and 5.2)
x_1	Real variable associated to biodiesel concentration (in sections 3.1 and 5.1) and vegetal oil concentration (in sections 3.2 and 5.2)
x_2	Real variable associated to vegetal oil concentration (in sections 3.1 and 5.1) and m-butanol concentration (in sections 3.2 and 5.2)
Y	Molar fraction (-)

Greek letters

Δh	Latent heat of vaporization (kJ/kg)
γ	Specific Heats Ratio (-).
η_f	Fuel Conversion Efficiency (%)
η_i	Indicated Efficiency (%)
η_m	Mechanical Efficiency (%)
η_v	Volumetric efficiency (%)
θ	Crank angle (°)
λ	Lambda (-)
μ	Dynamic Viscosity (kg/(m.s))
υ	Kinematic Viscosity (mm^2/s)
ρ	Specific Gravity (kg/m^3)
ω	Absolute moisture content (-)

PUC-Rio - Certificação Digital Nº 1312923/CA

Subscript

air, d	Dry air
air, w	Wet air
B	Biodiesel
b	Brake
D	Diesel fuel
DBE	Diesel-Biodiesel-Ethanol blends
$EtOH$	Ethanol
f	Fuel
i	Indicated
inj	Injected
m	Mass basis
max	Maximum
n	Molar basis
r	Reference
s	Stoichiometric
w	Water

PUC-Rio - Certificação Digital Nº 1312923/CA

1 Introduction

1.1. Brazilian Energy Matrix

The worldwide fuel crisis of the 1970s initiated awareness about the vulnerability to oil embargoes and shortages among the countries of the world [Shahir, 2014]. Moreover, most scenarios developed by economists are based on a regular growth of global energy demand over the next twenty years. In this balance, nuclear and renewable energy (wind, hydro, solar, etc.), although in full expansion, will remain marginal compared to fossil fuels, growing from 19% nowadays to 25 %, in 2040. Oil demand for transport and petrochemical is expected to grow by over 15% until 2040 [IEA, 2014].

Considering more specifically the Brazilian scenario [Pottmaier, 2013], the country is incorporating two strategies regarding the energy sector:

(i) Keeping the matrix clean and renewable, focusing on its potentials to produce energy from hydraulic, for electricity generation, and from biomass, for liquid fuels for transportation (in particular, sugarcane ethanol);

(ii) Promotion of conservation and efficient use of energy, through several governmental programs, such as the *Programa de Controle de Poluição do Ar por Veículos Automotores* (PROCONVE), the *Programa de Controle da Poluição do Ar por Motociclos e Veículos Similares* (PROMOT), the *Programa Nacional de Controle de Qualidade do Ar* (PRONAR), the *Programa de Incentivo à Inovação Tecnológica e Adensamento da Cadeia Produtiva de Veículos Automotores* (INOVAR-AUTO) and *RenovaBio* program (public consultation opened in March 2017).

The results of this policy are illustrated in Figure 1 in which the Brazilian domestic energy supply in 2015 is given.

PUC-Rio - Certificação Digital Nº 1312923/CA

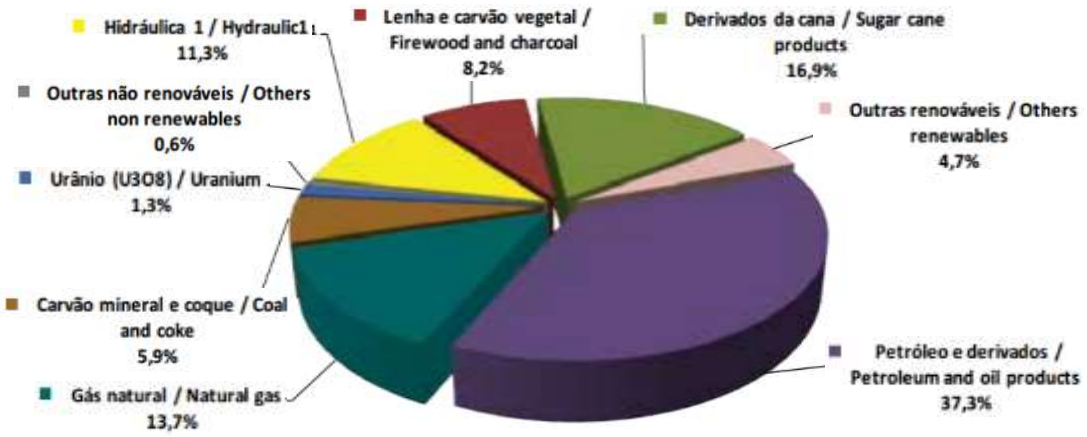

[1] Includes electricity imports originated from hydraulic sources.

Figure 1: Domestic energy supply in 2015 [EPE, 2016].

In 2015, renewable sources represented 41.1% of the domestic energy supply. This proportion was almost the double of the worldwide average, showing that Brazil has a relatively green energy mix. Nevertheless, such proportion remained equal to the contribution of petroleum and oil products, as seen in Figure 1 [EPE, 2016]. Moreover, the prevision of distribution of the Brazilian energy matrix showed that the dependence on oil will remain high (41.9% in 2024) [MME/EPE, 2015]. Figure 2 shows the consumption of oil products by sector over the period 1970-2015.

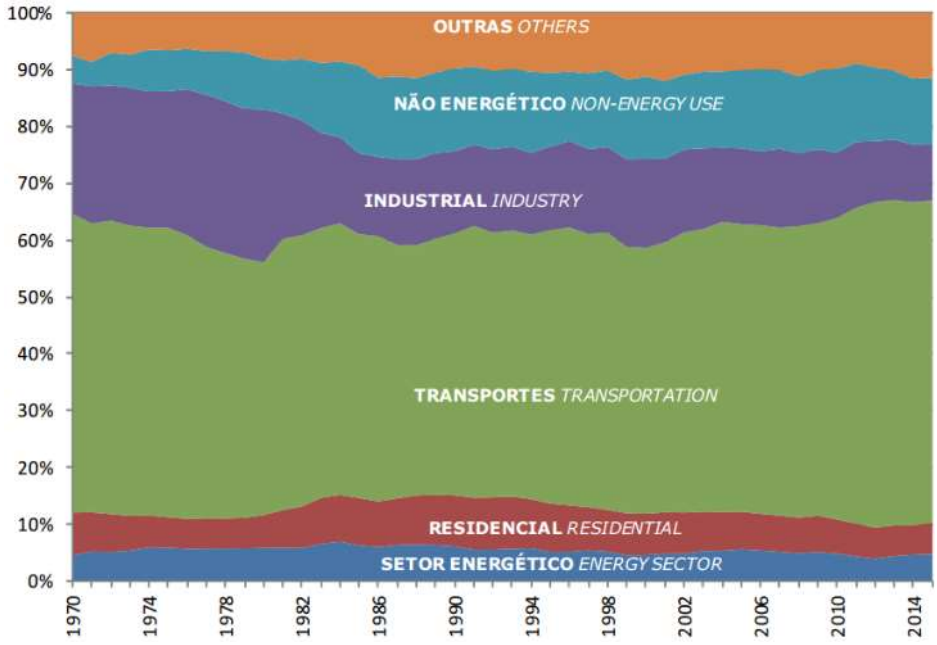

Figure 2: Oil products consumption by sector over the period 1970-2015 [EPE, 2016].

PUC-Rio - Certificação Digital Nº 1312923/CA

Such dependency on oil is due to transportation sector, that represented, in 2015, 32.5% of the final energy consumption and 57% of the oil products consumption [EPE, 2016]. Figure 3 gives the distribution of the different fuels used in the transportation sector over the period 1975-2015.

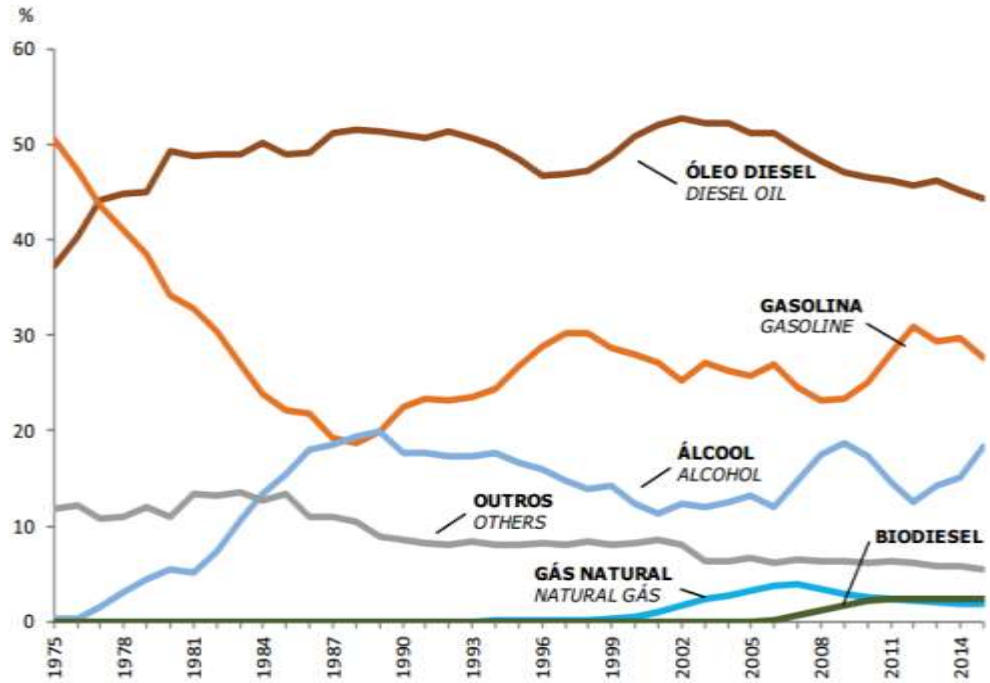

Figure 3: Transportation sector energy consumption over the period 1975-2015 [EPE, 2016].

It can be seen in this figure that, among petroleum products, diesel fuel continues to represent an essential source for the Brazilian economy (44.4% of the derivates from petroleum used in transportation sector in 2015) due to its intense use in ground transportation area cargo and passenger public transportation (Figure 3) [EPE, 2016].

According to the decennial plan (2014-2024) from the Brazilian Ministry of Mines and Energy *(Ministério de Minas e Energia*) [MME-EPE, 2015], diesel fuel demand should reach almost 72 billion litres in 2024. The projection of diesel fuel is based on the demand for transport derives from the use of heavy road vehicles (buses and trucks), light commercial vehicles and transportation by boat and rail. The Figure 4 presents the projection of the number of light vehicles (passenger cars and light-weight commercial vehicles) fueled with diesel fuel for the period 2015-2024.

PUC-Rio - Certificação Digital Nº 1312923/CA

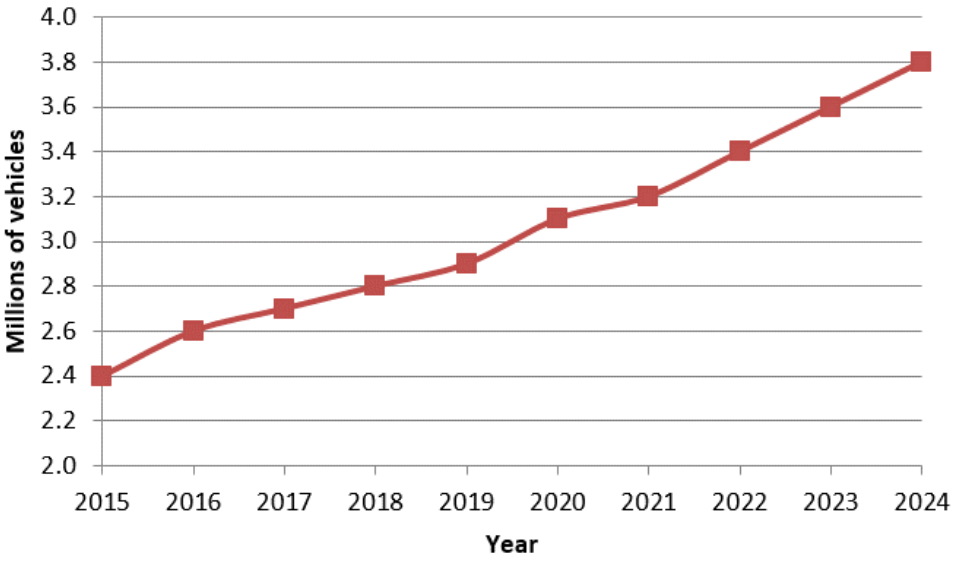

Figure 4: Profile of light vehicles (passenger cars and light-weight commercial vehicles) fueled with diesel fuel for the period 2015-2024 [MME-EPE, 2015].

Compared to 2015, it is expected an increase of 27% of the diesel fuel demand that can be associated to the increase of 58% of the number of light vehicle fueled with diesel fuel over the same period.

Although Brazil is the second largest oil producer in South America and it produces more crude oil than its domestic demand, the country does not meet a situation of self-sufficiency and it needs to import diesel fuel to supply the national demand. Table 1 gathers data on production, importation and exportation of fossil diesel fuel in Brazil.

PUC-Rio - Certificação Digital Nº 1312923/CA

Table 1: Fossil diesel fuel in Brazil over the period 2006-2015 [EPE, 2016].

Flow (10^3 m^3)	2006	2007	2008	2009	2010	2011	2012	2013	2014	2015
Production	38,660	39,111	41,077	42,443	41,429	42,891	45,576	49,168	49,302	49,059
Import	3,545	5,099	5,829	3,515	9,007	9,333	9,719	10,024	11,275	6,940
Export	-1,337	-1,804	-1,557	-2,010	-1,545	-1,110	-792	-1,030	-936	-768
Stock variations, losses and adjustments [1]	95	442	352	441	251	156	341	-379	-265	331
Total Consumption	40,963	42,489	45,702	44,389	49,142	51,270	54,844	57,783	59,375	55,562

[1] Biodiesel not included

Moreover, it can be seen in this table an increase of the importation and decrease of exportation of diesel fuel since 2010, with exception of 2015 (probably associated to the reduction of economic activity), due to the increase of domestic demands, in particular for commodity production. As already observed by Duran (2013), this contributes to the deficits on the Brazilian balance of trade [Brasil, 2016b; EPE, 2016].

To partially substitute the fossil fuel demand, reduce the importation and the greenhouse gases emissions, biodiesel was progressively introduced into fossil diesel fuel. Moreover, the Brazilian biodiesel production federal program encourages small farmers (family farms), mainly in the North and Northeast regions, to produce feedstock for biodiesel production and to become an important part of this biofuel production chain [Bergmann, 2013]. Since 2008, the blend of pure biodiesel in diesel fuel has become mandatory. Between January and June 2008, the mix was of 2 vol% of biodiesel, before increasing to 3 vol% between July 2008 and June 2009 and to 4 vol% between July and December 2009. The incorporation content increased to 5 vol% in January 2010 and 6 vol% in July 2014. Since November 2014, 7 vol% of biodiesel is added to commercial diesel fuel. Consequently, as given in Table 2, the biodiesel consumption triplicated since 2008 and an average annual increase of 10% since 2010 [EPE, 2016].

PUC-Rio - Certificação Digital Nº 1312923/CA

Table 2: Biodiesel in Brazil over the period 2006-2015 [EPE, 2016].

Flow (10^3 m^3)	2006	2007	2008	2009	2010	2011	2012	2013	2014	2015
Production	69	404	1,167	1,608	2,397	2,673	2,717	2,917	3,420	3,937
Stock variations, losses and adjustments	0	0	-46	-50	-51	-126	36	-33	-29	10
Total Consumption	69	404	1,121	1,558	2,347	2,547	2,754	2,885	3,391	3,947

The law n° 13.263 from March 23rd 2016 stipulated the augmentation in 8, 9 and 10 vol% of biodiesel content in a period of 12, 24 and 36 months, respectively [Brasil, 2016a]. Moreover, this decision was also based on a publication of the Resolution n°03 of the *Conselho Nacional de Política Energética (CNPE)* on the *Diário Oficial da União da Resolução n° 03* allowing the commercialization and the volunteer use of biodiesel into fossil diesel fuel up to 20 vol% in captive fleets and 30 vol% for rail and for agricultural and industrial use [Brasil, 2015a].

Table 3 presents the biodiesel plants (methyl esters) in Brazil over the period 2005-2014.

Table 3: Biodiesel plants in Brazil over the period 2005-2014 [EPE, 2016].

Specification	2006	2007	2008	2009	2010
Total Raw Materials (m^3)	-79,010	-463,596	-1,313,681	-1,813,945	-2,666,289
Methanol	-9,998	-57,495	-136,043	-199,111	-278,650
Soybean oil	-65,764	-35,3233	-967,326	-1,250,590	-1,980,346
Palm oil	-2,431	-3,821	-2,728	-5,209	-3,201
Cottonseed oil	0	-1,904	-24,109	-70,616	-57,054
Peanut oil	0	0	-2,551	-2,667	-406
Radish oil	0	-159	0	-444	-1,579
Sunflower oil	0	0	-1,125	-4,127	-171
Castor oil	0	-336	-115	-111	0
Sesame oil	0	0	0	0	-144
Canola oil	0	0	0	0	0
Tallow	-816	-34,445	-153,275	-253,703	-297,243
Other fatty materials	0	-12,197	-23,975	-22,939	-37,181
Chicken fat	0	0	-150	-873	-2,416
Pork fat	0	0	-1,123	-1,190	-2,800
Used frying oil	0	-6	-1,160	-2,366	-5,099
Biodiesel production (m^3)	69,002	404,329	1,167,128	1,608,448	2,386,399

Specification	2011	2012	2013	2014	2015
Total Raw Materials (m^3)	-2,974,662	-3,025,130	-3,253,873	-3,795,320	-4,378,456
Methanol	-301,890	-305,233	-332,867	-379,953	-439,584
Soybean oil	-2,171,113	-2,105,334	-2,231,464	-2,625,558	-3,061,027
Palm oil	-1,748	-5,230	-9,990	-1,026	-3,336
Cottonseed oil	-98,230	-116,736	-64,359	-76,792	-78,840
Peanut oil	-225	0	0	0	0
Radish oil	0	0	-672	0	0
Sunflower oil	-420	0	0	0	0
Castor oil	0	0	0	0	0
Sesame oil	0	0	0	0	0
Canola oil	0	-501	0	0	-158
Tallow	-348,983	-444,676	-563,860	-644,382	-712,670
Other fatty materials	-29,182	-22,361	-8,383	-14,119	-39,656
Chicken fat	-670	-2,653	-639	-15,831	-1,797
Pork fat	-9,034	-10,693	-13,928	-15,648	-24,452
Used frying oil	-13,168	-11,713	-27,711	-22,110	-16,935
Biodiesel production (m^3)	2,672,760	2,717,483	2,917,488	3,419,838	3,937,269

PUC-Rio - Certificação Digital Nº 1312923/CA

Due to its great biodiversity and diversified climate and soil conditions, Brazil has different vegetable oils sources, including soybean, coconut, castor seed, cottonseed, palm trees, and others (mainly beef tallow). Since Brazil is the second largest soybean producer in the world and it has a well-developed soybean-processing industry, soybean is the main source for biodiesel production. The Table 3 also shows that beef tallow is the second source of biodiesel in the country [Pousa, 2007; EPE, 2016].

1.2. Biofuels in Compression Ignition (CI) Engines

With the continued depletion of oil reserves and the increasingly stringent emission standards concerning gases and particulate matters causing the greenhouse effect within the earth's atmosphere and local pollution, it is important to develop new internal combustion engines – fuel systems with low emissions, high fuel efficiency, high specific power and the same drivability quality [Lei, 2012]. Distribution and supply, fuel delivery reliability to the engine and engine stability have to be considered [Hansen, 2005]. Another very important factor to be considered for assessment is the difference between the modern state-of-the-art vehicles and the older technologies, which represents the majority of current vehicle fleet, in particular, existing engines and exhaust gas post-treatment. Extreme environmental conditions also play a vital role in assessing a fuel [Shahir, 2014].

In this context, the use of biofuels presents an attractive potential. Biofuels are produced from biomass and, therefore, as long as the growing cycle is respected, constitute renewable energy source, contributing much less to global warming than fossil fuels. In addition, the development of biofuel production chains can participate in the energy independence in many countries [Ballerini, 2007]. Among them, biodiesel and bioethanol present a high potential to be used in compression ignition (CI) engines.

Diesel-biodiesel blends are already used on existing engines to achieve both environmental and energy benefits [Carneiro, 2017]. Biodiesel has properties similar to those of traditional fossil diesel fuel and it can substitute diesel fuel with little or no engine modification, depending of the concentration. Depending on the

PUC-Rio - Certificação Digital Nº 1312923/CA

engine and load, substantial reduction in particulate and CO emissions can be obtained through the addition of biodiesel to diesel fuel [Pang, 2006; Shi, 2006].

As biodiesel cannot entirely replace fossil diesel fuel demand, ethanol is also considered as an alternative. Due to the availability in large volume among all the renewable fuel sources, bioethanol can be a good option, especially for the second-generation pathway. Bioethanol is produced by fermentation from various feedstocks like sugarcane, corn, beet, molasses, cassava root, barley sugar, starch, cellulose, etc. or, more marginally, from reacting ethane and steam [Shahir, 2014]. Nevertheless, due to the different polarity of ethanol and hydrocarbons in diesel fuel, ethanol cannot be blend in all proportion into the fossil fuel. Three main techniques have emerged during recent years to use ethanol with diesel fuel [Abu-Qudais, 2000; Boretti, 2012; Pauferro, 2012]:

(i) **Alcohol fumigation** where alcohol is added to the intake air charge, displacing up to around 50% of diesel fuel demand. Injection of ethanol in the intake may permit large percentages of ethanol. However, this method requires a second port injector for the ethanol and separate fuel tanks, lines, pumps and controls. Diesel Port Fuel Injection injectors and pumps, specifically developed for ethanol, are required.

(ii) **Dual injection** where each fuel is separately injected requiring two separate injection system, displacing up to 90% of diesel fuel demand. The dual fuel direct injection is a method by which only a small amount of diesel fuel supplements the main injection of ethanol. The drawbacks of this method include the second direct injector and separate fuel tanks, lines, pumps and control. The dual injector requires space in the combustion chamber where the injector can be effective. Diesel Direct fuel injection injectors and pumps are available, but specifically developed ethanol injectors and pumps are needed. Two theses on this subject were formerly submitted at *Pontifícia Universidade Católica do Rio de Janeiro* (PUC-Rio), presenting experimental study on rapid compression machine (RCM) [Loaiza, 2014] and on engine [Egúsquiza, 2011]

(iii) **Ethanol-diesel blends (E-diesel or diesohol)** where the fuels are mixed prior to injection, displacing up to 25% of diesel fuel demand.

PUC-Rio - Certificação Digital Nº 1312923/CA

This method is the easiest since ethanol could be used in the form of solutions, without technical modifications.

The first investigations done on E-diesel were carried out in South Africa, in the late 1970s. Research continued in Germany and in the United States during the 1980s. More recently, since the late 1990s, it has been used on heavy-duty and light-duty diesel engines in order to modify their emission characteristics. The high number of publications and patents about E-diesel published in the past few years could testify new interest in this issue [Weber de Menezes, 2006; Ribeiro, 2007]. The present thesis investigated some issues related to this technological option.

1.3. Potential of Ethanol-Diesel Blends (E-Diesel)

The literature showed that many technical barriers exist to the direct use of E-diesel blend in the CI engine [Ajav, 1999; Hansen, 2001a; Hansen, 2001b; Satgé de Caro, 2001; Li, 2005; Pang, 2006; Ribeiro, 2007; Török, 2009; Pidol, 2012; Shahir, 2014; Yilmaz, 2014]:

(i) Ethanol is not accurately described as either miscible or immiscible in diesel fuel. Very small proportion (less than 5 vol%) of ethanol shows complete miscibility in diesel fuel. Miscibility of ethanol in diesel fuel depends on the hydrocarbon composition and wax content of the base diesel fuel, ethanol content, moisture and the temperature of the diesel fuel.

(ii) Specific gravity, viscosity, lubricity and flash point of the blend are affected, implying some adaptation of the storage and injection of the blends. The cetane number and calorific value energy content of the E-diesel blend are much lower than the fossil diesel fuel, influencing the combustion. The expected torque and power reduction due to the lower heating value and specific gravity is approximately 2% for every 5% ethanol added. Therefore, ignition improvers and other additives are required to improve the durability and ignition of diesel engines when E-diesel fuels are used.

(iii) The use of E-diesel can increase unburned hydrocarbons, NOx emissions, and aldehyde emissions, perhaps due to the cooling effects of

PUC-Rio - Certificação Digital Nº 1312923/CA

alcohols. Nevertheless, higher total hydrocarbon emissions might offer a reducer that regenerates NOx adsorbers.

(iv) Material compatibility and corrosiveness are also important factors that must be considered.

Nevertheless, there are some very important advantages considering E-diesel blend as a potential fuel for the existing compression ignition engines:

(i) The E-diesel blend can significantly reduce particulate matter (PM) emissions in the motor vehicles [Ahmed, 2001; He, 2003; Beer, 2007; Xing-Cai, 2004; Lei, 2011], when compared to conventional low sulphur diesel fuel. Moreover, this ethanol-diesel blend yielded substantial reductions in urban emissions of greenhouse [Shahir, 2014], as ethanol has naturally zero sulphur content (considered a soot precursor). However, this advantage seems to gradually fade away, due to the continuous desulfurization of the fossil diesel fuel [Giakoumis, 2013].

(ii) Minor variations in the fuel delivery system are required while using E-diesel as fuel, mainly due to material compatibility [Gerdes, 2001; El-Awad, 2004; Ghobadian, 2006].

(iii) Similar energy output can be attained compared to fossil diesel fuel, as for instance, with a blend of diesel B30 with 5 vol% of anhydrous ethanol (Raslavicius and Bazaras (apud [Shahir, 2014])).

(iv) By adding ethanol to the diesel fuel, the cold flow properties (cloud point, cold filter plugging point (CFPP) and pour point) are improved compared to fossil diesel fuel [Kwanchareon, 2007; Barabás, 2009].

Indeed, diesel engines cannot normally operate on E–diesel blend without special additives. There are two additive-based approaches to maintain stable blends: adding surfactants (or emulsifiers) that produce stable (micro)emulsions or adding co-solvents that produce stable homogeneous solutions [Ribeiro, 2007].

1.4. Potential of Diesel-Biodiesel-Ethanol (DBE) Blends

Biodiesel are primarily used because of their similarity to diesel fuel concerning physicochemical characteristic [Fazal, 2011], which allows the use of ester-diesel blends in any proportion. Moreover, biodiesel is miscible with alcohols and diesel fuel. This addition increases the oxygen level in the blend. Its

PUC-Rio - Certificação Digital Nº 1312923/CA

addition prevented phase separation up to 20 vol% of ethanol, acting as an amphiphile, and improved the tolerance to water [Fernando, 2004; Shi, 2005; Shi, 2006; Kwanchareon, 2007; Rahimi, 2009; Shudo, 2009; Chotwichien, 2009; Moretti, 2013; Silveira, 2013; Shahir, 2014].

The main advantages of using biodiesel, rather than using any artificial additive synthesized in the laboratory, are listed below [Balat, 2008; Murugesan, 2009; Jain, 2010; Rajasekar, 2010; Jayed, 2011; Ong, 2011; Xue, 2011; Mehta, 2012; Mofijur, 2012; Shahir, 2014]:

(i) By using biodiesel, it will increase the supply of domestic renewable energy and the oxygen level in the blend, and reduce the sulphur content of the blends.

(ii) When biodiesel is added to E-diesel, the flash point of this ternary blend can become high enough to safely store it.

(iii) When biodiesel is added to the E-diesel, lower viscosity and specific gravity of the E-diesel can be compensated and it can remain within the standard diesel fuel prescribed limits.

(iv) By adding biodiesel, heating value, cetane number and lubricity of the ternary blend approach to the fossil diesel fuel and enable the use of this ternary blend in the existing CI engines.

(v) Compared to E-diesel blends, investigations showed that diesel-biodiesel-ethanol blends can reduce NOx emissions while increasing CO and HC emissions [Yilmaz, 2014]. These results are strongly dependent of the fuel composition, the engine characteristics and loads. As a consequence, other studies showed opposite tendency, as for example, Raslavicius and Bazaras (apud [Suppes, 2000]). They tested a vehicle fueled with a blend of 70% of diesel fuel + 30% of biodiesel admixed with the anhydrous ethanol additive (5 vol%) and they found a dramatic decrease in PM (40%), HC (25%) and CO (6%) emissions compared to fossil diesel fuel. NOx emissions from diesel–biodiesel–ethanol blends were lower than the B30 (up to 4%), but remained higher than in the diesel fuel.

PUC-Rio - Certificação Digital Nº 1312923/CA

1.5. Brazilian Experience

In Brazil, at the end of the 70s, the hypothesis of a partial substitution of diesel fuel by its mixtures with ethanol in diesel engines was studied, motivated by the oil crisis and Proálcool program. As this substitution resulted in some problems of adaptation (for instance, material compatibility and expensive ignition improver), these initiatives were abandoned [Reyes, 2009a].

In the late 90s, the interest for this technology re-emerged with the aim of reducing emissions of greenhouse gas and diversifying the energetic mix. Based on the positive results obtained on heavy-duty compression ignition engines in Sweden, Australia, Chile, Germany and Thailand, a Technical Group (*Grupo Técnico*, GT II) was created in 1997, coordinated by the Ministry of Sciences and Technology (*Ministério da Ciência e Tecnologia*, MCT), to study the technical feasibility of the mixture, bringing together governmental agencies, research institutions, private sector and non-governmental organizations. This group integrated the executive committee of the Interministerial Council of Sugar and Alcohol (*Conselho Interministerial de Açúcar e do Álcool*, CIMA). The Alcohol & Diesel Program was developed in two directions: one project coordinated by the Union of Cities producing Sugar Cane in the State of São Paulo (*União dos Municípios Canavieiros do Estado de São Paulo*, Unica) and another, by the Association of the Producers of Alcohol and Sugar of Paraná (*Associação dos Produtores de Álcool e Açúcar do Paraná*, Alcopar). The two differed on technical aspects: the mixture proposed by Unica contained 3% to 10% hydrous ethanol to form an emulsion, while the Alcopar contained 8% to 12% of anhydrous alcohol with stabilizing additives to form a solution [Ecomat, 1999; MCT–CIMA, 2000; Oliveira, 2003; Weber de Menezes, 2006; Koike, 2006; Koike, 2007; Reyes, 2009a].

Among the works sponsored by the MCT, some presented a technical alternative for hydrated alcohol-diesel emulsions with additives to increase the homogeneity of the mixture and to improve cetane number and lubricity. This alternative was endorsed by Methanex, a Canadian multinational group and one of the largest methanol producers in the world that commercializes an emulsifier agent named Dalco, fabricated by the Australian Apace (Sosalla). In São Paulo, it was tested a mixture of hydrous alcohol, Dalco additive (0.5% to 0.8% vol.), anti-

PUC-Rio - Certificação Digital Nº 1312923/CA

corrosion additives and cetane rating improvers. These tests, financed also by the Company of Public Transport of São Paulo (*Companhia de Transportes Coletivos de São Paulo*, CTC-SP), were carried out in laboratory and in field. The assays were made with up to 20% vol. of hydrous alcohol. This experiment was abandoned due to the dependence on a single supplier of emulsifier, specific conditions to keep stability and deposit formation in injection pump [Kremer, 2000; Santos, 2000; Oliveira, 2003; Weber de Menezes, 2006; Koike, 2006; Koike, 2007; Reyes, 2009a].

Subsequently, other studies investigated various types of emulsions with the use of anhydrous alcohol and other stabilizing additives: AEP-102, BIO-7 and Promad-1 [Strapasson, 2006].

The additive BIO-7, produced in England, was used in two buses in Piracicaba, São Paulo in a solution of 7% of anhydrous ethanol, 91% of diesel fuel and 2% of BIO-7 blends. Results showed a lower performance as the driver needed to use lower shift in comparison to conventional fuel [Oliveira, 2003].

The additive AEP-102 acts as a cetane improver and presents good solubility and lubricity properties. Researchers had successfully tested, in urban buses, a blend of 86.2% diesel fuel, 11.2% anhydrous alcohol and 2.6% AEP-102 additive. The mixture with 89.4% diesel fuel, 8% ethanol, and 2.6% AEP-102 presented excellent performance in studies carried out in twenty urban busses of the metropolitan fleet of Curitiba, as a part of the test program realized by the laboratories of the Institute of Technology of Paraná (*Instituto de Tecnologia do Paraná*, Tecpar), the Institute for Technological Researches (*Instituto de Pesquisas Tecnológicas*, IPT), in São Paulo (SP), and the National Institute of Technology (*Instituto Nacional de Tecnologia*, INT), in Rio de Janeiro (RJ). The blend was consumed for several years in fleets and it fed vehicles which have covered about 260,000 km in the cities of Curitiba (PR), Cuiabá (MT) and Campo Grande (MS) [Ecomat, 1999; Oliveira, 2003; Koike, 2006; Koike, 2007; Ribeiro, 2007; Reyes, 2009a; Reyes, 2009b].

Other initiatives for formulation of mixtures of anhydrous ethanol to diesel fuel and the main results of the tests conducted in Brazil are related to the following:

(i) Independent tests have been developed in some plant with mixtures containing anhydrous ethanol in the range of 3 to 10 vol%, without

PUC-Rio - Certificação Digital Nº 1312923/CA

additives. The use of this mixture, named MAD3, with 3 vol% of ethanol, was monitored in Curitiba bus fleet use. It was also experienced in the city of São Paulo. Since 1998, Copersucar, Brazilian ethanol and sugar company, leads tests with 3%, 5%, 7% and 10 vol% anhydrous ethanol blended in diesel fuel without additives [Koike, 2006; Koike, 2007; Reyes, 2009a].

(ii) In 2004, the Dedini Agro Group conducted tests on service trucks of the *Usina São Luis* in Pirassununga (SP) consuming a mixture of diesel fuel with 10 vol% ethanol and 0.5 vol% of additive Octimise D 7001 [Reyes, 2009a].

(iii) Tests with anhydrous ethanol blended with diesel fuel without any additive in the proportion of 7 vol%, was initiated in 1998, in Virgolino de Oliveira S/A Sugar and Alcohol, better known as Catanduva Plant, in Ariranha (SP) [Koike, 2006; Koike, 2007; Reyes, 2009a].

(iv) In *Usina São Martinho de São Paulo*, a fleet of eleven trucks consumed diesel fuel with 10 vol% of anhydrous ethanol without additive in 2002. This mixture was prepared and consumed daily to ensure its stability. Between 2003 and 2005, forty trucks used the mixture with a new formulation (diesel fuel with 5 vol% of anhydrous ethanol without additives). Under the new conditions, the mixture remained stable for five days, considering the environmental characteristics of the region [Reyes, 2009a].

Researchers of the *Laboratório de Desenvolvimento de Tecnologias Limpas* of the Department of Chemistry of *Universidade de São Paulo / Ribeirão Preto* (LADETEL-USP/RP) proposed to conduct intensive studies, field trials and engine test benches, for the use of a new ternary mixture (90% diesel fuel, 5% anhydrous ethanol and 5% ethyl esters of soybean) developed internally. This fuel showed promise results in isolated tests with midsize vehicles [Reyes, 2009a].

1.6. Objectives

As formerly shown, DBE blends were already investigated by several research groups to find technological solutions to increase the incorporation of ethanol in the blends, to evaluate the physicochemical properties and to assess the

PUC-Rio - Certificação Digital Nº 1312923/CA

impact in the greenhouse gases after combustion in a CI engine. However, there are still some points to be further investigated, like those that will be studied in this work. The present thesis has the following goals:

(i) To find a way to enhance the miscibility of ethanol in diesel fuel and to stabilize DBE mixture, by formulating a new and original additive from renewable compounds. For this purpose, the study initially investigated current blends with commercial fuels. However, adequacy to potential future fuel, such as higher incorporation of biodiesel or other ethanol quality, were assessed.

(ii) To study the interaction between the various compounds of the blends: diesel fuel, biodiesel and ethanol and to determine the factors influencing the stability, such as concentration of ethanol, additive content, temperature, and aging time.

(iii) To assess several critical physicochemical properties involved in the proper operation of the fuel line (stability issue, fuel consumption, behavior under cold weather, safety concerns, interaction between the fluid and the surface, and combustion quality) for a large range of ethanol content.

(iv) To define the potential of the blends to be used in current engine and vehicles through engine tests. Fuel consumption, engine efficiency, ignition delay and combustion characteristics were assessed for different experimental condition of blends and loads in an Euro III engine. Based on these experimental results, recommendations for future works were given in order to adequate the blends to current engines.

PUC-Rio - Certificação Digital Nº 1312923/CA

1.7. Performed Activities and Organization of the Thesis

A state-of-the-art on miscibility of ethanol in E-diesel and DBE blends were performed to define the ethanol miscibility issue. A large review of additives studied in literature allowed to define compounds with high potential to enhance ethanol miscibility. Based on literature review and promising Lei's results [Lei, 2012], the present thesis focused on the formulation of ternary additives composed of biodiesel, vegetal oil and *n*-butanol.

Based on the literature data, a first set of additives was formulated to stabilize Brazilian diesel S10 fuel (with 7 vol% of biodiesel, B7) blended with hydrous ethanol, both commercial. The tested additives were synthesized through a Doehlert design of experiments (DOE), considering all the possible combinations of biodiesel-vegetal oil from soybean and castor oil. Such sources was chosen as, on the one hand, soybean is the main sources of biodiesel in Brazil and its production at industrial scale is already mature and, on the other hand, castor oil showed to be part of an efficient additive already in an article published in literature. All compounds of the additive can be obtained from renewable sources (even if the *n*-butanol used in the experimental section was from fossil source). Based on the stabilization impact of 2 vol% of additive, the best additive for each couple was defined. As the blends presented high instability due to high moisture content, tests assessing the impact of temperature were done using anhydrous ethanol. Based on the experimental results, additives with higher refined vegetal oil fraction were tested to increase the bridging power of the co-solvent and ethanol with low moisture content has to be used to guarantee the stability.

Consequently, a second set of additives was studied to stabilize Brazilian diesel S10 fuel blended with anhydrous ethanol. As biodiesel can be directly blended into diesel fuel and the tendency is to increase its concentration in commercial diesel fuel, different concentrations of biodiesel (B7, B15 and B30) were also investigated. Based on the experimental results formerly obtained, new additive formulations, with vegetal oil as main compound, were investigated through a Doehlert DOE, considering the same combinations of biodiesel and vegetal oil from soybean and castor oil. For each concentration of biodiesel, the impact of 2 vol% of such additive to stabilize DBE blends was studied. Based on these results, the best additive was defined. A short and long-term study of its stabilizing effect at different temperature was performed to define the optimum concentration, the stability range and the impact on miscibility of ethanol. The synthesized additive increased substantially the miscibility of ethanol in the blends and the stability range was higher. It was used for the further investigations.

Then, some critical physicochemical properties were assessed for DBE blends with 2.0 vol% and without additive:

PUC-Rio - Certificação Digital Nº 1312923/CA

(i) The kinematic viscosity, the specific gravity and the surface tension were measured in the Laboratory of Fluid Characterization (*Laboratório de Caracterização de Fluidos*, LCF) at PUC-Rio.

(ii) The contact angle was measured in the Laboratory of Microhydrodynamics and Flow in Porous Media (*Laboratório de Micro Hidrodinâmica e Meios Porosos*, LMMP) at PUC-Rio.

(iii) The lubricity was measured in the Laboratory of Fuels and Lubricants (*Laboratório de Combustíveis e Lubrificantes*, LACOL) at the National Institute of Technology (*Instituto Nacional de Tecnologia*, INT)

(iv) The cetane number was defined in the Laboratory of Engines and Fuels (*Laboratório de Motores e Combustíveis*, LAMOC) at the National Institute of Metrology, Quality and Technology (*Instituto Nacional de Metrologia, Qualidade e Tecnologia*, INMETRO).

(v) The flash point, the cold filter plugging point and the corrosiveness to copper were measured in the Centre of Research and Characterization of Crude Oil and Fuels (*Centro de Pesquisas e Caracterização de Petróleo e Combustíveis*, COPPEComb) at UFRJ.

(vi) The lower heating value (LHV) was calculated based on the LHV values of the used compounds obtained through a bibliographic revision.

Based on the crossed results of stability study and physicochemical properties, the use of at least 1.0 vol% of additive is recommended and their specific properties were defined. Such blends were used to test an engine on dynamometer with diesel B15 fuel blended with 0, 5, 10, 15 and 20 vol% of anhydrous, with 1.0 vol% of additive and compared to current commercial diesel B7 fuel. The instrumentation designed to measure the engine performance, available in the Laboratory of Vehicular Engineering (*Laboratório de Engenharia Veicular*, LEV) at PUC-Rio allowed to obtain data to calculate fuel consumption, engine efficiency and combustion characteristics.

A large bibliographic review of the theme is available in the Chapter 2 of the present work. Variables influencing DBE stability were discussed and the different additives tested on literature were listed and classified by main chemical moieties. The impact of biodiesel and ethanol content in some physicochemical properties, combustion and pollutants emission were also assessed.

PUC-Rio - Certificação Digital Nº 1312923/CA

The material and experimental procedure were described in Chapter 3. Characterization of the raw materials and methodology followed in the present thesis were detailed. The methodology of DOE was also described in Chapter 4, just as the reduction of engine test data and the assessment of uncertainty.

Chapter 5 presented the main results and discussed the experimental uncertainties. Adequacy of the blends to current engine and vehicles was discussed and recommendations were given. Chapter 6 gave the main conclusion and suggested future works.

PUC-Rio - Certificação Digital Nº 1312923/CA

2 Literature Review

2.1. Blend Stability Issue

2.1.1. Miscibility of Ethanol in Diesel Fuel

2.1.1.1. Fuel Composition

One of the main targets of using E-diesel blends in the diesel engines is to keep the engine modification minimal. A solution is a single-phase liquid system, homogeneous at the molecular level. It was seen that such blends are technically suitable to run without modifications in existing diesel engines. The major drawback is that E-diesel blends are not accurately described as either miscible or immiscible. Miscibility of ethanol in diesel fuel depends on the hydrocarbon composition and wax content of the base diesel fuel, ethanol content (a low ethanol concentration has reduced immiscibility), and the temperature of the diesel fuel [Ribeiro, 2007].

Figure 5 gives the temperature of phase separation for ethanol blends with different compounds present in commercial diesel blends.

PUC-Rio - Certificação Digital Nº 1312923/CA

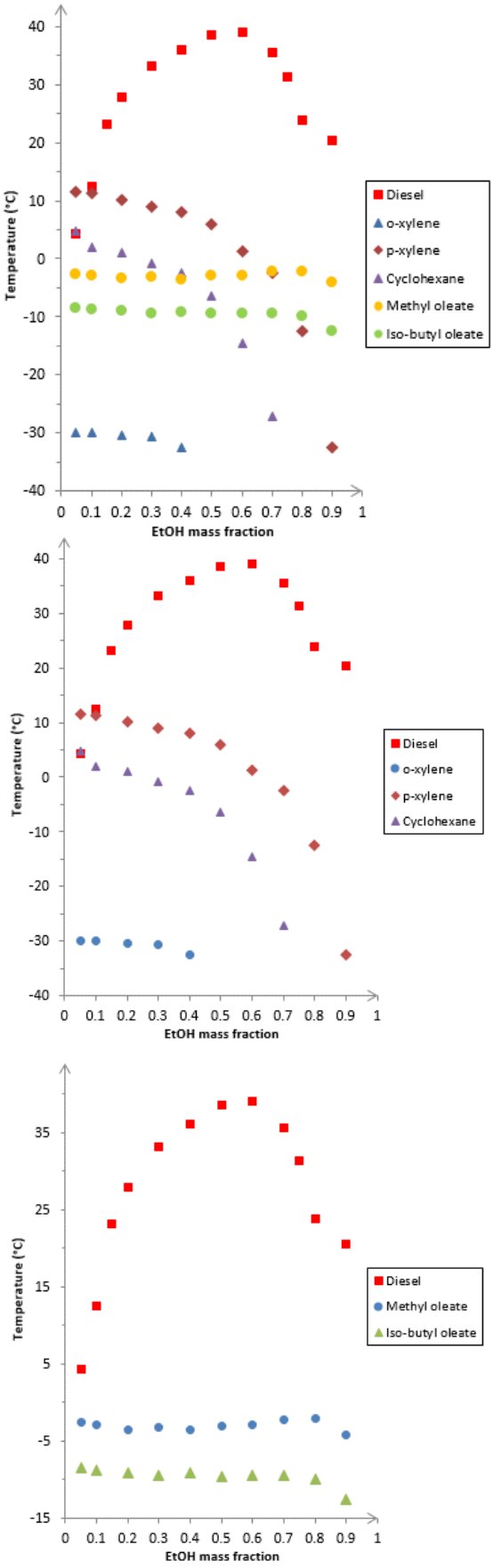

Figure 5: Temperature of phase separation for ethanol blends with paraffinic and olefinic blends (top), aromatic and naphthenic blends (middle) and ester blends (bottom) [Caetano, 2003].

PUC-Rio - Certificação Digital Nº 1312923/CA

Aromatic contents and intermediate distillate temperatures has a significant impact on the miscibility limits [Gerdes, 2001; Can, 2004]. It was verified that, for blends of ethanol with paraffinic and olefinic hydrocarbons, the temperature of phase separation gradually decreases with the increase of the molecular mass and the number of unsaturations of the hydrocarbon. Comparing ethanol blends with olefinic and paraffinic hydrocarbons with the same carbon number, it appears that the presence of unsaturation increases the miscibility of the mixture. Naphthenic and aromatic hydrocarbons show low temperatures of phase transition, as they perform as bridging agents and co-solvents to some degree. The polar nature of ethanol induces a dipole in the aromatic molecule, allowing them to reasonably strongly interact, while the aromatics stay compatible with other hydrocarbons in diesel fuel [Hansen, 2005; He, 2003]. It has been found that the presence of ethanol in any proportion in a mixture with esters in biodiesel does not cause phase separation, under the conditions of use in Brazil. This is because the obtained temperatures of phase transition were negative, as observed in Figure 5 [Caetano, 2003].

One of the main parameters of E-diesel is the stability at low temperatures. Anhydrous ethanol easily blends with diesel fuel to form stable solutions containing up to 5 vol% ethanol at ambient temperature. However, at temperatures below 10°C, ethanol is almost immiscible in diesel fuel, and the blend separates into two phases. This fact affects the fluidity and good filterability of the E-diesel in cold climatic conditions [Ribeiro, 2007]. Moreover, Rahimi *et al.* found that the temperature of phase separation up to 4–5% ethanol in typical diesel fuel is identical to the cloud point of the pure diesel fuel [Rahimi, 2009; Jackson, 2003].

In 2005, Da Silva studied the effect of the carbon chain on alcohol miscibility. His results are given in Figure 6.

PUC-Rio - Certificação Digital Nº 1312923/CA

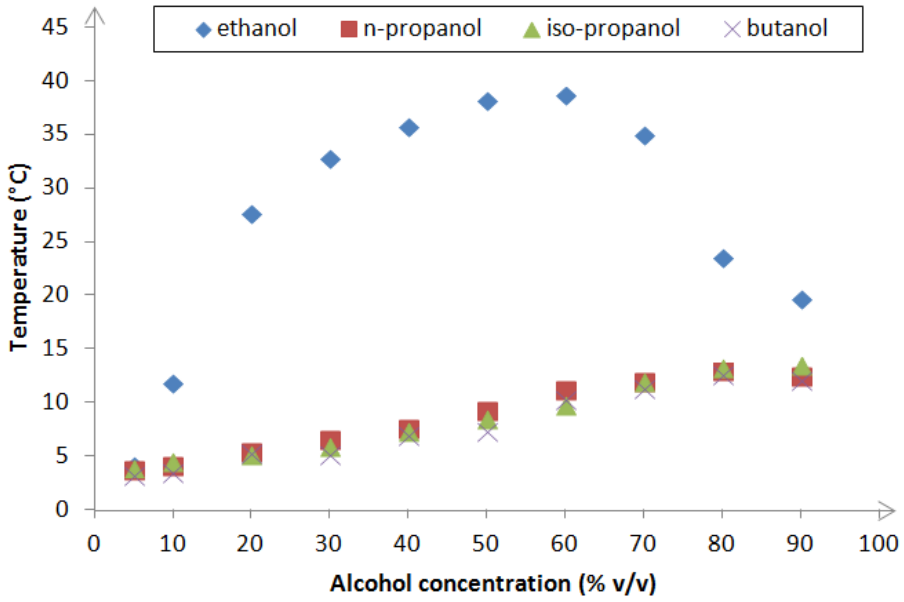

Figure 6: Miscibility of diesel fuel in function of alcohol content [Caetano, 2003; Da Silva, 2005].

He observed that methanol was fully immiscible with diesel fuel, even at very low concentration. Looking at the Figure 6, temperature of phase transition of ethanol slowly increased until a maximum value for 60 vol% of ethanol, when it began to decrease rapidly. Similar results were observed by Caetano (2003) and Cutrim *et al* (2013). For more than 3 carbon atoms, miscibility was almost invariant due to apolar tendency of these alcohols [Da Silva, 2005].

2.1.1.2. Temperature

In 2007, Lapuerta *et al.* (2007) studied the effect of temperature by means of a level curve map for different water and additive contents. Each level curve corresponds to a different maximum separation ratio (SR_{max}), indicating the maximum volume of separated ethanol phase (V_{sep}) with respect to the initial ethanol content in the blend (V_e), as described in equation 1.

$$SR_{max} = \frac{V_{sep}}{V_e} \quad (1)$$

Figure 7 gives the level curves for SR_{max} in the map temperature/ethanol content.

PUC-Rio - Certificação Digital Nº 1312923/CA

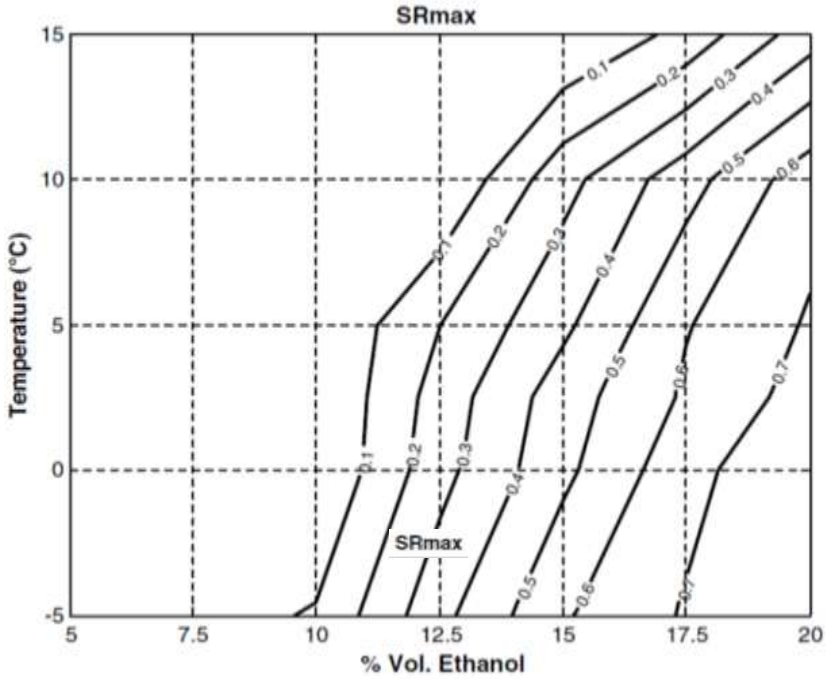

Figure 7: Level curves for SR_{max} in the map temperature/ethanol content [Lapuerta, 2007].

PUC-Rio - Certificação Digital Nº 1312923/CA

Lapuerta *et al.* (2007) showed that, when the initial ethanol content increased and the temperature decreased, the maximum separation ratio of the alcohol phase increased. As a blend was considered unstable when SR_{max} is, at least, 0.1, the region located at the left side of curve 0.1 corresponds to the stability zone of the blends. As temperature increased, the average solubility increased.

2.1.1.3. Water Content

Miscibility also depends on the water content of ethanol. Ethanol is hygroscopic and easily picks water up from ambient air and from the distribution system (mainly during transport and in the gas station). Anhydrous ethanol is highly miscible in diesel fuel at low (0-30 vol%) and high (70-100 vol%) contents. Within these zones, the miscibility and the cloudiness in the mixture followed by phase separation were observed when the water content of the ethanol exceeded 1 vol% [Satgé de Caro, 2001; Fernando, 2004; Weber de Menezes, 2006; Ribeiro, 2007]. As temperature increased, the mean solubility increased. The presence of water reduced the solubility of ethanol in diesel fuel. This effect was more important as temperature increased. However, the opposite effect was

observed when additive was added. Figure 8 illustrates the effect of water and additive on the mean solubility at different temperatures.

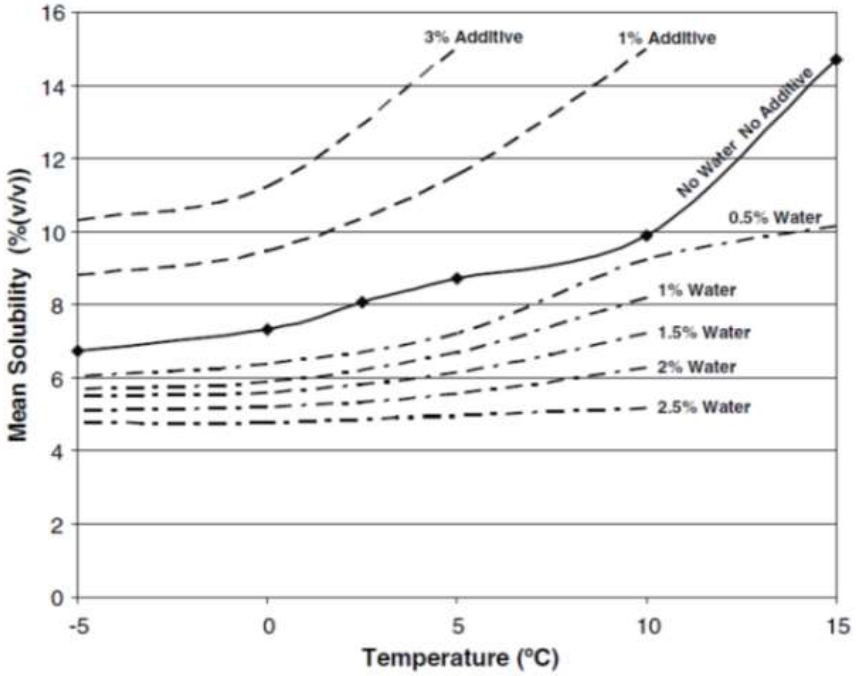

Figure 8: Effect of water and additive on the mean solubility at different temperatures [Lapuerta, 2007].

To stabilize the blend in presence of high water content and to ensure fuel homogeneity under all conditions of the temperature, additives are indispensable in E-diesel. However, these additives increase the fuel's cost. The presence of water (in blends without additive) and additive (without water addition) also affected the miscibility of alcohol in diesel fuel, as shown in Figure 8 [Lapuerta, 2007].

In 2004, Fernando *et al.* developed ternary phase diagrams for diesel-biodiesel-ethanol systems with low-sulphur diesel (LSD, 500 ppm of sulphur) and ultralow-sulphur diesel fuels (ULSD, 15 ppm of sulphur) and observed that the phase stability of blends using ULSD had better low-temperature phase stabilities than those with LSD fuel. They also showed that the type of ethanol had a significant effect on the phase behavior of the ternary system, as illustrated in Figure 9.

PUC-Rio - Certificação Digital Nº 1312923/CA

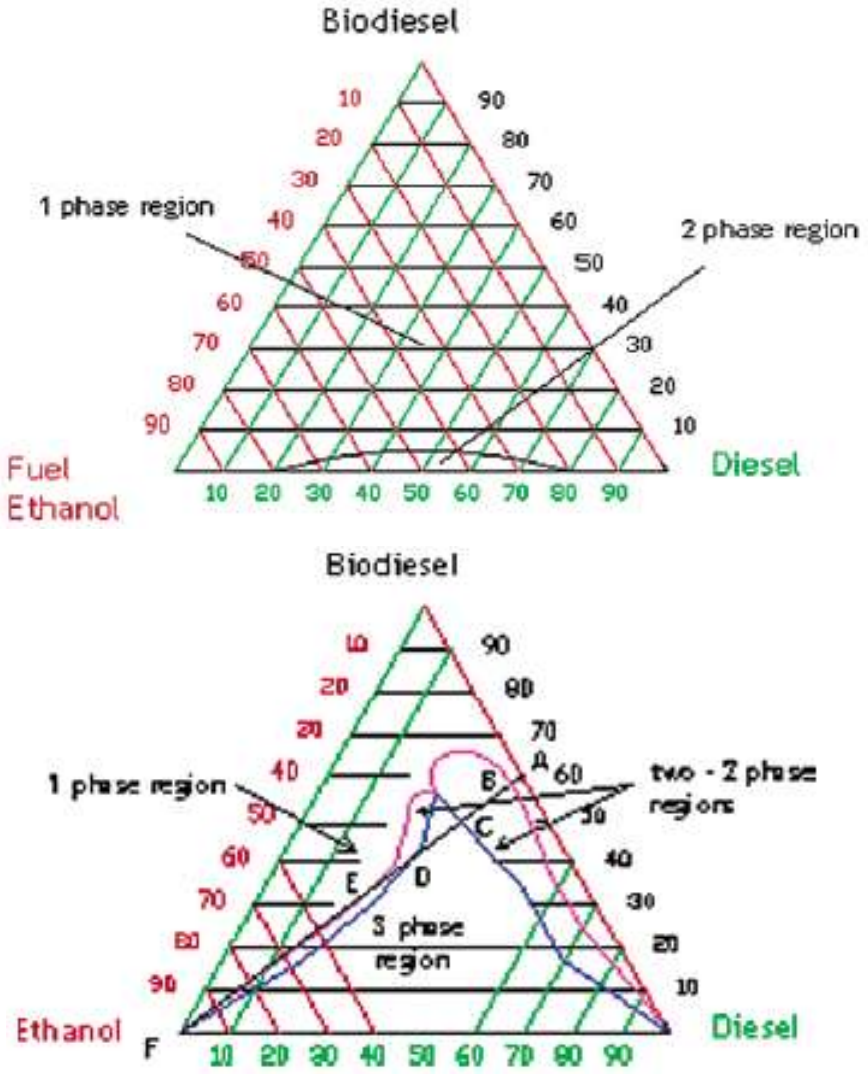

Figure 9: Effect of ethanol on the phase behavior of the ternary system for various quality of ethanol: fuel ethanol (top) and SD-1 denatured ethanol (bottom) [Fernando, 2004].

At 20°C, 200-proof ethanol (anhydrous ethanol) was completely miscible in North American grade No. 2 diesel fuel (middle distillate diesel fuel heavier than grade No. 1 and lighter than grade No. 4), at all concentrations. Fuel ethanol was completely miscible in diesel fuel when the diesel fuel concentration in the E-diesel mix was inferior to 30 vol% or when the diesel fuel concentration was superior to 85 vol%. A SD-1 denatured ethanol showed much more complex phase behavior, forming single-phase, two-phase and three-phase regions [Fernando, 2004; Ribeiro, 2007].

PUC-Rio - Certificação Digital Nº 1312923/CA

2.1.2. Additive-Based Strategies

There are two additive-based approaches to maintain stable blends: adding surfactants (or emulsifiers), that produce stable emulsions, or microemulsions, or adding co-solvents to have stable solutions. [Ribeiro, 2007; Guarieiro, 2009].

A microemulsion consists of droplets or micelles of ethanol dispersed in the diesel fuel phase, but a small amount of emulsifier and water is required for its formation. The addition of an emulsifier acts by lowering the surface tension of two or more substances. Preparing an E-diesel blend with surfactants generally requires a heating and stirring step.

Co-solvents act as a bridging agent through molecular compatibility by modifying the power of solvency for the pure solvent and bonding to produce a homogeneous blend. Co-solvents can be prepared by splash blending, which can be done by just pouring the components together into a tank.

In both cases, the percentage of required additive is dominated by the lower limit of temperature at which the blend is needed to be stable. Accordingly, ethanol-diesel blend requires fewer additives in summer conditions as compared to the winter ones.

It is also important to note that both concepts are commonly used as synonyms in literature. Nevertheless, the present work is focusing on homogeneous blends by the use of co-solvent.

PUC-Rio - Certificação Digital Nº 1312923/CA

2.1.2.1. Biodiesel as Additives for E-Diesel

Among the applicable co-solvents, Fatty Acid Methyl Esters (FAME), also known as biodiesel, are primarily used because of their similarity to the diesel fuel concerning physicochemical characteristic, which allows the use of ester-diesel blends in any proportion. Moreover, biodiesel is miscible with alcohols. Its addition prevents phase separation (biodiesel can act as an amphiphile and form micelles), improves the tolerance to water and the lubricating properties, and its high cetane number improves the low cetane number of diesel–ethanol blended fuels [Hansen, 2001a; Fernando, 2004; Shi, 2005; Shi, 2006; Kwanchareon, 2007; Ribeiro, 2007; Lapuerta 2009; Rahimi, 2009; Shudo, 2009; Chotwichien, 2009; Randazzo, 2011a; Randazzo, 2011b; Shahir, 2014]. Nowadays, it is becoming the preferred co-solvent because it has the advantage of increasing the biofuel

concentration in diesel fuel, which is one of the targets proposed by the European Union to promote the use of biofuels for transport [Guarieiro, 2009; Torres-Jimenez, 2011; Yilmaz, 2014]. The instantaneous phase behavior indicated that the system formulates stable blends over a large region of the ternary phase diagram, depending on the concentrations of the different components. As seen in Figure 9, the phase diagram indicated that the ratio of biodiesel to ethanol in the system should be greater than 1:1 at higher diesel fuel concentrations to formulate stable blends [Zöldy, 2011].

A lot of studies were published since 1980 using DBE blends with anhydrous ethanol (up to 30 vol%) or hydrous ethanol (up to 10 vol%) and using different biodiesel sources. The influence of some parameters related to biodiesel is discussed in the following paragraphs.

Pidol *et al.* (2012) used rapeseed methyl ester (RME) to stabilize the diesel fuel and anhydrous ethanol blend. They determined that, to carry out the better blend stability, the blends needs to be prepared in two steps. First, FAME was blended with the ethanol and, lastly, regular diesel fuel was added to the blend.

Makareviciene *et al.* (2005) studied the solubility of rapeseed oil ethyl ester (REE) and rapeseed oil methyl ester (RME) in E-diesel blends for various moisture contents in ethanol (0.2, 1.5 and 6.0 vol% of water), as illustrated in Figure 10.

PUC-Rio - Certificação Digital Nº 1312923/CA

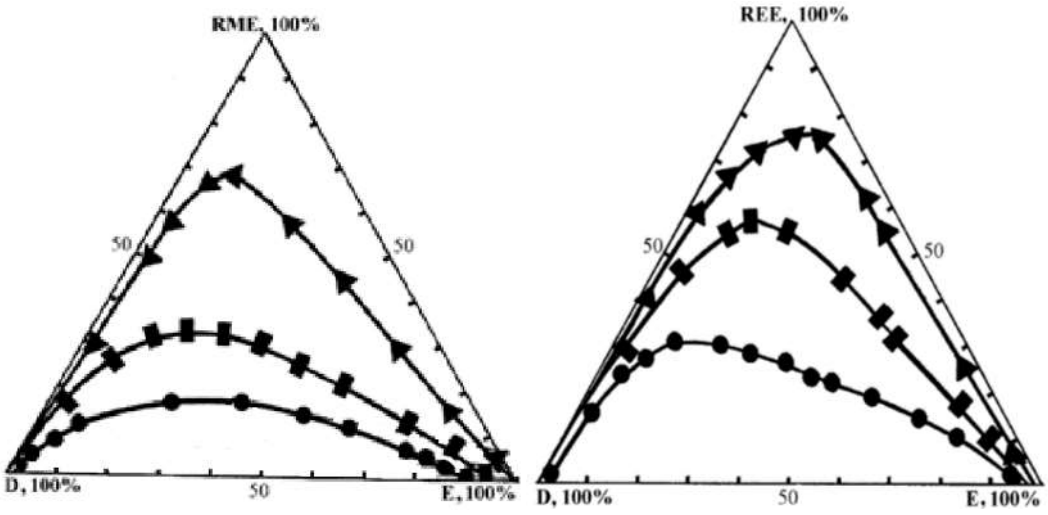

[(●) 99.8 vol%, (■) 98.5 vol%, (△) 94.0 vol%] [(●) 99.8 vol %, (■) 97.9 vol %, (△) 95.6 vol %]

Figure 10: Isotherms of solubility of diesel – ethanol – RME (left) and diesel – ethanol – REE (right) system using different concentration of ethanol [Makareviciene, 2005].

When 94 vol% ethanol was used, ethanol and diesel fuel were immiscible in each other. The miscibility limit of diesel fuel in 98.5 vol% ethanol was 5.4 vol%. In the case of 99.8 vol% ethanol, the miscibility limit of diesel fuel in ethanol and ethanol in diesel fuel increased to 8.7 vol% and 0.9 vol%, respectively. Using absolute ethanol (99.8 vol%), stable ternary mixtures in a relatively wide range of concentrations could be produced. Miscibility in the case of REE was slightly lower, showing that miscibility is function of the length of the carbon chain. The results indicated that methyl ester was better than ethyl ester in improving the miscibility of the E–diesel blend.

They also studied the solubility of diesel-RME-ethanol at different temperatures. The results are given in Figure 11. As expected, miscibility of diesel fuel and ethanol decreased when the temperature decreased: 8.7 vol% of diesel fuel was soluble in ethanol at 20°C, only 2.9 vol% at 0°C. At -10°C, the range of stable blends was less than half the size of the miscibility field at 20°C. For obtaining stable solutions with wider ethanol concentration, the ratio of RME and diesel fuel in mixtures would have to be increased [Makareviciene, 2005].

PUC-Rio - Certificação Digital Nº 1312923/CA

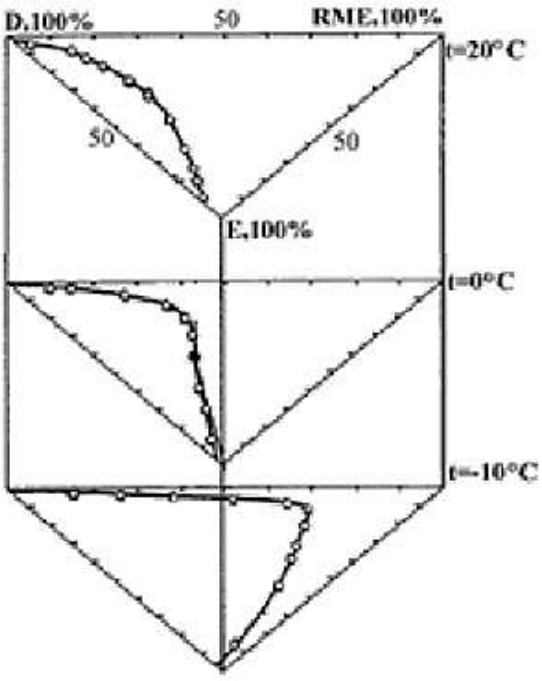

Figure 11: Polytherm of solubility of diesel – ethanol – RME system [Makareviciene, 2005].

Lapuerta *et al.* (2009) studied the stability diagrams of diesel-biodiesel-anhydrous ethanol blends at different temperatures. It was found that biodiesel

acted as a stabilizer component in E-diesel blends, except at low temperatures, where it favored the formation of a gelatinous phase. Their main results are presented in Figure 12.

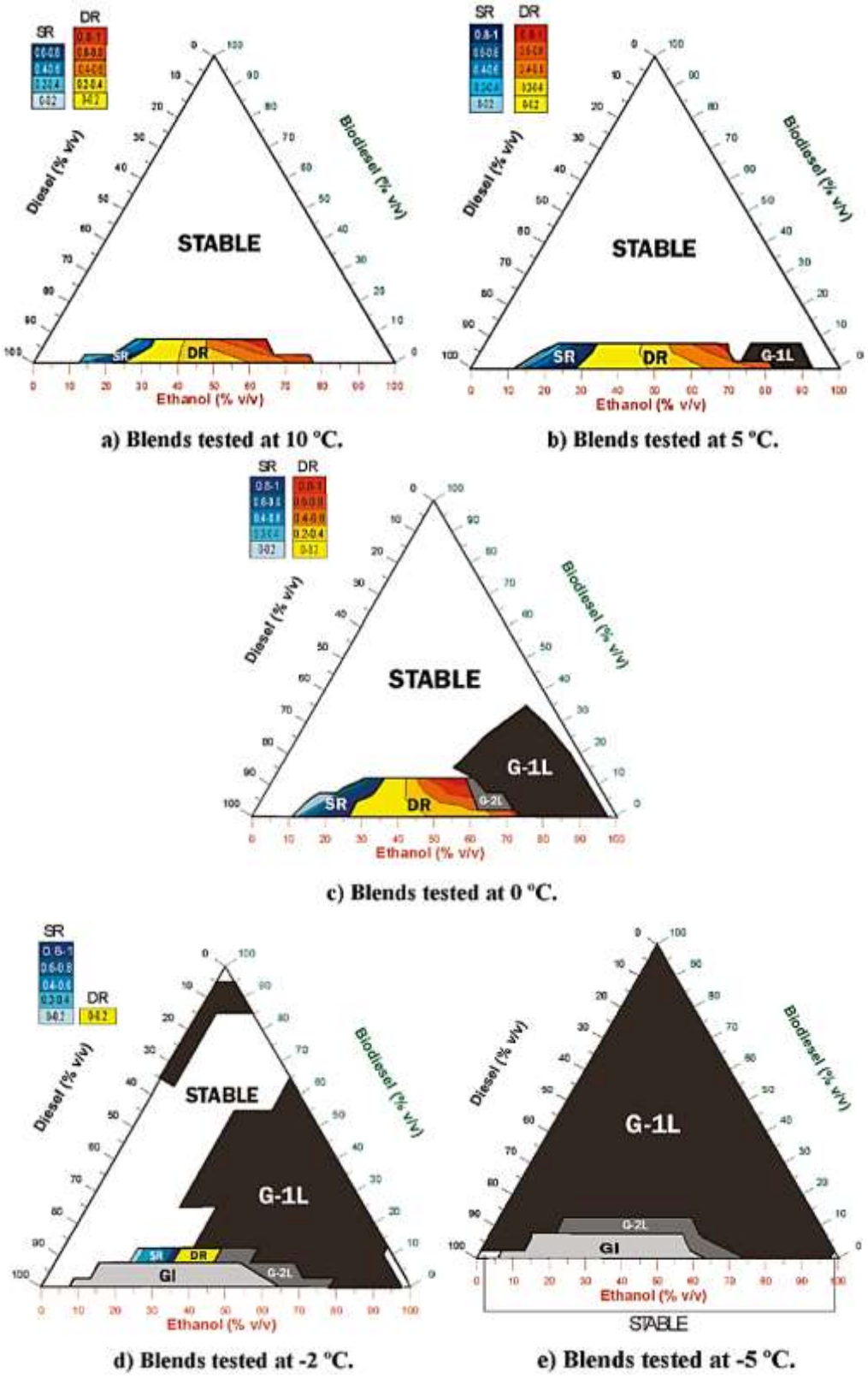

Figure 12: Stability results at different temperatures [Lapuerta, 2009].

PUC-Rio - Certificação Digital Nº 1312923/CA

In Figure 12, two zones can be distinguished in the unstable liquid region corresponding to blends that present a certain separation ratio (SR) and blends defined by their dragging ratio (DR). The dragging ratio, indicating the content of diesel fuel, biodiesel, or both that is present in the separated phase. It is defined as the ratio between the volume of the separated phase (diesel fuel and biodiesel) and that corresponding to the initial diesel-biodiesel blend, as given in equation 2:

$$DR = \frac{V_{sep} - V_e}{V_{blend} - V_e} \quad (2)$$

In the SR zone, it can be observed that, the higher the ethanol content, the higher the separated phase, while biodiesel generates the opposite effect because it acts as a stabilizer. In the DR region, the separated phase is not only composed of ethanol. DR indicates that biodiesel is not the only component that can be dragged by ethanol. Biodiesel improves stability, but in the DR region, the higher the biodiesel content in the blends, the higher the DR values [Lapuerta, 2009].

At 5°C, although this is a temperature far from the cold-filter plugging point values of fuels, a gelatinous phase (G-1L) appears in the bottom of the cell glass when the ethanol content is very high (75%) and the content of biodiesel is less than 10%. Above this gelatinous layer, a homogeneous and clear phase is formed. At 0°C, a new region appears where unstable blends present a gelatinous phase in the bottom of glass cell and two liquid phases appear in the upper part (G-2L). At -2°C, an important increase of the unstable region is observed with respect to that obtained at 0°C. Above -2°C, all diesel-biodiesel and ethanol-biodiesel blends remain stable, but, at this temperature, there are some ethanol-biodiesel blends in which the gelatinous phase appears. Most of the blends situated in the SR or DR zone at positive temperatures show a gelatinous interphase (GI) between two liquid phases. At -5°C, only pure ethanol, pure diesel fuel, and the E-diesel blends up to 5% of alcohol remain stable [Lapuerta, 2009].

Such behavior at low temperature is due to the crystallization of fatty acid methyl esters. Hanna *et al.* (1996) blended methyl tallowate with ethanol and No. 2 diesel fuel in different ratios. Crystallization characteristics of these blends were studied at temperatures ranging from 22 to -16°C. Blending ethanol with methyl tallowate reduced crystal formation at all temperatures. As the temperature of the blends was reduced from 22 to 0°C, there was no effect on crystal formation of

PUC-Rio - Certificação Digital Nº 1312923/CA

saturated vs. unsaturated fatty acids. Below 0°C, the saturated fatty acids crystallized at a much faster rate than the unsaturated fatty acids.

Lin *et al.* (2013) developed a nonlinear optimization model to analyze diesel-biodiesel–ethanol ternary blending processes. The model established optimal blends to improve the system profitability given production costs, market demand, and fuel prices while meeting multiple property criteria such as kinematic viscosity, density, lower heating value, cloud point, cetane number, fuel stability, and sulphur content. Pertinent fuel mixing rules for predicting the fuel properties of DBE blends were extrapolated from previous works and applied as constraints to the present model. They considered various representative biomass, such as corn, switchgrass, and food wastes for ethanol and soybean oil, algae and waste cooking oil for biodiesel. Figure 13 illustrates a ternary diagram of the DBE blend based on blend fuel requirements, the predicted fuel specifications and defined a feasible region.

PUC-Rio - Certificação Digital Nº 1312923/CA

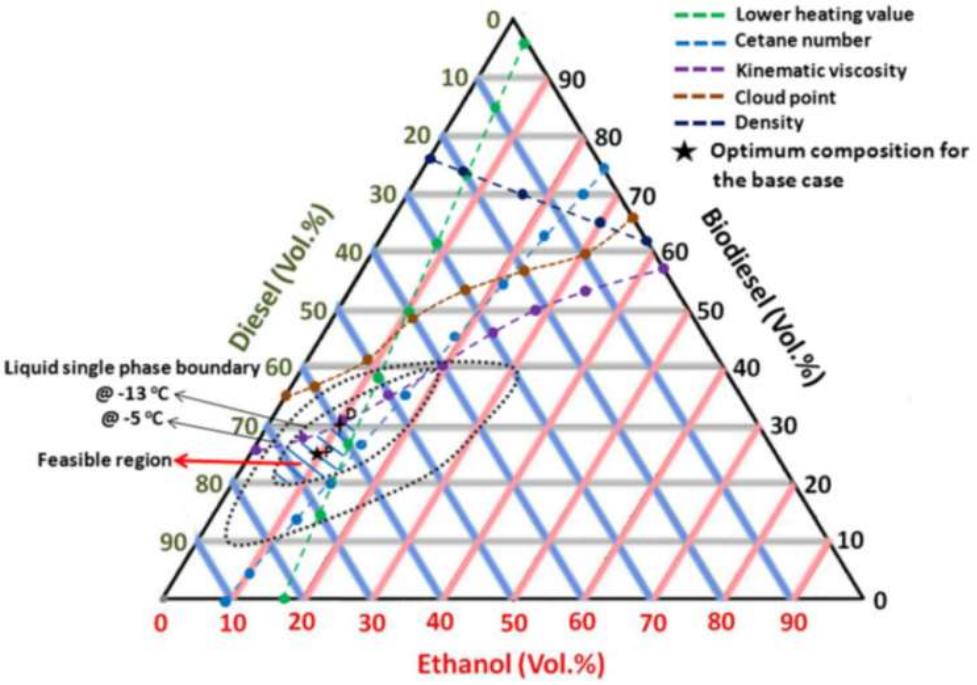

Figure 13: Ternary diagram of regular DBE blends [Lin, 2013].

Graphically, the optimum formulation of regular blends was gradually moving from point P (the base case) towards Point D, which was the optimum composition predicted for year 2040.

2.1.2.2. Other Additives for E-Diesel in the Literature

Besides biodiesel that are complex mixture of esters, numerous works were done since 1980's assessing different kind of additives. They are listed below in function of their chemical families:

(i) **Alcohols:** Isopropanol [Can, 2004; Ribeiro, 2007]; *n*-butanol [Boruff, 1982; Hansen, 2001a; Rangel, 2002; Ribeiro, 2007; Huang, 2009; Lei, 2012]; propanol [Murayama, 1982], pentanol [Murayama, 1982], 2-ethyl-1-hexanol [Odziemkowska, 2016]; octanol [Murayama, 1982; Lei, 2012], dodecanol [Murayama, 1982; Di, 2009; Sayin, 2010; Lei, 2012], tridecanol [Hancsók, 2011]; hexadecanol or cetanol [Murayama, 1982; Lei, 2012]; fatty-alcohol [Hancsók, 2011];

(ii) **Ethers:** Methyl *tert*-butyl ether (MTBE) [Yaginuma, 1999], ethyl *tert*-butyl ether (ETBE) [Yaginuma, 1999; Weber de Menezes, 2006], *tert*-amyl methyl ether (TAME) [Yaginuma, 1999], *tert*-amyl ethyl ether (TAEE) [Weber de Menezes, 2006]; tetrahydropyran (THP) [Yaginuma, 1999]; 1,4-dioxane [Yaginuma, 1999]; tetrahydrofuran (THF) [Yaginuma, 1999; Hansen, 2001a; Hansen, 2005; Kim, 2008; Lei, 2012]; methyltetrahydrofuran [SAGA Fuel Systems, 2002];

(iii) **Polymers:** Styrene-butadiene copolymer in diesel fuel and polyethyleneoxide-polystyrene copolymer in hydrated alcohol [Demirbas, 2008]; polyalkyl-succinimide [Hancsók, 2011]; various silanes, celluloses, polystyrenes, poly(alkyl oxide) and copolymers [Da Silva, 2005].

(iv) **Esters:** Ethyl acetate [Hansen, 2001a; Hansen, 2005; Lei, 2012]; isobutyl oleate [Da Silva, 2005]; octyl oleate [Da Silva, 2005]; trimethylolpropane trioleate [Da Silva, 2005]; poly(ethylene glycol) dioleate [Da Silva, 2005]; ethyl laurate [Cutrim, 2013]; ethyl oleate [Cutrim, 2013]; ethyl estearate [Cutrim, 2013]; ethyl miristate [Cutrim, 2013]; ethyl palmitate [Cutrim, 2013]; laurel acid glyceride, stearic acid glyceride [Lei, 2012].

(v) **Fatty acids and carboxylic acids:** C_{14}-C_{18} fatty acids from biodegradable sources [Ikura, 2002]; caprylic acid [Da Silva, 2005]; oleic acid [Cutrim, 2013]; castor oil [Lei, 2012; Guarieiro, 2009]; tea oil [Lei,

PUC-Rio - Certificação Digital Nº 1312923/CA

2012]; soybean oil [Guarieiro, 2009]; fluorine oil [Lei, 2012]; tung oil [Lei, 2012].

(vi) **Surfactants:** Tridecanol based additive (MX 1625) [Marsi, 2008; Nagy, 2007]; decaglycerol mono-oleate (MO 750) [Xu, 2001; Fernando, 2004; Ribeiro, 2007; Surisetty, 2011]; sorbitan monooleate (Span 80) [Reyes, 2009a; Reyes, 2009b; Lei, 2012]; sorbitan trioleate (Span 85) [Da Silva, 2005]; Tween80 [Lei, 2012]; various families of surfactants (anionic, cationic and non-ionic) [Xu, 2001; Da Silva, 2005].

(vii) **Aromatics compounds:** Benzene [Murayama, 1982]; *n*-butyl-4-hydroxybenzoate [Da Silva, 2005].

(viii) **Nitrogen compounds:** Amines and amides [Da Silva, 2005]; octyl nitrate [Putrasari, 2013]; nitrite glycol [Putrasari, 2013]; triethylene glycol dinitrate (TEGDN) [Putrasari, 2013]; alkanolamides [Fernando, 2004; Ribeiro, 2007; Surisetty, 2011].

(ix) **Other petrochemical compounds:** Gasoline [Murayama, 1982]; iso-octane [Murayama, 1982].

(x) **Elaborated formulations:** N,N-dimethylethanoamine and commercially available grade of soybean fatty acids low in saturates [Boruff, 1982; Hansen, 2001; Ribeiro, 2007]; additive composed of a nitric ester as active agent; a vegetal oil as lubricant, an anti-corrosive agent such as an aromatic or aliphatic amine, a morpholine, an alcohol amine or a benzotriazole; and a stabilizing agent such as ketones, aliphatic alcohols, glycolic ethers and esters of glycolic ethers [Oxiteno, 1985]; additive synthesized from unsaturated fatty acid, a polymer (not specified), xylene, tetrabutylphthalate and lecithin and an ignition improver (isooctyl nitrate) [He, 2003; Ribeiro, 2007]; an additive composed of one or more alcohols having from between about 6 and 12 carbon atoms or one or more ethoxylated alcohols having between about 13 and 18 carbon atoms, where the ethylene oxide add-on is less than 5 moles, a fatty acid of the structure with alkyl, alkenyl or alkynyl chain having from about 10 to 24 carbon atoms, with a source of nitrogen in an anhydrous state or as an hydrous solution of ammonia (compositions of iso-propanol, octanol, 2-ethyl-hexanol, linoleic acid, oleic acid, ammonia, and water are preferred) [SAGA Fuel Systems, 2002].

PUC-Rio - Certificação Digital Nº 1312923/CA

(xi) **New organic compounds:** Organic additives with glycerol skeleton bearing heteroatoms and amino-ether, hydroxyl, nitrate, and nitramine functional groups (1-octylamino-3-octyloxy-2-propanol and dinitrated derivative N-(2-nitrato-3-octyloxy propyl),N-octyl nitramine) [Satgé de Caro, 1997a; Satgé de Caro, 1997b; Satgé de Caro, 2001]; a fatty acid methyl ester containing polyisobutylene-succinic derived used with a co-solvent (fatty-acid-alkyl-esters and different carbon number alcohols) [Hancsók, 2011].

Based on this review, it was decided to focus on a combination of renewable compounds to stabilize the DBE blends. Two specific articles had oriented the further experimental studies and they are described in the following paragraphs.

Guarieiro *et al.* (2009) studied the phase stability of both binary (E-diesel) and ternary (DBE) blends with both anhydrous ethanol (99.5 vol%) and hydrous ethanol (95 vol%). They also found that hydrous ethanol (95 vol%) was insoluble in diesel fuel for the investigated concentration of co-solvents. On the other hand, when they added 10 vol% anhydrous ethanol (99.5 vol%) in the diesel fuel, they found no phase separation, even after 90 days. However, they observed that adding a greater percentage of anhydrous ethanol (15 vol%) to the binary mixture caused phase separation on the first day. So, they studied blends using a higher percentage of anhydrous ethanol, diesel fuel and a co-solvent. Soybean biodiesel (SB), castor oil biodiesel (CB), residual biodiesel (RB), soybean oil (SO) and castor oil (CO) were tested as co-solvents. They found out that some of the blends were stable even after 3 months of observation while most of them were separated into phases. Thus, they selected the following stable blends for further studies:

(i) Diesel fuel / ethanol – 90/10 vol%;

(ii) Diesel fuel / ethanol / SB – 80/15/5 vol%;

(iii) Diesel fuel / ethanol / CB – 80/15/5 vol%;

(iv) Diesel fuel / ethanol / RB – 80/15/5 vol%;

(v) Diesel fuel / ethanol / SO – 90/7/3 vol%;

(vi) Diesel fuel / ethanol / CO – 90/7/3 vol%.

Lei *et al.* (2012) studied the stability of E-diesel blends with single and mixed (bi- and tri-components) emulsifiers. They also assessed the effects of temperature on emulsification properties. Sixteen reagents were chosen as single emulsifier, including castor oil, tea oil, biofuel esterificated from wasted food,

PUC-Rio - Certificação Digital Nº 1312923/CA

fluorine oil, butanol, octanol, acid glyceride, laurel acid glyceride, tung oil, hexadecanol, dodecanol, stearic acid glyceride, tetrahydrofuran, ethyl acetate, Span80, and Tween80.

When the ambient temperature was above 25°C, E–diesel blend with 10 vol% of ethanol could keep its physical stability with all single emulsifiers. For lower temperature, E–diesel blends with a single emulsifier became unstable. Castor oil, tea oil, biofuel esterificated from wasted food, and fluorine oil were able to reduce the temperature of phase separation of ethanol–diesel blends to 15°C. For E15 blends, separation occurred below 20°C.

Then, bicomponent emulsifiers (volume ratio 1:1) were tested and it was observed that the bicomponent emulsifiers have better performance than the single emulsifiers do. The mixed emulsifier formulated with castor oil and biofuel had the best emulsification performance, with the occurrence of phase separation were at 10°C in E10 diesel fuel.

Furthermore, the tricomponent emulsifiers were prepared based on castor oil and biofuel with a third component at a volume ratio 1:1:1. It can be seen that the tricomponent emulsifiers perform better than the bicomponent emulsifiers do. Among them, castor oil, biofuel, and butanol emulsifier were the best additive, since phase separation occurred at 10°C in E10 and E15 diesel fuels.

A new emulsifier, called ‘‘CLZ’’, was developed based on biodiesel, castor oil and other single emulsifiers (not specified in the publication). Figure 14 showed the stability of E–diesel blends with different concentration of CLZ additive.

PUC-Rio - Certificação Digital Nº 1312923/CA

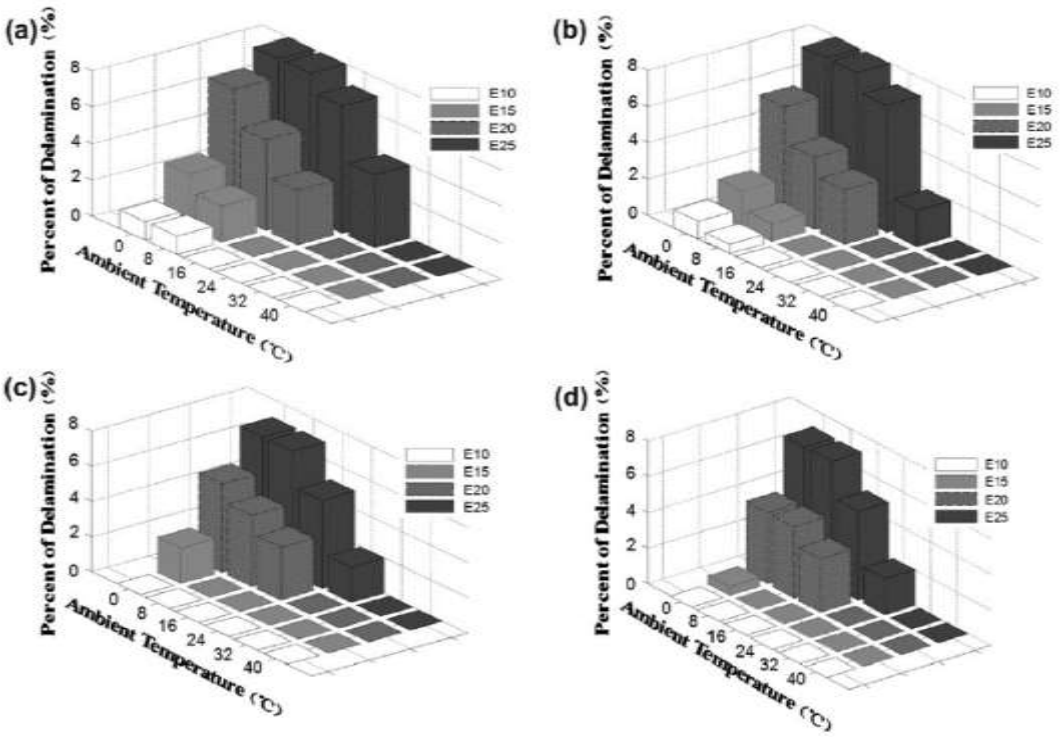

Figure 14: Stability performance of ethanol–diesel blends with emulsifier ''CLZ'' for addition (a) 0.4%, (b) 0.6%, (c) 0.8% and (d) 1.0% of CLZ [Lei, 2012].

E10 blends remained stable for temperature between 0 to 35°C. The additive stabilized E15 blends in a wide range of temperature, and could also emulsify E20 and E25 at temperature in the range of 20-25°C. At 0°C, E10 with 0.8% CLZ was kept clear, transparent and uniform after 60 days of standing.

2.1.3. Commercial Additives for E-Diesel

Besides the additives studied in the literature, commercial additive package were developed. In 2007, Ribeiro *et al.* listed the five predominant blend additive packages, from different suppliers, that allowed the preparation of stable E-diesel blends. Four of them were co-solvent-based produced from renewable resources [McCormick, 2001; Hansen, 2005; Ribeiro, 2007]:

(i) Puranol, created by Pure Energy Corporation (PEC), is a mixture of fatty acid alcohols, a polymeric material, or a combination of both. The blend is flexible and can be engineered for different applications and geographic regions. Additive had to be added at the concentration of 2–5 vol% with 15 vol% of anhydrous ethanol and proportionately less for 10 vol% blends. Higher dosage are required for extreme temperatures and

PUC-Rio - Certificação Digital Nº 1312923/CA

wet conditions. For instance, in the United States, PEC specified 5 vol% of additive for stability at temperatures below -18°C, making it suitable for winter fuel formulation. In summer, the additive requirement drops to 2.35 vol% with spring and autumn concentrations is 3.85 vol% [Pure Energy Corporation, 2000; Ahmed, 2001; Pure Energy Corporation, 2001a; Pure Energy Corporation, 2001b; Pure Energy, 2015].

(ii) OxyDiesel, from AAE Technologies, was tested in a 7.7 and 10.0 vol% ethanol in diesel fuel containing 1% and 1.25 vol%. Tests were performed in Ireland, Brazil, and the United States [Hansen, 2001a; Peeples, 2015].

(iii) Beraid ED-10, provided by Akzo Nobel. This additive was studied by Aydogan *et al.* in blends using 2 vol% of additive and 5 to 15 vol% of ethanol with low sulphur diesel fuel [Aydogan, 2013].

(iv) PuriNox, also known as Proformix, from Lubrizol Corporation. No publication using this additive was encountered during the literature review.

The other additive is provided by GE Betz (formerly Betz-Dearborn, a division of General Electric, Inc.) and it is an emulsifier derived purely from petroleum products [Hansen, 2001a; Ribeiro, 2007]. Rakopoulos *et al.* used 1.5 vol%. of this emulsifier in blends with 5, 10 and 15 vol% of ethanol in conventional diesel fuel [Rakopoulos, 2007; Rakopoulos, 2011].

Reyes *et al.* (2009a; 2009b) listed the fundamental characteristics of several additives that have been patented as co-solvents for anhydrous ethanol-diesel blends:

(i) The SPAN 80 additive is composed by sorbitan monooleate and it is commercialized in Brazil by the Oxiteno Company. This additive improves the solubility of ethanol in diesel fuel and also it has the property of increasing the cetane number and the lubricity of the blend. Depending on the fatty acids used in the ester synthesis, products with different values of HLB (hydrophile – lipophile balance) can be obtained [Oxiteno, 2015].

(ii) The AEP-102 additive, produced by the *Ecológica Mato Grosso Indústria e Comércio Ltda* (Ecomat), is a biodegradable co-solvent for alcohol-diesel blends and it allows its homogenization with a simple

PUC-Rio - Certificação Digital Nº 1312923/CA

agitation system. The additive is an inflammable biodegradable soybean methyl ester. Typical blend formulation, involves the following: 89.4 vol% diesel fuel, 8 vol% anhydrous ethanol, 2.6 vol% AEP-102. In this blend, the additive guarantees the stability until absorbed water contents of 1,200 ppm, even to temperatures between 0 and 5°C [Ecomat, 1999].

(iii) Octimise D 7001 is commercialized in Brazil by the Química Fina Company, representative of the North-American Company Octel. The additive works as a co-solvent in a blend with 10 vol% anhydrous ethanol and 0.5 vol% additive. According to the company, this additive, as well as guaranteeing the stability of the blend, contains compounds that improve the ignition quality and the lubricity [Química Fina, 2005].

2.2. Blend Properties Issues

Two reviews dealing with the properties of E-diesel [Torres-Jimenez, 2011] and DBE blends [Shahir, 2014] were published. The main results are given in this section. Moreover, the properties discussed in this section and the stability behavior of different blends described in literature were summarized in the Appendix A.

2.2.1. Viscosity

Viscosity is an important fuel property as it affects the fuel drop size, the jet penetration, the quality of atomization, the spray characteristics, and the combustion quality. On the one hand, fuel with low viscosity typically results in smaller droplet diameters, significantly influencing the evaporation characteristic time, and, in extreme case, could cause the fuel system leakage. On the other hand, high viscosity of the fuel can cause poor fuel atomization, incomplete combustion and increase the engine deposits. More viscous fuels also require more energy to pump the fuel. Moreover, problems are also met in cold weather because the viscosity increases as the temperature decreases. Thus, viscosity should be low enough to flow freely at its lowest functioning temperature [Heywood, 1988; Shahir, 2014].

When ethanol is blended in E-diesel blends, kinematic viscosity decreased because ethanol has a kinematic viscosity of approximately 1.10 mm^2/s at 40°C.

PUC-Rio - Certificação Digital Nº 1312923/CA

Wrage and Goering (apud [Hansen, 2005] and [Shahir, 2014]) built the graph shown in Figure 15 which studied the deviation of kinematic viscosity in function of the ethanol content the blend.

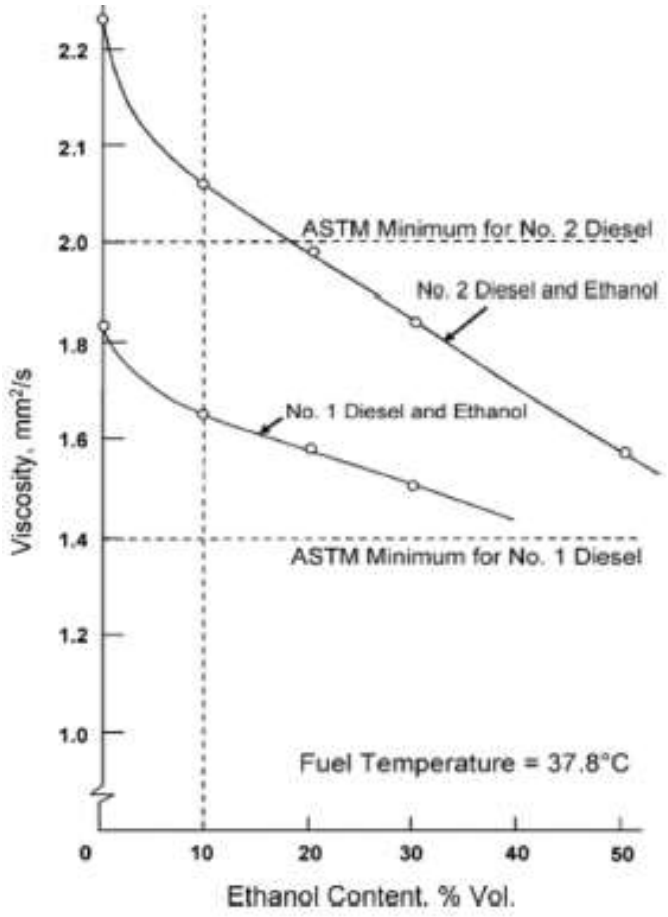

Figure 15: Effect of ethanol content on fuel viscosity [Shahir, 2014].

For ethanol content higher than 20 vol%, the viscosity of the blend is lower than the value required by the ASTM D975 as the minimum.

Figure 16 shows the kinematic viscosity of ethanol-diesel (20:80) blends in function of biodiesel concentration.

PUC-Rio - Certificação Digital Nº 1312923/CA

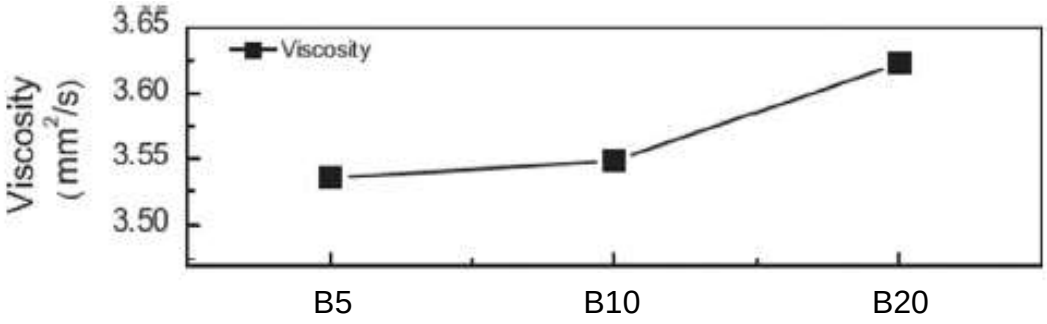

Figure 16: Variation of kinematic viscosity in E-diesel blends (20 vol% of ethanol) in function of biodiesel content at 15°C [Park, 2012].

It can be seen in this figure that, when biodiesel is added to this blend, the kinematic viscosity increases and it can compensate the low values of the parameter in E-diesel blends. Furthermore, viscosity mostly rises with the increase of the chain length [Knothe, 2005b; Knothe, 2005c].

Moreover, Barabás *et al.* (2010) prepared several blends with different concentrations of diesel, biodiesel and ethanol. As the temperature increases, the differences with reference diesel fuel decreases due to the low temperature of vaporization of ethanol (approximately 78°C), allowing the vaporization at the operating injector temperatures.

Zöldy (2011) measured the dynamic viscosity of DBE blends and established an empirical formula (equation 3) in the range of 30–60°C for the viscosity:

$$\mu_{DBE} = 0.91(2n_d\mu_d + 3n_{bd}\mu_{bd} + 2n_e\mu_e + 0.71) \quad (3)$$

where μ_{DBE} is the dynamic viscosity of the blend; n_i is the volumetric ratio of components (e – ethanol, bd – biodiesel, d – diesel fuel); μ_i is the viscosity of components (e – ethanol, bd – biodiesel, d – diesel fuel).

2.2.2. Lubricity

Lubricity is the ability of the fuel to lubricate metal surfaces forming boundary films that prevent metal-to-metal contact that leads to wear under light to moderate loads. From a macroscopic point of view, the frictional behavior of a lubricated contact is quantified by the friction coefficient μ, which is the ratio between the tangential (rolling and/or sliding) force and the applied normal load. In general, friction coefficient strongly depends on the relative speed between

PUC-Rio - Certificação Digital Nº 1312923/CA

surfaces (V), the lubricant dynamic viscosity (μ) and the applied normal load (F_N). The three parameters are traditionally grouped to form the Gumbel number, Gu, as given in equation 4:

$$Gu = \frac{V\mu}{F_N} \tag{4}$$

Three different forms of lubrication can be identified for lubricated contacts, constituting the so-called Stribeck curve, as given in Figure 17.

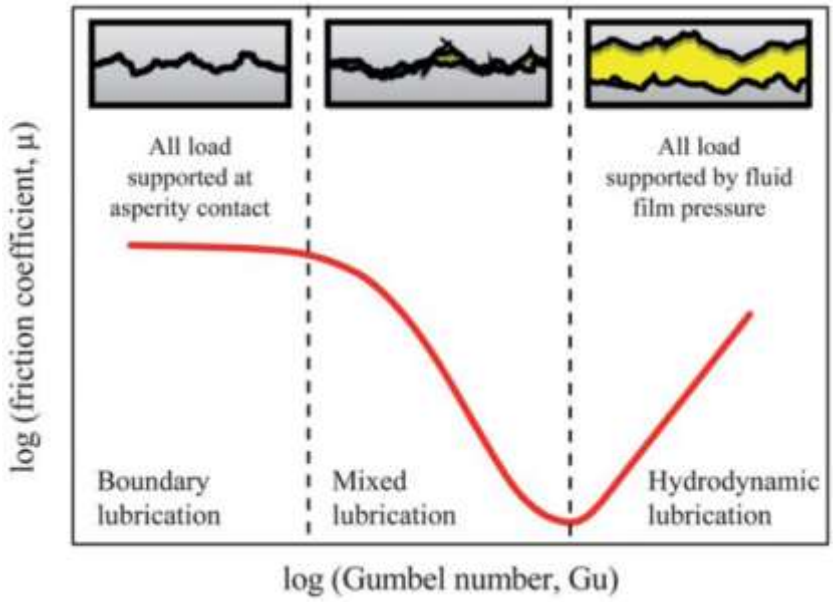

Figure 17: Typical Stribeck curve showing the variation in frictional drag (expressed as the friction coefficient) with the Gumbel number for a lubricated contact [Andablo-Reyes, 2011].

Hydrodynamic or full film lubrication is the condition when the load carrying surfaces are separated by a relatively thick film of lubricant due to viscous force, which support the applied load. This is a stable regime of lubrication and metal-to-metal contact does not occur during the steady state operation of the bearing, associated to high value of Gumbel number. Partial or mixed lubrication regime deals with the condition when the speed is low, the load is high or the temperature is sufficiently large to significantly reduce lubricant viscosity, the highest asperities of the bounding surfaces will protrude through the film and they will, occasionally, come in contact. Boundary lubrication is the condition when the fluid films are negligible and there is considerable asperity contact. The physical and chemical properties of thin surface films are of significant importance while the properties of the fluid lubricant are insignificant.

PUC-Rio - Certificação Digital Nº 1312923/CA

Consequently, the Gumbel number is low in such lubrication mode [Rahnejat, 2010; Andablo-Reyes, 2011].

Fuel pump lubrication and injectors are also affected by the fuel lubricity, especially those incorporated with rotary distributor injection pumps. They rely completely on the fuel for lubrication within the high pressure pumping mechanism. In the case of the common rail accumulator fuel-injection system, the fuel delivered to the rail by the high pressure pump also depends on the fuel for lubrication. There is less dependence on the fuel for lubrication in the case of in-line pumps and unit injectors, but there are still few metal interfaces like the interface between the piston and cylinder require lubrication by the fuel. Injector lubrication, particularly at the needle guide-nozzle body interface, is also affected. To ensure the durability of the fuel injection system and the reliability of starting the engine when it is hot, minimum viscosity and lubricity of the blends are mandatory [Hansen, 2001a; Shahir, 2014].

The lubricity of the biodiesel is higher than the diesel fuel. But, the lubricity of the DBE blends decreases if the ethanol content increases. Zöldy's researches showed that low biofuel content (up to 10% of each biofuel) blends fulfil the European diesel fuel's lubricity requirements [Zöldy, 2007].

Lapuerta *et al.* (2010b) tested different DBE blends, based on the addition of different anhydrous ethanol contents into both commercial pure diesel fuel and a diesel B30 blend at 25 and 60°C. He observed that the addition of ethanol into both kinds of blends decreases lubricity (increases the wear scar) in almost all cases, as a consequence of the lower lubricity of ethanol. However, the increase in the size of the wear scar is not linear, as the concentration of ethanol increased. This is probably a consequence of the combined effect of the following properties of the blends: tribological properties, volatility, blending stability, and of the different sensitivity of these properties to the fuel temperature. In comparison with E-diesel blends, DBE blends led to smaller wear scars and to flatter lubricity curves (less sensitive to the ethanol concentration). The results proved that blending ethanol in diesel-biodiesel blends, within the previously studied range of stability, could guarantee the engine preservation to friction wear. At 60°C, a certain synergistic effect was observed, since the lubricity of some of the tested blends with intermedium ethanol content became even better than those of their separate components. Additionally, at this range of ethanol concentration, the

PUC-Rio - Certificação Digital Nº 1312923/CA

effect of temperature was the opposite to the usual, which means it improved lubricities under hot conditions. Both effects can be explained because the ethanol evaporation losses compensate the poorer tribological properties of ethanol. Joaquim studied the lubricity behavior of E-diesel blends and he proposed modifications in test apparatus (closed vessel) and test procedure (recirculation of fuel) to avoid the vaporization of ethanol and to have reliable results [Joaquim, 2007].

A friction modifier can also be added to the blend to prevent such problems. They comprise a range of surface-active chemicals [McCormick, 2001; Ribeiro, 2007; Pidol, 2012]. Biodiesel and vegetal oil can also be used for this purpose.

Literature showed that fatty acid esters derived from vegetable oils have increased diesel fuel lubricity at concentrations of less than 1%. The lubricity improvement observed from vegetable-oil-based methyl ester additives is greater than that observed when the methyl ester of only one fatty acid is added at the same concentrations [Anastopoulos, 2001; Dmytryshyn, 2004; Anastopoulos, 2005; Goodrum, 2005]. It has been also observed that the fatty acid composition of FAME mixtures may have an impact on their effectiveness as lubricity enhancers. Factors such as saturation, chain length, and hydroxylation could influence the performance of these additives as lubricity enhancers [Geller, 2004]. The hydroxyl group is significant because it facilitates plasticization and adhesion of the oil esters by formation of hydrogen-bonded complexes that enhance the lubricity of mixtures containing these components. When the unsaturation of these FAMEs increases, lubricity enhancement also increases. Oils, which contain a high concentration of hydroxylated fatty acids, such as castor oil, produce a FAME mixture with much more effective lubricity than oils that do not contain any hydroxylated fatty acids.

Two studies [Hu, 2005; Knothe, 2005a] showed that the addition of biodiesel improves the lubricity of low-sulphur diesel fuel (LSD) more than pure fatty esters. The addition of polar compounds, such as free fatty acids or monoacylglycerols, improves the lubricity of low-level blends of esters in diesel fuel. Methyl esters and monoacylglycerols determine the lubricity of biodiesel. Free fatty acids and diacylglycerols can also affect the lubricity of biodiesel, but not as much as monoacylglycerols. Triacylglycerols almost have no effect on the lubricity. Pure free fatty acids, monoacylglycerols, and glycerol possess better

PUC-Rio - Certificação Digital Nº 1312923/CA

lubricity than pure esters because of their free OH groups, confirming former studies. Additionally, a classification of oxygenated moieties enhancing lubricity was obtained: COOH > CHO > OH > $COOCH_3$> C-O > C-O-C.

2.2.3. Cetane Number

Cetane number (CN) of a CI engine fuel is a measurement of the ability of the fuel to auto ignite when injected into the engine. The cetane number is a scale based on two compounds, hexadecane, with a CN of 100, and heptamethylnonane, with a CN of 15. An increase in CN decreases the delay between injection and ignition. Based on the cetane number of the constituents and the mass composition of the blend, the cetane index of the blend can be assessed [Bamgboye, 2008; Barabás, 2011].

The requirements of a minimum CN depend on the engine design, size, speed and load variations (starting, brake or acceleration), as well as atmospheric conditions. Low values could cause rough operation of the engine (difficult starting, especially in the cold weather or at high altitudes) [Randazzo, 2011a]. Low CN fuels can accelerate the formation of lube oil sludge and they also can be the cause of larger engine deposits, which results in extra smoke, higher exhaust emissions and greater engine wear. Depending on the engine, the cetane number can have a reduced influence. To increase the efficiency of the fuel-engine system, the CN should be in a certain range, because high values do not increase the performance. Indeed, lower is the CN, higher is the ignition delay, allowing more time for the fuel to vaporize before combustion starts. Initial burn rates are higher and the conversion process of heat to work is more efficient [Shahir, 2014].

The CN of diesel fuels generally varies from 45 to 50. Ethanol has a low CN and the CN of the blend decreases proportionately to the ethanol content [Hansen, 2001a; Barabás, 2010]. Hardenberg and Ehnert (1981a) projected the cetane number of ethanol in between 5 and 15 (the value is too low to be determined experimentally). More recently, Rahimi *et al.* (2009) and Kwanchareon *et al.* (2007) found that the CN of ethanol was in the range of 5 to 8. The CN of biodiesel ranges from 48 to 67 depending on several parameters such as oil processing technology, climate conditions where the feedstock was collected and, mainly, the fatty acid composition of the base oil. CN is especially affected by the

PUC-Rio - Certificação Digital Nº 1312923/CA

structural features of the various fatty esters. The increase of unsaturations reduces the CN, meanwhile the increase in chain length increases the CN [Demirbas, 2009].

Olivares (2012) and Rocha (2014) studied the cetane number of Brazilian DBE blends and ternary mixtures created by mixing biodiesel, anhydrous ethanol and diesel fuel, respectively, using an ASTM-CFR cetane research engine. Their results, given in Figure 18, confirmed the general trend described before.

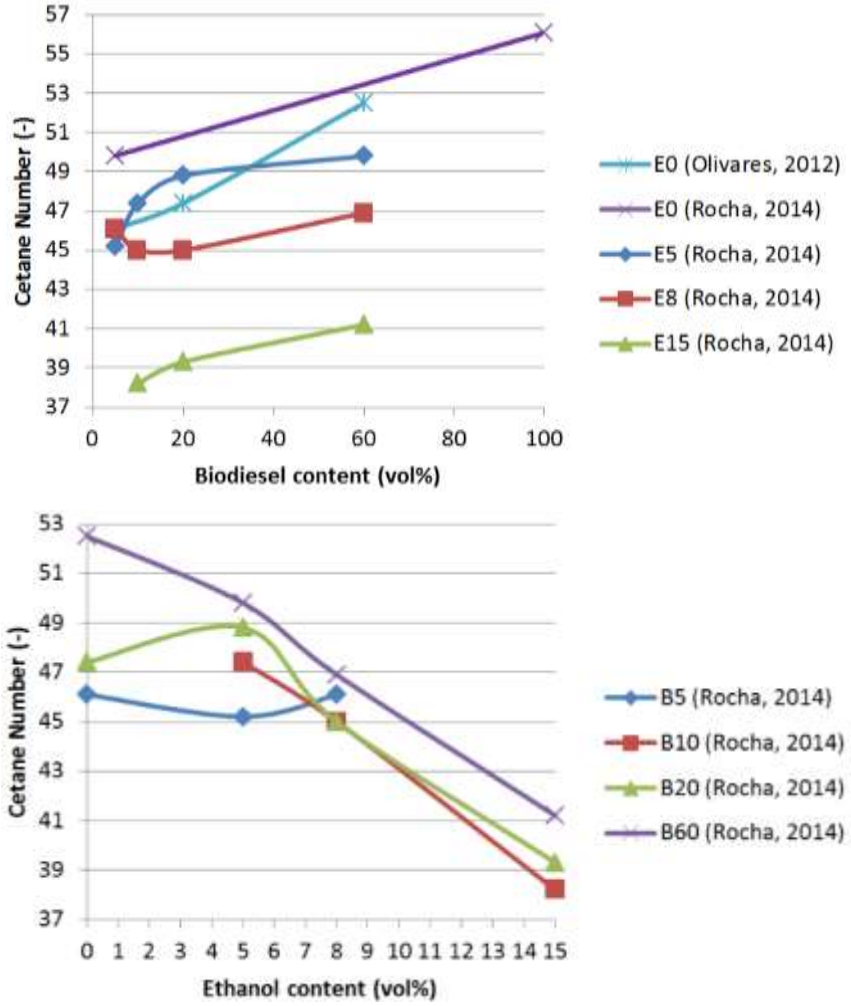

Figure 18: Variation of cetane number in ethanol-diesel blends in function of biodiesel content (top) and ethanol content (bottom).

Zöldy (2011) studied the CN of different ternary blends and developed a linear model (equation 5), which can be applied to assess the impact of adding ethanol and biodiesel to diesel fuel:

$$CN_{bl} = CN_d - 0.59n_e + 0.55n_{bd} \quad (5)$$

PUC-Rio - Certificação Digital Nº 1312923/CA

where CN_{bl} is the calculated cetane number of the blend; CN_d is the cetane number of diesel fuel; n_e and n_{bd} are the volumetric ratio of ethanol and biodiesel in the blend, respectively. The equation suggested that these two components should be blended approximately at a 1:1 ratio with the diesel fuel to hold the cetane number of the blend at its original value.

Additives can play an important role, in this case, providing adjustment of the CN value that could not be fitted only by the composition of the DBE blends. Because cetane-enhancing additives are expensive, the lowest cost approach is to use only enough cetane additives to bring the CN up to the level of the blending diesel fuel [Hansen, 2001a; McCormick, 2001; Ribeiro, 2007].

One alternative is to use fatty acids, as illustrated in literature. A combination of oleic acid and stearic acid were tested [Duffield, 1998]. Such fuel could be used in warmer rather than cooler climates because of the decreased cold properties associated with increased saturated fatty acid content. Later, to combine CN with enhanced lubricity, Kinney and Clemente suggested the mixture of oleic acid and ricinoleic acid in soybean oil [Kinney, 2005; Ribeiro, 2007].

Hardenberg and Schaefer (1981b) found triethylene glycol dinitrate (TEGDN) as the most suitable ignition improver in tests performed in Brazil, particularly because it could be produced from ethanol. Meiring *et al.* (apud [Shahir, 2014]) found the ignition delay of a 30 vol% diesel–ethanol blend as same as the diesel fuel by adding 4.5 vol% octyl nitrate ignition improver. According to Corporan *et al.* (2004), the most widely used cetane-improving additive is 2-ethylhexyl nitrate (2-EHN). The additive is thermally unstable and decomposes at high temperatures to release radicals that accelerate oxidation, and thus, promote combustion. They also evaluated isobutyl nitrate to assess effects of nitrates with different alkyl groups.

Oleochemical carbonates (esters of carbonic acid) have recently found increasing interest in commercial applications due to their relatively direct synthesis in addition to their properties. Kenar *et al.* studied the physical and fuel properties including the CN of eight oleochemical carbonates. These compounds showed CNs ranging from 47 to 107, depending on carbon chain length and branching. The carbonates did not significantly affect cold or lubricity properties at concentrations up to 10 000 ppm [Kenar, 2005].

PUC-Rio - Certificação Digital Nº 1312923/CA

Serdari *et al.* (2005) studied various amines as potential diesel additives, with the aim of stating the impact of the structure of these compounds on diesel fuel and biodiesel quality. It was found that methylation seemed to increase the CN to a larger extent than ethylation. It was concluded that the mono-dianol polyamides investigated enhanced the CN and they also have good cold-flow performance. The tertiary methylated fatty amines have the additional advantage of being produced from renewable raw materials. Tetrakis (dimethylamino) ethylene showed the best performance, but its oxidation stability must be evaluated in more detail because of its olefinic nature.

Dimethyl ether (DME) has also been considered as an additive to biodiesel and diesel-biodiesel blends due to its high CN. However, its addition significantly reduces the viscosity of the mixture, what is the limiting factor [Bhide, 2003; Ribeiro, 2007].

2.2.4. Specific Gravity

Specific gravity directly affects the engine performance characteristics, especially fuel atomization efficiency and combustion characteristics. Other properties like cetane number and heating value are also influenced by the specific gravity [Alpetkin, 2009; Shahir, 2014]. As the injection system used for diesel fuel measures the volumetric flow of the injected fuel, the variation of the specific gravity affects the output power of the engine due to an alteration of the mass. Generally, higher specific gravity causes greater fuel flow resistance, which results in higher viscosity, which may lead to inferior fuel injection.

Specific gravity of ethanol is inferior to diesel fuel specific gravity. Meanwhile, the specific gravity of biodiesel is higher than for diesel fuel. Consequently, the specific gravity of the blends decreases proportionally to the increase of ethanol content in the blends and it increases when the percentage of biodiesel increases.

Kwanchareon *et al.* (2007) prepared DBE blends and they found that the specific gravity values at 20°C of all blends were within the limits for the standard diesel engines. The same trend were described in earlier works [Guarieiro, 2009; Park, 2009; Lapuerta, 2010a; Park, 2012; Park, 2013]. Moreover, Barabás *et al.* (2010) tested the impact of temperature (0–80°C) on specific gravity of several

PUC-Rio - Certificação Digital Nº 1312923/CA

DBE blends and they found that the specific gravity of these ternary blends were very close to the diesel fuel specific gravity on the entire considered temperature domain.

2.2.5. Heating value

Heat of combustion (also known as calorific value) of a fuel is another important property to determine its suitability as an alternative to diesel fuel. It gives the total energy released as heat when a substance undergoes complete combustion with oxygen, under standard conditions. Lower heating value (or net calorific value) of a fuel influences the power output of an engine.

The calorific value of both biodiesel and ethanol is lower than the diesel fuel. Thus, their addition to the diesel fuel decreases the calorific value of the blend and it implies an increase of specific fuel consumption to have the same power output [Ajav, 2002; Fernando, 2004; Chotwichien, 2009; Park, 2012; Pidol, 2012]. However, the blends containing lower than 10 vol% of ethanol seemed to have a heating value nearer to fossil diesel fuel [Kwanchareon, 2007].

2.2.6. Wetting Properties: Surface Tension and Contact Angle

Surface tension influences the droplet formation, since the shape of a liquid droplet depends in this parameters, and combustion of fuel. A high surface tension make more difficult to form droplets of fuel [Ejim, 2007; Shu, 2008; Barabás, 2009].

Park *et al.* (2013) reported that surface tension of the compounds increased in the following order (values were given at 15°C): ethanol (21.7 mN/m), diesel fuel (26.9 mN/m) and biodiesel (31.1 mN/m). Barabás and Todorut (2009) studied ternary blends containing 5–25 % biodiesel and 5–10 % ethanol. Their results are gathered in Table 4.

PUC-Rio - Certificação Digital Nº 1312923/CA

Table 4: Surface tension for the investigated DBE blends at 20°C [Barabás, 2009].

Surface tension (mN/m)		Biodiesel content (vol%)						
		0	5	10	15	20	25	100
Ethanol content (vol%)	0	29.0	-	-	-	-	-	38.6
	5	-	30.7	34.6	34.9	32.8	34.9	-
	10	-	28.5	29.3	30.6	31.7	-	-
	100	19.2	-	-	-	-	-	-

The surface tension of the blends linearly increases with biodiesel content and it decreases when the ethanol concentration is higher.

The contact angle is defined as the angle formed by the intersection of the liquid-solid interface and the liquid-vapor interface (geometrically acquired by applying a tangent line from the contact point along the liquid-vapor interface in the droplet profile). The contact angle is expected to be characteristic for a given solid-liquid system in a specific environment. A contact angle less than 90° indicates that wetting of the surface is favorable, and the fluid will form a film over on the surface (complete wetting occurs when the contact angle is 0°); while contact angles greater than 90° means that wetting of the surface is unfavorable so the fluid minimize its contact with the surface and form a compact liquid droplet. [Yuan and Lee, 2013]. This parameter is important to avoid dewetting issues and lubrication issue. Nevertheless, in the literature review, it was not found any study on the contact angle of DBE blends.

PUC-Rio - Certificação Digital Nº 1312923/CA

2.2.7. Fuel Oxygen Content

The use of oxygenated fuel improves fuel combustion and reduces the engine emission level, as more oxygen is available to oxidize the fuel. Several oxygenated compounds were used for this purpose, but the most common ones are biodiesel, alcohols and ethers. Figure 19 shows the effect of fuel oxygen content on HC and CO emissions.

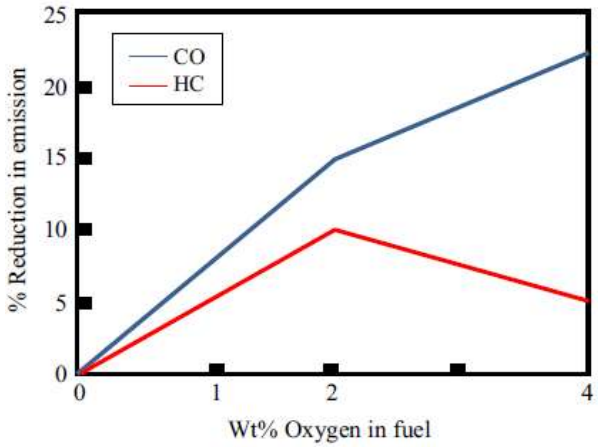

Figure 19: Effect of fuel oxygen content on HC and CO emissions [Rahimi, 2009].

It can be observed that 2 wt% of oxygen is more suitable because of the peak HC reduction observed by Rahimi *et al.* (2009). They also determined the oxygen content of the studied prepared blends. They found the oxygen content of bioethanol, diesel fuel and biodiesel as 34 wt%, 0.0 wt% and 11.01 wt% respectively. The oxygen content of DBE blends were calculated from the following relation (equation 6):

$$M_{bl} = 0.34\rho_e V_e + 0.11\rho_{bd} V_{bd} \quad (6)$$

where M_{bl} is the mass of oxygen in the blends (g); ρ_e is the specific gravity of bioethanol (g/cm^3); ρ_{bd} is the specific gravity of biodiesel (g/cm^3); V_e is the volume of bioethanol in the blends (cm^3); and V_{bd} is the volume of biodiesel in the blends (cm^3) [Rahimi, 2009].

2.2.8. Flammability Limits, Flash Point and Auto-ignition Temperature

Flammability limits and flash point of a fuel describe the ability of a substance to ignite. At a specified temperature and pressure, flammability limits can be described as the upper and lower concentrations of a combustible vapour in the air that can be ignited. The flash point is the temperature of the lowest value, corrected to a barometric pressure of 101.3 kPa, at which the vapor overhead the sample supports a momentary flame across its surface after the application of an ignition source under specified test conditions. It gives an estimation of the temperature at which the vapor pressure reaches the lower flammable limit. Auto-ignition temperature is the lowest temperature at which the fuel spontaneously

PUC-Rio - Certificação Digital Nº 1312923/CA

ignites in normal atmosphere without an external source of ignition. This temperature is required to supply the activation energy needed for combustion and is higher than the flash point. These properties do not directly affect the combustion [NFPA, 2014; Shahir, 2014].

In the fuel tank headspace, increase of temperature produces fuel vapors, which richness vary from a too-lean-to-burn to too-rich-to-burn mixture [Boruff, 1982]. The ignition rarely happens since it requires the presence of a source of ignition, such as static discharge, external sparks or smoking material. Another source of ignition is the electric fuel pumps used in the fuel tank. It has been found that the usual amount of energy in a spark initiated by a brake in the inductive circuit is sufficiently strong to ignite a flammable mixture [Shahir, 2014].

Battelle (apud [Hansen, 2005] and [Shahir, 2014]) provided a comparison for diesel fuel, ethanol and gasoline, which showed that anhydrous ethanol had a behavior between diesel fuel and gasoline in terms of flashpoint, auto-ignition temperature, and flammability limits. These results are available in Table 5.

PUC-Rio - Certificação Digital Nº 1312923/CA

Table 5: Approximate fuel characteristics related to flammability of neat diesel fuel, ethanol and gasoline (Battelle apud [Hansen, 2005] and [Shahir, 2014]).

Fuel characteristics	Diesel fuel	Ethanol	Gasoline
Vapor pressure at 37,8°C (kPa)	0.3	17	65
Flash point (°C)	64	13	-40
Auto-ignition temperature (°C)	230	366	300
Flammability limits (%)	0.6 - 5.6	3.3 – 19.0	1.4 – 7.6
Flammability limits (°C)	64 to 150	13 to 42	-40 to 18

However, both the minimum and maximum concentration limits were higher than those of diesel fuel and gasoline were. The flash point of biodiesel is greater than 120°C and it is higher than 55°C for fossil diesel fuel, while, in the case of bioethanol, it should be below 16°C [Barabás, 2011].

Consequently, the formation of ignitable vapor at normal ambient temperature is easier in ethanol and gasoline and consequently requires some precautions for storage, handling and transportation. Some authors measured the flash point of many E- diesel blends and found that, whatever the ethanol ratio was, the two fuel mixture reaches to a flash point value measured between 12 and 17 °C, which is close to the value of pure ethanol [Ajav, 2002; Fernando, 2004;

Li, 2005; Kwanchareon, 2007; Rahimi, 2009; Pidol, 2012; Shahir, 2014]. The flammability characteristics of E-diesel blends were more similar to ethanol than diesel fuel. Temperature in the fuel tank on a diesel fueled vehicles is raised to approximately 93 °C due to the recirculation of the fuel. This recirculation of fuel is essential for cooling the fuel injection system.

Meanwhile, for diesel–biodiesel blends, the flash point increases as the biodiesel content in the blends increases [Alptekin, 2009]. Nevertheless, as observed by Barabás *et al.* (2009) and shown in Table 6, flash point for DBE blends are very close to ethanol flashpoint with values in the range of 14 to 18°C.

Table 6: Measured flash point for the investigated DBE blends [Barabás, 2009].

Flash point (°C)		Biodiesel content (vol%)						
		0	5	10	15	20	25	100
Ethanol content (vol%)	0	126	-	-	-	-	-	155
	5	-	17	14	16	17	18	-
	10	-	15	15	15	16	-	-

Thus, the storage, handling and transportation of E-diesel blends require special attention compared to fossil diesel fuel and precautions are needed to avoid fire and explosions, quite similar to the solution used in the distribution chain of ethanol and gasoline. The flash point of these ternary blends is such, that it could be classified as a Class II liquid according to the NFPA 497 standard [NFPA, 2009]. It should be handled safely while filling a fuel tank and it has to use the same infrastructures as used for gasoline and ethanol [Chotwichien, 2009].

Several liquid hydrocarbons were studied by Pidol *et al.* (2012) in order to produce an over-rich fuel/air mixture in the empty space that will not ignite when exposed to a potential ignition source. It was found the iso-pentane (C_5) as the most suitable one, as it is non-toxic and it exhibits a low flash point (> -51°C) which permits reducing the incorporation proportion (7 vol% in the study). Due to this iso-pentane, the flash point of the blends decreases below -17°C, which ensures the neighboring gaseous phase is too-rich-to-burn inside the fuel tank.

PUC-Rio - Certificação Digital Nº 1312923/CA

2.2.9. Cold Properties: Cloud Point, Cold Filter Plugging Point (CFPP) and Pour Point

Three parameters can be assessed when dealing with cold properties, as shown in Figure 20:

(i) Cloud Point: The cloud point is defined as the temperature at which the first solid particles appear in a fluid.

(ii) Cold Filter Plugging Point (CFPP): The CFPP is the highest temperature at which a given volume of fuel fails to pass through a standardized filtration device in a specified time, when cooled under standardized conditions.

(iii) Pour Point: The pour point is the lowest temperature at which a liquid can flow, as the blend forms a gel

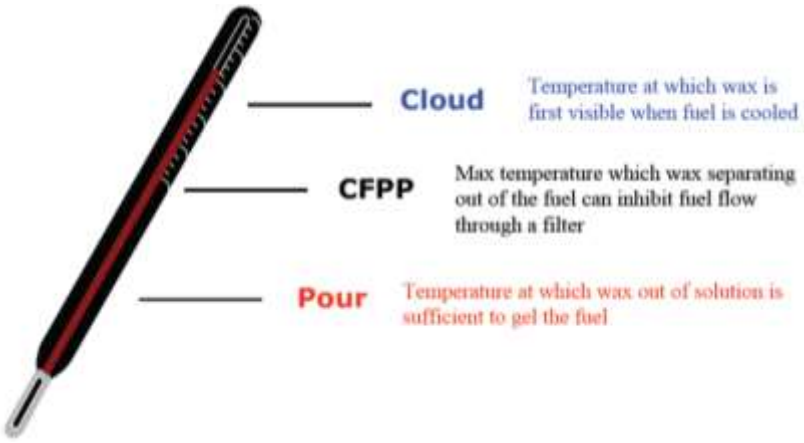

Figure 20: Difference between Cloud Point, CFPP and Pour Point.

The potential of a fluid to wax precipitation is measured by the cloud point of the fluid. Nevertheless, in the literature review, it was not found any study on the cloud point of the DBE blends. One possible explanation for this fact is that this property is only part of the fuel specifications following the North-American standard ASTM D 975 and it is poorly studied. Only CFPP is measured in the European and Brazilian specifications (cloud point is also studied for European winter diesel fuel in arctic climatic zones).

The trouble-free flow of a fuel at the lowest temperature is estimated by measuring the Cold Filter Plugging Point. It is a requirement for the fuel, which is a climate-dependent (between -20°C and 5°C for temperate climate) [Barabás,

PUC-Rio - Certificação Digital Nº 1312923/CA

2011]. Moreover, the CFPP depends on the raw materials of the biodiesel [Murugesan, 2009]. Barabás *et al.* (2009) measured CFPP for different DBE blends, as shown in Table 7.

Table 7: Measured CFPP for the investigated DBE blends [Barabás, 2009].

CFPP (°C)		Biodiesel content (vol%)						
		0	5	10	15	20	25	100
Ethanol content (vol%)	0	-9	-	-	-	-	-	-14
	5	-	-18	-17	-13	-17	-16	-
	10	-	-14	-6	-4	-7	-	-

They observed that, in comparison to diesel fuel, when rapeseed biodiesel content increased, CFPP decreased in the case of blends containing 5% ethanol, but it had a higher value for the blends containing 10% ethanol. Such behavior is due to the limited miscibility of ethanol.

Concerning the pour point, as the temperature of a fuel approaches to its pour point, it becomes cloudy due to the formation of crystals (cloud point) and, finally, the crystals solidify. This causes major problems [Knothe, 2005b].

Due to the extremely low pour point of ethanol, its addition to the diesel fuel decreases significantly the pour point of the final blend. Although biodiesel has high pour point (max 12°C) than diesel fuel and ethanol, it does not seem to affect the pour point of the final blend [Cheenkachorn, 2006; Chotwichien, 2009; Hussan, 2013].

Kwanchareon *et al.* (2007) studied this parameter and they observed that all of the test DBE blends, except samples containing 90% diesel fuel and 10% biodiesel, and 85% diesel fuel and 15% biodiesel, were found to have the same pour point at 3°C, while the samples which contained only diesel fuel and biodiesel, without ethanol, had the same pour point as that of reference diesel fuel (6°C). As the diesel fuel was the main component of the ternary blends, they did not find much deviation in the pour point from the fossil diesel fuel pour point value.

PUC-Rio - Certificação Digital Nº 1312923/CA

2.2.10. Materials Compatibility Issue

Several material compatibility studies were made during the early 80s for the use of ethanol in the gasoline engines and some of the conclusions are also applicable for E-diesel blends in the diesel engines [Hansen, 2001a].

The quality of the ethanol has a strong influence on its corrosive effects. The problems of ethanol corrosion are commonly divided into three categories: general corrosion, dry corrosion and wet corrosion. General corrosion is caused by ionic impurities, mainly chloride ions and acetic acid. Dry corrosion is attributed to the ethanol molecule and its polarity. De la Harpe (apud [Shahir, 2014]) reviewed reports of dry corrosion of metals by ethanol and he found that magnesium, lead and aluminum were susceptible to chemical attack by dry ethanol. Wet corrosion is caused by azeotropic water, which oxidizes most metals. Freshly formulated blends containing pH neutral dry ethanol would be expected to have relatively little corrosive effect. However, if a blend has been standing in a tank for sufficient time to allow the ethanol to absorb moisture from the atmosphere, it may tend to be more corrosive.

Non-metallic components have been affected by ethanol with particular reference to elastomeric components such as seals and O-rings in the fuel injection system. These seals tend to swell and stiffen. Resin-bonded or resin-sealed components are also susceptible to swelling and seals may be compromised [Shahir, 2014].

The results of Thangavelu et al. (2016) revealed that the corrosion rate of metals in BDE fuels is in the order: aluminum < mild steel < copper. The degradation of fuel properties and corrosion rate of metals in DBE fuel blends are lower than neat biodiesel, whereas higher than fossil diesel fuel.

Nevertheless, corrosion inhibitors have been incorporated in some additive packages used in ethanol-diesel blends. Moreover, technologies used in flex fuel gasoline car can be adapted to E-diesel issue.

2.3. Combustion Characteristics

Hulwan *et al.* (2011) found an increase in ignition delay and the highest heat release rate at low loads due to the high latent heat of evaporation of ethanol and the low cetane number of the ternary blends. As formerly observed [Ali, 1995;

PUC-Rio - Certificação Digital Nº 1312923/CA

Park, 2009, Qi, 2010], ethanol leads to superior fuel mixing and atomization to form an air fuel mixture that burns more rapidly due to the lower viscosity, surface tension, and specific gravity. They also observed that ethanol in the blend slightly affects the spray cone angle and spray tip penetration, whereas the size of droplets of diesel–ethanol blend decreases with the ethanol blending ratio.

The indicated pressure diagram obtained for different blends and BMEP at 1,200 and 1,600 rpm are given in Figures 21 and 22, respectively.

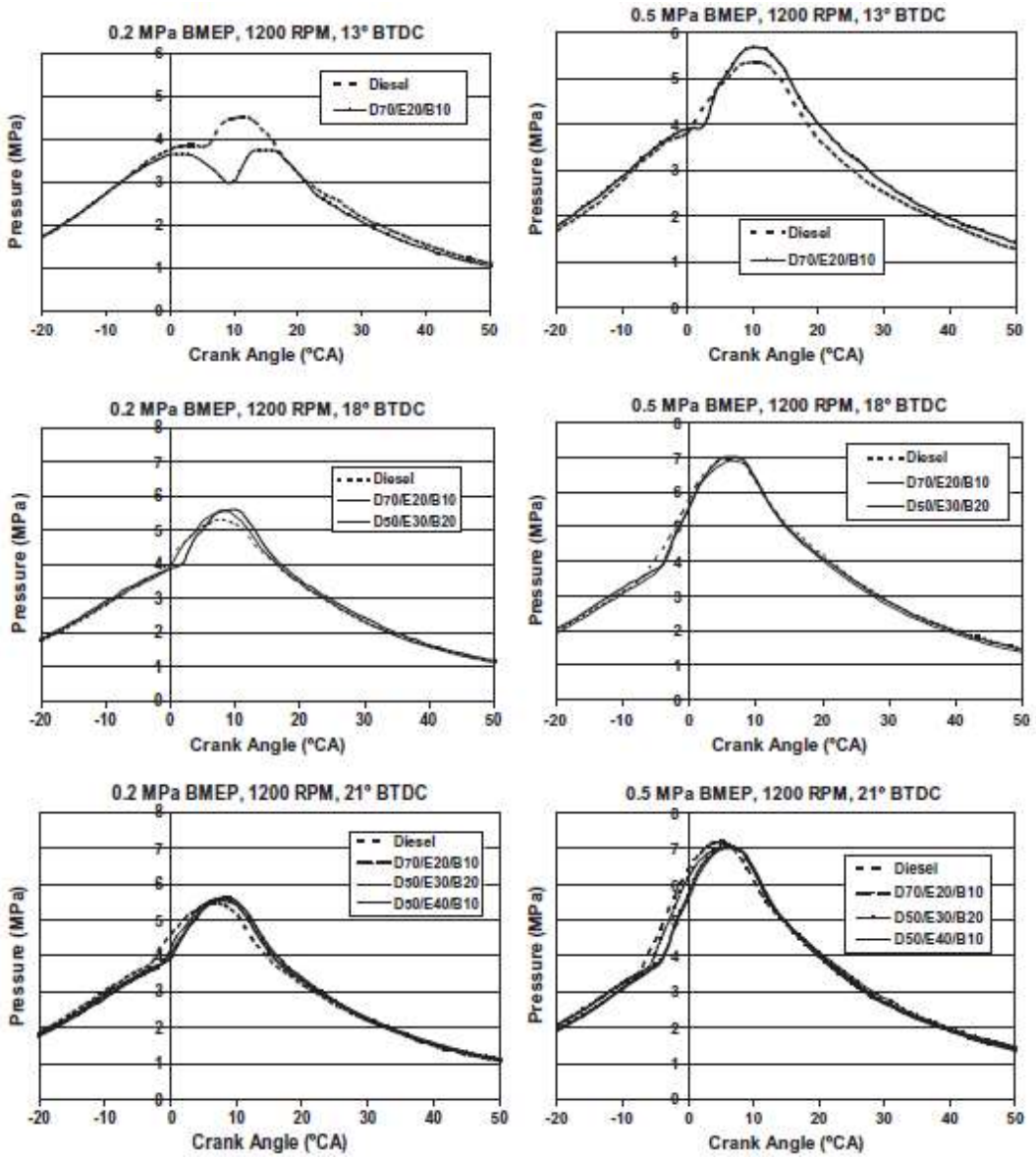

Figure 21: Indicated pressure diagram at 1,200 rpm for different blends and BMEP [Hulwan, 2011].

PUC-Rio - Certificação Digital Nº 1312923/CA

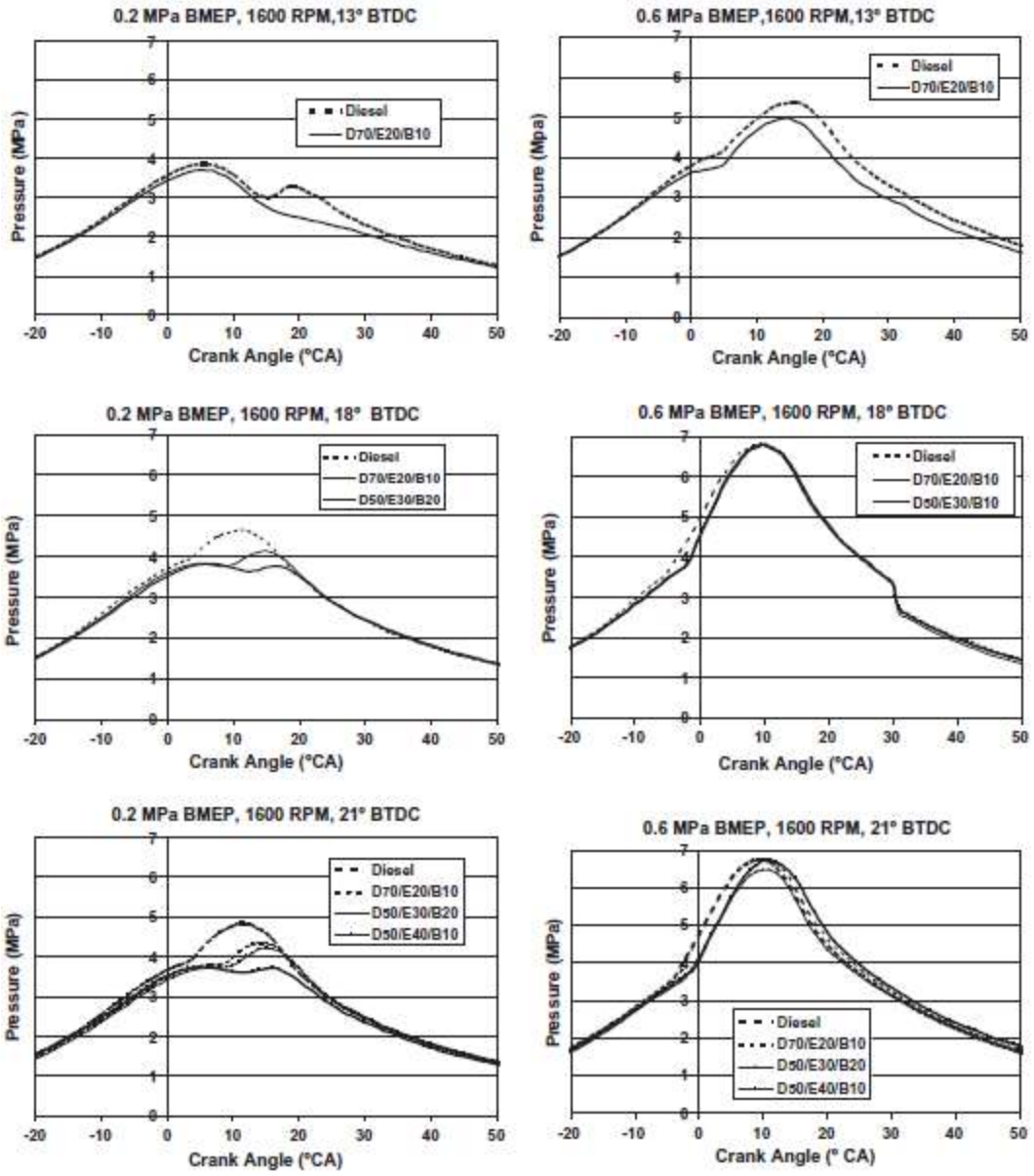

Figure 22: Indicated pressure diagram at 1,600 rpm for different blends and BMEP [Hulwan, 2011].

Although the ignition delay is higher, the end of heat release remains at nearly the equal crank angle as the one observed for diesel fuel. This indicates the decrease of diffusive combustion due to the improved mixing, atomization and access availability of oxygen. From the rate of heat release analysis, they concluded in higher thermal power output [Hulwan, 2011].

They also noticed variations in the combustion characteristics of the blends with respect to engine speed. The durable premixed burning phase resulted to the peak cylinder pressure, which is near the TDC (Top Dead Centre) at low engine load of 1,200 rpm. On the other hand, the entire combustion process is shifted in

PUC-Rio - Certificação Digital Nº 1312923/CA

the expansion stroke by the increased ignition delay, which is caused at low load of 1600 rpm. They found that, especially in the blends with high ethanol content, the initialization of combustion is delayed compared to diesel fuel. Consequently, the impact of a low cetane number of the blends is reduced on the ignition delay at high engine load.

Kannan (2013) tested a DBE blend (50:40:10) at 6.2 bar BMEP (Brake Mean Effective Pressure) condition. He found a maximum cylinder gas pressure 1.5% higher than for diesel fuel. He also investigated the variation of ignition delay for the blend at different injection timings and pressures. He found that the ignition delay decreased with the increasing BMEP. Lapuerta *et al.* (2017b) also observed this behavior. Overall, the blends showed a higher ignition delay compared to diesel fuel concerning injection timing and pressure.

Park *et al.* compared the DBE blends of 10, 20 and 30 vol% of ethanol with 5% of biodiesel [Park, 2010] and DBE blends of 20% of ethanol with 5, 10 and 20 vol% of biodiesel [Park, 2012]. They also observed that the increase of the ignition delay caused by the blended ethanol in diesel fuel is due to the reduction in cetane number. In addition, they associated the phenomenon to the consumption reaction of the hydroxyl radical (–OH), which confines the heat release. In assessment of the B5, B10 and B20, the ignition delay is found to be shorter in length as the quantity of biodiesel fuel increases. In addition, they also studied the shape of the spray behavior of some blends and the main characteristics are given in Figure 23.

PUC-Rio - Certificação Digital Nº 1312923/CA

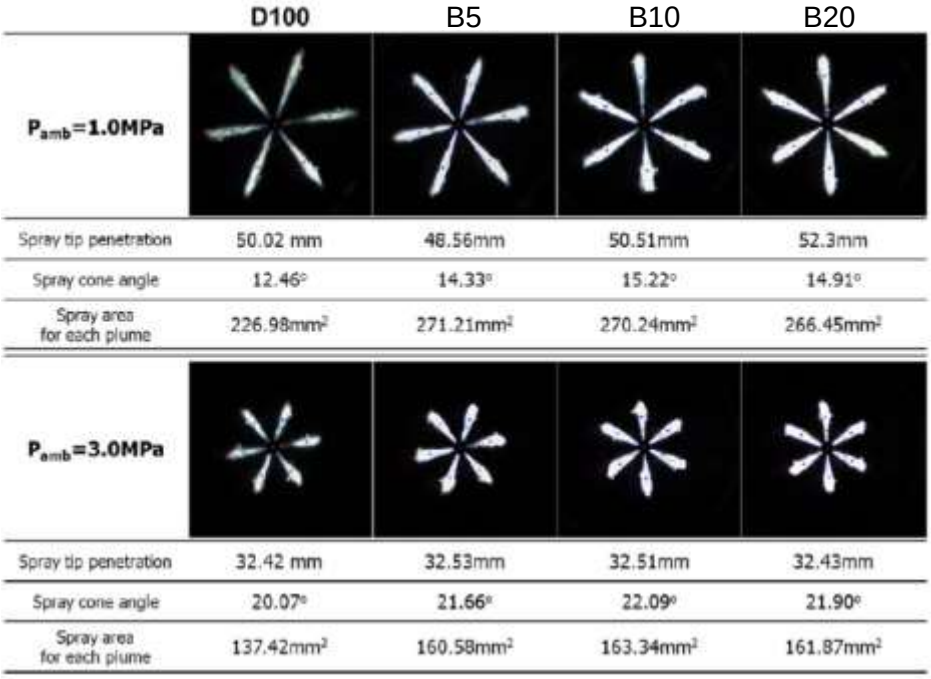

Figure 23: Spray behavior characteristics in the constant volume chamber (P_{inj} = 100 MPa, m_{fuel} = 10 mg, time after the start of energizing = 0.8 ms (about 5.76° of crank angle)) [Park, 2012].

PUC-Rio - Certificação Digital Nº 1312923/CA

The blends containing 5, 10 and 20 vol% biodiesel are found to have relatively wide spray shape in the combustion chamber, which is the effect of active evaporation of ethanol. This affects the higher peak combustion pressure in the blended fuels compared to conventional diesel fuel.

In DBE blends, this combustion phenomenon can be described in the following steps. The relatively undersized ignition delay, caused by the escalation of biodiesel portion, makes the premixed duration decrease. Nevertheless, the higher oxygen content and the cetane number ended in a better mixture formation in comparison to pure diesel fuel. Thus, the premixed combustion is independent to the biodiesel contents. The ignition delay for all test fuels considerably increased when the injection timing advances. In addition, the rise of biodiesel content in the blends caused the decrease of the IMEP (Indicated Mean Effective Pressure). It can be explained by (i) the premixed combustion phasing and the advancement of ignition timing, (ii) the increase of negative work before the TDC and (iii) the reduction of LHV and the low combustion pressure in the expansion stroke. Calculating the heat release using the law of thermodynamics from the curve of combustion pressure [Heywood, 1988], they showed that the event of heat release marginally advanced based on the growth of biodiesel portion. The

highest rate of heat release for the blends did not show a clear tendency, but it was either equal or higher than that of diesel fuel. This is the result of the extended ignition delay and the rise of premixed mixture [Park, 2012]

2.4. Pollutants Emission

Several studies investigated the effect of the biodiesel on exhaust emissions when compared to diesel fuel. Most of these studies showed that using of biodiesel in diesel engines can reduce carbon monoxide (CO), particulate matter (PM) emissions, unburned hydrocarbon (HC) and smoke, with an increase of carbon dioxide (CO_2). As the case of nitrogen oxides (NO_x) is strongly dependent on the fuel, the engine and the load, there is no global tendency. As reported by Fang *et al.* (2013), smoke emissions decreased because of higher oxygen content and longer ignition delay allowing to the air-fuel mixture to be more homogeneous.

Generally, it may be concluded that the studied DBE blends have lower pollution levels, except for CO_2 and NO_x, in which cases the recorded values are superior to those recorded for diesel fuel. However, the percentages of decreased or increased exhaust emission were different for different studies.

The ethanol's presence in mixture is an increasing factor of the unburned HC emissions, while the biodiesel's presence leads to their reduction [Barabás, 2010; Park, 2012]. Consequently, some authors observed an increase of HC [He, 2003; Li, 2005; Shi, 2005; Rakopoulos, 2007; Kim, 2008; Lapuerta, 2009; Subbaiah, 2010a; Zhu, 2011; Lei, 2012; Pidol, 2012; Yilmaz, 2012; Fang, 2013; Aydin and Ogut, 2017], due to lower combustion temperature, and others observed a decrease of this pollutant [Ali, 1995; Pang, 2006; Shi, 2006; Chen, 2007; Pang, 2008; Rahimi, 2009; Barabás, 2010; Sayin, 2010; Lei, 2011; Randazzo, 2011b; Park, 2012; Khoobbakht, 2016; Roy, 2016].

Moreover, DBE blends led to a slight increase of acetaldehyde, propionaldehyde and acetone emissions [He, 2003; Pang, 2006; Shi, 2006; Pang, 2008; Guarieiro, 2009].

Ali *et al.* (1995) also observed that SO_2 emissions did not change with an increase in methyl tallowate-ethanol content in the blend at a time were high

PUC-Rio - Certificação Digital Nº 1312923/CA

content of sulphur where present in the blends. Aydin and Ogut (2017) observed a decreased up to 67% of the diesel fuel emission under the investigated conditions.

Nitrogen oxides emission may increase [Shi, 2005; Pang, 2006; Shi, 2006; Chen, 2008; Kim, 2008; Pang, 2008; Barabás, 2010; Sayin, 2010; Subbaiah, 2010a; Aydin and Ogut, 2017]. On the contrary, some studies also reported the decrease of NO_x [He, 2003; Rakopoulos, 2007; Guarieiro, 2009; Lapuerta, 2009; Lebedevas, 2009; Park, 2010; Lei, 2011; Rakopoulos, 2011; Randazzo, 2011b; Zhu, 2011; Lei, 2012; Park, 2012; Pidol, 2012; Yilmaz, 2012; Fang, 2013; Yilmaz, 2014; Khoobbakht, 2016].

Others observed inconclusive behavior, with both increase and decrease, in function of the load, engine speed and injection time for NO_x, CO and/or unburned HC [Li, 2005; Shi, 2006; Chen, 2008; Guarieiro, 2009; Huang, 2009; Barabás, 2010; Park, 2010; Subbaiah, 2010b; Hulwan, 2011; Lei, 2012; Yilmaz, 2014; Roy, 2016; Aydin and Ogut, 2017, Tan, 2017].

The heterogeneity in the results and the explanation obtained by different authors can also be attributed to the test conditions of engine (model, load and engine speed) and the nature of the blends (proportions and nature of the biodiesel). Unfortunately, it was not possible to link the observed emissions to engine technology. Only four authors gave the Euro or Tier emission standards of the tested engine [Shi, 2005; Pidol, 2012; Khoobbakht, 2016; Roy, 2016], as shown on Appendix B. For instance, the exact amount of the emitted NO_x emerges as the competitive result between various factors, which act in favor of higher local gas temperatures (e.g., lower alcohol cetane number, lower EGR ratio) and various others that act in contradiction (e.g., higher alcohol heat of evaporation and lower C:H atom ratio, early injection strategy with a narrow angle injection system), with the higher amount of available oxygen, also playing a vital role [Giakoumis, 2013: Park, 2013: Pidol, 2012].

The CO_2 emissions were superior to those measured in case of the diesel engine function [Shi, 2006; Barabás, 2010; Subbaiah, 2010a and 2010b, Hulwan, 2011; Khoobbakht, 2016; Aydin and Ogut, 2017]. The increasing level of the CO_2 emissions can be put on the decreasing CO emissions, which further oxidizes because of the high oxygen content of the researched mixtures, providing a more complete combustion. Also, the oxygen excess made possible the CO oxidation during the evacuation process, including on the evacuation route of the

PUC-Rio - Certificação Digital Nº 1312923/CA

combustion gas. Nevertheless, with the aid of additive and ignition improver, CO, unburned ethanol and acetaldehyde emissions of the blends can be moderately decreased, even total hydrocarbon emissions were less than those of diesel fuel were. The results indicate the potential of diesel reformation for clean combustion in diesel engines [He, 2003].

2.5. Partial Conclusion

In the current CI engines, it is technically impossible to use E-diesel due to its physical properties. Such blends do not meet the diesel fuel standard and compromise the operational integrity of the engine. Nevertheless, after the reading the present review, it can be said that the DBE ternary fuel blend in the CI engine has a higher potential as no work showed insuperable difficulty to use such blends. This bibliographic review indicates that, from the point of view of fuel properties and with a small fuel consumption penalty (which is equal to the decrease of energy content), this blend can be suggested, for especially medium and small load engines. Maximum of 20–25 vol% biodiesel and 5 vol% ethanol can be added effectively and efficiently with the fossil diesel fuel.

However, there is a scope of research on suitable additive, which would increase the ethanol and biodiesel portion in this ternary blend. Consequently, this work is focusing to find a way to increase ethanol proportion in the blends. Based on the results of the bibliographic review, the present thesis focused on the formulation of ternary additives composed of biodiesel, vegetal oil and *n*-butanol. Vegetal oil and biodiesel from soybean and castor seeds were investigated. Such sources was chosen as, on the one hand, soybean is the main sources of biodiesel in Brazil and its production at industrial scale is already mature and, on the other hand, castor oil showed to be part of an efficient additive already in an article published in literature [Lei, 2012].

PUC-Rio - Certificação Digital Nº 1312923/CA

3 Experimental Section

The present section was divided into four distinct parts. The first part is relative to the attempt to formulate an additive to stabilize commercial diesel B7 fuel (7 vol% of biodiesel in diesel fuel) blended with hydrous and anhydrous ethanol. The second part deals with the formulation of an additive to stabilize diesel fuel blended with anhydrous ethanol and different biodiesel contents. The third part consists in the description of the methodology used to measure some physicochemical properties of the diesel B15 fuel (15 vol% of biodiesel in diesel fuel) blended with anhydrous ethanol. The fourth part deals with the engine efficiency of diesel B15 fuel blended with up to 20 vol% of anhydrous ethanol and 1.0 vol% of additive.

PUC-Rio - Certificação Digital Nº 1312923/CA

3.1. Formulation of an Additive to Blend Commercial Additivated Diesel B7 Fuel with Hydrous and Anhydrous Ethanol

3.1.1. Materials

The phase behavior of the E-diesel blends was studied using additivated S10 diesel B7 fuel and hydrous ethanol fuel samples, both commercial and obtained from a gas station in Rio de Janeiro, Brazil. Anhydrous ethanol with 99.9° INPM (provided by the company B'Herzog) was used in some blends. Some physical–chemical properties of the commercial fuels are given in Tables 8 (diesel fuel) and 9 (hydrous and anhydrous ethanol), respectively.

Table 8: Physicochemical properties of the Brazilian additivated S10 diesel B7 fuel studied.

Property	Unit	Method (Resolution No. 50, 2013) [Brasil, 2013]	Limit (Resolution No. 50, 2013) [Brasil, 2013]	Result
Aspect	-	Visual	Limpid and exempt of impurities	Limpid and exempt of impurities
Color	-	Visual	Colorless to yellow	Yellow
Color ASTM	-	ASTM D1500	max 3.0	1.5
Water by Karl Fischer	wt%	ASTM D6304	max 0.02	0.01
Total sulphur	mg/kg	ASTM D5453	max 10.0	9.6
Biodiesel content	vol%	EN 14078	7.0 ± 0.5	7.2
Flash Point	°C	ASTM D93	min 38.0	48.7
Cold Filter Plugging Point	°C	ASTM D6371	max 5.0	-4.0

Table 9: Physicochemical properties of the studied hydrous and anhydrous ethanol.

Property	Unit	Method (Resolution No. 19, 2015) [Brasil, 2015b]	Limit (Resolution No. 19, 2015) [Brasil, 2015b]	Hydrous ethanol	Anhydrous ethanol
Color	-	Visual	Orange	Yellow	Colorless
Aspect	-	ASTM D4176	Limpid and exempt of impurities	Limpid and exempt of impurities	Limpid and exempt of impurities
Specific gravity at 20°C	kg/m^3	ASTM D4052	Max hydrous: 810.1 Max anhydrous: 791.5	809.2	789-791
Alcohol content	wt%	ASTM D4052	Hydrous: 92.5 to 93.8 Anhydrous: min 99.3	93.21	99.5 – 99.9
pH at 25°C	-	NBR 10891	6.0 to 8.0	7.2	-
Total acidity	mg/L	NBR 9866	max 30	8.2	max 30
Electric conductivity	µS/m	NBR 10547	max 389	372.0	-
Evaporation residue	mg/100mL	NBR 8644	max 5.0	3.1	-

Biodiesel (methyl esters) and refined vegetal oil from soybean and castor oil and *n*-butanol, purity PA (provided by the company Vetec), have been used for additive synthesis. Their main properties are given in Tables 10, 11 and 12. An antioxidant (1000 ppm of butylated hydroxytoluene, BHT) was added into the biodiesel to prevent its oxidation.

PUC-Rio - Certificação Digital Nº 1312923/CA

Table 10: Physicochemical properties of the soybean and castor oil biodiesel.

Property	Unit	Method (Resolution No. 45, 2014) [Brasil, 2014]	Limit (Resolution No. 45, 2014) [Brasil, 2014]	Soybean biodiesel	Castor oil biodiesel
Aspect	-	NBR 16048	Limpid and exempt of impurities	Limpid and exempt of impurities	Limpid and exempt of impurities
Specific gravity at 20°C	kg/m^3	NBR 14065	850.0 to 900.0	882.1	923.3
Kinematic viscosity at 40°C	mm^2/s	NBR 10441	3.0 to 6.0	4.290	15.99
Water by Karl Fischer	mg/kg	ASTM D6304	max 200	998.00	331
Flash Point	°C	NBR 14598	min 100.0	142.1	-
Esters content	wt %	NBR 15764	min 96.5	96.9	94.5
Total sulphur	mg/kg	ASTM D5453	max 10.0	4.06	-
Sodium and Potassium content	mg/kg	NBR 15556	max 5	0.1	12.4 / < 1.0
Calcium and Magnesium content	mg/kg	NBR 15553	max 5	0.5	1.8 / 1.6
Phosphorus content	mg/kg	NBR 15553	max 10	0	-
Cold Filter Plugging Point	°C	NBR 14747	max 8.0	-3.0	-
Total acidity	mg(KOH)/g	ASTM D664	max 0.50	0.47	0.31
Free glycerol content	wt %	ASTM 6584	max 0.02	0.009	-
Total glycerol content	wt %	ASTM 6584	max 0.25	0.144	0.14
Monoglyceride content	wt %	ASTM 6584	max 0.7	0.455	-
Diglyceride content	wt %	ASTM 6584	max 0.20	0.121	-
Triglyceride content	wt %	ASTM 6584	max 0.20	0	-
Methanol and/or ethanol content	wt %	NBR 15343	max 0.20	0.11	-
Stability to oxidation	h	EN 14112	min 8	3.24	-

In soybean biodiesel, the only physicochemical property out of the limit was water content. It is probably due to contamination of the sample by moisture during the storage.

It can also be seen in this table that castor oil biodiesel is denser and more viscous than the values allowed by the ANP's resolution No. 45 of 2014 [Brasil, 2014]. Castor oil biodiesel is commonly used only for industrial and cosmetic purposes since their property are out of the specifications for its use as fuel. The ester content is also lower than the inferior limit value given by ANP, while the sodium content is higher than the permitted maximum value. Additional purification steps would be necessary to fit to the specifications.

PUC-Rio - Certificação Digital Nº 1312923/CA

Table 11: Physicochemical properties of the soybean oil and castor oil.

Property	Unit	Method	Soybean oil	Castor oil
Aspect	-	Visual	Limpid and exempt of impurities	Limpid and exempt of impurities
Specific gravity at 20°C	kg/m^3	NBR 14065	920.7	959.5
Kinematic viscosity at 40°C	mm²/s	NBR 10441	33.19	252.6
Water by Karl Fischer	mg/kg	ASTM D6304	635.0	1742
Lovibond Color 5 ¼" (R; Y)	-	AOCS Cc 13b-45	(0.9; 6.2)	
Iodine - Wijs	cg I2/g	AOCS Cd 1-25	121.1	73.1
Free glycerol content	wt %	ASTM D6584	0	-
Total glycerol content	wt %	ASTM D6584	12.473	-
Monoglyceride content	wt %	ASTM D6584	0.008	-
Diglyceride content	wt %	ASTM D6584	1.258	-
Triglyceride content	wt %	ASTM D6584	117.665	-
Total acidity	mg(KOH)/g	AOCS Ca 5a-40	-	1.05
Saponification	mg(KOH)/g	AOCS Cd 3-25	-	192
Unsaponifiable material	wt %	AOCS Ca 6a-40	-	0.7
Sodium content	mg/kg	NBR 15553	-	< 1.0
Potassium content	mg/kg	NBR 15553	-	< 1.0
Calcium content	mg/kg	NBR 15553	-	< 1.0
Magnesium content	mg/kg	NBR 15553	-	< 1.0
Phosphorus content	mg/kg	NBR 15553	-	8.2
Saturated triglyceride content	wt %	Gas chromatography	-	1.7
Monounsaturated triglyceride content	wt %	Gas chromatography	-	0.5
Di-unsaturated triglyceride content	wt %	Gas chromatography	-	6.5
Polyunsaturated triglyceride content	wt %	Gas chromatography	-	2.0
Ricinoleic triglyceride content	wt %	Gas chromatography	-	89.2
Average molecular mass	g/mol	ASTM D2503	-	1089.8

Table 12: Physicochemical properties of the *n*-butanol.

Property	Unit	Result
Purity	%	min 99.4
Titrable Acid	meq/g	max 0.0008
Water content	%	max 0.1
Carbonyl compounds (including butyraldehyde)	%	max 0.01
Color APHA	%	max 10
Butyl ether content	%	max 0.2
Evaporation residue	%	max 0.005

PUC-Rio - Certificação Digital Nº 1312923/CA

To evaluate the impact of temperature, samples were stored in a biochemical oxygen demand (BOD) incubator (model 101M/3 from ELETROlab) which allows a control of temperature in the range of -6 to 60°C, with a precision of 0.3°C.

3.1.2. Methodology

Most processes are optimized by development of univariate methodology (one variable at each time). This simple optimization methodology is supposed to have an easier interpretation. However, this process requires a large number of experiments, expends a great amount of materials and time, and it is only valid if the variables to be optimized do not interact. Procedures involving optimization by multivariate techniques have been increasingly used as they are faster, more economical and effective, and allow more than one variable (or factor) to be simultaneously optimized [Ferreira, 2012].

In this context, the formulation of the ternary additive was determined using an adapted experimental design. It was chosen to use a two variables Doehlert matrix. As the experiments are uniformly in the experimental space, the Doehlert matrix design allows a good knowledge of the whole experimental domain without proposing, *a priori*, a model representing the response and the identification of critical points such as maximum, minimum or saddle points, at each step of the optimization process. This method is relatively inexpensive in term of experiments cost. When compared to other experimental designs conventionally used such as factorial, Box-Behnken and central composite designs. Doehlert matrix does not give the same level number to each of the variables. This property allows the free choice of factors to be assigned either to a large or to a small number of levels (minimum of 3), in function of the interest of each factors and experimental considerations [CNAM, 2011; Ferreira, 2012].

Consequently, the two chosen factors were the concentrations of biodiesel and vegetal oil: the concentration of biodiesel varied from 0-95 vol% whereas the concentration of vegetal oil was maintained in the range of 0-10 vol%. This reduced range was imposed by the restriction that the sum of the two concentrations can not be higher than 100 vol%. Three levels were assigned to vegetal oil content (0, 5 and 10 vol%) and five levels were given to biodiesel

PUC-Rio - Certificação Digital Nº 1312923/CA

concentration (5, 27.5, 50, 72.5 and 95 vol%). One sample formulation was repeated three times in order to evaluate the repeatability of the experiments (samples 1, 8 and 9). Table 13 shows the concentrations of biodiesel, vegetal oil and *n*-butanol for each sample define for a given couple of biomass for biodiesel and vegetal oil.

Table 13: Doehlert matrix in term of real coordinates for each biodiesel-oil combination.

Sample reference	X_1 (Biodiesel content, vol%)	X_2 (Vegetal oil content, vol%)	*n*-butanol content, vol%
1	50.0	5.0	45.0
2	95.0	5.0	0.0
3	72.5	10.0	17.5
4	27.5	10.0	62.5
5	5.0	5.0	90.0
6	27.5	0.0	72.5
7	72.5	0.0	27.5
8	50.0	5.0	45.0
9	50.0	5.0	45.0

All the experimental conditions were investigated for each couple of biomass for biodiesel and vegetal oil: soybean - soybean, soybean - castor oil, castor oil - soybean and castor oil - castor oil. These sources were chosen due to the predominance of soybean biodiesel in Brazil and the fact that castor oil was part of the best additive formulated in the literature. Table 14 gives the tests conditions of each additive.

Table 14: Summary of the performed tests conditions described in Section 3.1.2.

Sections	Diesel fuel quality	Ethanol quality	Additive set	Additive content	Temperature	Test duration	Description
3.1.2.1. and 5.1.1.	Commercial diesel B7 fuel	Commercial hydrous ethanol	Set 1 (36 additives)	2.0 vol%	Ambient (20°C)	1, 2 and 3 hours	Stability of ethanol-diesel blends (49:51)
3.1.2.2. and 5.1.2.				2.0 to 5.0 vol %		1 and 2 hours	Influence of additive concentration in ethanol-diesel (49:51) blends on stability
3.1.2.3. and 5.1.3.				Variable		15 minutes	Maximum miscibility of ethanol in diesel fuel with initially 4 vol% of additive
3.1.2.4. and 5.1.4.		Anhydrous ethanol	Best additives from Set 1 (4 additives)	2.0 vol%	10, 20 and 30°C	1, 2 and 3 days	Influence of temperature in the stability of diesel fuel blended with ethanol (from 0 to 100 vol%)

PUC-Rio - Certificação Digital Nº 1312923/CA

3.1.2.1. Stability Study of Ethanol- Diesel-Additive Blends (48:50:2) at Ambient Temperature

All additives were tested at the concentration of 2 vol% in pure diesel B7 fuel and hydrous ethanol, to confirm the miscibility of the additive in these fuels, and in 200 mL of ethanol-diesel-additive blends (proportion 48:50:2). For all unstable samples, the separation ratio (SR, previously defined in equation 1) was calculated, after 1, 2 and 3 hours of decantation at 20 ± 2°C. A sample with the same proportion of diesel fuel and ethanol without additive was used as a reference to evaluate the stability effect.

3.1.2.2. Influence of Additive Concentration in Ethanol-Diesel (49:51) Blends at Ambient Temperature

The additive concentration was tested in the range of 2, 3, 4 and 5 vol% in 200 mL of ethanol-diesel blends (proportion 49:51). The volume ratio between the inferior diesel fuel phase and the superior ethanol phase were measured after 1 and 2 hours of decantation (when an apparent equilibrium was observed) at 20 ± 2°C. A sample with the same proportion of diesel fuel and ethanol without additive was used as a reference to evaluate the stability effect.

3.1.2.3. Maximum Addition of Hydrous Ethanol in Diesel Fuel with 4 vol% of Additive until Phase Separation at Ambient Temperature

Moreover, the maximum addition of hydrous ethanol in diesel B7 fuel initially additivated with 4 vol% of co-solvent was determined. This concentration of additive was chosen in order to have 2 vol% of additive in a mixture ethanol - diesel B7 fuel (50:50). For this purpose, hydrous ethanol was added, by step of 2 mL, in 100 mL of diesel fuel until a phase separation could be observed after 15 min of decantation at 20 ± 2°C. After the observation of phase separation, an supplementary addition was done to confirm the previous observation. At the equilibrium (after one day of decantation), the separation ratio SR was calculated. Again, an E-diesel sample without additive was used for comparison.

PUC-Rio - Certificação Digital Nº 1312923/CA

3.1.2.4. Influence of Temperature in the Stability of Anhydrous Ethanol – Diesel Blends with 2 vol% of Additive

Based on the precedent results, the best additive composition for each biodiesel-vegetal oil combination was defined. Best additives for all combinations biodiesel – vegetal oil were tested at the concentration of 2 vol% in 200 mL E-diesel blends. Concentration of anhydrous ethanol varied, from 0 to 100 vol%, by step of 10 vol%. Three temperatures were investigated to represent different climatic conditions: 10, 20 and 30°C. Again, separation ratios SR were measured after 1, 2 and 3 days of decantation for unstable blends.

3.2. Formulation of an Additive to Blend Diesel B0 fuel with Variable Anhydrous Ethanol and Biodiesel's Content

3.2.1. Materials

The phase behavior of the E-diesel blends was studied using S10 diesel B0 blended with biodiesel and anhydrous ethanol 99.9° INPM. Biodiesel used was a mixture of 85% of soybean methyl esters and 15% of tallow biodiesel, characteristic mixture of Brazilian biodiesel added to diesel fuel. An antioxidant (1000 ppm of butylated hydroxytoluene, BHT) was added into the biodiesel to prevent its oxidation. Some physicochemical properties of the diesel fuel and biodiesel are given in Tables 15 and 16, respectively. Anhydrous ethanol properties are the same as described in the previous section and they are available in Table 9.

Biodiesel, refined vegetal oil (from soybean and castor oil) and *n*-butanol used as additives were the same as formerly described (Tables 10, 11 and 12). Samples were stored in a biochemical oxygen demand (BOD) incubator (model 101M/3, ELETROlab) which allowed a control of temperature in the range of -6 to 60°C, with a precision of 0.3°C.

PUC-Rio - Certificação Digital Nº 1312923/CA

Table 15: Physicochemical properties of the studied Brazilian S10 diesel B0 fuel.

Property	Unit	Method (Resolution No. 50, 2013) [Brasil, 2013]	Limit (Resolution No. 50, 2013) [Brasil, 2013]	Value
Aspect	-	ASTM D4176	Limpid and exempt of impurities	Limpid and exempt of impurities
Color	-	Visual	Colorless to yellow	Yellow
Color ASTM	-	ASTM D1500	max 3.0	0.5
Specific Gravity at 20°C	kg/m^3	ASTM D4052	815.0 to 850.0	829.8
Distillation temperature **T10** **T50** **T95**	°C	ASTM D86	 min 180.0 245.0 to 295.0 max 370.0	 220,2 275,1 366,8
Flash Point	°C	ASTM D93	min 38.0	63.0
Cold Filter Plugging Point	°C	ASTM D6371	max 5.0	-4.0
Kinematic viscosity at 40°C	mm^2/s	ASTM D445	2.0 to 4.5	3.087
Total acidity	mg(KOH)/g	ASTM D664		0.02
Total sulphur	mg/kg	ASTM D5453	max 10.0	4.4
Aromatic Content and Polynuclear Aromatic Content	wt %	ASTM D5186	max 11	1,58
Cetane number	-	ASTM D613	min 48	56
Carbon residue	wt %	ASTM D524	max 0.25	0.05
Ash	wt %	ASTM D482	max 0.010	< 0,0010
Water by Karl Fischer	mg/kg	ASTM D6304	max 200	49
Water sediment	vol %	ASTM D2709	-	< 0.050
Total contamination	mg/kg	EN 12662	max 24	1.5
Corrosiveness to Cu, 3h at 50°C	-	ASTM D130	max 1	1
Lubricity by HFRR	mm	ASTM D6079	max 520	190
Stability to oxidation	mg/100mL	ASTM D5304	max 2.5	0.2
Electrical conductivity	pS/m	ASTM D2624	min 25	84

PUC-Rio - Certificação Digital Nº 1312923/CA

Table 16: Physicochemical properties of the biodiesel (85% soybean and 15% beef tallow).

Property	Unit	Method (Resolution No. 45, 2014) [Brasil, 2014]	Limit (Resolution No. 45, 2014) [Brasil, 2014]	Value
Aspect	-	NBR 16048	Limpid and exempt of impurities	Limpid and exempt of impurities
Specific gravity at 20°C	kg/m^3	NBR 14065	850.0 to 900.0	879.9
Kinematic viscosity at 40°C	mm²/s	NBR 10441	3.0 to 6.0	4.166
Water by Karl Fischer	mg/kg	ASTM D6304	max 200	176
Total contamination	mg/kg	EN 12662	max 24	13.5
Flash Point	°C	NBR 14598	min 100.0	125.5
Ester and linolenic acid methyl ester contents	wt %	EN 14103	min 96.5	99.0
Total sulphur	mg/kg	ASTM D5453	max 10.0	1.8
Sodium and Potassium content	mg/kg	NBR 15556	max 5	< 0.8
Calcium and Magnesium content	mg/kg	NBR 15553	max 5	< 2.0
Phosphorus content	mg/kg	NBR 15553	max 10	< 1.0
Cold Filter Plugging Point	°C	NBR 14747	max 8.0	0.0
Total acidity	mg(KOH)/g	ASTM D664	max 0.50	0.23
Free glycerol content	wt %	ASTM 6584	max 0.02	0.006
Total glycerol content	wt %	ASTM 6584	max 0.25	0.188
Monoglyceride content	wt %	ASTM 6584	max 0.7	0.602
Diglyceride content	wt %	ASTM 6584	max 0.20	0.132
Triglyceride content	wt %	ASTM 6584	max 0.20	0.058
Methanol content	wt %	NBR 15343	max 0.20	0.06
Iodine value	g(I)/100g	EN 14111	-	114
Stability to oxidation	h	EN 14112	min 8	12.4

PUC-Rio - Certificação Digital Nº 1312923/CA

3.2.2. Methodology

Based on the results of Part 1 of the experimental section, it was decided to evaluate the impact of a higher content of vegetal oil with lower *n*-butanol content. Again, a Doehlert matrix design was used and, in this case, the two factors were the concentrations of vegetal oil and *n*-butanol. The concentration of vegetal oil varied from 0-95 vol%, while the concentration of *n*-butanol was maintained in the range of 0-10 vol%. Three levels were assigned to *n*-butanol content (0, 5 and 10 vol%) and five levels were given to vegetal oil concentration (5, 27.5, 50, 72.5 and 95 vol%). Table 17 summarizes all the experimental conditions investigated for each couple of biomass for biodiesel and vegetal oil.

Table 17: Doehlert matrix in term of real coordinates for each biomass source.

Sample reference	X_1 (Vegetal oil content, vol%)	X_2 (*n*-butanol, vol%)	Biodiesel content, vol%
1	50.0	5.0	45.0
2	5.0	5.0	90.0
3	27.5	10.0	62.5
4	27.5	0.0	72.5
5	72.5	10.0	17.5
6	72.5	0.0	27.5
7	95,0	5.0	0.0

The repeatability of the test is assumed equal to the observed values in section 3.1.2. Table 18 gives the tests conditions described in the next sub-sections.

Table 18: Summary of the performed tests conditions described in Section 3.2.2.

Sections	Diesel fuel quality	Ethanol quality	Additive set	Additive content	Temperature	Test duration	Description
3.2.2.1. and 5.2.1.	Diesel B7, B15 and B30 fuels	Anhydrous ethanol	Set 2 (28 additives)	2.0 vol%	10 to 30°C	1 and 2 hours	Stability study in ethanol-diesel blends (40:60) at different temperatures and biodiesel concentrations
3.2.2.2 and 5.2.2.	Diesel B15 fuel		Best additive from Set 2	0.0, 0.5, 1.0 and 2.0 vol%	10 to 25°C	2 hours and 1, 2 and 3 weeks	Impact of the additive in diesel fuel blended with ethanol (from 0 to 100 vol%) in function of temperature and additive content at short to long terms

PUC-Rio - Certificação Digital Nº 1312923/CA

3.2.2.1. Stability Study of the Additives in DBE Blends at Different Temperatures and Different Biodiesel Concentration

All additives were tested at the concentration of 2 vol% in diesel BX fuel - anhydrous ethanol blends in proportion 60:40. The blends were prepared according to the following steps: first, biodiesel was blended with the ethanol and then, regular diesel fuel was added to the blend. BX corresponds to three values of concentration of biodiesel in diesel fuel: 7, 15 and 30 vol%. A blend without additive was used as a reference to evaluate the stabilization effect and the partition of the compounds into the phases when separation was observed.

First of all, for each family of additives, diesel B7 fuel stability was investigated at an initial temperature of 30°C after 1 and 2 hours of decantation.

For the unstable samples, the separation ratio (SR) was calculated. For the others, temperature was decreased, by step of 5°C, until only one sample was stable or a higher separation ratio was defined for all biphasic samples.

Then, diesel B15 and B30 fuels were investigated using the same procedure and considering as initial temperature, the last temperature investigated for blends with lower biodiesel concentration. Such blends were prepared by addition of ethanol, biodiesel and additive according to the Table 19.

Table 19: Added volume of each compound of the blends.

Biodiesel content	Ethanol addition (mL)	Diesel addition (mL)	Biodiesel addition (mL)	Additive addition (mL)
B7	80.0	111.6	8.4	4.08
B15	7.5	0	11.4	0.38
B30	18.7	0	28.1	0.94

Based on the precedent results, mathematical models allowed the determination of the best additive composition.

3.2.2.2. Impact of the Best Additive in Anhydrous Ethanol-Diesel B15 Blends at Different Ethanol Concentration in Function of Temperature and Additive Content

The best additive determined in the former step was tested at the concentration of 0; 0,5; 1 and 2 vol% in 200 mL of E-diesel B15 blends, which concentrations of anhydrous ethanol varied from 0 to 100 vol%, by step of 10 vol%. Four temperatures were investigated: 10, 15, 20 and 25°C. If separation was observed, the separation ratios were calculated after 1 and 2 hours of decantation for the blends. This process was duplicated to calculate the uncertainty. The results allowed describing the ranges of anhydrous ethanol concentration and temperature where stable blends were observed.

The long term stability (up to 3 weeks) of the blends, with and without 2 vol% of additive, was evaluated at the four temperatures investigated in 200 mL of E-diesel B15 blends. This duration was chosen to represent the maximum period when a car is parked, since experimental observation showed that agitation due to throttle / brake variation is sufficient to mix again the separated phase. The concentrations of anhydrous ethanol varied from 0 to 100 vol%, by step of 10

PUC-Rio - Certificação Digital Nº 1312923/CA

vol%. If separation was observed, the separation ratios were calculated after 1, 2 and 3 weeks of decantation of the blends.

3.3. Assessment of Some Physicochemical Properties for Anhydrous Ethanol – Diesel B15 Blends

3.3.1. Materials

The materials used in this part were the same as used in section 3.2.

3.3.2. Methodology

3.3.2.1. Specific gravity at 20 and 25°C

Specific gravity were measured for anhydrous ethanol – diesel B15 blends in the Fluids' Characterization Laboratory (LCF) at PUC-Rio, according to the ASTM D4052 or NBR 14065. Concentrations of anhydrous ethanol varied from 0 to 100 vol%, by step of 10 vol%, in regular and additivated blends (2.0 vol%). An additional sample with 20 vol% of ethanol and 1.0 vol% of additive was also analyzed.

Specific gravity was obtained using a 10 mL Gay-Lussac pycnometer (Roni Alzi) with a precision of 0.002 mL, a water bath model TV 4000 from Tamson and a Ohaus Explorer E02140 Balance (range 0.1 mg - 210 g; uncertainty: ± 0.0004 g). Figure 24 shows the equipments used to measure this property.

Figure 24: Gay-Lussac pycnometer, water bath model TV 4000 (Tamson) and a Ohaus Explorer E02140 Balance (from left to right).

PUC-Rio - Certificação Digital Nº 1312923/CA

A clean and dry pycnometer of volume V was previously weighted (m_0). The pycnometer was filled with the samples to be analysed, that have been previously stabilized at a temperature closed to the set point. The excess of liquid after stabilization at the studied temperature was removed and the filled pycnometer was weighted (m). The specific gravity was calculated according to equation 7:

$$\rho = \frac{m - m_0}{V} \tag{7}$$

The resolution n°50 of the ANP from December, 23rd 2013 [Brasil, 2013] specified that the experiment should be realized at 20°C. Nevertheless, as phase separation was observed at 20°C for some blends, the specific gravity was measured for the each phase of the unstable blends and the specific gravity of the blends was calculated using the volumetric fraction of each phase. The only exception was for blends with 70 vol% of ethanol and 2.0 vol% of additive where the volume of inferior phase was not sufficient to perform the measure. In that case, the specific gravity of the blends was measured and the specific gravity of the inferior phase was calculated.

Moreover, specific gravity was also experimentally measured at 25°C, because no separation are observed at this temperature and this value is closed to the value specified by the ANP.

PUC-Rio - Certificação Digital Nº 1312923/CA

3.3.2.2. Kinematic Viscosity at 40°C

As specified by the resolution n°50 from the ANP of December, 23rd 2013 [Brasil, 2013], the kinematic viscosity at 40°C was measured for anhydrous ethanol – diesel B15 blends in the Fluids' Characterization Laboratory (LCF) at PUC-Rio, according to the NBR 10441. As for specific gravity, concentrations of anhydrous ethanol varied from 0 to 100 vol%, by step of 10 vol%, in regular and additivated blends (2.0 vol%). An additional sample with 20 vol% of ethanol and 1.0 vol% of additive was also analyzed.

Viscosity was measured with an Ubbelohde glass capillary viscometer (Cannon) adapted to the range of the kinematic viscosity (number #1, for the range 2-10 mm²/s, constant C = 0.008956 ± 0.000037 mm²/s²). A water bath

model TV 4000 (Tamson) and a vacuum pump (Nova Técnica, model 613). The experimental equipment is illustrated in Figure 25.

Figure 25: Ubbelohde glass capillary viscometer (Cannon) and experimental equipment in the Fluids' Characterization Laboratory (LCF) at PUC-Rio.

PUC-Rio - Certificação Digital Nº 1312923/CA

The time is measured for a fixed volume of liquid to flow under gravity through the capillary of a calibrated viscometer under a reproducible driving head and at a closely controlled and known temperature. The kinematic viscosity υ is the product of the measured flow time (Δt) and the calibration constant of the viscometer (C), as given in equation 8:

$$\upsilon = C.\Delta t \tag{8}$$

Two determinations are needed. The average of the two acceptable values is the kinematic viscosity.

3.3.2.3. Surface Tension at 25°C

Surface tension at 25°C was semi automatically measured with a Lauda TE 1C tensiometer using a platinum ring for the stirrup method in the Fluids' Characterization Laboratory (LCF) at PUC-Rio. Figure 26 presents the equipment available in the laboratory.

Figure 26: Lauda TE 1C tensiometer (left) and zoom on the platinum ring (right) in the Fluids' Characterization Laboratory (LCF) at PUC-Rio.

PUC-Rio - Certificação Digital Nº 1312923/CA

Regular and additivated anhydrous ethanol – diesel B15 blends which concentrations of anhydrous ethanol varied from 0 to 100 vol%, by step of 10 vol%, were analyzed. An additional sample with 20 vol% of ethanol and 1.0 vol% of additive was also studied.

The Du Noüy ring tensiometry method, described in ASTM D1331, is based on pulling a ring out of a liquid and measuring the weight of the attached liquid meniscus. Platinum is used as the material for the ring, as this alloy is optimally wettable due to its very high surface free energy and, therefore, generally forms a contact angle θ of 0° with liquids. The material is also chemically inert and easy to clean.

The ring, initially outside the liquid, is moved in direction to the surface until it touched the liquid surface. At this moment, the measured tension (and, consequently, the force) slightly decreased due to buoyancy of the ring. Then, the ring was immersed into the liquid. This is the starting position of a surface tension experiment. The ring is moved out of the liquid with a constant speed. The liquid meniscus is pulled out by the ring and the measured force increases. The force reaches a maximum and decreases again. The maximum force corresponds to the surface tension of the measured liquid. Further pulling the ring led to a rupture of the meniscus [Sinterface, 2016; Kruss, 2016]. This procedure was repeated three times to obtain the average value of the maximum tension value.

With the Du Noüy ring method, a correction must be made to the measurement because the weight of the liquid wetting the ring increased the measured force, and because the maximum force does not occur at the inside and outside of the lamella at the same time. This correction factor is a function of the ring geometry and the liquid specific gravity [Sinterface, 2016; Kruss, 2016].

3.3.2.4. Contact Angle at 21°C

The contact angle of the blends was measured at 21°C in the Laboratory of Microhydrodynamics and Flow in Porous Media (LMMP) at PUC-Rio. Due to ethanol evaporation issue, this parameter was measured only for anhydrous ethanol – diesel B15 blends which concentrations of anhydrous ethanol varied from 0 to 20 vol%, by step of 5 vol%, until the evaporation of ethanol was observed. Contact angle was measured with an automated drop tensiometer Tracker S, from Teclis Scientific, as shown in Figure 27.

PUC-Rio - Certificação Digital Nº 1312923/CA

Figure 27: Tracker S (Teclis Scientific) automated drop tensiometer in the Laboratory of Microhydrodynamics and Flow in Porous Media (LMMP) at PUC-Rio.

The substrate used to determine the contact angle was a glass lamella. The cleaning process consisted in washing the glass lamella with detergent and water. After a quick drying, the substrate was put in an ultrasonic bath of isopropanol during 10 minutes to clean the last fatty compounds on the glass. The substrate was dried and, just before use, the solid particles on the surface were swept out the surface by a clean compressed air flow. The sample drop was deposited on the

surface using a micropipette and the focus and horizontality of the lamella were adjusted. The contact angle was immediately measured at ambient temperature (T=21±1°C), recorded by the computer. The Figure 28 showed the image of a drop (blend without additive and ethanol).

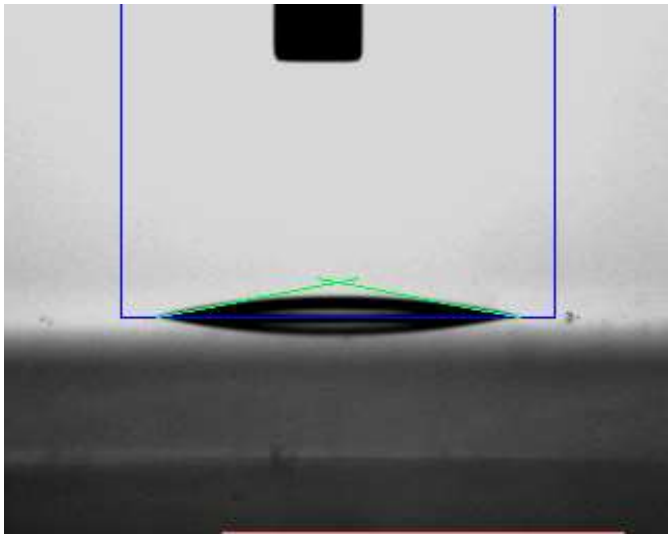

Figure 28: Image of a drop given by the software.

The grey region on the bottom represents the glass lamella and the blue line represents the frontier, chosen by the experimenter, to make the calculation. The green lines defined the contact angles.

To control the quality of the cleaning, a drop of water was deposited in the surface of each new lamella and the value was compared between the different lamellas. Some parameters are calculated from the image of a drop, such as area of the interface; volume, diameter and apex radius of the drop; temperature and angle, defined at the average value of the right and left angles.

3.3.2.5. Flash Point

As specified by the resolution n°50 from the ANP of December, 23rd 2013 [Brasil, 2013], the flash point was measured by tag closed cup tester (ASTM D56), method more adapted to samples with a flash point in the range -20 to +25°C. Anhydrous ethanol – diesel B15 blends, which concentrations of anhydrous ethanol varied from 0 to 100 vol%, by step of 10 vol% were analyzed. An additional sample with 20 vol% of ethanol and 1.0 vol% of additive was also

PUC-Rio - Certificação Digital Nº 1312923/CA

analyzed. Such tests were performed in the *Centro de Pesquisas e Caracterização de Petróleo e Combustíveis* (COPPEComb) at UFRJ. The schematic view of the equipment is available in Figure 29.

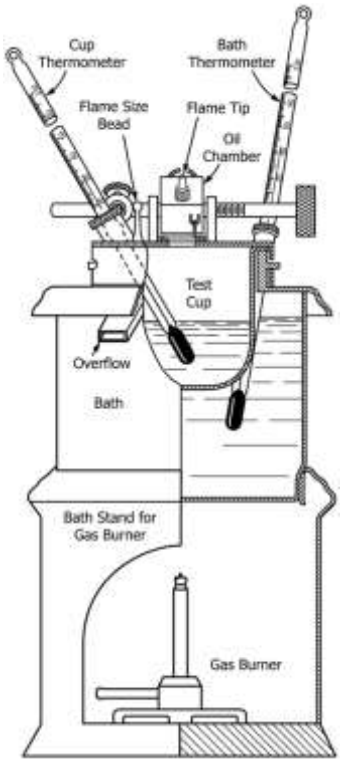

Figure 29: Schematic view of a manual tag closed cup tester [ATSM D56, 2010].

The method consists in heating, at a slow constant rate, the specimen placed in the cup of the tester with the lid closed. An ignition source is inserted into the cup at regular intervals. The flash point is taken at the lowest temperature in which the application of the ignition source causes vapor above the specimen to ignite. The equipment available in the lab is an automatic Flash Point Tester, model Atg-8l from Nakata, shown in Figure 30.

PUC-Rio - Certificação Digital Nº 1312923/CA

Figure 30: Tracker S (Teclis Scientific) automated drop tensiometer in the *Centro de Pesquisas e Caracterização de Petróleo e Combustíveis* (CoppeComb) at UFRJ.

Two determinations were made and the average value was used to calculate the final value, after a correction associated to the thermometer calibration.

3.3.2.6. Cold Filter Plugging Point (CFPP)

The cold filter plugging point (CFPP) was measured for anhydrous ethanol – diesel B15 blends which concentrations of anhydrous ethanol varied from 0 to 100 vol%, by step of 10 vol%, in the *Centro de Pesquisas e Caracterização de Petróleo e Combustíveis* (COPPEComb) at UFRJ. An additional sample with 20 vol% of ethanol and 1.0 vol% of additive was also analyzed. The protocol used followed the ASTM D6371 method, as specified by the resolution n°50 of the ANP from December, 23rd 2013 [Brasil, 2013]. The measurements were performed in a fully automated cold filter plugging point equipment, model NTL 450 from Normalab, as shown in Figure 31.

PUC-Rio - Certificação Digital Nº 1312923/CA

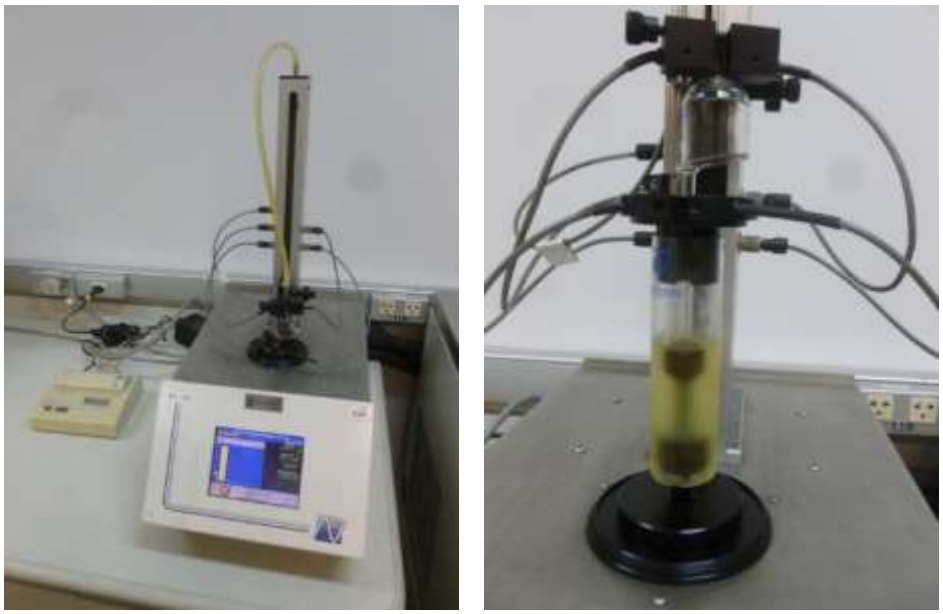

Figure 31: CFPP equipment, model NTL 450 from Normalab (left) and zoom on the wire mesh filter in the *Centro de Pesquisas e Caracterização de Petróleo e Combustíveis* (COPPEComb) at UFRJ.

PUC-Rio - Certificação Digital Nº 1312923/CA

The samples were cooled to the test temperature and drew through a wire mesh standard filter under vacuum. CFPP is defined as the lowest temperature at which 20 mL of fuel passes through the filter within 60 s. The cooling process was ensured by a 35L Proline heating thermostat from Lauda, model RP 1290, working at a temperature range from -88 to 200°C.

3.3.2.7. Corrosiveness to Copper at 50°C

Using the ASTM D130 method defined in the resolution n°50 of the ANP from December, 23rd 2013 [Brasil, 2013], the corrosiveness to copper was measured for anhydrous ethanol – diesel B15 blends which concentrations of anhydrous ethanol varied from 0 to 100 vol%, by step of 10 vol%, in the *Centro de Pesquisas e Caracterização de Petróleo e Combustíveis* (COPPEComb) at UFRJ. An additional sample with 20 vol% of ethanol and 1.0 vol% of additive was also analyzed.

A polished copper strip is immersed in test tube with the sample being tested and heated at 50 ± 1°C in an Ecoline immersion thermostat from Lauda, model E 100, as illustrated in Figure 32.

Figure 32: Ecoline immersion thermostat from Lauda, model E 100 used for corrosion test in the *Centro de Pesquisas e Caracterização de Petróleo e Combustíveis* (COPPEComb) at UFRJ.

At the end of the heating period (3 hours), the copper strip is removed, washed and the color and tarnish level assessed against the ASTM Copper Strip Corrosion Standard. The ASTM Copper Strip Corrosion Standard is a colored reproduction of strips characteristic of the descriptions given in Table 20.

PUC-Rio - Certificação Digital Nº 1312923/CA

Table 20: Copper Strip Classifications [ASTM D130, 2012].

Classification	Designation	Description
Freshly polished strip	Freshly polished strip	The freshly polished strip is included in the series only as an indication of the appearance of a properly polished strip before a test run; it is not possible to duplicate this appearance after a test even with a completely noncorrosive sample.
1	Slight tarnish	a. Light orange, almost the same as freshly polished strip b. Dark orange
2	Moderate tarnish	a. Claret red b. Lavender c. Multi-colored with lavender blue or silver, or both, overlaid on claret red d. Silvery e. Brassy or gold
3	Dark tarnish	a. Magenta overcast on brassy strip b. Multi-colored with red and green showing (peacock), but no grey
4	Corrosion	a. Transparent black, dark grey or brown with peacock green barely showing b. Graphite or lusterless black c. Glossy or jet black

3.3.2.8. Cetane Number (CN)

The cetane numbers of the E-diesel blends with (2 vol%) and without additive were measured. Blends with 0, 5, 10, 20 and 40 vol% of anhydrous ethanol were investigated. Additionally, an additional sample with 20 vol% of ethanol and 1.0 vol% of additive was also analyzed. This ethanol content limitation were related to the necessity of the blends to fit to standard fuels properties in order to prevent equipment failure and non-representative results. The property was measured in the *Laboratório de Motores e Combustíveis* (LAMOC) at the *Instituto Nacional de Metrologia, Qualidade e Tecnologia* (INMETRO), according to the ASTM D613.

The cetane number of a diesel fuel is determined by comparing its combustion characteristics in a test engine (CFR engine, as shown in Figure 33) with those for blends of reference fuels of known cetane number under standard operating conditions.

PUC-Rio - Certificação Digital Nº 1312923/CA

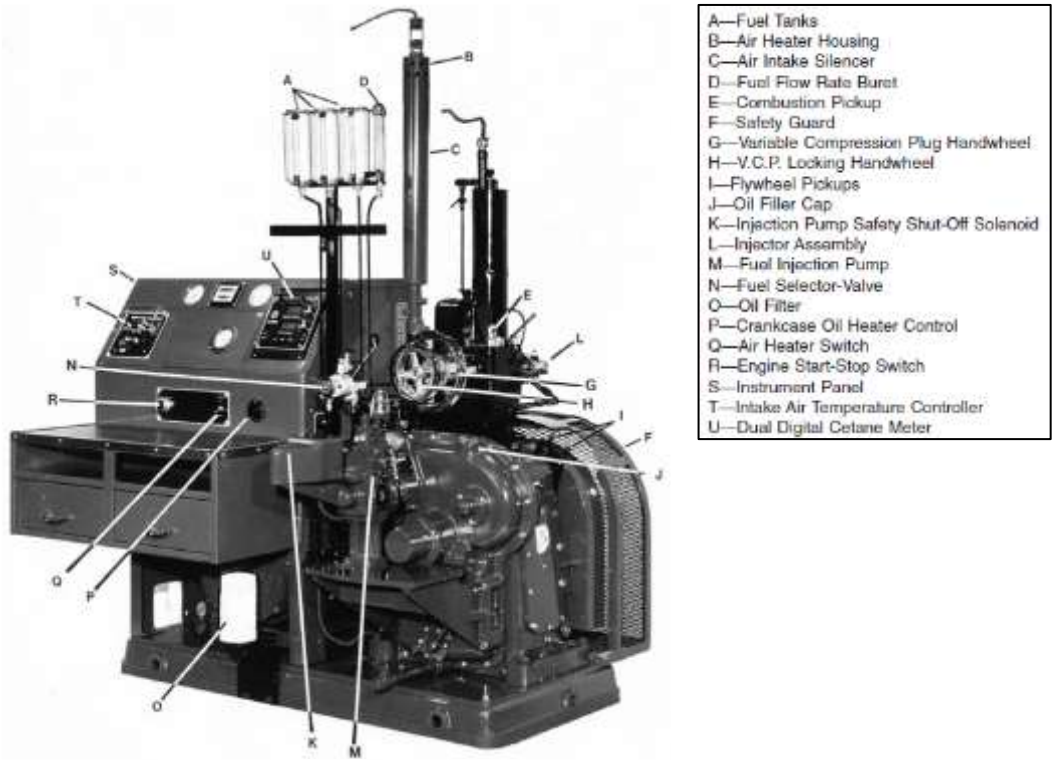

Figure 33: Cetane Method Test Engine Assembly [ASTM D613, 2013].

This is accomplished using the bracketing handwheel procedure which varies the compression ratio (handwheel reading) for the sample and each of two

bracketing reference fuels to obtain a specific ignition delay permitting interpolation of cetane number in terms of handwheel reading. The cetane number was calculated by interpolation of the average handwheel readings proportioned to the cetane numbers of the bracketing reference fuel blends in accordance with equation 9:

$$CN_S = CN_{LRF} + \left(\frac{HW_s - HW_{LRF}}{HW_{HRF} - HW_{LRF}}\right)(CN_{HRF} - CN_{LRF}) \quad (9)$$

where CN_i and HW_i are, respectively, the cetane number and handwheel reading of sample and i may represent the sample (*S*), the low reference fuel (*LRF*, generally n-cetane, also known as n-hexadecane with a CN of 15) and the high reference fuel (*HRF*, generally heptamethylnonane, also known as 2,2,4,4,6,8,8-heptamethylnonane with a CN of 100).

3.3.2.9. Lubricity at 25°C and 60°C

As for cetane number, the lubricity of the E-diesel blends with (2 vol%) and without additive were measured. Blends with 0, 5, 10, 20 and 40 vol% of anhydrous ethanol were investigated. Additionally, an additional sample with 20 vol% of ethanol and 1.0 vol% of additive was also analyzed. This ethanol content limitation was related to the necessity of have a fluid with a viscosity under the diesel fuel specifications. Lubricity was measured in the *Laboratório de Combustíveis e Lubrificantes* (LACOL) at the *Instituto Nacional de Tecnologia* (INT) using a high-frequency reciprocating rig (HFRR) according to the ASTM D6079:2004, shown in Figure 34.

PUC-Rio - Certificação Digital Nº 1312923/CA

Figure 34: PCS Instruments HFRR system in the *Laboratório de Combustíveis e Lubrificantes* (LACOL) at the *Instituto Nacional de Tecnologia* (INT).

PUC-Rio - Certificação Digital Nº 1312923/CA

The PCS Instruments HFRR system uses an electromagnetic vibrator to oscillate a moving steel ball loaded with a 200-g mass with a small amplitude (stroke length: 1 ± 0.02 mm, frequency: 50 ± 1 Hz) against a stationary steel disk completely submerged in a test fuel, as shown in the schematic diagram available in Figure 35.

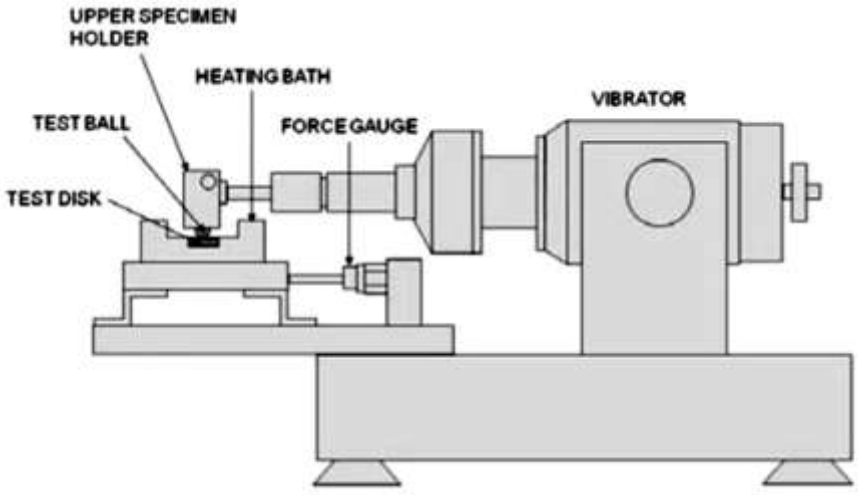

Figure 35: Schematic Diagram of HFRR [ASTM D6079, 2011].

The test disks were previously cleaned up in a beaker with heptane on an ultrasonic cleaner during 7 minutes and then, 2 minutes with acetone before

drying. A 2-mL test specimen of fuel is placed in the test reservoir with a surface area of 6 ± 1 cm² and adjusted to either of the standard temperature (25 or 60°C). The preferred test temperature is 60°C, except when there may be concerns about fuel loss because of its volatility or its degradation because of the temperature. After initial tests at 60°C with a cap to reduce ethanol evaporation, it was decided to reduce the temperature to 25°C for safety issues (low flash point) and for avoiding ethanol evaporation. The ambient relative humidity was maintained between 30 % and 70 %, in function of air temperature, as specified in Figure 36.

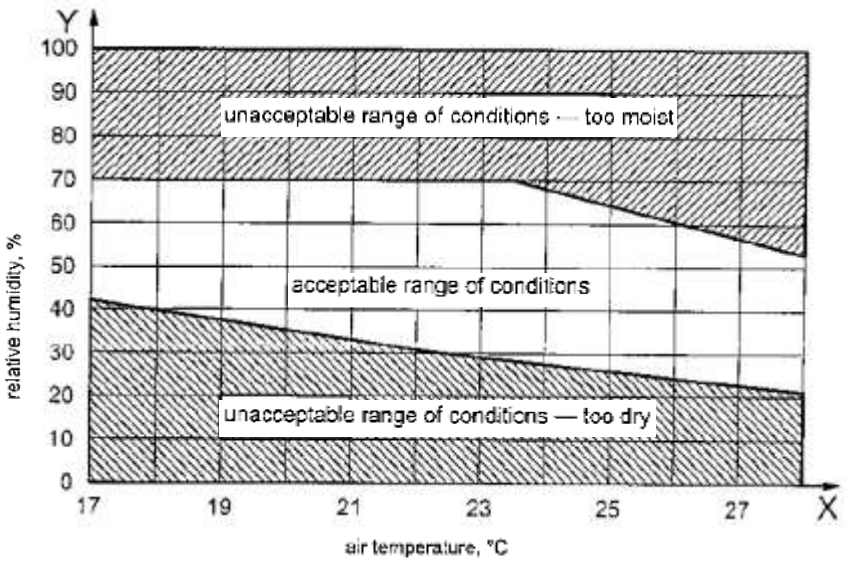

Figure 36: Laboratory air conditions [adapted from the ISO 12156-1, 2006].

At the conclusion of the test (75 minutes), the upper specimen holder is removed from the vibrator arm and cleaned with acetone. Using a microscope digital camera, the dimensions of the major (X) and minor axes (Y) of the wear scar are measured and are recorded by two different persons. Larger is the scar, lower is the lubricity. The mean wear scar diameter (MWSD) is calculated as follow:

$$MWSD = \frac{X + Y}{2} \tag{10}$$

During each test, the profile of temperature, film percentage (assessed through the measurement of contact resistance through the film) and coefficient of friction were recorded.

PUC-Rio - Certificação Digital Nº 1312923/CA

3.3.2.10. Lower Heating Value (LHV)

An evaluation of the lower heating value was done based on the value of the lower heating value (LHV) and specific gravity of all the used compounds. A bibliographic review allowed having some experimental values. An average value and standard deviation were determined for each kind of raw material. These results were used for the calculation of average values of LHV of biodiesel (85% from soybean + 15% from beef tallow), diesel fuel with 7 vol% and 15 vol% of biodiesel and additive. Then, the LHV of E-diesel blends were assessed as:

$$LHV_S = \sum_i \%_i \rho_i LHV_i \quad (11)$$

where LHV_i, ρ_i and $\%_i$ are the lower heating value (given in MJ/kg), the specific gravity and the volumetric ratio of the component *i*, respectively, and *i* can represent each the component of the studied blends (*i*).

At each step, the propagated uncertainty was calculated, using the formulation of Kline and McClintock.

3.4. Evaluation of the Engine Efficiency Running on Diesel B15 Fuel Blended with up to 20 vol% of Anhydrous Ethanol and 1.0 vol% of Additive.

3.4.1. Materials

3.4.1.1. Fuels

The fuel used in this section is S10 diesel B0 fuel blended with biodiesel and anhydrous ethanol 99.9° INPM (provided by B'Herzog). The main physicochemical properties of diesel fuel are given in Table 21, while anhydrous ethanol properties are the same as in the previous sections and they are available in Table 9.

PUC-Rio - Certificação Digital Nº 1312923/CA

Table 21: Physicochemical properties of the studied Brazilian S10 diesel B0 fuel.

Property	Unit	Method (Resolution No. 50, 2013) [Brasil, 2013]	Limit (Resolution No. 50, 2013) [Brasil, 2013]	Value
Aspect	-	ASTM D4176	Limpid and exempt of impurities	Limpid and exempt of impurities
Color	-	Visual	Colorless to yellow	Yellow
Color ASTM	-	ASTM D1500	max 3.0	1.0
Specific Gravity at 20°C	kg/m^3	ASTM D4052	815.0 to 850.0	836.6
Distillation temperature **T10** **T50** **T95**	°C	ASTM D86	 min 180.0 245.0 to 295.0 max 370.0	 187.3 260.0 366,8
Flash Point	°C	ASTM D93	min 38.0	46.0
Cold Filter Plugging Point	°C	ASTM D6371	max 5.0	-2.0
Kinematic viscosity at 40°C	mm^2/s	ASTM D445	2.0 to 4.5	2.590
Total acidity	mg(KOH)/g	ASTM D664		0.01
Total sulphur	mg/kg	ASTM D5453	max 10.0	6.2
Aromatic and Polynuclear Aromatic Content	wt %	ASTM D5186	max 11	25.4
Cetane number	-	ASTM D613	min 48	64.2
Ash	wt %	ASTM D482	max 0.010	< 0.0010
Water by Karl Fischer	mg/kg	ASTM D6304	max 200	7
Total contamination	mg/kg	EN 12662	max 24	2.0
Stability to oxidation	mg/100mL	ASTM D5304	max 2.5	0.2
Lower Heating Value	MJ/kg	ASTM D210		45.713

The diesel fuel had a high aromatic and polynuclear aromatic content, twice higher than the Brazilian specification.

Furthermore, the biodiesel used was a mixture of 80 vol% of soybean biodiesel and 20% of beef tallow biodiesel. These proportions are also characteristic of Brazilian biodiesel added to diesel fuel. This concentration was achieved blending three different biodiesels. The first one is the mixture of 85% of soybean biodiesel and 15% of tallow biodiesel described in the previous section. Pure soybean biodiesel and a mixture of 65% of soybean biodiesel and 35% of tallow biodiesel were also used. Their properties are given in Table 22. An antioxidant (1000 ppm of butylated hydroxytoluene, BHT) was added into the biodiesel to prevent its oxidation.

PUC-Rio - Certificação Digital Nº 1312923/CA

Table 22: Physicochemical properties of the different biodiesel blends used in this section.

Property	Unit	Method (Resolution No. 45, 2014) [Brasil, 2014]	Limit (Resolution No. 45, 2014) [Brasil, 2014]	80 vol% soybean and 20 vol% beef tallow biodiesel	65 vol% soybean and 35 vol% beef tallow biodiesel	100 vol% soybean biodiesel
Aspect	-	NBR 16048	Limpid and exempt of impurities	Limpid and exempt of impurities	Limpid and exempt of impurities	Limpid and exempt of impurities
Specific gravity at 20°C	kg/m^3	NBR 14065	850.0 to 900.0	879.7	878.3	880.9
Kinematic viscosity at 40°C	mm^2/s	NBR 10441	3.0 to 6.0	4.304	4.327	4.145
Water by Karl Fischer	mg/kg	ASTM D6304	max 200	249.0	170	-
Flash Point	°C	NBR 14598	min 100.0	148.1	133.0	-
Esters content	wt %	NBR 15764	min 96.5	98.5	97.4	-
Total sulphur	mg/kg	ASTM D5453	max 10.0	2.2	2.4	-
Sodium and Potassium content	mg/kg	NBR 15556	max 5	0.2	< 0.6	-
Calcium and Magnesium content	mg/kg	NBR 15553	max 5	0.2	< 2.0	-
Phosphorus content	mg/kg	NBR 15553	max 10	0	< 1.0	-
Cold Filter Plugging Point	°C	NBR 14747	max 8.0	3.0	4.0	-
Total acidity	mg(KOH)/g	ASTM D664	max 0.50	0.36	0.34	-
Free glycerol content	wt %	ASTM 6584	max 0.02	0.015	0.020	-
Total glycerol content	wt %	ASTM 6584	max 0.25	0.188	0.196	-
Monoglyceride content	wt %	ASTM 6584	max 0.7	0.615	0.548	-
Diglyceride content	wt %	ASTM 6584	max 0.20	0.089	0.157	-
Triglyceride content	wt %	ASTM 6584	max 0.20	0	0.100	-
Methanol content	wt %	NBR 15343	max 0.20	0.11	-	-
Stability to oxidation	H	EN 14112	min 8	10.76	10.6	-
Total contamination	mg/kg	EN 12662	max 24	-	17.8	-
Iodine value	g(I)/100g	EN 14111	-	-	106	-

The biodiesel blend with 80 vol% soybean and 20 vol% beef tallow presented a higher water content than the value allowed by the ANP's resolution No. 45, 2014) [Brasil, 2014]. It is probably due to contamination of the sample by moisture during the storage.

Moreover, soybean biodiesel and *n*-butanol used as additives were formerly described in Tables 10 and 12. Castor oil properties are given in Table 23.

PUC-Rio - Certificação Digital Nº 1312923/CA

Table 23: Physicochemical properties of the castor oil.

Property	Unit	Method	Value
Aspect at 25°C	-	Visual	Viscous, limpid and colorless to yellow liquid
Specific Gravity at 20°C	-	NBR 14065	0.9602
Specific Gravity at 25°C	-	AOCS Cc 10a-25	0.955
Free fatty acids	%	AOCS Ca 5a-40	0.82
Moisture	%	AOCS Ca 2e-84	0.11
Lovibond Color 5 ¼" (R; Y)	-	AOCS Cc 13b-45	22.0; .22
Iodine - Wijs	cg I2/g	AOCS Cd 1-25	85.73
Hydroxyl	mg(KOH)/g	AOCS Cd 13-60	160.01
Saponification	mg(KOH)/g	AOCS Cd 3-25	180.96

A commercial diesel B7 fuel, bought in a gas station from Rio de Janeiro, was used and its characteristics are given in Table 24.

Table 24: Physicochemical properties of the commercial Brazilian S10 diesel B7 fuel.

Property	Unit	Method [Brasil, 2013]	Limit [ANP, 2013]	Value
Aspect	-	ASTM D4176	Limpid and exempt of impurities	Limpid and exempt of impurities
Color	-	Visual	Colorless to yellow	Yellow
Color ASTM	-	ASTM D1500	max 3.0	1.5
Specific Gravity at 20°C	kg/m^3	ASTM D4052	815.0 to 850.0	833.7
Biodiesel content	vol%	EN 14078	7.0 ± 0.5	7.4
Total sulphur	mg/kg	ASTM D5453	max 10.0	6.56
Distillation temperature **T10** **T50** **T95**	°C	ASTM D86	 min 180.0 245.0 to 295.0 max 370.0	 233.0 289.5 351.5
Carbon residue	wt %	ASTM D524	max 0.25	0.14
Flash Point	°C	ASTM D93	min 38.0	68.5
Cold Filter Plugging Point	°C	ASTM D6371	max 5.0	-3.0
Kinematic viscosity at 40°C	mm^2/s	ASTM D445	2.0 to 4.5	3.466
Cetane number	-	ASTM D4737	min 48	56.6
Ash	wt %	ASTM D482	max 0.010	0.001
Water by Karl Fischer	mg/kg	ASTM D6304	max 200	95.0
Corrosiveness to Cu, 3h at 50°C	-	ASTM D130	max 1	1a

PUC-Rio - Certificação Digital Nº 1312923/CA

3.4.1.2. Engine

In this thesis, a four-stroke compression ignition engine with four-cylinder, model 4.10 TCA by MWM, with maximum power of 107 kW at 2,600 rpm and maximum torque of 430 Nm observed at 1,800 rpm was used and tested in the Laboratory of Vehicular Engineering (*Laboratório de Engenharia Veicular*, LEV) at PUC-Rio. Table 25 shows its main characteristics.

Table 25: Main characteristics of the engine model MWM 4.10 TCA [MWM International, 2007].

Characteristic	Value
Number of cylinders and arrangement	Four cylinder, in line
Number of valves per cylinder	2
Bore	103 mm
Stroke	129 mm
Connecting rod	207 mm
Total cylinder capacity	4.3 L
Compression ratio	15.8:1
Aspiration	Turbo / Aftercooler
Injection system	Mechanical direct injection
Dimension / Weight	796x801x745 mm / 450 kg
Oil lubricant and temperature	SAE 15W-40 / 90-110°C
Water temperature	80-90°C
Maximum working speed	2,600 rpm
Maximum torque	430 Nm a 1,800 rpm
Maximum power	107 kW a 2,600 rpm
Start of injection	9°14’ BTDC
Intake valve opening	3±3° BTDC
Intake valve closing	23±3° ATDC
Exhaust valve opening	33±3° ATDC
Exhaust valve closing	1±3° ATDC
Emission	Euro III

This Euro III emission engine is commonly used in the propulsion of light trucks and commercial vehicles. It was formerly used in the works of Pereira (2006) and Egúsquiza (2011). This is a model with turbo-charging and air aftercooler. Figure 37 gives a view of the engine, focusing on the heat exchanger.

PUC-Rio - Certificação Digital Nº 1312923/CA

Figure 37: View of the tested engine – model MWM 4.10 TCA.

As shown in Figure 38, the injection pump of the test engine is a VE distributor pump mechanically controlled axial-piston distributor fuel, manufactured by BOSCH.

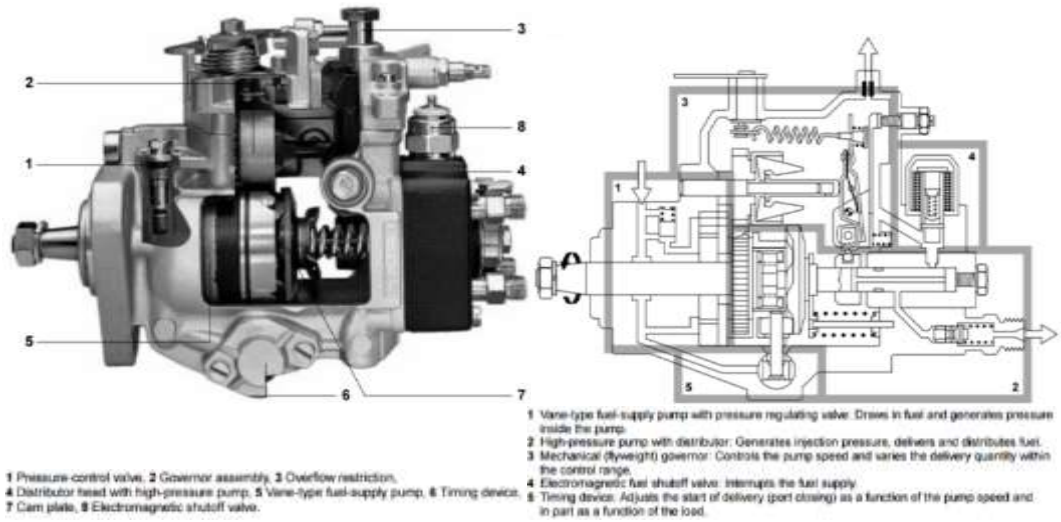

Figure 38: The subassemblies of the Bosch VE distributor pump [Bosch, 1999].

The recommendation provided by the engine manufacturer to adjust the injection advance indicates that when the piston number 1 is at the TDC, the distributor piston of the pump may have displaced 1.04 mm, defined by the distributor cam height. To do this, the withdrawal of the access screw allows the installation of a threaded device for attaching a dial indicator, whose probe must touch the end of the distributor piston inside the injection pump. Thus, by turning up the motor shaft manually when the piston reaches the TDC (determined by the

PUC-Rio - Certificação Digital Nº 1312923/CA

reference in the steering wheel), the dial must indicate a value of 1.04 mm. Figure 39 shows the dial indicator and the steering wheel.

Figure 39: Adjustment of the static injection advance.

Values below 1.04 mm indicate that the injection is delayed compared to the original injection advance, while higher values indicate an earlier injection. The value of 1.04 mm is a "static" adjustment of the start of injection, equivalent to an advance of 9°14’ BTDC. Thus, in order to compensate the lower cetane number of ethanol, we adjusted the start of injection to 10.5° BTDC by displacing 1.25 mm the distributor piston of the pump.

The engine tests were conducted on a dynamometer, model START, manufactured by AVL in the Laboratory of Vehicular Engineering (*Laboratório de Engenharia Veicular*, LEV) at PUC-Rio. This has electric brake ALPHA model 240 and it can test engines with maximum torque up to 550 Nm. The maximum permitted speed and power are 7,500 rpm and 240 kW (approximately 320 hp), respectively. Figure 40 shows the dynometer bench.

Figure 40: Views of the dynamometer bench for testing.

PUC-Rio - Certificação Digital Nº 1312923/CA

On the left of Figure 37, it can be seen a water/water shell-tube heat exchanger, that transfers the heat of the water of the cooling system into the water from a tower. The dynamometer includes a controller that regulates the flow of water tower to the heat exchanger to maintain stable the temperature of the water of the cooling system. To enable this mode of temperature control, the thermostatic valve of the engine was removed so that the cooling water freely circulate through the exchanger. On the right of Figure 37, the cooling of the admission air was conducted through an air / air heat exchanger.

With respect to the lubricating oil temperature, no specific control is made, although the test bank has a water / oil heat exchanger for this purpose. The tests were always carried out ensuring a representative value of the nominal temperature. The oil temperature was also recorded for different points tested.

3.4.1.3. Instrumentation

Figure 41 illustrates the laminar flowmeter model 50MC2-4 from Meriam, used to measure the combustion air intake consumption.

Figure 41: Laminar flowmeter used in the measurement of intake air.

Such equipment is internally constituted by a matrix of capillary tubes, which have the task to force the laminar regime of the intake air. Thus, the flow consumption has an almost linear relationship with the pressure difference measured between the input and the output of the device. Gauge pressure outlets appear at the top of this figure. To ensure proper operation of the laminar flowmeter, straight tubes were installed upstream and downstream of the

PUC-Rio - Certificação Digital Nº 1312923/CA

equipment, whose lengths correspond to ten and five times of the input / output diameter, respectively.

Figure 42 shows the Coriolis flowmeter brand MICRO MOTION, model CMF010 from Micro Motion, used in instant consumption measurements of DBE blends.

Figure 42: Coriolis flowmeter used in the measurement of DBE blends.

Basically, this machine has two components: the sensor (composed of one or two vibrating U-shaped tubes), and an electronic transmitter. When the fuel passes through the tube, the Coriolis effect occurs, causing an inclination on the tube in vibration. This slope is measured by position sensors, which send electric signals to the transmitter nonstandard where electrical signal is generated proportionally to the instantaneous mass flow flowing through the tube. In the fuel supply lines, the connections to Coriolis flowmeter were made via flexible hoses.

A piezoelectric pressure transducer, model 6052CS31U20 from Kistler, capable of measuring dynamic pressures up to 300 bar was installed on the head of the cylinder number 4. Since the output of the piezoelectric transducer is an electric charge, it is necessary to use an amplifier (model FlexiFEM from AVL), which is converted to an amplified voltage signal. Then, the signal is collected by INDIMETER 619 and processed through the INDICOM software, both manufactured by AVL, as shown in Figures 43 and 44.

PUC-Rio - Certificação Digital Nº 1312923/CA

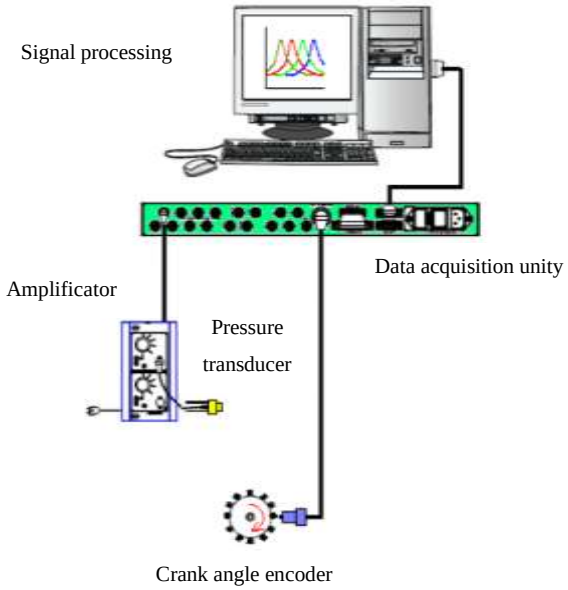

Figure 43: Scheme of the measurement of pressure and crank angle.

Figure 44: Instrumentation used for the measurement of pressure and crank angle.

The angular position was measured using a crank angle encoder (Kistler 2614A1), which have a resolution of 0.1 degree. The transducer is also connected to the INDIMETER 619, relying the pressure reading to the crank angle position. This equipment, in turn, multiplies the number of pulses in order to have a resolution of 1° of the crankshaft axis.

It is important to note that, in order to perform a thermodynamic analysis, measures given by piezoelectric transducer give absolute pressure, using a piezoresistive transducer installed in the engine intake manifold. Indeed, the procedure considered that the pressure in the cylinder at the BDC is equal to the average value of the absolute pressure in the manifold. It can be considered that,

PUC-Rio - Certificação Digital Nº 1312923/CA

at that moment of the cycle, the piston is practically stopped, while the exhaust valve is closed and the intake valve is opened. Therefore, at this instant, the average pressure of the intake manifold is an accurate estimation of the absolute pressure in the cylinder. However, the pressure adjustment factor was calculated considering a measurement interval equal to 5° (beginning at the BDC), in order to reduce the possible noise effects during the measurement. After defining the pressure adjustment factor in this angular range, it was used to estimate the absolute pressures for each value of the crank angle, from their respective dynamic pressures.

Three piezoresistive pressure transducers installed in several location of the engine measured the differential (used to calculate the wet air mass flow) and stationary pressures of inlet air and the pressure of the exhaust gas. All of them were manufactured by Sensotec (FP 2000 series). Moreover, atmospheric humidity was registered with a transducer manufactured by Omega. Type K thermocouples were used to record the temperature of inlet air (also equal to the room temperature) and exhaust gas. The temperature of the fluid in the cooling system of the engine (lubricating oil, engine water and heat exchanger water) were also registered.

PUC-Rio - Certificação Digital Nº 1312923/CA

3.4.2. Methodology

For carrying out the tests, it was adopted a strict criteria in the definition of torque – engine speed pairs. Intermediate engine speeds and torques were selected to facilitate comparative analysis of similar charges (in terms of brake power) at the different engine speeds. Thus, experimental points were determined for three engine speeds (1,500, 1,800 and 2,100 rpm). The values were centered around 1,800 rpm, which is the engine speed where the maximum torque was found. For each fuel and engine speed, the conditions of torque were defined in function of the fraction of maximum torque measured for commercial diesel B7 fuel. Thus, conditions corresponding to 25, 50 and 75% (if possible) of the maximum observed torque for diesel B7 fuel were investigated for each fuel. The other value for torque was defined as the maximum torque observed for the studied blends.

Different fuels were investigated:

(i) Commercial diesel B7 fuel: This fuel was used to assess the values of the torque and to define a baseline, with the performance of the motor with the current fuel;

(ii) Diesel B15 fuel, without ethanol and additive: This fuel was used to assess the contribution of biodiesel in comparison to current commercial diesel;

(iii) Diesel B15 fuel with 5 vol% of anhydrous ethanol and 1 vol% of additive;

(iv) Diesel B15 fuel with 10 vol% of anhydrous ethanol and 1 vol% of additive;

(v) Diesel B15 fuel with 15 vol% of anhydrous ethanol and 1 vol% of additive;

(vi) Diesel B15 fuel with 20 vol% of anhydrous ethanol and 1 vol% of additive.

During a typical series of tests, it was necessary to wait that the temperatures of the cooling water and lubricating oil stabilized around their nominal values (85 and 90°C, respectively) to attain the permanent regime. Then, dynamometer parameters were adjusted to operate the engine to the different operating points with the fuel under study. Then, it was necessary to purge the fuel line, clean the filter (one filter was used for commercial diesel B7 fuel and one other for all DBE blends) and the stabilization of the parameters for the new fuel. The substitution ratio of diesel B15 fuel by anhydrous ethanol was gradually increased and, for each experimental condition, the characteristics of the engine performance were recorded (accelerator position, torque and engine speed, fuel flow and air velocity, pressure in the combustion chamber and displacement of the piston, room and oil temperatures, ambient moisture, temperature and pressure in the exhaustion, oil and cooling water temperature).

To assess the repeatability of the test and an eventual change in the motor performance after running with DBE blends, the test with commercial diesel B7 fuel was repeated.

For each condition examined, the acquisition system is programmed to record 300 cycles of the engine and to calculate the average representative value

PUC-Rio - Certificação Digital Nº 1312923/CA

of the pressure for each value of the crank angle. From the recorded data, several parameters were calculated as described in Chapter 4:

(i) Fuel and air consumptions; air to fuel ratio, lambda, specific fuel consumption for the blends and for ethanol;

(ii) Brake power, Brake Mean Effective Pressure (BMEP), Indicated power and Indicated Mean Effective Pressure (IMEP);

(iii) Combustion characteristics: Polytropic coefficient, Ignition delay, Chemical energy release, CA10, CA50, CA90, maximum pressure, maximum pressure rate and maximum gross heat release rate;

(iv) Efficiency parameters: Fuel Conversion Efficiency ($\boldsymbol{\eta_f}$), Volumetric Efficiency ($\boldsymbol{\eta_v}$), Indicated Efficiency ($\boldsymbol{\eta_i}$), mechanical efficiency ($\boldsymbol{\eta_m}$), ratio of released energy by the injected energy.

PUC-Rio - Certificação Digital Nº 1312923/CA

4 Calculation Procedure

This chapter presents the methodology used in data reduction and analysis of the experimental uncertainties.

4.1. Design of Experiments: Doehlert design

It was chosen to use a two variables Doehlert matrix, a second order design with interaction of order two, which is described by the equation 12:

$$Y = b_0 + b_1X_1 + b_2X_2 + b_{11}X_1^2 + b_{22}X_2^2 + b_{12}X_1X_2 + \varepsilon_{X_1,X_2} \qquad (12)$$

where Y is the experimental response, X_1 and X_2 represent the variables to be optimized, b_0 is an independent term, b_1 and b_2 are the coefficients of the linear terms, b_{11} and b_{22} are the coefficients of the quadratic terms, b_{12} is the coefficient of the interaction (or rectangular) term and ε_{X_1,X_2} is the residue associated to the experimental or model errors.

For a number of factors k, the Doehlert matrix consists of N_o experiments in the center of the domain (generally, N_o=3) and k^2+k experiments uniformly distributed in an hypersphere of radius 1 to form a rhombic lattice (an hexagon in the case of two variables, as shown in Figure 45).

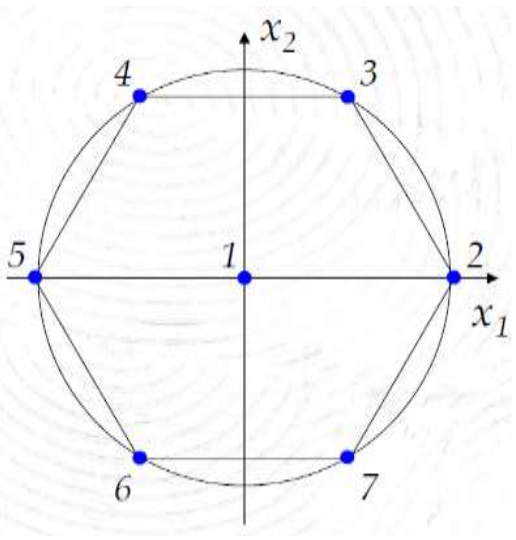

Figure 45: Spatial representation of the Doehlert matrix design [CNAM, 2011].

PUC-Rio - Certificação Digital Nº 1312923/CA

Table 26 gives the coordinates of the experiments in term of reduced variables.

Table 26: Doehlert matrix design in term of reduced variables.

Sample reference	X_1	X_2
1	0	0
2	1	0
3	0.5	0.866
4	-0.5	0.866
5	-1	0
6	-0.5	-0.866
7	0.5	-0.866

In Doehlert matrix, each variable does not have the same number of level, as shown in this table. This property allows the free choice of factors to be assigned either to a large or to small number of levels (minimum of 3), in function of the interest of each factors and the experimental considerations [CNAM, 2011; Ferreira, 2012].

One of its main characteristics is to allow a sequential approach in relation to the domain, as illustrated in Figure 46.

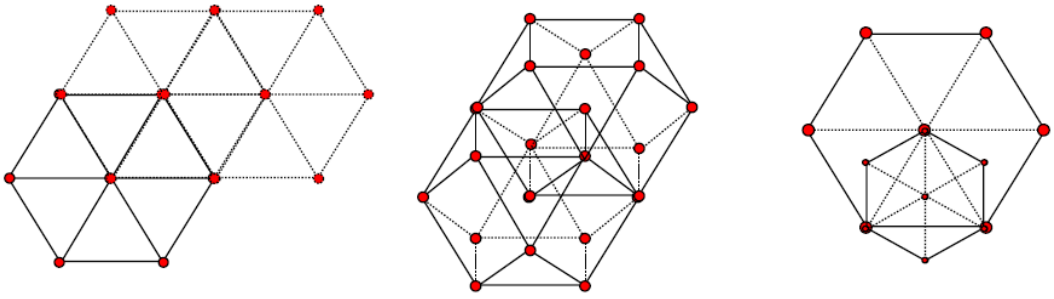

Figure 46: Sequential properties in relation to the experimental domain: translation of the domain for 2 and 3 factors and reduction of the domain (from left to right) [CNAM, 2011].

If the interested experimental domain is adjacent to the studied domain, it is possible to build a new set of experiments around one of the points of the original domain. This comprises part of simulations already carried out, without destroying the existing uniformity. These plans also allow reducing the domain by changing the size of the initial simplex [CNAM, 2011].

PUC-Rio - Certificação Digital Nº 1312923/CA

There is also a sequential property in relation to the number of factors. The Figure 47 illustrated this property.

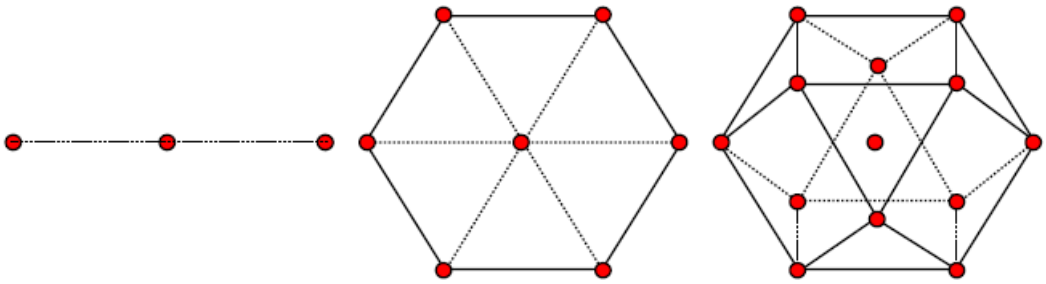

Figure 47: Sequential properties in relation to the number of factors for 1, 2 and 3 factors (from left to right) [CNAM, 2011].

As each simplex is deductible from the simplex of inferior dimension, it is easy to increase the number of variables (or factors) gradually when the initial field of exploration is not suitable.

For a given number of factors k, the minimum number of distinct points of a Doehlert matrix is k^2+k+1. This turns the method relatively inexpensive in term of experiments cost for large k in comparison to other experimental designs conventionally used such as factorial, Box-Behnken and central composite designs. However, the uniformity of the matrix induces a loss of information due to the alignment in space. For two factors, the plan meets the criteria of isovariance but not those of quasi orthogonality or uniform precision: the variance prediction function is identical for all points equidistant from the center of the field [CNAM, 2011].

Defining by Y the vector with the n observed responses, ε the vector with the n residues and B the vector with p parameters, the mathematical model can be written in function of a matrix as given in the equation 13:

$$Y = X.B + \varepsilon \tag{13}$$

where the matrix of effect $X_{(n\times p)}$ and the vector of coefficient B are respectively:

PUC-Rio - Certificação Digital Nº 1312923/CA

$$X = \begin{bmatrix} 1 & X_{1,1}X_{1,1} & X_{1,2}X_{1,2} & X_{1,1} & X_{1,2} & X_{1,1}X_{1,2} \\ 1 & X_{2,1}X_{2,1} & X_{2,2}X_{2,2} & X_{2,1} & X_{2,2} & X_{2,1}X_{2,2} \\ 1 & X_{3,1}X_{3,1} & X_{3,2}X_{3,2} & X_{3,1} & X_{3,2} & X_{3,1}X_{3,2} \\ 1 & X_{4,1}X_{4,1} & X_{4,2}X_{4,2} & X_{4,1} & X_{4,2} & X_{4,1}X_{4,2} \\ 1 & X_{5,1}X_{5,1} & X_{5,2}X_{5,2} & X_{5,1} & X_{5,2} & X_{5,1}X_{5,2} \\ 1 & X_{6,1}X_{6,1} & X_{6,2}X_{6,2} & X_{6,2} & X_{6,2} & X_{6,1}X_{6,2} \\ 1 & X_{7,1}X_{7,1} & X_{7,2}X_{7,2} & X_{7,1} & X_{7,2} & X_{7,1}X_{7,2} \\ 1 & X_{8,1}X_{8,1} & X_{8,2}X_{8,2} & X_{8,1} & X_{8,2} & X_{8,1}X_{8,2} \\ 1 & X_{9,1}X_{9,1} & X_{2,9}X_{2,9} & X_{9,1} & X_{2,9} & X_{9,1}X_{2,9} \end{bmatrix}, B = \begin{bmatrix} b_0 \\ b_{11} \\ b_{22} \\ b_1 \\ b_2 \\ b_{12} \end{bmatrix} \quad (14)$$

As the response vector Y is known and contains the experimental response, the vector of coefficient B has to be determined in a way to have the lower predictive error. The last square method leads defines the solution as:

$$B = (X^t X)^{-1} X^t Y \quad (15)$$

The variance – covariance matrix is:

$$Var_B = (X^t X)^{-1} \sigma^2 \quad (16)$$

where σ^2 is the estimation of residual variance defined, in function of the rank of the matrix, as:

$$\sigma^2 = \frac{(Y - XB)^t . (Y - XB)}{n - rank(X)} \quad (17)$$

The response surface is estimated as:

$$Y^s = X . B \quad (18)$$

To define the reduced of coordinates of the optimum (minimum, maximum or saddle point), it is necessary to solve the following equations system:

$$\begin{cases} \frac{dY^s}{d\mathrm{X}_1} = 0 & (19) \\ \frac{dY^s}{d\mathrm{X}_2} = 0 & (20) \end{cases}$$

With $Y^s = \mathrm{b}_0 + \mathrm{b}_1\mathrm{X}_1 + \mathrm{b}_2\mathrm{X}_2 + \mathrm{b}_{11}\mathrm{X}_1^2 + \mathrm{b}_{22}\mathrm{X}_2^2 + \mathrm{b}_{12}\mathrm{X}_1\mathrm{X}_2$ (21)

$$\Leftrightarrow \begin{cases} \frac{dY^s}{d\mathrm{X}_1} = \mathrm{b}_1 + 2\mathrm{b}_{11}\mathrm{X}_1 + \mathrm{b}_{12}\mathrm{X}_2 = 0 & (22) \\ \frac{dY^s}{d\mathrm{X}_2} = \mathrm{b}_2 + 2\mathrm{b}_{22}\mathrm{X}_2 + \mathrm{b}_{12}\mathrm{X}_1 = 0 & (23) \end{cases}$$

$$\Rightarrow \begin{cases} \mathrm{X}_1 = \frac{2\mathrm{b}_1\mathrm{b}_{22} - \mathrm{b}_2\mathrm{b}_{12}}{b_{12}^2 - 4\mathrm{b}_{11}\mathrm{b}_{22}} & (24) \\ \mathrm{X}_2 = -\left(\frac{\mathrm{b}_1}{\mathrm{b}_{12}} + \frac{2\mathrm{b}_{11}}{\mathrm{b}_{12}}\mathrm{X}_1\right) & (25) \end{cases}$$

PUC-Rio - Certificação Digital Nº 1312923/CA

The kind of optimum depends on the sign of the second derivatives defined in function of the parameters as:

$$\begin{cases} \dfrac{d^2Y^s}{dX_1{}^2} = 2b_{11} & (26) \\ \dfrac{d^2Y^s}{dX_2{}^2} = 2b_{22} & (27) \end{cases}$$

If both second derivatives are negative, the optimum is a maximum. If both second derivatives are positive, the optimum is a minimum. If the two derivatives have different signal, the optimum is a saddle point.

If the stationary point is not inside the experimental domain, the best conditions are calculated in the frontier of the experimental defined as:

$$X_1^2 + X_2^2 = 1 \Leftrightarrow X_2 = \pm\sqrt{1 - X_1^2} \quad (28)$$

Then, the response function can be rewritten as:

$$Y^s = (b_0 + b_{22}) + b_1X_1 \pm (b_2 + b_{12}X_1)\sqrt{1 - X_1^2} + (b_{11} - b_{22})X_1^2 \quad (29)$$

and the determination of the stationary point is resumed as:

$$\frac{dY^s}{dX_1} = \mathrm{b_1} \pm \mathrm{b_{12}}\sqrt{1 - \mathrm{X_1^2}} \pm \frac{\mathrm{X_1(b_2 + b_{12}X_1)}}{\sqrt{1 - \mathrm{X_1^2}}} + 2(\mathrm{b_{11} - b_{22}})\mathrm{X_1} = 0 \quad (30)$$

The sign of X_2 is chosen after determining the value of the response function to eliminate the inadequate value.

4.2. Engine and Combustion Parameters

In this chapter, the methodology used to calculated engine and combustion parameters is presented.

In a general way, it was necessary to process the experimental data to calculate some key parameters that are described in the present section. Some of them required the derivative of pressure, volume and speed, which were calculated as the discrete derivative in the central, except for the first and last point where it was used, respectively, the derivative back and forward, as given in equation 31:

$$\left.\frac{dX}{d\theta}\right|_i = \frac{X_{i+1} - X_{i-1}}{2\Delta\theta}, \left.\frac{dX}{d\theta}\right|_1 = \frac{X_2 - X_1}{\Delta\theta}, \left.\frac{dX}{d\theta}\right|_{\mathrm{N}} = \frac{X_{\mathrm{N}} - X_{\mathrm{N-1}}}{\Delta\theta}, X = p, V \quad (31)$$

PUC-Rio - Certificação Digital Nº 1312923/CA

To eliminate noise due to the measures, the derivative of the pressure was smoothed before any treatment, using a polynomial model and the method of weighted least squares, at the Matlab software.

4.2.1. Geometrical Properties

From the engine geometry data, it was necessary to calculate, for each crank angle, the volume of the combustion chamber in function of the displaced volume V_d and the clearance volume V_c.

$$V_d = \pi \frac{B^2}{4} L, V_c = \frac{V_d}{r_c - 1} \tag{32}$$

where L is the stroke, B is the bore and r_c is the compression ratio.

Therefore, it is necessary to define the ratio of connecting rod length (l) to crank radius (a) and the distance between the crank axis and the piston pin axis (s) (equation (33))

$$a = \frac{L}{2}, s = acos\theta + \sqrt{l^2 - a^2 sin^2\theta} \tag{33}$$

Then, the cylinder volume V at any crank position is given by:

$$V = V_c + \pi \frac{B^2}{4}(l + a - s) \tag{34}$$

As the cylinder geometry is well known, the piston speed profile can be calculated by finite difference from the derivative of the volume divided by the surface of the cylinder base:

$$\frac{dv}{d\theta} = \frac{4}{\pi B^2} \frac{dV}{d\theta} \tag{35}$$

4.2.2. Fuel and Air Consumption

In engine tests, the fuel consumption is measured as a mass flow rate $\dot{m}_f$. A more useful parameter is the specific fuel consumption (*sfc*), define as the fuel flow rate per unit power output:

$$sfc = \frac{\dot{m}_f}{P_b} \tag{36}$$

The mass flow rate of DBE blends ($\dot{m}_f$) and brake power (P_b) were experimentally measured. It measures how efficiently an engine is using the fuel supplied to produce work and it is given in kg/(kW.h).

PUC-Rio - Certificação Digital Nº 1312923/CA

The ethanol specific fuel consumption (sfc_{EtOH}) is calculated from the sfc of the blend, the weight fraction of ethanol in the blends and the sfc of the free-alcohol diesel B15 fuel in the same condition of engine speed and torque (sfc_{B15}):

$$sfc_{EtOH} = \frac{sfc - (1 - \%_{EtOH}^{wt})sfc_{B15}}{\%_{EtOH}^{wt}} \quad (37)$$

The conversion of a determined element of the blends is assessed multiplying its specific fuel consumption by its lower heating value

$$Conversion_i = sfc_i . LHV_i, \qquad i = EtOH, B7, B15 \quad (38)$$

In reference to atmospheric conditions (25°C and 101,325 kPa), the mass flow of moist air consumed by the engine, $\dot{m}_{air,w}$, was determined based on the measurements of the volumetric flow, $\dot{V}_{air,w}$, and the specific gravity $\rho_{air,w}$, as:

$$\dot{m}_{air,w} = \dot{V}_{air,w} . \rho_{air,w} \quad (39)$$

where

$$\dot{V}_{air,w} = \dot{V}_r \left(\frac{\mu_r}{\mu_{air,w}}\right)\left(\frac{T_r}{T_{air,w}}\right)\left(\frac{p_{air,w}}{p_r}\right)\left(\frac{\rho_{air,w}}{\rho_r}\right) \quad (40)$$

The laminar flowmeter calibration curve gives the expression for the volumetric air flow $\dot{V}_r$ in function of the measured pressure difference Δp given in in_{H_2O}:

$$\dot{V}_r(ft^3/min) = 54.1288\Delta p - 0.200199\Delta p^2 \quad (41)$$

However, this ratio was determined using dry air at reference conditions. Thus, in equation (40), the ratio of viscosity, temperature, pressure, and specific gravity represent the correction factors needed to calculate the volumetric flow rate of the moist air mixture. The details of the calculation of these correction factors are given in Appendix C.

The mass flow rate of dry air admitted in the engine $\dot{m}_{air,d}$ was calculated using the values of the mass flow rate of moist air $\dot{m}_{air,w}$ and absolute moisture content ω:

$$\dot{m}_{air,d} = \frac{\dot{m}_{air,w}}{(1 + \omega)} \quad (42)$$

Lambda λ is the ratio of air fuel ratio $(A/F_{DBE})_m$ to the stoichiometric air fuel ratio $(A/F_{DBE})_m^s$. It provides an intuitive way to express leanness conditions mixtures of fuel and air.

PUC-Rio - Certificação Digital Nº 1312923/CA

$$\lambda = \frac{(A/F_{DBE})_m}{(A/F_{DBE})_m^s} \tag{43}$$

The details of the calculation of stoichiometric air fuel ratio are given in Appendix D.

4.2.3. Brake Power (P_b), Brake Mean Effective Pressure (BMEP) and Indicated Mean Effective Pressure (IMEP)

According to Heywood (1988), the brake power (P_b) delivered by the engine and absorbed by the dynamometer is the product of torque (To) and crankshaft engine speed N:

$$P_b = 2\pi NTo \tag{44}$$

Torque is a valuable measure of a particular engine's ability to do work and it depends on engine size. A more useful relative engine performance measure is called the brake mean effective pressure (BMEP) and is calculated dividing the work per cycle by the cylinder volume displaced per cycle (V_d) [Heywood, 1988]:

$$BMEP(kPa) = \frac{P_b.n_R}{V_d.N} = 12{,}56\frac{To(N.m)}{V_d(dm^3)} \tag{45}$$

where n_R is the number of crank revolutions for each power stroke per cylinder (two in the case of a four-stroke cycle).

The indicated work per cycle W (per cylinder) is obtained by integrating around the curve to obtain the area below the curve on the Clapeyron diagram:

$$W = \int p.dV \tag{46}$$

Consequently, the power per cylinder is related to the indicated work per cycle by:

$$P_i = \frac{W.N}{n_R} = \frac{V_d.IMEP.N}{2} \tag{47}$$

where IMEP is the indicated mean effective pressure, the average pressure acting on a piston during the cycle. IMEP is calculated as the sum of the trapezoids under the curve in the Clapeyron diagram:

$$IMEP = \frac{1}{V_d}\sum_{i=1}^{n-1}\left(\frac{p_{i+1}+p_i}{2}\right)(V_{i+1}-V_i) \tag{48}$$

PUC-Rio - Certificação Digital Nº 1312923/CA

where p_i and p_{i+1} are the pressure inside the combustion chamber at two consecutive instants i and i+1, respectively, and V_i and V_{i+1} are the volume of the combustion chamber at the same two consecutive intants i and i+1, respectively.

4.2.4. Combustion Characteristics

With regard to the ignition delay, the beginning of the ignition was determined by analyzing the compression polytropic exponent, and calculating the derivative of the pressure in the cylinder, as described in the following paragraphs.

During the compression and expansion phases of the engine cycle, the relationship between pressure, p, and volume, V, of the cylinder gas mixture is strictly described by the polytropic equation:

$$pV^n = constant \tag{49}$$

Thus, the polytropic exponent can reflect the different characteristics of such processes, including heat exchange with the surrounding. In the initial stage of the compression, the temperature of the mixture is lower than the temperature of the walls of the cylinder. Initially, the polytropic exponent n is higher than the ratio of specific heats ratio γ ($\gamma = c_p/c_v$). As the piston moves, the mixture continues to increase its temperature and its pressure, resulting in a decrease of heat exchange between the walls and the admitted fluid and a decrease of the polytropic exponent. When $n = \gamma$, there is an instantaneous adiabatic process $(T_{wall} = T_{fuel})$ and, as the compression continues, the mixture temperature rise reverses the passage of thermal energy towards the border ($n < \gamma$). This phase extends until the piston reaches the position corresponding to the start of combustion.

Despite the variations in the polytropic exponent, it is considered in many cases an average value representative of the compression process. The estimation of this value is made possible in the logarithmic diagram log(p)-log(V), where the curve is substantially a straight line from the start of the compression until the start of combustion. Therefore, the slope value is equivalent to the average value of the polytropic exponent. A similar phenomenon occurs in the process of expansion, after the end of combustion. In the logarithmic diagram, the points corresponding to the beginning and end of combustion are marked by a notable

PUC-Rio - Certificação Digital Nº 1312923/CA

distance from the linear trend, as the effect of combustion is equivalent to the addition of heat, with a consequent change in values. Thus, the various test conditions, the position was determined by identifying the end point of the straight line associated with compression. Such procedure was described by Egúsquiza (2011) as a reliable procedure.

According to Heywood (1988), the chemical energy or gross heat release rate is given by:

$$\frac{dQ}{d\theta} = \frac{\gamma}{\gamma - 1} p \frac{dV}{d\theta} + \frac{1}{\gamma - 1} V \frac{dp}{d\theta} \tag{50}$$

The value of ratio of specific heat, γ, varies with cylinder gas temperature and, according to Adhikesavan *et al.* (2014), can be calculated through the equation 51:

$$\gamma = \left(1 - \frac{R}{c_p}\right)^{-1} \; with \; \frac{c_p}{R} = A_0 + A_1 T + A_2 T^2 + A_3 T^3 + A_4 T^4 \tag{51}$$

where c_p is the specific heat of the gas at constant pressure (J/(kg.K)), T is the temperature in the cylinder at a particular crank angle (K) and the values of the constants are:

$A_0 = 3.04473$,

$A_1 = 1.33805\ 10^{-3}\ K^{-1}$,

$A_2 = -4.88256\ 10^{-7} K^{-2}$,

$A_3 = 8.55475\ 10^{-11}\ K^{-3}$,

and $A_4 = -5.70132\ 10^{-15}\ K^{-4}$.

The wall heat transfer and blow by losses are not considered to find the heat released due combustion of fuel inside cylinder. This helps to eliminate additional approximation in the analysis of heat release.

To determine the temperature in the cylinder, it is assumed that the unique gas inside the cylinder was wet air. The temperature at a particular crank angle is calculated using the ideal gas law given and as in equation 52:

$$T = \frac{pV}{mR} \tag{52}$$

where m is the mass of wet air (kg) and R is the constant gas of wet air (J/(kg.K)).

According to Merker *et al.* (2006), the start of ignition was determined as the crank angle where 3% of the total heat was released. Then, the time between

PUC-Rio - Certificação Digital Nº 1312923/CA

injection in the diesel engine (10.5° BTDC) and start of combustion, defined as the ignition delay, was calculated.

The combustion progress were represented by the CA10, CA50, CA90, which are respectively the crank angles where 10%, 50% and 90% of the energy due to combustion has been released, maximum pressure, maximum pressure rate and maximum gross heat liberation rate. The total heat released during the combustion process was determined integrating the equation 50, as given in equation (53).

$$Q = \frac{\gamma}{\gamma - 1}\sum_{i=1}^{n-1}\left(\frac{p_{i+1} + p_i}{2}\right)(V_{i+1} - V_i) + \frac{1}{\gamma - 1}\sum_{i=1}^{n-1}\left(\frac{V_{i+1} + V_i}{2}\right)(p_{i+1} - p_i) \quad (53)$$

4.2.5. Efficiency Calculation: Fuel Conversion Efficiency (η_f), Volumetric Efficiency (η_v), Indicated Efficiency (η_i) and Mechanical Efficiency (η_m)

The ratio of the work produced per cycle with the amount of fuel energy supplied per cycle that can be released in the combustion process (the lower heating value, LHV) defines the fuel conversion efficiency η_f [Heywood, 1988].

$$\eta_f = \frac{P_b}{\dot{m}_f . LHV} = \frac{1}{sfc . LHV} \quad (54)$$

The parameter used to measure the effectiveness of an engine's induction process is the volumetric efficiency η_v. It is defined as the ratio of the volume of air induced to the swept volume of the cylinders and can be expressed as:

$$\eta_v = \frac{2\dot{m}_{air,d}}{\rho_{air,d} . V_d . N} \quad (55)$$

where $\rho_{a,i}$ is the dry air specific gravity is given by the ideal gas law:

$$\rho_{air,d} = \frac{p(atm) . M(kg . mol^{-1})}{R . T_{air,d}(K)} \quad (56)$$

with $R = 8{,}2057 . 10^{-5}\ \frac{m^3 . atm}{mol . K}$ and $M = 28{,}96 . 10^{-3}\ \frac{kg}{mol}$.

The indicated efficiency is calculated as:

$$\eta_i = \frac{P_i}{\dot{m}_f . LHV} \quad (57)$$

PUC-Rio - Certificação Digital Nº 1312923/CA

The ratio of the brake (or useful) power delivered by the engine to the indicated power is called the mechanical efficiency η_m:

$$\eta_m = \frac{P_b}{P_i} = \frac{\eta_f}{\eta_i} \tag{58}$$

4.3. Uncertainties

4.3.1. Experimental Uncertainties

The experimental uncertainties of the experimental results are given in the section 5. When more than one measurement was performed, the average value $\bar{x}$ and the standard deviation σ were calculated as defined in equation 59:

$$\bar{x} = \sum_{i=1}^{N} \frac{x_i}{N}, \sigma = \sqrt{\sum_{i=1}^{N} \frac{(x_i - \bar{x})^2}{N-1}} \tag{59}$$

4.3.2. Propagated Uncertainties

All values are given with a standard deviation and a propagated uncertainty calculated according to the formulation of Kline and McClintock. If δR is the uncertainty in the results and δx_1, δx_2, ... , δx_n are the uncertainties in the independent variables (with a 95% confidence interval), then the uncertainty in the result having these odds is given as:

$$\delta R = \left[\left(\frac{\partial R}{\partial x_1}\delta x_1\right)^2 + \left(\frac{\partial R}{\partial x_2}\delta x_2\right)^2 + \cdots + \left(\frac{\partial R}{\partial x_n}\delta x_n\right)^2\right]^{1/2} \tag{60}$$

The values of experimental and propagated uncertainties are given in Appendixes E, F and H and discussed in the section 5.

PUC-Rio - Certificação Digital Nº 1312923/CA

5 Results and Discussion

The results of the tests described in the Experimental Section are given and analyzed in the next paragraphs. To make easier the understanding, the investigated conditions, in terms of diesel fuel and ethanol quality, additive nature and content, temperature and decantation duration, a short description of the performed tests are given in Table 27.

Table 27: Summary of the performed tests conditions, given in chronological order.

Sections	Diesel fuel quality	Ethanol quality	Additive set and content	Temperature / Decantation duration	Description
3.1.2.1. and 5.1.1.	Commercial diesel B7 fuel	Commercial hydrous ethanol	Set 1 (36 additives) / 2.0 vol%	20°C / 1, 2 and 3 hours	Stability of ethanol-diesel blends (49:51)
3.1.2.2. and 5.1.2.	Commercial diesel B7 fuel	Commercial hydrous ethanol	Set 1 (36 additives) / 2.0 to 5.0 vol %	20°C / 1 and 2 hours	Influence of additive concentration in ethanol-diesel (49:51) blends on stability
3.1.2.3. and 5.1.3.	Commercial diesel B7 fuel	Commercial hydrous ethanol	Set 1 (36 additives) / Variable	20°C / 15 minutes	Maximum miscibility of ethanol in diesel fuel with initially 4 vol% of additive
3.1.2.4. and 5.1.4.	Commercial diesel B7 fuel	Anhydrous ethanol	Best additives from Set 1 (4 additives) / 2.0 vol%	10, 20 and 30°C / 1, 2 and 3 days	Influence of temperature in the stability of diesel fuel blended with ethanol (from 0 to 100 vol%)
3.2.2.1. and 5.2.1.	Diesel B7, B15 and B30 fuels	Anhydrous ethanol	Set 2 (28 additives) / 2.0 vol%	10 to 30°C / 1 and 2 hours	Stability study in ethanol-diesel blends (40:60) at different temperatures and biodiesel concentrations
3.2.2.2 and 5.2.2.	Diesel B15 fuel	Anhydrous ethanol	Best additive from Set 2 / 0.0, 0.5, 1.0 and 2.0 vol%	10 to 25°C / 2 hours and 1, 2 and 3 weeks	Impact of the additive in diesel fuel blended with ethanol (from 0 to 100 vol%) in function of temperature and additive content at short to long terms
3.3. and 5.3	Diesel B15 fuel	Anhydrous ethanol	Best additive from Set 2 / 0.0 and 2.0 vol% + 1.0 vol% for E20 blend	NA / NA	Assessment of some physicochemical properties for ethanol – diesel B15 blends
3.4. and 5.4	Diesel B15 fuel	Anhydrous ethanol	Best additive from Set 2 / 1.0 vol%	NA / NA	Evaluation of the engine efficiency of diesel B15 fuel blended with up to 20 vol% of anhydrous ethanol and 1.0 vol% of additive.

PUC-Rio - Certificação Digital Nº 1312923/CA

5.1. Formulation of an Additive to Blend Commercial Additivated Diesel B7 Fuel with Anhydrous and Hydrous Ethanol

5.1.1. Stability Study of Ethanol-Diesel-Additive Blends (48:50:2) at Ambient Temperature

All tested additives were miscible at ambient temperature (20 ± 2°C) in pure diesel B7 fuel and pure hydrous ethanol at the concentration of 2 vol% after 1, 2 and 3 hours. Table 28 gathers the values of separation ratio (SR) for each biodiesel (B) – vegetal oil (O) sources after 3 hours of decantation.

Table 28: Separation ratio (SR) for each biodiesel (B) – vegetal oil (O) sources after 3 hours of decantation.

Samples (B-O source)	1	2	3	4	5	6	7	8	9	Ref
Soybean-Soybean	1.167	1.188	1.167	1.181	1.188	1.188	1.198	1.181	1.194	1.120
Soybean-Castor oil	1.188	1.188	1.167	1.167	1.208	1.194	1.167	1.188	1.188	1.113
Castor oil-Soybean	1.167	1.160	1.146	1.188	1.201	1.188	1.167	1.167	1.146	1.127
Castor oil-Castor oil	1.109	1.042	1.063	1.104	1.125	1.111	1.069	1.104	1.104	1.120

In term of stabilization of the DBE blends, only the additive 7 with 72.5 vol% of biodiesel and 27.5 vol% vegetal oil from soybean delayed the separation by less than 2 hours. Nevertheless, it can be observed in this sample the formation of three phases: a limpid diesel fuel phase (bottom), a cloudy intermediary phase (it can be supposed that there are crystals of biodiesel in suspension) and a limpid ethanol phase (superior). For other additives, phase separation was observed after a few minutes. Samples 1, 8 and 9 had similar behavior, showing a good repeatability of the experiments.

According to Table 28, all additivated and reference samples presented a separation ratio (SR) higher than 1. This indicated that, diesel fuel, biodiesel or additive compounds were dragged with the ethanol into the superior phase.

Values significantly higher than 1 are preferable when phase separation occurred, as it indicates that ethanol interacts better with diesel fuel and biodiesel and their amount dragged into the ethanol phase was higher. Moreover, the SR of

PUC-Rio - Certificação Digital Nº 1312923/CA

additivated samples were higher than the reference samples. Such results showed the efficiency of the additives since more hydrocarbons and esters were dragged into ethanol phase when additive was added to the blends. Some exceptions were found for samples 1 to 4 and 6 to 9 for the additive made of vegetal oil and biodiesel from castor oil. This behavior could be related to the chemical structure of the main compounds of oil and biodiesel. The chemical structure of the linoleic acid (main compound in soybean oil) and ricinoleic acid (main compound in castor oil) is shown in Figure 48.

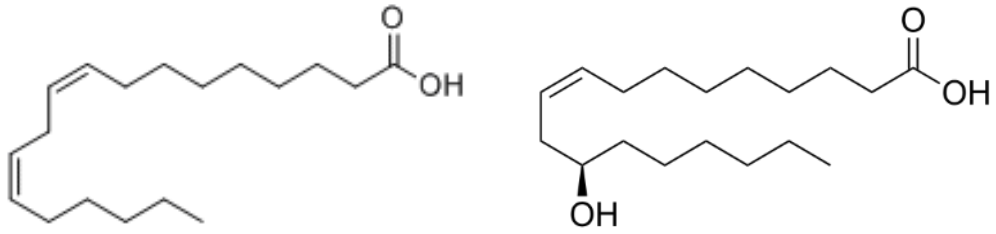

Figure 48: Chemical structure of the main compound of both vegetal oils: linoleic acid in soybean oil (left) and ricinoleic acid in castor oil (right).

PUC-Rio - Certificação Digital Nº 1312923/CA

Indeed, both main compounds from the two different studied sources of oil and biodiesel have the same number of carbon in their chain. However, the material from castor oil has an additional double bound while material from soybean has an alcohol function instead, allowing hydrogen interaction with ethanol (Figure 48). Furthermore, the behavior of samples 5 could be related to the higher affinity of *n*-butanol, main compounds of the additive, with ethanol and water than with diesel fuel, through hydrogen bounds.

5.1.2. Influence of Additive Concentration in Ethanol-Diesel (49:51) Blends at Ambient Temperature

The increase of additive content in the studied range (2 to 5 vol%, by step of 1 vol%) did not influence the miscibility of ethanol in the E-diesel blends since phase separation was observed. An apparent equilibrium was observed after 1 hour of decantation. Figure 49 gives the volumetric ratio between the ethanol phase and diesel fuel phase after decantation for different additive's content.

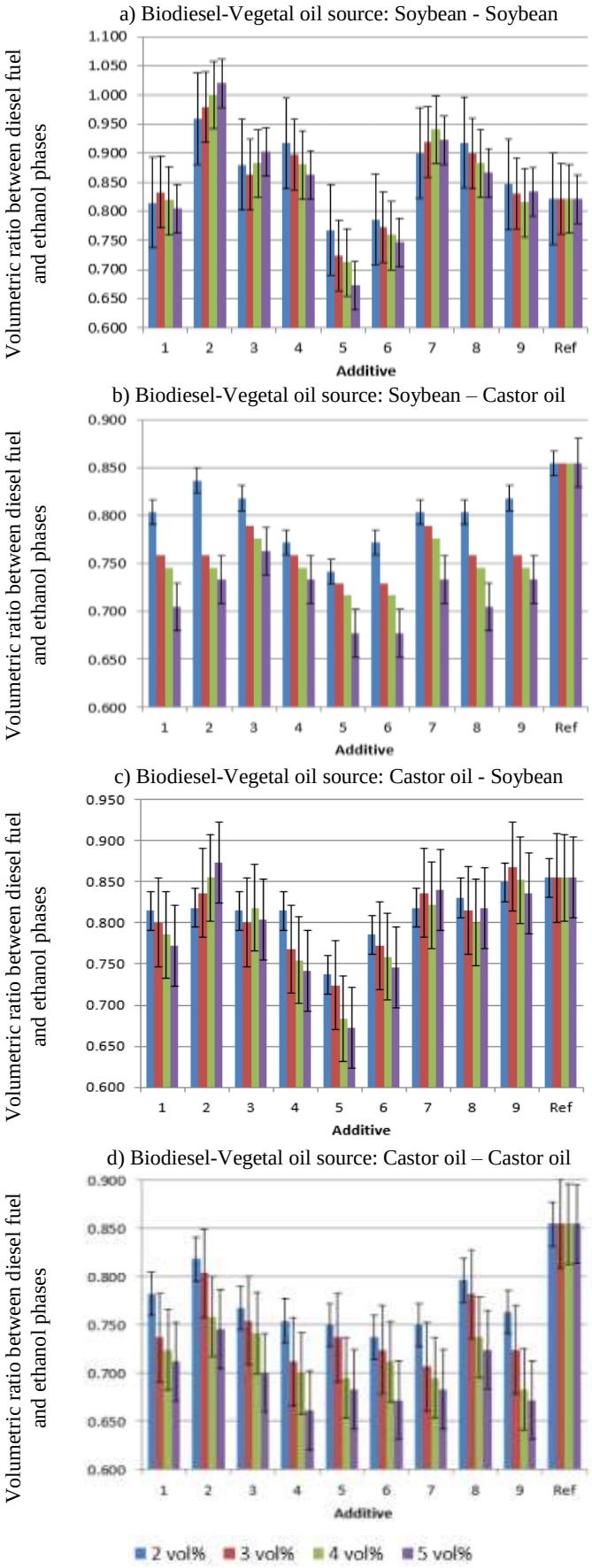

Figure 49: Volumetric ratio between the ethanol phase and diesel fuel phase after decantation for different additive's content.

PUC-Rio - Certificação Digital Nº 1312923/CA

Moreover, in most of the cases, the additive went into the ethanol phase, as the volumetric ratios between diesel fuel and ethanol phases decreased with the addition of additive. Nevertheless, the additives with high biodiesel content from castor oil had the opposite behavior. Again, this indicates that materials from soybean have higher affinity with diesel fuel than materials from castor seeds. For additives with biodiesel from soybean, all volumetric ratios between diesel fuel and ethanol phases were lower than for the reference sample confirming the affinity of these materials with ethanol. Repetition of samples 1, 8 and 9 (in the center of the Doehlert design) presented the same tendency, even if the values were different due to the experimental error, mainly temperature variation. This fact can also explain some apparent random behavior (for instance, samples 8 and 9 from castor oil biodiesel and soybean oil.

5.1.3. Maximum Addition of Hydrous Ethanol in Diesel Fuel with 4 vol% of Additive until Phase Separation at Ambient Temperature

Figure 50 presents the iso-lines of maximum volumetric fraction of hydrous ethanol according to the mathematical models given by the Doehlert design (Appendix E) in terms of reduced variables.

PUC-Rio - Certificação Digital Nº 1312923/CA

a) Biodiesel-Vegetal oil source: Soybean - Soybean

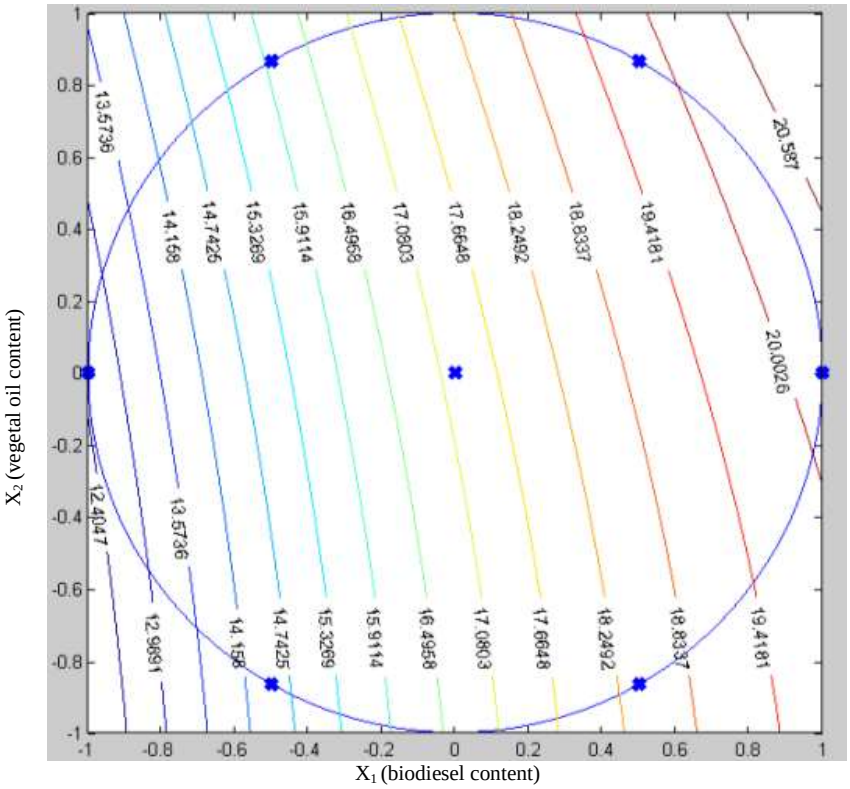

b) Biodiesel-Vegetal oil source: Soybean – Castor oil

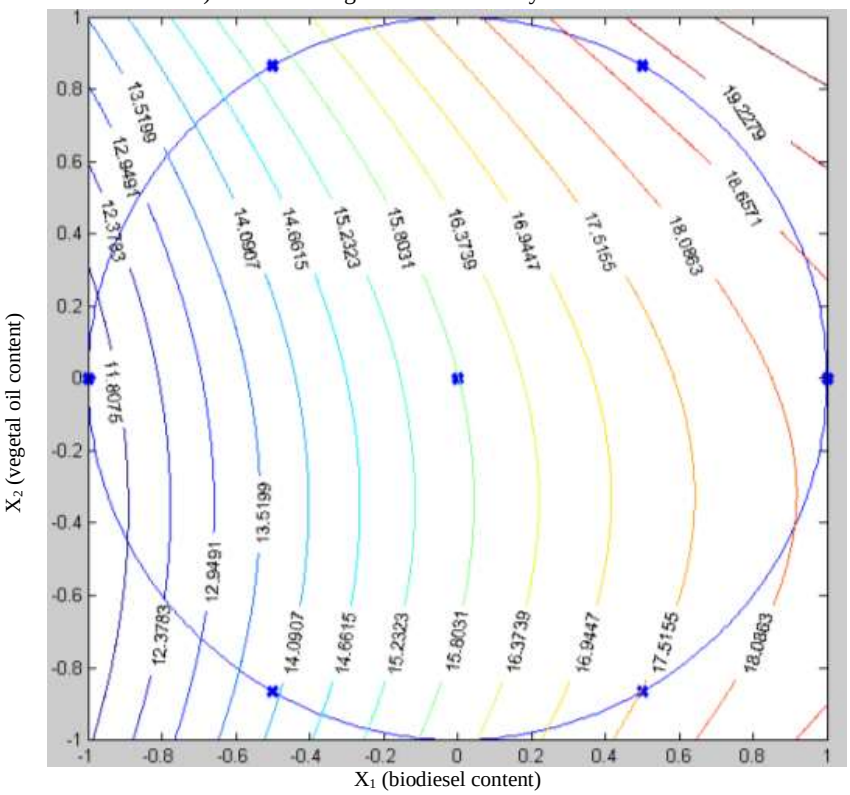

Figure 50: Maximum volumetric fraction (%) of ethanol in 100 mL of diesel fuel with 4 vol% until phase separation after 15 min of decantation (Part 1 of 2).

PUC-Rio - Certificação Digital Nº 1312923/CA

c) Biodiesel-Vegetal oil source: Castor oil - Soybean

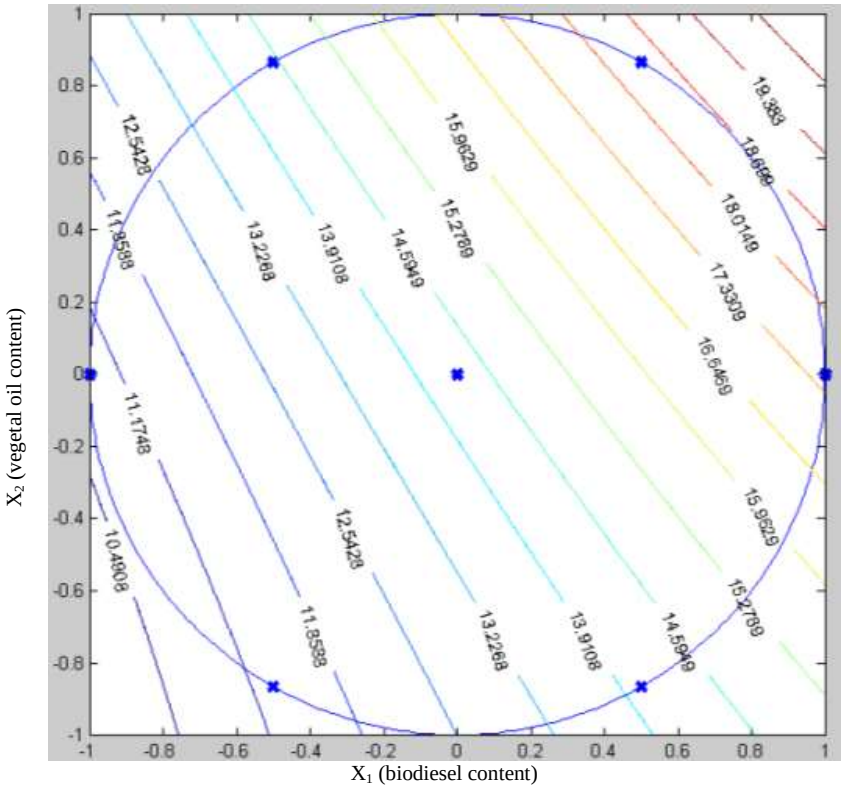

d) Biodiesel-Vegetal oil source: Castor oil – Castor oil

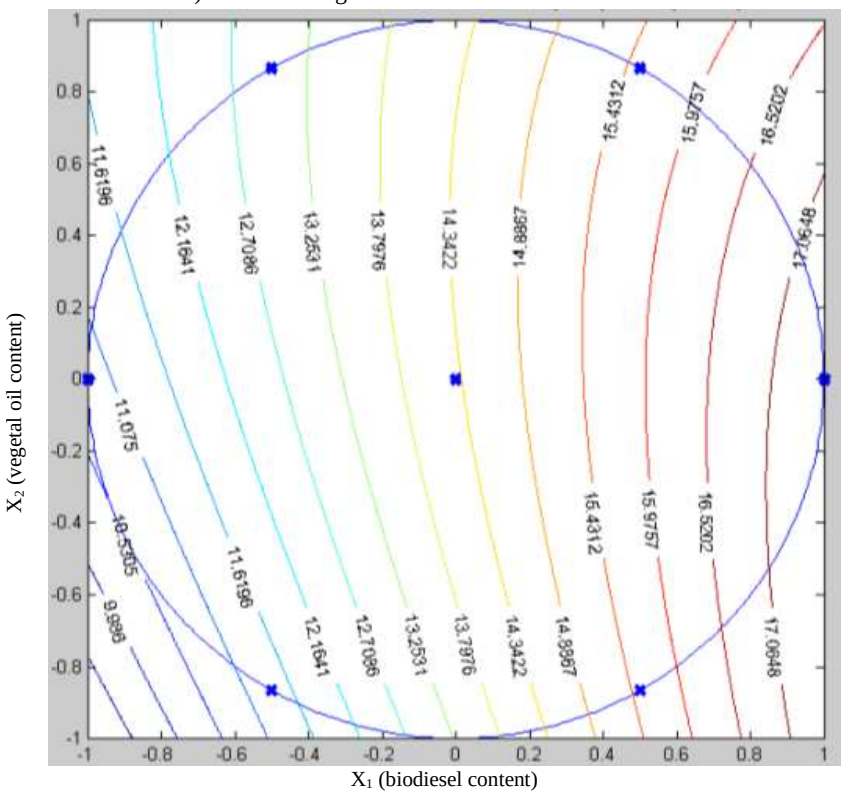

Figure 50: Maximum volumetric fraction (%) of ethanol in 100 mL of diesel fuel with 4 vol% until phase separation after 15 min of decantation (Part 2 of 2).

PUC-Rio - Certificação Digital Nº 1312923/CA

In this figure, it could be observed that a maximum of approximately 20 vol% can be added to 100 mL of diesel fuel without separation after 15 minutes of decantation. Such maximum was observed for the additive with high concentration of biodiesel and vegetal oil from soybean.

For all combination soybean-soybean, soybean – castor oil, castor oil - soybean and castor oil – castor oil, it could be seen that the additives with high *n*-butanol content did not contribute to stabilization. Furthermore, they had an opposite effect as samples with these additives had lower miscibility than E-diesel blends without additives: *n*-butanol acted as an extraction solvent, enhancing phase separation.

In general, additives with high biodiesel and high vegetal oil content presented higher stabilizing ability. Biodiesel and vegetal oil present a good miscibility with ethanol because of their polar characteristic and their long lipophilic carbon chain contributes to the stability with diesel fuel. For additive with biodiesel and vegetal oil from castor oil, the vegetal oil content had lower effect than in the other additives.

At the equilibrium, the separation ratios of all samples were calculated and presented in Table 29.

PUC-Rio - Certificação Digital Nº 1312923/CA

Table 29: Separation ratio (SR) for each biodiesel (B) – vegetal oil (O) sources.

Samples (B-O source)	1	2	3	4	5	6	7	8	9	Ref
Soybean-Soybean	1.000	1.000	0.929	0.909	1.000	1.000	0.923	0.917	0.917	1.120
Soybean-Castor oil	1.000	1.000	1.000	1.000	1.000	1.000	1.000	1.000	1.000	1.113
Castor oil-Soybean	1.400	1.250	1.231	1.500	1.500	1.500	1.400	1.400	1.400	1.127
Castor oil-Castor oil	0.800	0.750	0.750	0.778	0.750	0.750	0.833	0.800	0.800	1.120

It can be observed a good repeatability of the experiments. Only samples additivated with biodiesel from castor oil and vegetal oil from soybean had SR higher than the reference samples. This indicates that these additives dragged more diesel fuel, biodiesel or additive compounds than the others into the ethanol

phase. Considering this aspect, additives from castor oil biodiesel and soybean oil allowed a higher miscibility of ethanol in diesel fuel.

Based on the results of the maximum volume before separation, the mathematical models allowed the determination of the optimum composition of the best additives for each combination biodiesel–vegetal oil. The stationary points given by the model (see Appendix E) were outside of the experimental domain. Consequently, an alternative procedure was used. A qualitative inspection of the results showed that better results were obtained for vegetal oil content higher than 5.0 vol% (positive value of X_2). The composition defined by this procedure was given in Table 30.

Table 30: Best additive's composition for each biodiesel – vegetal oil sources.

Additive number	Biodiesel – Vegetal oil source	Biodiesel content (vol%)	Vegetal oil content (vol%)	*n*-butanol content (vol%)
1	**Soybean-Soybean**	91.6	7.2	1.2
2	**Soybean-Castor oil**	78.9	9.4	11.7
3	**Castor oil-Soybean**	83.3	8.9	7.8
4	**Castor oil-Castor oil**	95.0	5.0	0.0

In Table 30, it can be observed that biodiesel was the main contributor to the additive, since ethanol presents a good miscibility with biodiesel because of its polar character. Moreover, vegetal oil content was higher in the additive formulation when biodiesel and vegetal oil came from different sources, showing a synergy between them offered by the variety of carbon chain length.

5.1.4. Influence of Temperature in the Stability of Anhydrous Ethanol – Diesel Blends with 2 vol% of Additive

In order to define a reference situation and assess the impact of the additives, the stability of E-diesel blends without additive was investigated at 10, 20 and 30°C. The separation ratios (SR) after 3 days of decantation in function of temperature of anhydrous ethanol-diesel fuel without additive at 10, 20 and 30°C are given in Figure 51. Stable blends are represented by null SR ratio. The uncertainty on the results was calculated from the results of section 5.1.2 and is equal to ± 0.028.

PUC-Rio - Certificação Digital Nº 1312923/CA

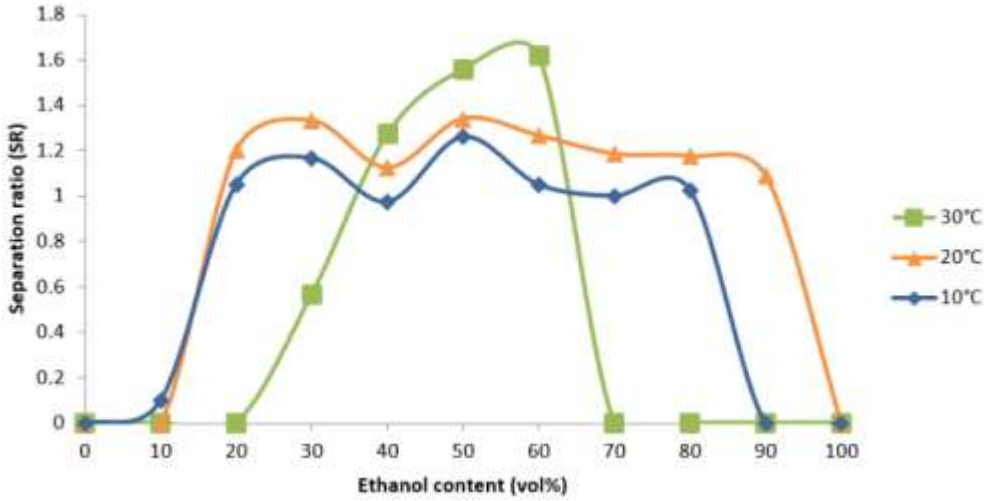

Figure 51: Separation ratio (SR) after 3 days of decantation in function of temperature of anhydrous ethanol-diesel fuel without additive at 10, 20 and 30°C.

Figure 51 shows that, at a determined temperature, the separation ratios were *quasi* constant for the unstable two-phase' blends (stable blends are represented by null SR ratio). When temperature decreased, the range of stability decreased and tended to 1.0, as low temperatures were not favorable to drag other compounds (diesel fuel, biodiesel or additive) into ethanol phase.

Moreover, when fuels were not miscible, it could be observed, at 10°C, the formation of a multiphasic solution. From 2 to 5 phases could be observed and white crystals could be also observed in blends with 80 and 90 vol% of anhydrous ethanol, as illustrated in Figure 52.

Figure 52: Multiple phases system for blends with 40 vol% of ethanol (left) and crystals observed in blends with 90 and 80 vol% of anhydrous ethanol (right), after 3 days of decantation at 10°C.

PUC-Rio - Certificação Digital Nº 1312923/CA

Figure 53 presents the separation ratio (SR) after 3 days of decantation in function of anhydrous ethanol content at 20°C and 10°C in ethanol-diesel fuel. Stable blends are represented by null SR ratio, as defined previously. The uncertainty on the results was calculated from the results of section 5.1.2 and is equal to ± 0.028.

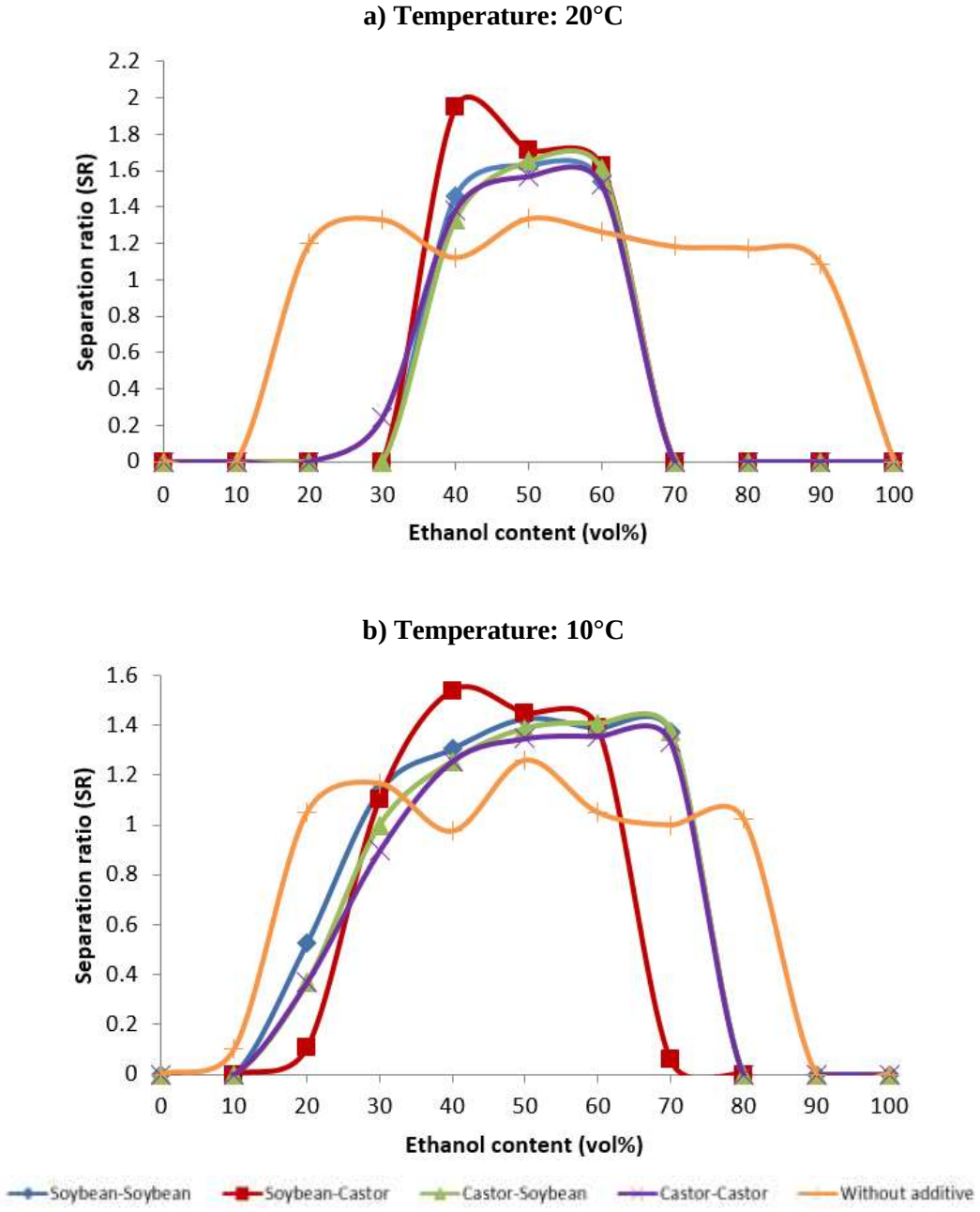

Figure 53: Separation ratio (SR) after 3 days of decantation in function of anhydrous ethanol content at 20°C (top) and 10°C (bottom) in ethanol – diesel fuel.

PUC-Rio - Certificação Digital Nº 1312923/CA

At 30°C, all additivated samples were homogeneous while in absence of additive, ethanol-diesel blends formed 2 phases when ethanol content varied from 30 to 60 vol%. At 20°C, samples with anhydrous ethanol content between 30 and 60 vol% presented phase separation while at 10°C, only blends with ethanol concentration in the ranges of 0 to 10 and 80 to 100 vol% were stable. Nevertheless, at such low temperature and for high ethanol content (80 and 90 vol%), white deposits were observed at the bottom of the vessel, probably crystals of biodiesel.

Moreover, the presence of additive led to a better stability of ethanol-diesel blends since no separation was observed at 30°C. The range of instability was narrower and the separation ratio was higher with additive at 20 and 10°C: even if blends were immiscible, the ethanol phase contained organic compounds. Based on this observation, additive with biodiesel from soybean and vegetal oil from castor oil was the best tested additive, showing a synergy between the variety of carbon chain length and moieties.

PUC-Rio - Certificação Digital Nº 1312923/CA

5.1.5. Partial Conclusion

The additives synthesized from the experimental design showed that, for all combination of biodiesel – vegetal oil, the additives with high *n*-butanol content did not contribute to stabilization. It acted as an extraction solvent, due to the higher affinity of *n*-butanol through hydrogen bounds with alcohols and water than with diesel fuel. It can be observed that biodiesel is always the main compounds in the formulation of the best additives. In a general point of view, additives with high biodiesel and high vegetal oil contents presented higher stabilizing ability. Biodiesel and vegetal oil have both a polar character, due to the carboxylic acid moiety, and an apolar character, due to the long lipophilic carbon chain. Consequently, they have a good miscibility in ethanol and in diesel fuel. Moreover, vegetal oil content was higher in the additive formulation when biodiesel and vegetal oil came from different sources, showing a synergy between them offered by the variety of carbon chain length.

The increase of additive content in the studied range did not influence the miscibility of ethanol in the E-diesel blends as phase separation was observed. Moreover, the additive was generally going into the ethanol phase, but the

additives with high content biodiesel from castor seeds had the opposite behavior, due to the chemical structure of the compounds.

Considering the ability of the best additives for each combination of biodiesel and vegetal oil to improve miscibility of blends with anhydrous ethanol, the presence of additive led to a better stability of diesel fuel-anhydrous ethanol blends. No separation was observed at 30°C and, at 20°C and 10°C, the range of instability was narrower and the separation ratio was higher with additive. Even if blends were immiscible, the ethanol phase contained organic compounds. Among the tested additives, additive with biodiesel from soybean and vegetal oil from castor seeds (additive No 2 in Table 28) presented the best stabilizing properties, showing a synergy between the variety of carbon chain length and moieties.

Based on the presented results, additives with higher refined vegetal oil fraction could be tested to increase the bridging power of the co-solvent and ethanol with low moisture content has to be used to guarantee the stability. Moreover, as the Resolution n°03 of the *Conselho Nacional de Política Energética (CNPE)* published on the *Diário Oficial da União da Resolução n° 03* [Brasil, 2015a] allowed the commercialization and the volunteer use of biodiesel into fossil diesel fuel up to 20 vol% in captive fleets and 30 vol% for rail and for agricultural and industrial use, it was decided to investigate diesel fuel blends with up to 30 vol% of biodiesel.

PUC-Rio - Certificação Digital Nº 1312923/CA

5.2. Formulation of an Additive to Blend Diesel B0 Fuel with Variable Anhydrous Ethanol and Biodiesel's Content

5.2.1. Stability Study of the Additives in DBE Blends at Different Temperatures and Different Biodiesel Concentration

All tested additives were miscible at ambient temperature (20 ± 2°C) in both pure B7, B15 and B30 diesel fuels and in pure anhydrous ethanol. Figure 54 presents the separation ratio (SR) after 2 hours of decantation for diesel B7 fuel at 25°C and 30°C for all tested additives.

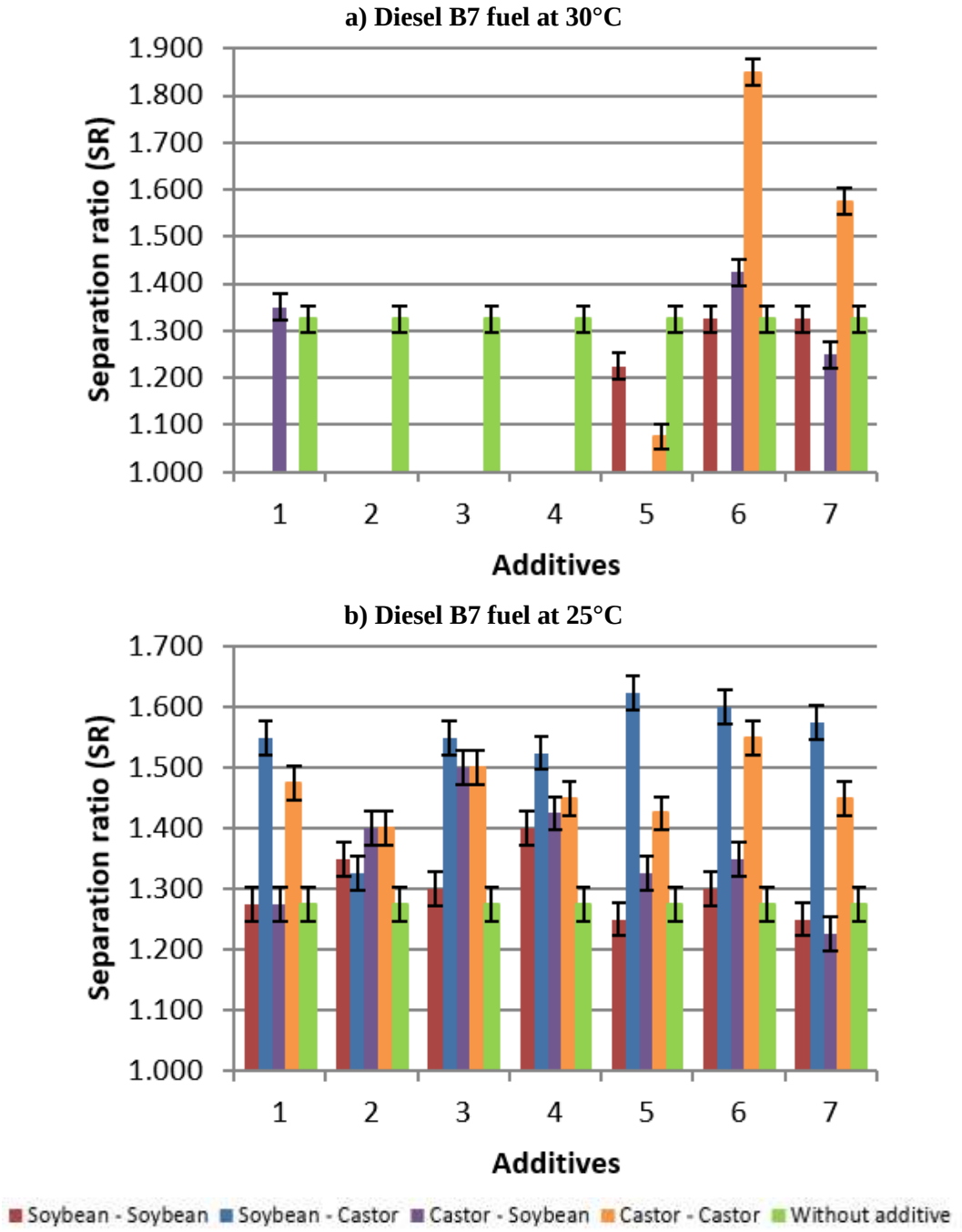

Figure 54: Separation ratio (SR) after 2 hours of decantation for diesel B7 fuel at 30°C (top) and 25°C (bottom) for all tested additives.

According to Figure 54, commercial diesel B7 fuel used as reference sample separated into two phase (SR = 1.300) at 30°C, but all family of additives had at least 4 additives resulting into a stable solution (SR = 0.000). At 25°C, no sample was stable and the best tested additive was the sample 5, with biodiesel from soybean and the vegetal oil from castor seeds.

At 25°C, all additivated and reference diesel B15 fuel samples were stable. At 20°C, separation was observed in the reference sample (SR = 2.273), but all

PUC-Rio - Certificação Digital Nº 1312923/CA

additivated samples remained stable. Figure 55 presents the separation ratio (SR) after 2 hours of decantation for diesel B15 fuel at 15°C and 10°C for all tested additives

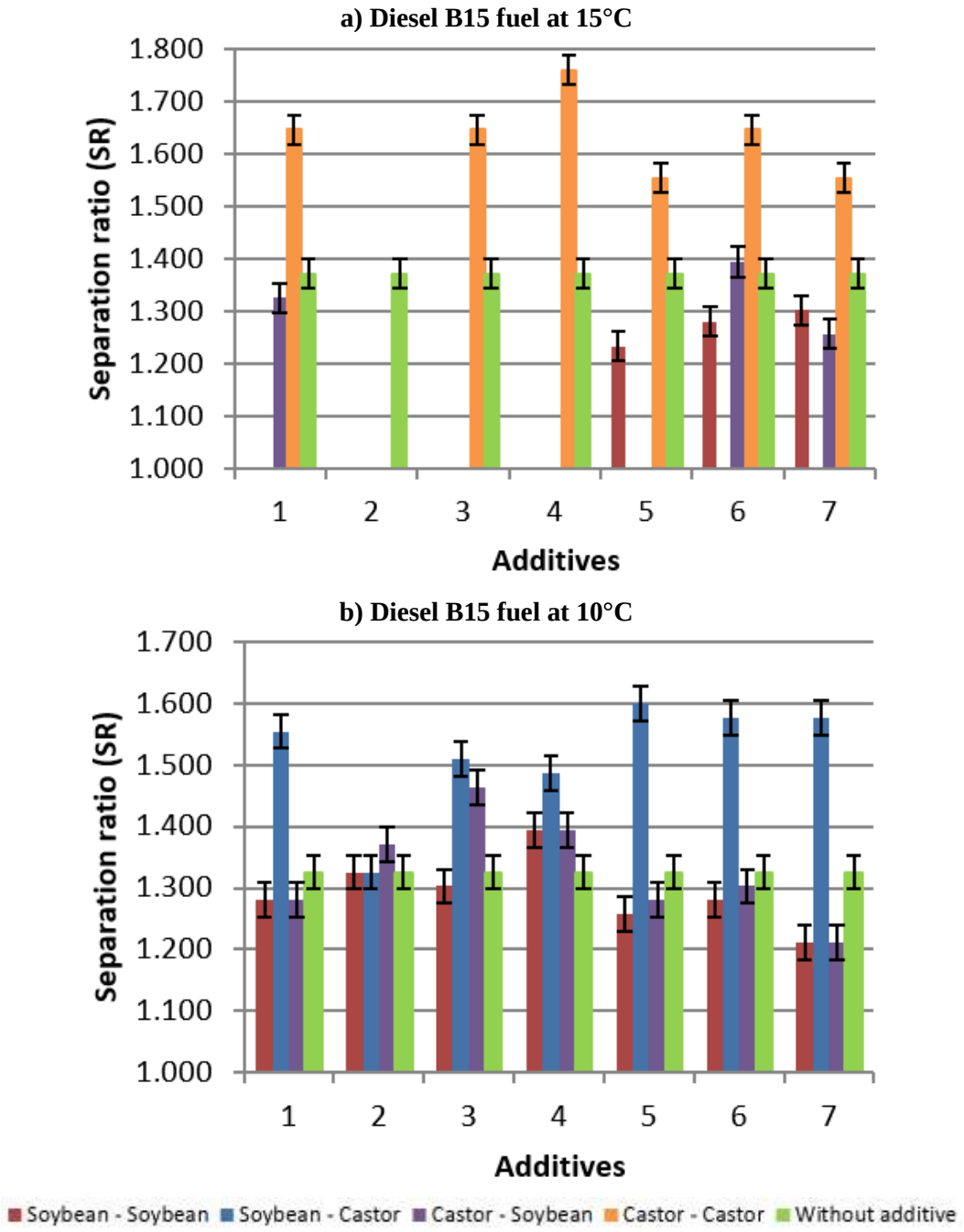

Figure 55: Separation ratio (SR) after 2 hours of decantation for diesel B15 fuel at 15°C (top) and 10°C (bottom) for all tested additives.

According to Figure 55, at 15°C, all samples with biodiesel from soybean and the vegetal oil from castor seeds were stable while only one sample was stable (Sample 2) for the additives based only on castor seeds biomass. Other

PUC-Rio - Certificação Digital Nº 1312923/CA

combinations of biomass presented, at least, 4 stable blends. At 10°C, no sample was stable and the best tested additive was, again, the sample 5, with biodiesel from soybean and the vegetal oil from castor seeds. The separation ratio of the reference sample decreased with temperature (SR = 1.336 at 15°C and 1.290 at 10°C).

In Figures 54 and 55, some samples had a lower separation ratio than the reference, indicating that the additive acted as an extraction solvent and not as a co-solvent.

For diesel B30 mixtures, all blends were stable, but a white solid appeared in solution for temperatures inferior to 0°C. Such behavior was expected and it is in accordance with literature [Lapuerta, 2009]. Again, it can be supposed that it was related to the crystallization of biodiesel [Hanna, 1996]. The effect of ethanol was hidden by the high content of biodiesel.

Comparing additives with the same proportion of each compound, but from different sources, the additives formulated with biodiesel from soybean and the vegetal oil from castor seeds for both tested diesel BX - ethanol blends always presented the best performance. Moreover, it can be seen that such combination allowed a higher tolerance to experimental variation on the formulation of the additive, in particular for higher temperature. The only exception is the formulation of the sample 2 (worst additive) with 5 vol% of castor oil and 5 vol% of *n*-butanol. This showed the necessity of a synergy between the vegetal oil and the other compounds of the additive to stabilize the DBE blends.

When phase separation was observed, all tested blends had a higher separation ratio than 1.000. Values significantly higher than 1 are recommended when phase separation occurred, as it indicates that ethanol interacts better with diesel fuel and biodiesel. Moreover, the biofuel theoretical separation ratio considering that ethanol and biodiesel were both going into the superior phase (SR = 1.105 for B7 and 1.226 for B15) was lower than the experimental values. For this reason, it can be supposed that all biodiesel from the blend was going into the ethanol phase, dragging a small volume of diesel fuel with it.

The separation ratios (SR) after 2 hours of decantation and volumetric ratio for ethanol and both biofuels for diesel B7 and B15 fuels in function of the investigated temperature are presented in Figure 56.

PUC-Rio - Certificação Digital Nº 1312923/CA

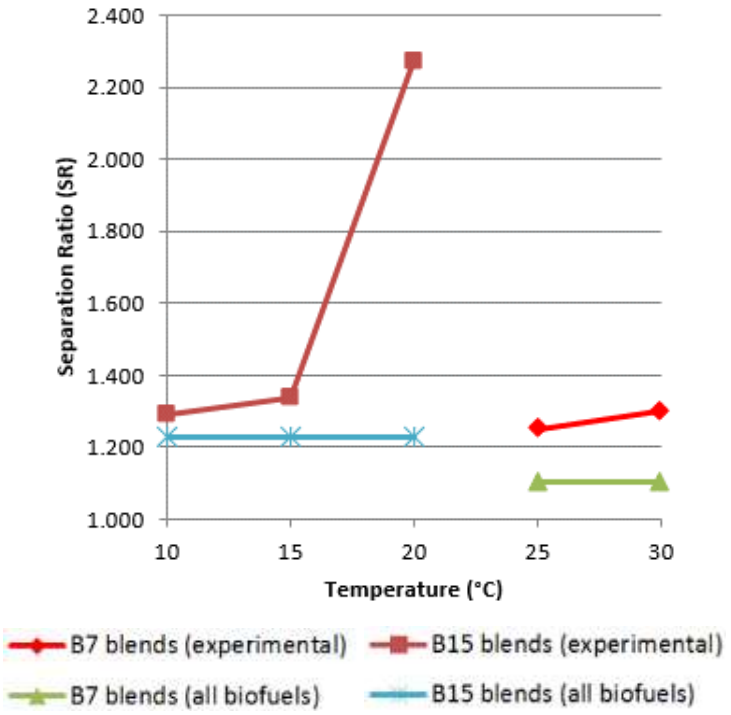

Figure 56: Separation ratio (SR) after 2 hours of decantation and volumetric ratio for ethanol and both biofuels for diesel B7 and B15 fuels in function of the investigated temperature (°C).

PUC-Rio - Certificação Digital Nº 1312923/CA

Based on Figure 56, it is a good hypothesis to assume that the separation ratio tends to the value of the biofuel (ethanol and biodiesel) separation ratio when temperature decreases: $SR_{bio} = \frac{V_{sep}}{V_e + V_{bd}}$.

Based on the previous comments, the best additive was the mixture of soybean biodiesel and castor oil for the tested DBE blends, in particular diesel B7 and B15 fuels. Consequently, mathematical models allowing the determination of the optimum composition of the best additives were used for diesel B7 fuel at 25°C and diesel B15 fuel at 10°C. Nevertheless, both solutions were not in the experimental domain. Consequently, the best additive was defined as a mixture of 72.5 vol% of castor oil, 17.5 vol% of soybean biodiesel and 10 vol% of *n*-butanol.

Moreover, as a biodiesel content of 30 vol% in diesel fuel is a long-term perspective of a commercial blend for compression ignition engine, it was decided to investigate diesel fuel blends with 15 vol% of biodiesel that can be a reality in at a medium term.

5.2.2. Impact of the Best Additive in Anhydrous Ethanol-Diesel B15 Blends at Different Ethanol Concentration in Function of Temperature and Additive Content

At 25°C, all tested samples were stable. The 15 vol% of biodiesel added to diesel fuel was sufficient to maintain the stability of the blends at this temperature. The experimental results at lower temperatures were gathered in the Table 31 and Figures 57 and 58. The uncertainty on the results was calculated from the results of section 5.1.2 and is equal to ± 0.028.

Table 31: Separation ratio (SR) and stability range for E-diesel (B15) blends in function of the ethanol content, additive content and temperature.

<table>
<tr><td rowspan="3">Ethanol content (vol%)</td><td colspan="4">T = 20°C</td><td colspan="4">T = 15°C</td><td colspan="4">T = 10°C</td></tr>
<tr><td colspan="12">Additive content (vol%)</td></tr>
<tr><td>0.0</td><td>0.5</td><td>1.0</td><td>2.0</td><td>0.0</td><td>0.5</td><td>1.0</td><td>2.0</td><td>0.0</td><td>0.5</td><td>1.0</td><td>2.0</td></tr>
<tr><td>0</td><td colspan="4" rowspan="2">Stable blends without additive</td><td colspan="4" rowspan="2">Stable blends without additive</td><td colspan="4" rowspan="2">Stable blends without additive</td></tr>
<tr><td>10</td></tr>
<tr><td>20</td><td colspan="4" rowspan="2">Stable blends without additive</td><td>0.350</td><td colspan="3" rowspan="2">Stability gain</td><td>0.200</td><td>0.250</td><td colspan="2">Stability gain</td></tr>
<tr><td>30</td><td>0.673</td><td>0.909</td><td>0.967</td><td>0.900</td><td>0.825</td></tr>
<tr><td>40</td><td>1.550</td><td>1.733</td><td colspan="2">Stability gain</td><td>1.375</td><td>1.425</td><td>1.535</td><td>1.667</td><td>1.338</td><td>1.350</td><td>1.375</td><td>1.436</td></tr>
<tr><td>50</td><td>1.660</td><td>1.604</td><td>1.683</td><td>1.824</td><td>1.440</td><td>1.480</td><td>1.564</td><td>1.608</td><td>1.394</td><td>1.400</td><td>1.440</td><td>1.505</td></tr>
<tr><td>60</td><td>1.502</td><td>1.520</td><td>1.536</td><td>1.586</td><td>1.417</td><td>1.452</td><td>1.503</td><td>1.505</td><td>1.400</td><td>1.403</td><td>1.419</td><td>1.454</td></tr>
<tr><td>70</td><td colspan="4" rowspan="3">Stable blends without additive</td><td>1.414</td><td>1.414</td><td colspan="2">Stability gain</td><td>1.385</td><td>1.386</td><td>1.371</td><td>1.414</td></tr>
<tr><td>80</td><td colspan="4" rowspan="3">Stable blends without additive</td><td colspan="4" rowspan="3">Stable blends without additive</td></tr>
<tr><td>90</td></tr>
<tr><td>100</td></tr>
</table>

PUC-Rio - Certificação Digital Nº 1312923/CA

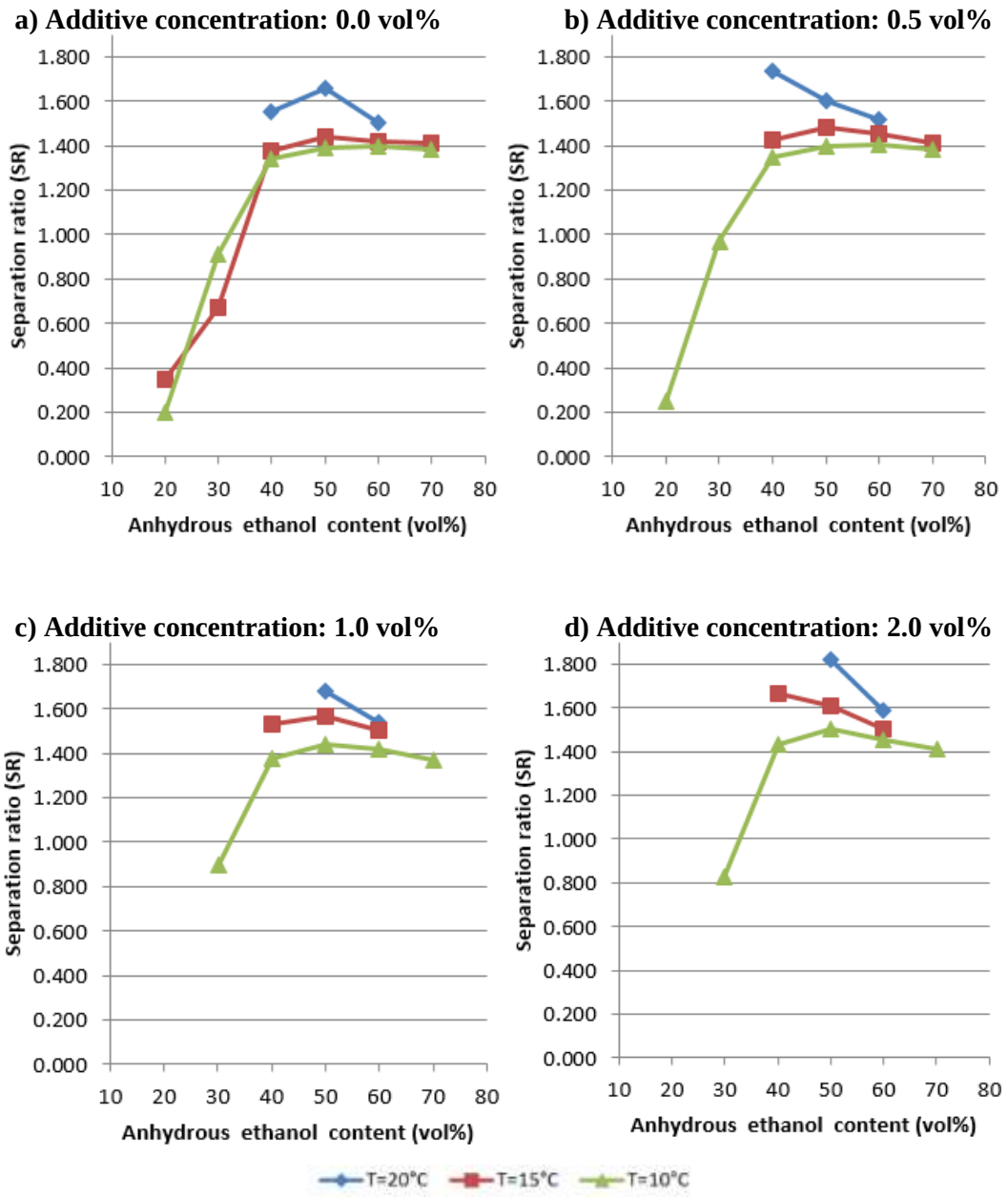

Figure 57: Separation ratio (SR) for E-diesel (B15) unstable blends in function of the ethanol content and temperature for a) 0.0, b) 0.5, c) 1.0 and d) 2.0 vol% of additive.

For lower temperatures, unstable regions appeared, but the addition of additive implied a higher stability region (10 to 30 vol% higher than the non additivated blends) and an increase of the separation ratio. Few exceptions of the former described behavior were observed.

PUC-Rio - Certificação Digital Nº 1312923/CA

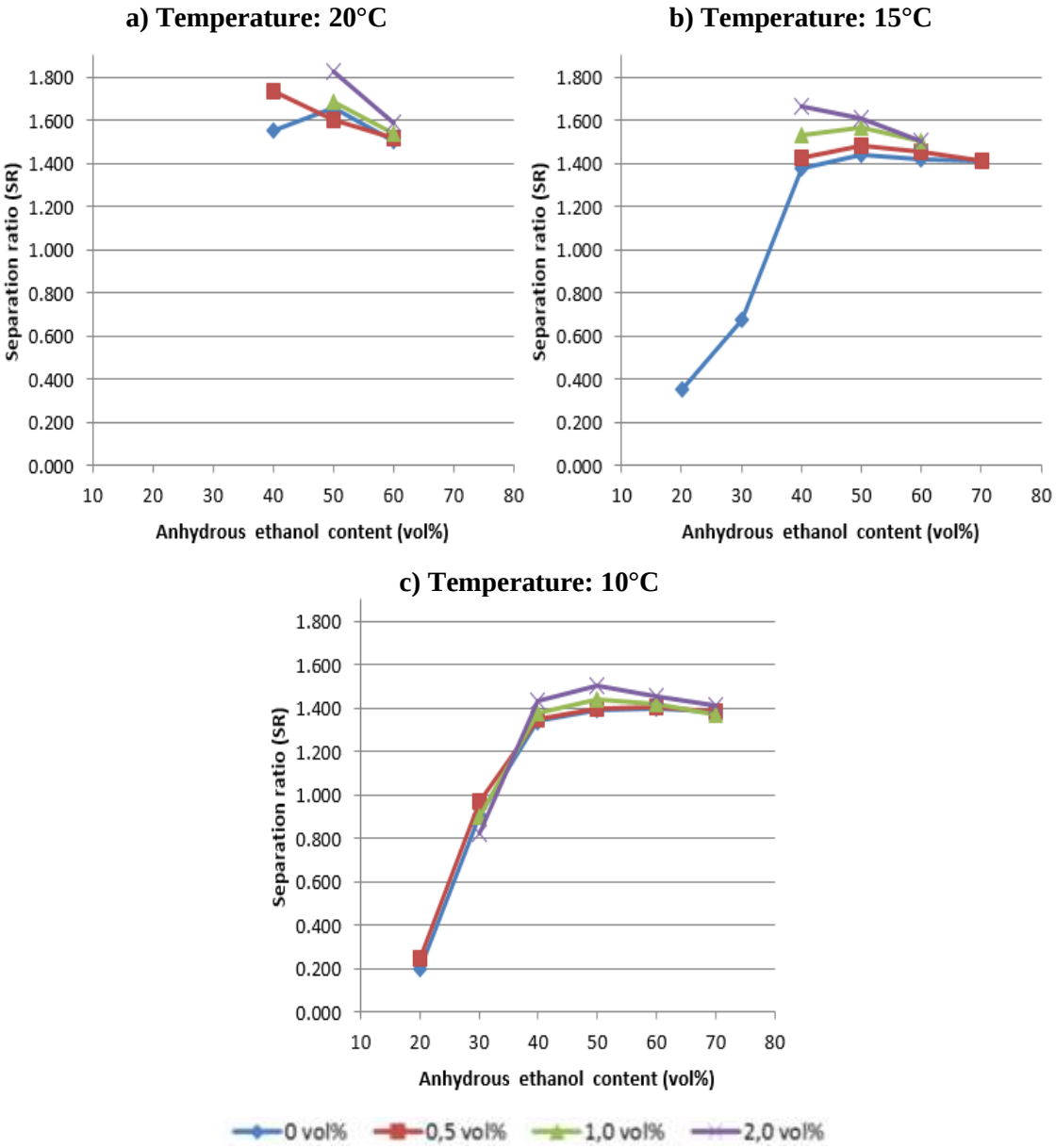

Figure 58: Separation ratio (SR) for E-diesel (B15) unstable blends in function of the ethanol content and additive content at a) 20, b) 15 and c) 10°C.

In Figure 58, it can be observed that, at 10°C, the impact of additive content on separation ratio was reduced. The temperature was the key parameter. Only the addition of 2.0 vol% seemed to have a better performance on SR. At 15°C, separation ratios inferior to 1.000 were observed for ethanol content of 20 and 30 vol%, without additive. Such values were also observed at 10°C for ethanol content of 20 vol% (with 0.0 and 0.5 vol% of additive) and 30 vol% (for all additive contents). In such cases, ethanol was dragged into the diesel fuel phase. Nevertheless, values close to 1.000 were not recommended as, in a first approximation, there was poor blending between the ethanol and the diesel fuel.

PUC-Rio - Certificação Digital Nº 1312923/CA

Poor properties of ethanol are not compensated by the addition of diesel fuel compounds and no renewable fuel substituted fossil diesel fuel.

The long-term stability of the blends without and with 2 vol% of additive at the four temperatures investigated was assessed up to 3 weeks. At 25 and 20°C, the equilibrium was observed after the first week while, at 15 and 10°C, the equilibrium seemed to be reached after 2 weeks. Figure 59 shows the evolution of SR with time. The uncertainty on the results was calculated from the results of section 5.1.2 and is equal to ± 0.028.

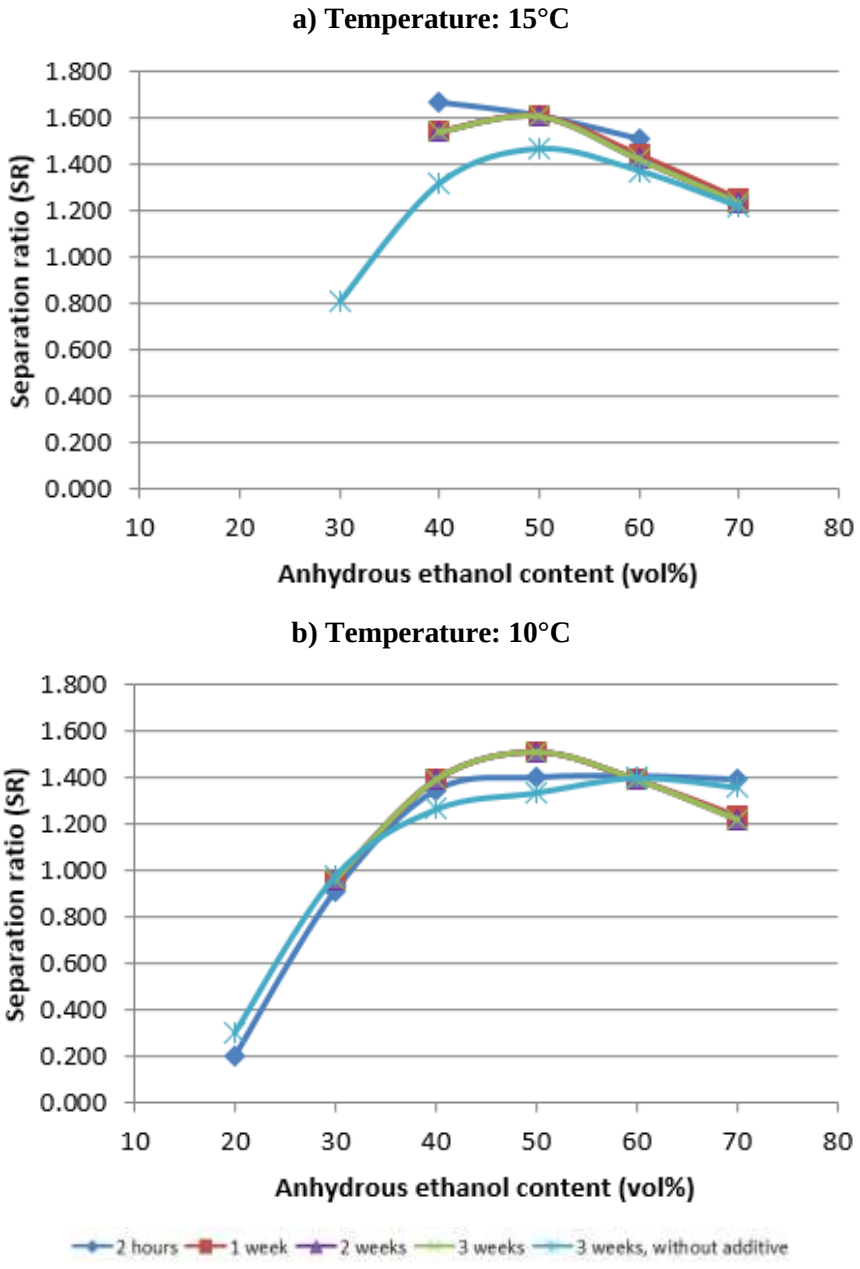

Figure 59: Kinetics of decantation measuring separation ratio (SR) up to 3 weeks of decantation for E-diesel (B15) blends for different ethanol content at a) 15 and b) 10°C.

PUC-Rio - Certificação Digital Nº 1312923/CA

At both temperatures, the results obtained after 1, 2 and 3 weeks were almost the same and the curve are overlaid in the figure. At 15°C, instability was observed after 2 hours for ethanol content in the range of 40 to 60 vol% while for 1, 2 and 3 weeks, two phases were also observed for 70 vol% of anhydrous ethanol. SR was decreasing with time. When compared with blend without additive stored 3 weeks, the additive implied a narrower unstable region and a higher separation ratio.

At 10°C, instability was observed after 2 hours for ethanol content in the range of 20 to 70 vol% while, after 1, 2 and 3 weeks, two phases were observed in the range of 30 to 70 vol% of anhydrous ethanol. This reduction of the range of instability can be related to a separation observed under kinetics condition while the blends are stable under thermodynamic conditions. It seems that, at 10°C, SR was slightly increasing with time, except for high ethanol content. When compared with blend without additive stored for 3 weeks, the additive implied a narrower unstable region, but the separation ratios were similar.

The separation ratios (SR) after 3 weeks of decantation of E-diesel (B15) blends for different ethanol content and temperature without additive and with 2.0 vol% of additive are plotted in Figure 60. The uncertainty on the results was calculated from the results of section 5.1.2 and is equal to ± 0.028.

PUC-Rio - Certificação Digital Nº 1312923/CA

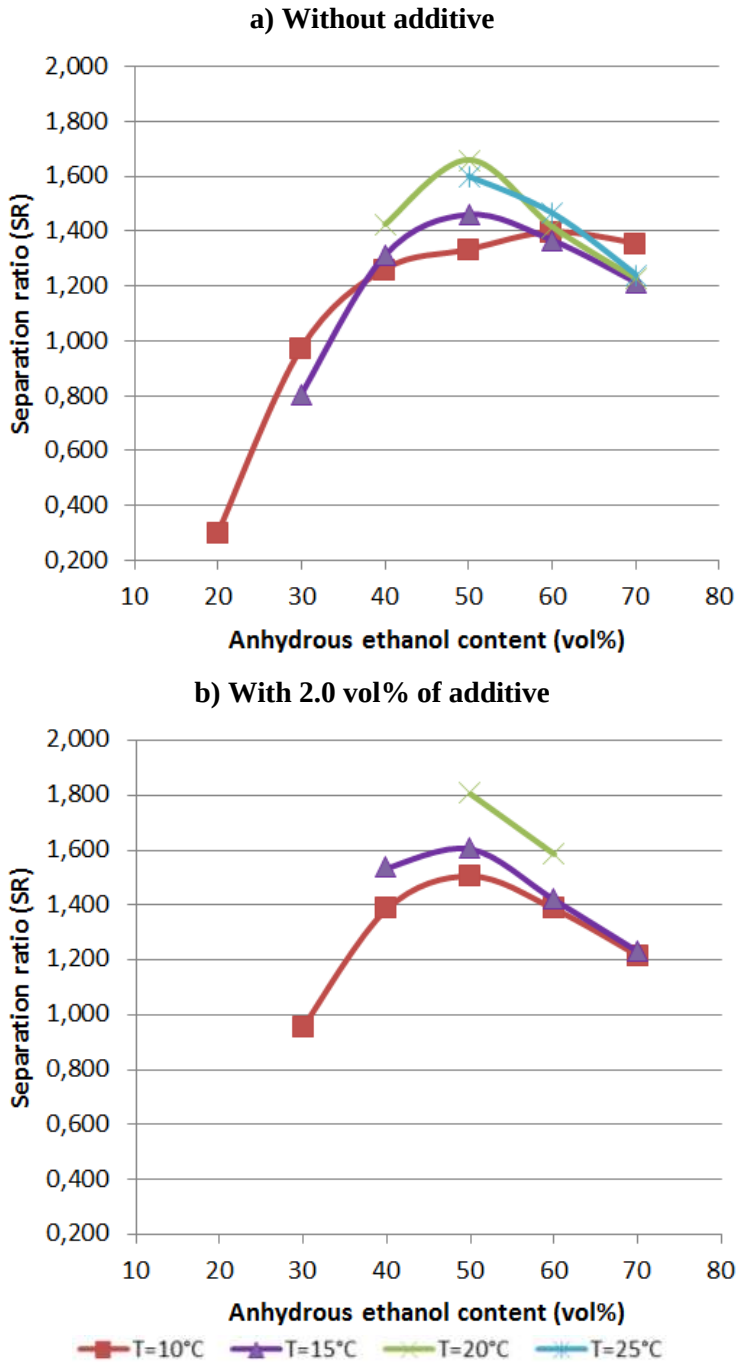

Figure 60: Separation ratio (SR) after 3 weeks of decantation of E-diesel (B15) blends for different ethanol content and temperature a) without additive and b) with 2.0 vol% of additive.

It can be observed on Figure 60 that the additive reduced significantly the instability domain, in particular at 25°C when all additivated blends remained stable after 3 weeks of storage. When phase separation was observed, the additive generally lead to higher separation ratio. In comparison with the results obtained after 2 hours of decantation, the tendency was to broaden the instability region with the duration of storage. Moreover, in absence of additive, some blends stored for more than 1 week began to separate at 25°C.

PUC-Rio - Certificação Digital Nº 1312923/CA

The results showed that a minimum addition of 1.0 vol% is required to have a sufficient short term and long-term stability at temperatures higher than 10°C and ethanol content up to 20 vol%. However, when 2 vol% of additive was added, the stability region was the same, but the separation ratio increased. Thus, when phase separation was observed, more compounds were dragged into the ethanol phase (in particular, biodiesel and diesel fuel).

5.2.3. Partial Conclusion

These results confirmed the bridging agent function of vegetal oil as it is the main compound of the additive. Again, diversity on the carbon chain length and moieties were required to improve the miscibility of ethanol in diesel fuel. It is important to note that the same species were involved in the formulation of the best additive (biodiesel from soybean and the vegetal oil from castor seeds) as in the previous section.

The best additive determined in this section was used for the next steps of the study since the biodiesel content can be fixed directly by blending it into the diesel fuel. Its use is justified by the observed stability gain, in particular at 15°C and 10°C (see Table 29). In further investigations, DBE blends were tested using a base of diesel B15 fuel based on the experimental results obtained in this section. Moreover, this decision was also based on the Brazilian biofuels policy that showed a tendency of increase of its addition in commercial diesel fuel. For instance, a resolution published in 2015 allowed the commercialization and the volunteer use of biodiesel into fossil diesel fuel up to 20 vol% for captive fleets and 30 vol% for rail and for agricultural and industrial use [Brasil, 2015a]. Moreover, another example is the law n° 13.263 from March 23rd 2016 that stipulated the augmentation in 8, 9 and 10 vol% of biodiesel content in a period of 12, 24 and 36 months, respectively.

5.3. Assessment of Some Physicochemical Properties for Anhydrous Ethanol – Diesel B15 Blends

In the following subsections, comments are made about the evolution of each physicochemical property in function of ethanol and additive contents. DBE blends using diesel B15 fuel were also investigated. Concentration of anhydrous

PUC-Rio - Certificação Digital Nº 1312923/CA

ethanol varied from 0 to 100 vol%, by step of 10 vol%, except when technical limitation implied a reduction of the investigated range. Moreover, DBE blends with 0.0 and 2.0 vol% of additive were investigated to assess the impact of the additive. An additional sample with 20.0 vol% of anhydrous ethanol and 1.0 vol% of additive were investigated. It represents the critical blend tested in the engine in the next section.

All the experimental results are given in the Appendix F with their respective uncertainties.

5.3.1. Specific Gravity at 25°C and 20°C

The values of specific gravity of DBE blends at 25°C and 20°C are given in Figures 61 and 62, respectively. As expected, the specific gravity decreased with the ethanol content, at both temperatures, because specific gravity of ethanol is lower than for diesel B15 fuel.

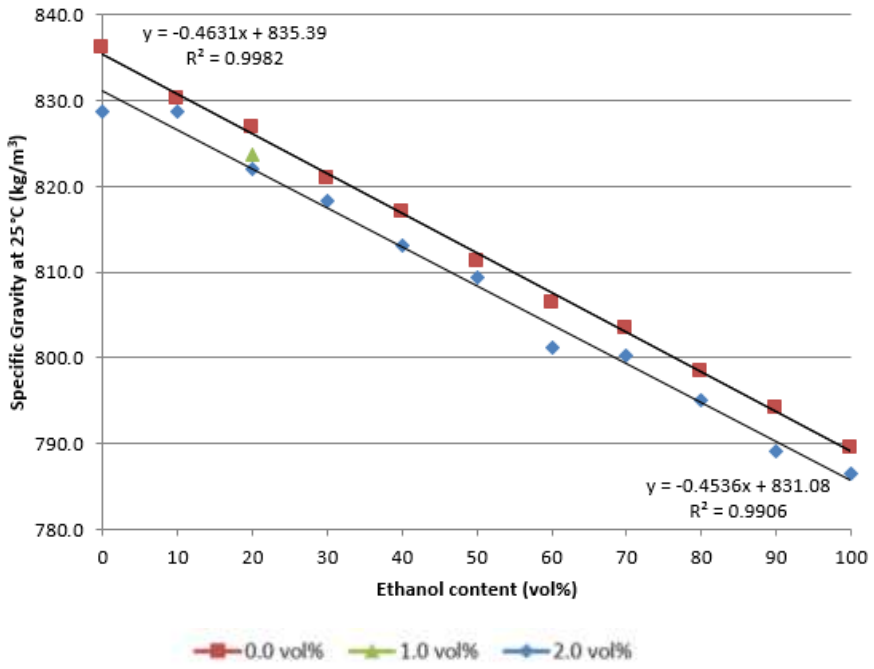

Figure 61: Specific gravity (kg/m³) at 25°C of DBE blends, in function of additive and ethanol content.

Linear regression for specific gravity at 25°C in function of ethanol content fitted well with the experimental data (determination coefficient R^2 of 0.9906 and 0.9982 for blends without and with 2.0 vol% of additive, respectively). As expected, the results confirmed that a dilution law was adapted to the specific

PUC-Rio - Certificação Digital Nº 1312923/CA

gravity at 25°C. The differences observed with experimental values were mainly due to experimental uncertainties during the blending.

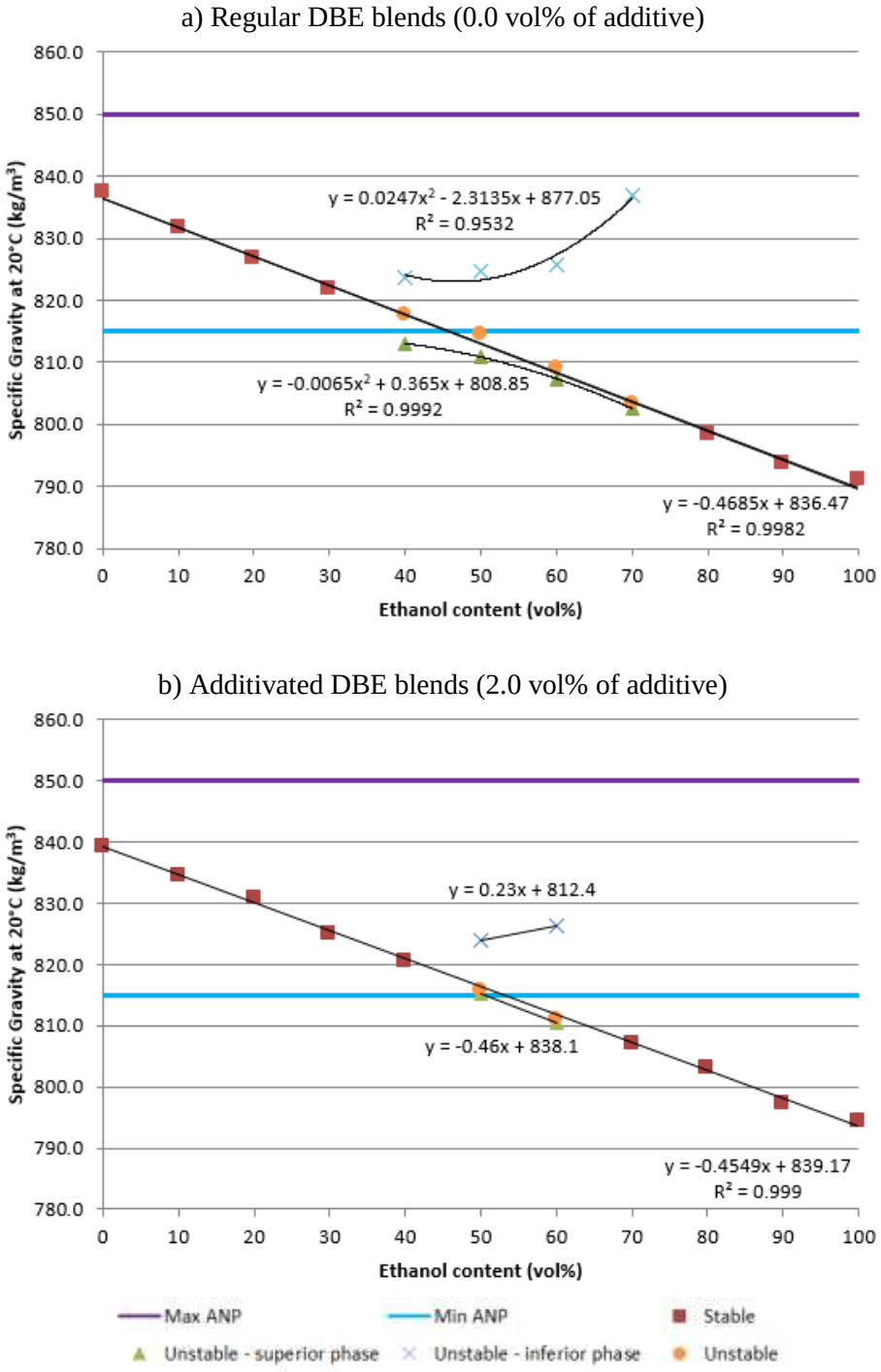

Figure 62: Specific gravity (kg/m^3) at 20°C of E-diesel blends a) without and b) with 2 vol% additive, in function of ethanol content.

Additivated blends were slightly denser than the original blends due to the higher specific gravity of the additive (931.9 kg/m^3 at 20°C). In average, specific

PUC-Rio - Certificação Digital Nº 1312923/CA

gravity was 0.39% higher at 25°C and 0.38% higher at 20°C. The linear regression at 20°C calculated with experimental measures for stable blends had determination coefficients R^2 of 0.9982 and 0.9990 for blends without and with 2.0 vol% of additive, respectively. These results showed a good adequacy of the results to the theoretical dilution law. When phase separation was observed, it can be seen that the calculated specific gravity for the blends fitted well with the experimental linear regression. The specific gravity of inferior phase increased with ethanol content and the one of superior phase decreased with ethanol content. This showed that, the miscibility of ethanol in diesel fuel decreased with the ethanol content. Moreover, as the curve of specific gravity of inferior phase was asymptotically tending to the specific gravity of the blends, it shows that the miscibility of diesel fuel in ethanol increased.

It was expected that the blends with 1.0 vol% presented intermediate values of specific gravity at both temperature. Such behavior was observed at 25°C as given in Table 32.

PUC-Rio - Certificação Digital Nº 1312923/CA

Table 32: Specific gravity (kg/m³) for the DBE blends with 20 vol% of anhydrous ethanol at 20 and 25°C.

Additive content (vol %)	0.0	1.0	2.0
Specific gravity at 20°C (kg/m³)	826.7	826.1	830.8
Specific gravity at 25°C (kg/m³)	822.0	823.7	826.8

However, at 20°C, the value for intermediate additive content was slightly lower than the value for 2.0 vol% of additive. This can be explained by the experimental uncertainty and a partial evaporation of ethanol.

Figure 62 showed that the blends with up to 30 vol% of anhydrous ethanol without additive had specific gravity in the range define by the current legislation of the ANP for diesel B7 fuel (minimum value of 815 kg/m³, Min ANP, and maximum value of 850.0 kg/m³, Max ANP). The additive allowed to use up to 40 vol% of anhydrous ethanol content. The inferior phases of unstable blends also respected the Brazilian specifications. Moreover, it could be observed that the specific gravity at 20°C of additivated pure anhydrous ethanol was higher (794.4 kg/m³) than the legislation maximum limit (791.5 kg/m³) while pure ethanol respected the specification.

5.3.2. Kinematic Viscosity at 40°C

The values of kinematic viscosity of DBE blends at 40°C are given in Figure 63.

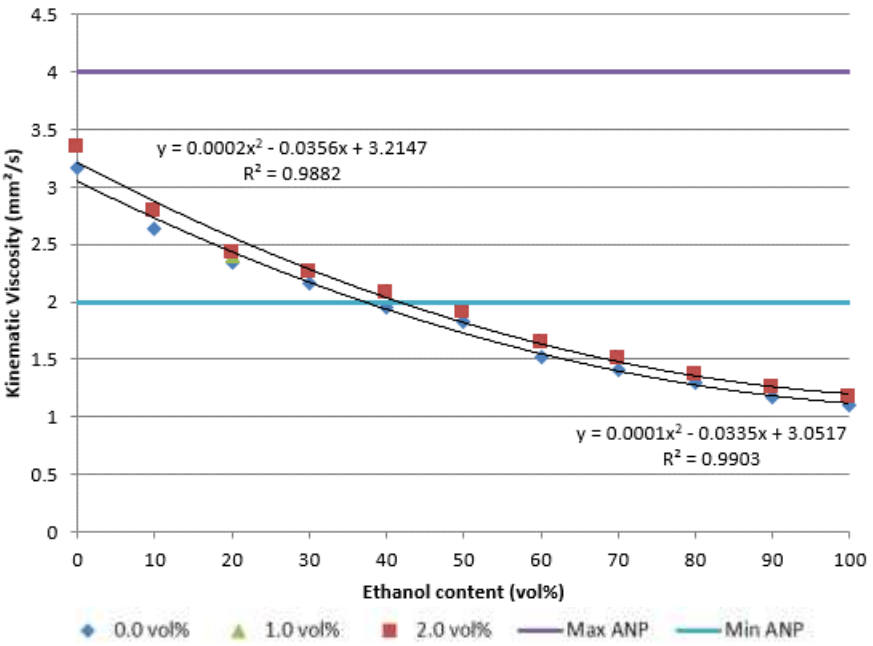

Figure 63: Kinematic viscosity (mm²/s) at 40°C of DBE blends, in function of additive and ethanol content.

Increasing ethanol content implied a diminution of the viscosity. Additivated blends with 2.0 vol% were, in average, 6.0% more viscous than the regular blends, due to the higher kinematic viscosity of the additive (55.09 mm²/s at 40°C). Quadratic regression for kinematic viscosity matched quite well with the experimental data (determination coefficient R^2 of 0.9882 for additivated blends and 0.9903 for regular blends). As expected, the blends with 20.0 vol% of anhydrous ethanol and 1.0 vol% of additive presented intermediate values of kinematic viscosity.

The results showed that the blends, additivated or not, with up to approximately 40 vol% of anhydrous ethanol respected the current legislation of the ANP for diesel B7 fuel. This results is coherent to the results of Lapuerta *et al.* (2017b) who showed that only ethanol blends with alcohol content lower than 36 vol% fulfill this requirement of the European standard.

PUC-Rio - Certificação Digital Nº 1312923/CA

5.3.3. Surface Tension at 25°C

The values of surface tension at 25°C of DBE blends in function of additive and ethanol content are given in Figure 64.

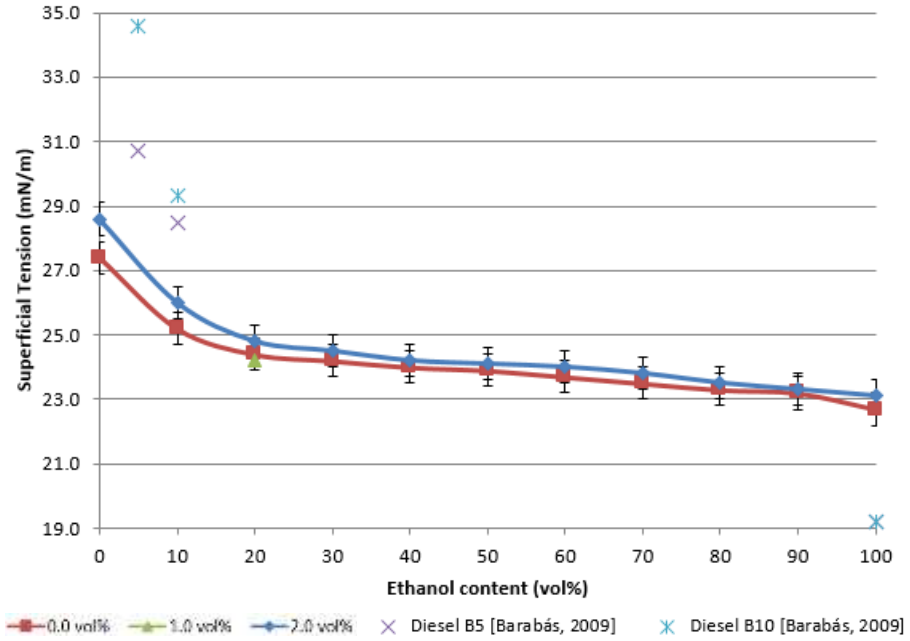

Figure 64: Surface tension (mN/m) at 25°C of DBE blends, in function of additive and ethanol content.

Increasing ethanol content implied a diminution of the surface tension, as observed by Barabás *et al.* (2009) at 20°C in blends with diesel B5 and B10. The ethanol content had a great impact for low concentrations (approximately up to 20 vol%) while, for higher concentration (superior to 20 vol%), the surface tension decreased slightly. Additivated blends with 2.0 vol% had, in average, a surface tension 1.6% higher than the regular blends, making more difficult the appropriate formation of droplets in the spray. Nevertheless, for ethanol concentration superior to 20 vol%, the difference of superficial tension between the blends without and with 2.0 vol% of additive was inferior to the uncertainty of the method (± 0.5 mN/m).

The blends with 20 vol% of ethanol and 1.0 vol% presented slightly lower surface tension than the regular blends. Nevertheless, considering the experimental uncertainty, the values of the surface tension for all the blends with 20 vol% of ethanol can be considered equal.

PUC-Rio - Certificação Digital Nº 1312923/CA

5.3.4. Contact Angle at 21°C

The cleanness of the three glass lamellas was controlled measuring the contact angle of a drop of distillate water over each substrate. The results presented a good repeatability, as given in Table 33.

Table 33: Water drop properties used to control the cleanness of the glass lamella.

Property	Lamella 1	Lamella 2	Lamella 3	Average	Standard deviation
Area (mm^2)	4.820	4.882	5.314	5.005	0.206
Volume (mm^3)	1.242	1.249	1.441	1.311	0.087
Diameter (mm)	2.147	2.176	2.252	2.192	0.040
Apex radius (mm)	1.254	1.317	1.309	1.293	0.026
Temperature (°C)	20.6	20.7	20.7	20.7	0.0
Contact angle (°)	60.1	59.4	60.3	59.9	0.4

The variation of the contact angle at 21°C of DBE blends and the drop volume are given in Figures 65 and 66, respectively.

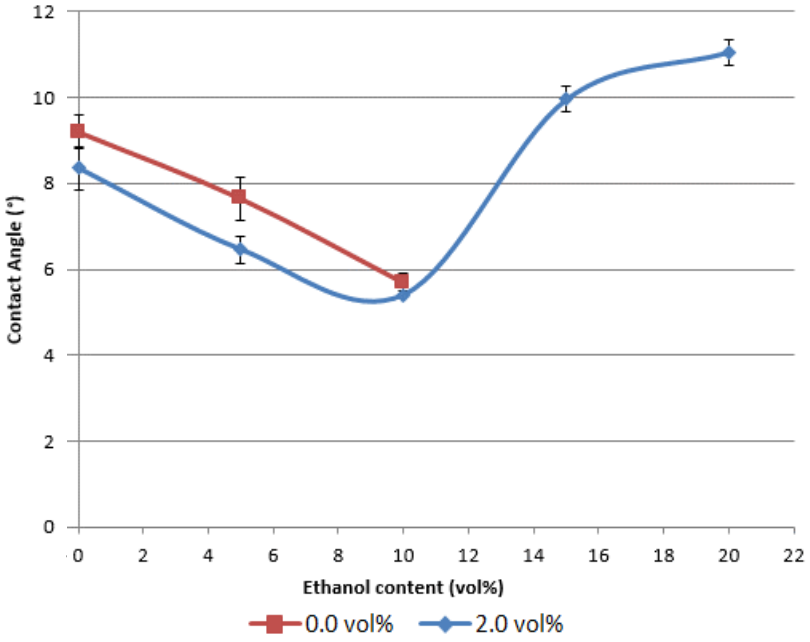

Figure 65: Contact angle (°) at 21°C of DBE blends, in function of additive and ethanol content.

PUC-Rio - Certificação Digital Nº 1312923/CA

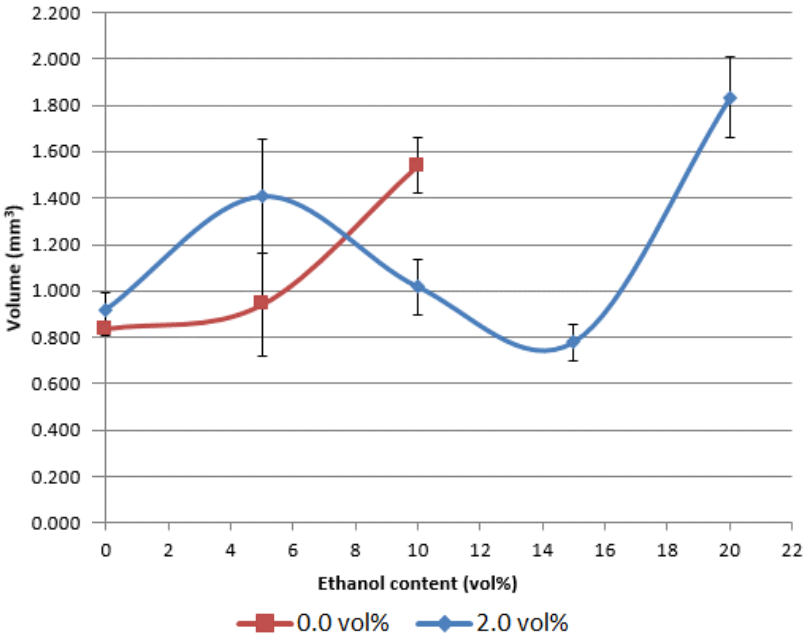

Figure 66: Drop volume (mm^3) of DBE blends, in function of additive and ethanol content.

In regular blends, the contact angle decreased with ethanol content as ethanol is more wettable in the glass substrate than the diesel fuel. It was possible to measure contact angle for ethanol concentration up to 10 vol% of anhydrous ethanol. In fact, due to the rapid evaporation of the drop for low volume, it was necessary to increase gradually the volume of the drop up to 50% its initial value, as shown in Figure 66. For further ethanol content, the drop immediately evaporated on the glass lamella and a residual irregular film remained on the substrate (probably diesel fuel and biodiesel).

In blends with 2.0 vol% of additive, an initial reduction of the contact angle was also observed up to 10.0 vol% of anhydrous ethanol. For higher ethanol content, the contact angle increased to a value higher than the initial values. Such behavior can be related to the evaporation of the fraction of ethanol in the blends, which required higher volume for the drop. The decrease of the volume in the range 5 to 15 vol% can be related to a partial evaporation on the micropipette, even if drop was formed on the substrate. For higher ethanol content, the increase of drop volume is necessary to avoid evaporation on the micropipette and after drop formation. It was impossible to measure contact angle for anhydrous ethanol concentration higher than 20 vol% due to the immediate evaporation of the drop on the glass lamella.

PUC-Rio - Certificação Digital Nº 1312923/CA

5.3.5. Flash Point

The values of flash point of DBE blends are given in Figure 67.

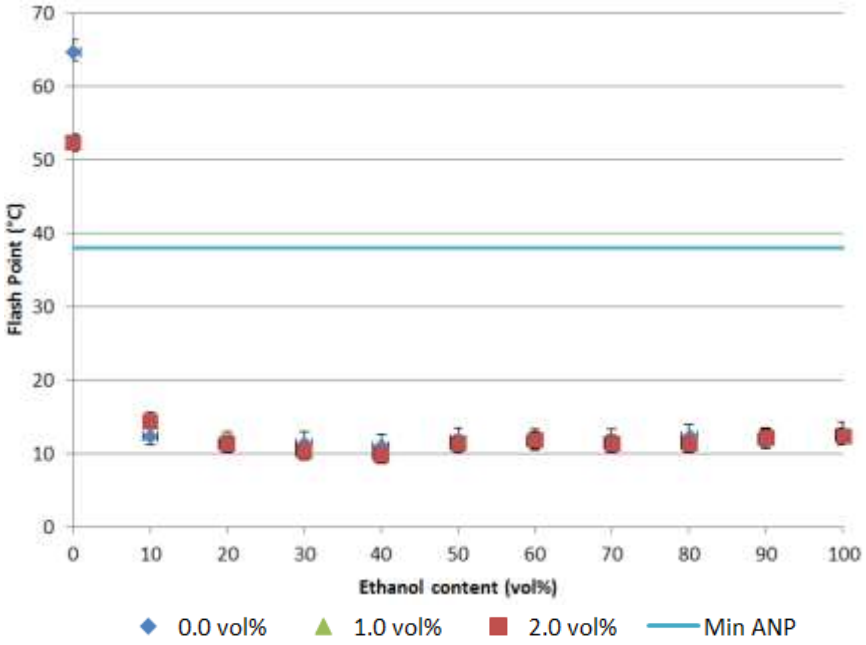

Figure 67: Flash point (°C) of DBE blends, in function of additive and ethanol content.

The increase of ethanol content implied a diminution of the flash point. The ethanol content had a great impact on the lowest concentrations (approximately up to 10 vol% of alcohol) while, for higher concentration, the flash point was almost constant. Blends without and with 2.0 vol% of additive only had a different behavior in absence of ethanol. Without alcohol, additivated blends had a flash point 19% lower than the regular blends. In the other case, the values were almost constant, slightly varying around the value of 11.7°C, within the range of the ASTM repeatability (±1.2°C for flash point lower than 60°C). These values were slightly lower than the flash point of ethanol (12.6 °C).

The results showed that the blends, additivated or not, with up to approximately 5 vol% of anhydrous ethanol respect the current legislation of the ANP for diesel B7 fuel. For higher ethanol concentration, the blends did not meet the Brazilian specification for diesel fuel. Nevertheless, this parameter has no direct impact on the combustion. It indicates that the fuel must be handled carefully. Technical solution used for flex fuel gasoline vehicles can be adapted to these blends, such as [National Renewable Energy Laboratory, 2016]:

PUC-Rio - Certificação Digital Nº 1312923/CA

(i) Modified electrical wiring and connectors for submersed components, such as the fuel-level sensor and fuel pump;

(ii) Increased evaporative emissions carbon canister capacity;

(iii) Modified fuel tank vapor pressure sensor, pump, injectors and engine valves;

(iv) Adapted material for pressure regulator diaphragms, fuel injector O-rings and valve seat.

5.3.6. Cold Filter Plugging Point (CFPP)

The values of CFPP for the tested DBE blends are given in Figure 68.

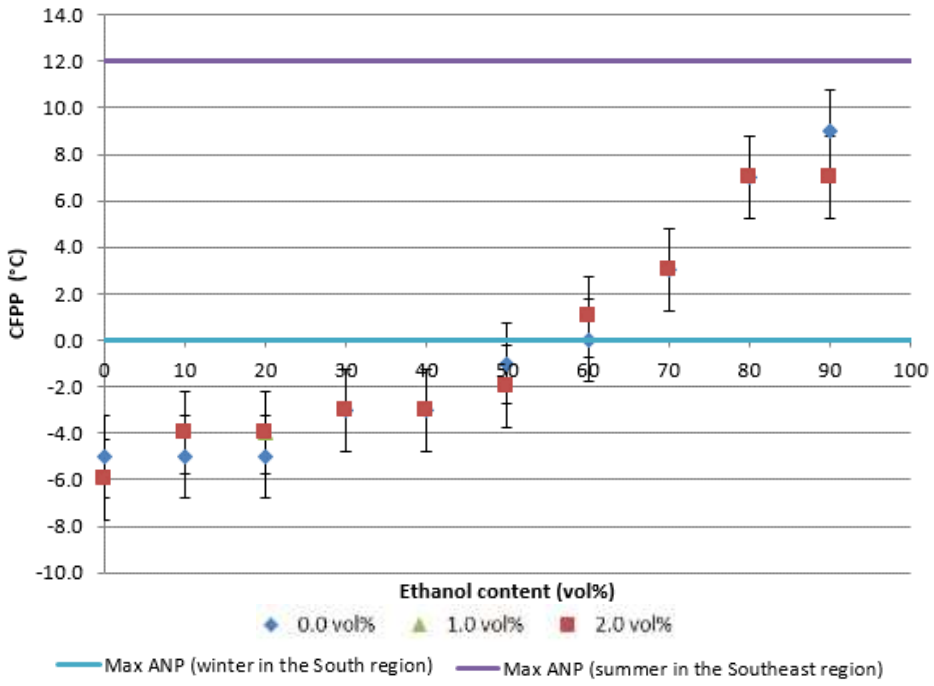

Figure 68: Cold Filter Plugging Point (°C) of DBE blends, in function of additive and ethanol content.

It was not possible to measure the CFPP point of anhydrous ethanol, without or with 2.0 vol% of additive. Nevertheless, it can be assumed that the CFPP of these blends were close to the freezing point of ethanol (approximately -114°C).

The higher was the ethanol content, the higher was the value of the CFPP. In most of the case, the differences between regular and additivated blends were lower than 1.0°C and the ASTM repeatability (±1.76°C). Only the samples with 90 vol% of ethanol presented a difference higher than the repeatability. In that case, the CFPP of the additivated blends were lower than of the regular blend.

PUC-Rio - Certificação Digital Nº 1312923/CA

This can be explained by the slightly higher content of biodiesel and oil content in the blends that led to a faster clogging of the filter.

The blends with 20 vol% of ethanol and 1.0 vol% of additive presented a CFPP equal to the additivated blend and both had a CFPP slightly higher than the value for regular blends.

The maximum value of CFPP authorized by the Brazilian legislation depends on the geographical localization and the month of the year, as given in Figure 69.

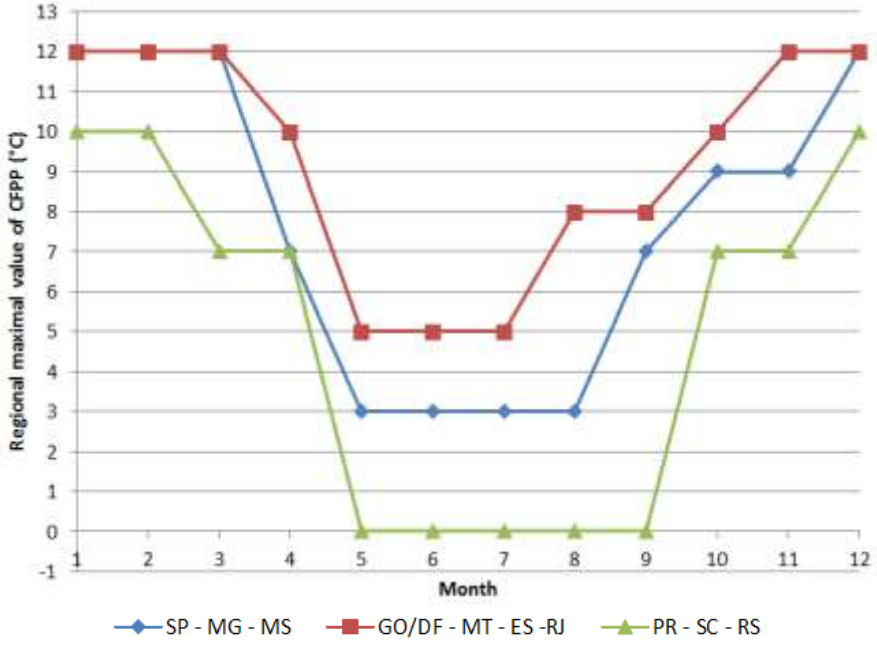

Figure 69: Brazilian maximum value of CFPP (°C) according to the month [Brasil, 2013].

These values vary from 0 to 12°C. The results showed that the blends, additivated or not, with up to approximately 60 vol% of anhydrous ethanol respected the lowest maximum limit for CFPP value (0°C) in the current legislation of the ANP for diesel B7 fuel. Considering the most favorable case, blends in all proportions can be used.

5.3.7. Corrosiveness to Copper at 50°C

All studied blends gave the same results after the heating period and they presented the same light orange color, almost the same as the freshly polished strip (classification 1a), according to the ASTM copper strip corrosion standard shown in Figure 70.

PUC-Rio - Certificação Digital Nº 1312923/CA

Figure 70: ASTM Copper Strip Corrosion Standard.

That means that all samples had an acceptable low degree of corrosiveness. According to the ASTM D130, the statistician determined that there is nominally a 5% chance that a difference between any of the two ratings will exceed 1 lettered category within classification (ratings 1, 2 and 3) and 2 lettered category within classification (rating 4).

5.3.8. Cetane Number (CN)

The values of CN of DBE blends and the relative impact of additive are shown in Figure 71.

PUC-Rio - Certificação Digital Nº 1312923/CA

a) Cetane Number (CN)

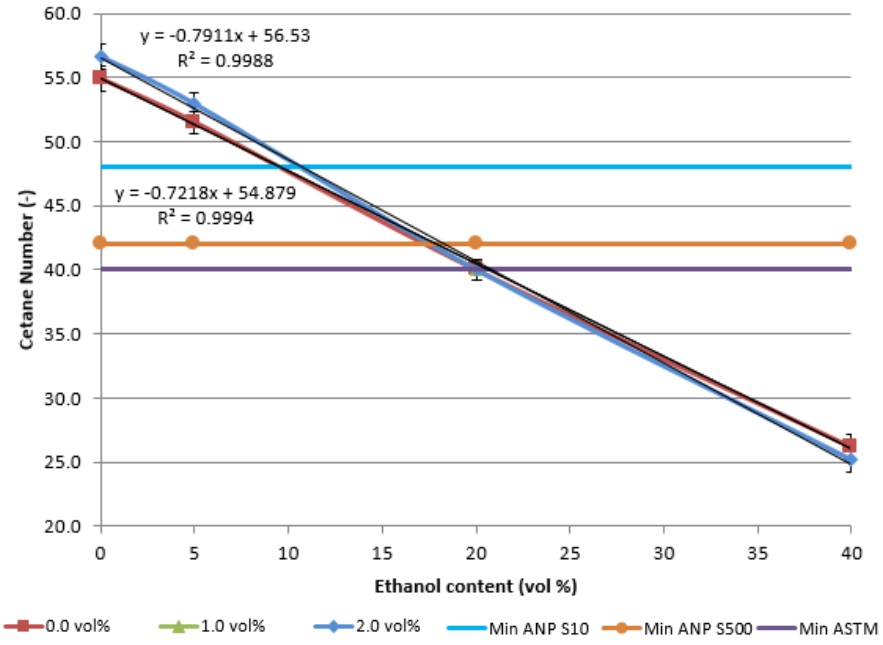

b) Relative impact of additive on CN (%)

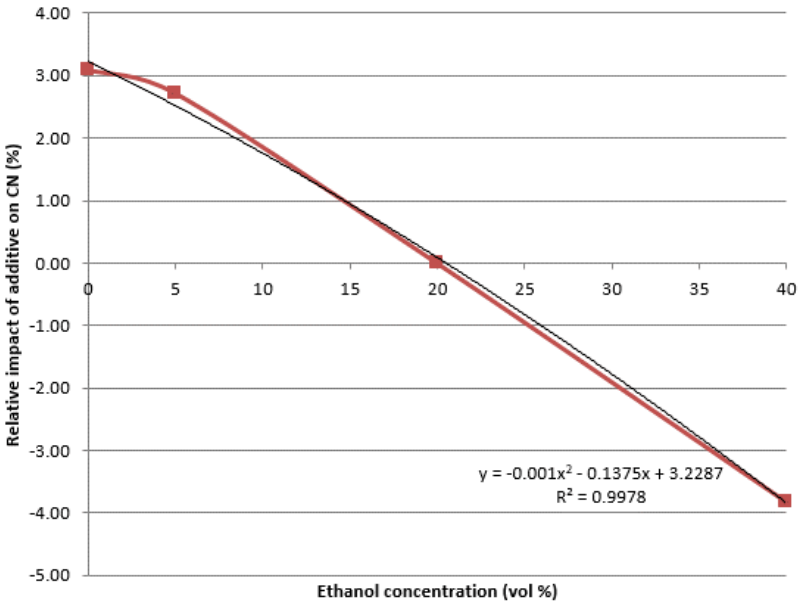

Figure 71: a) Cetane Number of DBE blends and b) Relative impact of additive on CN, in function of additive and ethanol content.

For low ethanol content, additivated blends had higher cetane number (increase of 1.4-1.7), while for high ethanol content, the trend was reverse (decrease of 1.0). Based on the investigated experimental condition, such inversion of behavior happened at ethanol concentration of 20 vol% and the relative diminution of cetane number fitted well with a polynomial regression. The linear regression obtained for CN allowed the determination of the maximum

PUC-Rio - Certificação Digital Nº 1312923/CA

value of ethanol content that respect the Brazilian and North-American legislations.

It is also important to note that experimental instability was observed for additivated samples during the analysis. As described formerly, one step of the method consists in fixing the ignition delay at 13° ± 0.2 BTDC by adjusting the injection timing and the compression ratio. Indeed, the sample had both stability and instability periods. No clear tendency on the variation of injection advance can be defined as higher and lower values of injection time were observed.

Up to 10.8 vol% of ethanol can be added to additivated blends while only mixtures without additive with up to 9.5 vol% of ethanol had cetane number higher than 48, as specified by the ANP legislation for diesel S10 fuel [Brasil, 2013]. Considering the minimum cetane number allowed for diesel S500 fuel in Brazilian legislation (CN higher than 42), the maximum ethanol addition increased to 17.8 and 18.3 vol% in regular and additivated blends, respectively. When considering the ASTM limit (minimum of 40), in both cases, the maximum concentration of ethanol of 20.0 vol% respected the limitation.

5.3.9. Lubricity at 25°C and 60°C

The values of lubricity parameters (mean wear scar diameter, film percentage and friction coefficient) of DBE blends without and with 2 vol% of additive were measured for 0, 5, 10, 20 and 40 vol% of anhydrous ethanol. The results at 25°C and partial results obtained at 60°C are given in Figure 72.

PUC-Rio - Certificação Digital Nº 1312923/CA

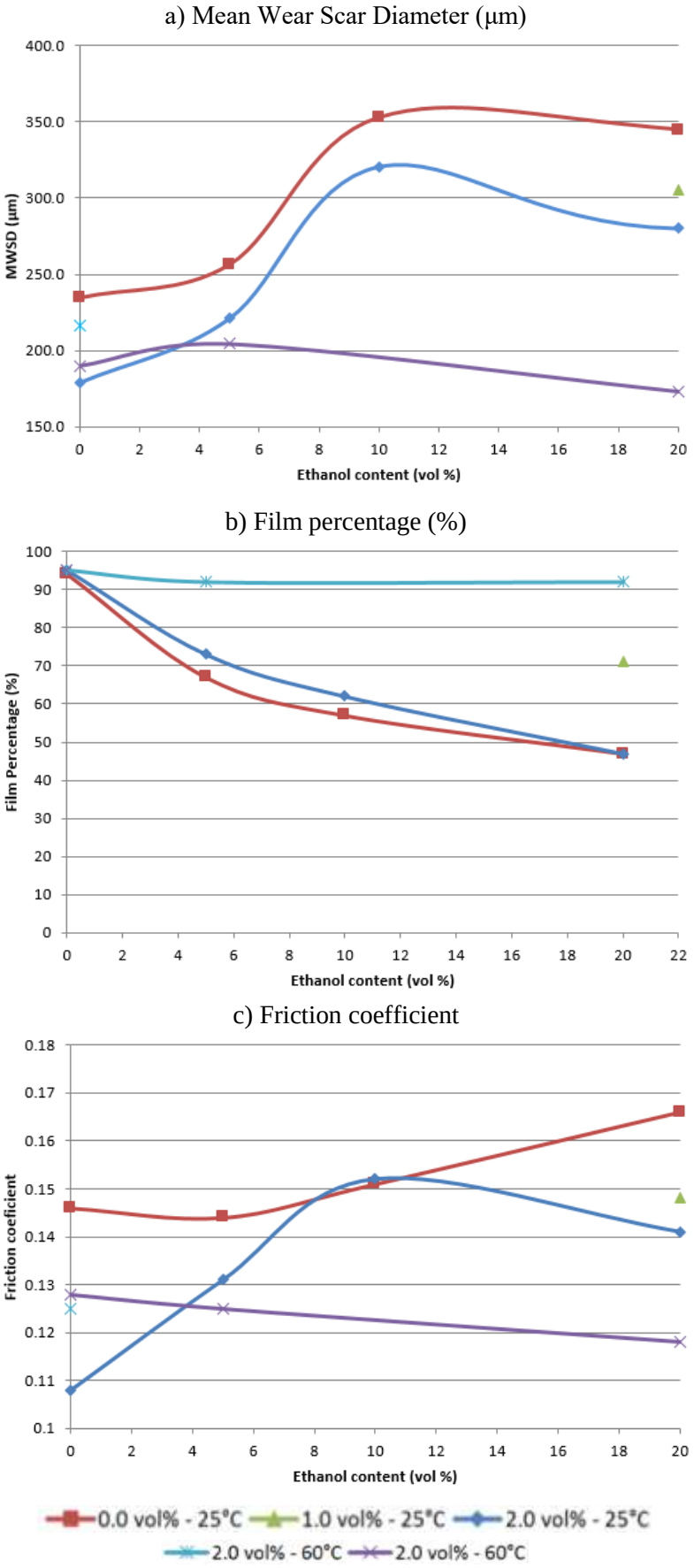

Figure 72: Mean wear scar diameter (µm), b) film percentage (%) and c) friction coefficient of DBE blends at 25°C and 60°C, in function of additive and ethanol content (up to 20 vol%).

PUC-Rio - Certificação Digital Nº 1312923/CA

At 25°C, each condition was repeated twice or three times. The average value and standard deviation, with an interval confidence of 95%, were calculated. The uncertainty was lower than 10% of the nominal values, except for the additivated sample with 40 vol% of anhydrous ethanol, where relative uncertainty was higher (21%). Nevertheless, this uncertainty interval was always lower than the repeatability of the method (80 μm).

At 25°C, the mean wear scar diameter increased with ethanol content as a loss of lubricity is expected. Moreover, the mean wear scar diameter (MWSD) was higher in regular blends than in additivated blends up to around 40% of ethanol, when an inversion was observed. Such inversion should be confirmed by further investigation as the uncertainty was significant in this blend. An evaporation of ethanol could explain this reduction. These results were also coherent with the results of Lapuerta *et al.* (2010b) who stated that there is an optimum value of biodiesel content at which MWSD is reduced and more biodiesel it is not necessarily synonym of better lubricant proprieties. For both kind of blends, the film percentage decreased with ethanol content from an initial value of 94-95% to 47% for 20 vol% of anhydrous ethanol. At a concentration of 40 vol% of alcohol, the values increased slightly (50%) in regular blends, meanwhile, for additivated samples, the increase was higher (59%). The same behavior can be observed for the friction coefficient, with a clear increase for additivated blends with 40 vol% (+256% when compared to regular blends). Such differences were coherent to the observed inversion of lubricity.

At 60°C, it was possible to observe a slight decrease of the three parameters in the additivated blends in function of ethanol concentration. This effect could be explained by the compensation of the expected loss of lubricity (due to the presence of ethanol) by the increase of its evaporation losses from the lubricating layer. Lapuerta *et al.* (2010b) had already observed this tendency. In all investigated conditions, lubricity is lower than the maximum limit defined by the Brazilian legislation (460 μm for S10 diesel fuel and 520 μm for S500 diesel fuel) [Brasil, 2013].

For free ethanol blends, the additive decreased the MWSD of the fuel, as expected from literature, at both temperatures. Without ethanol, the MWSD decreased as the temperature increased in regular blends. Such behavior, already observed by Lapuerta *et al.*, is related to the reduction of fuel viscosity and,

PUC-Rio - Certificação Digital Nº 1312923/CA

consequently, of the metallic contact resistance. A similar decrease in lubricity can be observed in the case of the additivated blend, although, in this case, the effect of temperature is lower (half of the reduction). It can be noted that the additive provide a significant benefit in lubricity: in average, the mean wear scar diameter is 33.5 μm lower in additivated blends. Temperature had significant impact on the evaporation loss as it can be seen.

5.3.10. Lower Heating Value (LHV)

A bibliographic revision gave some experimental values of the lower heating value on a mass basis (Table 34) and specific gravity at 20°C (Table 35). The average and standard deviation were calculated based on the results.

Table 34: Values available in literature of the LHV of the different compounds.

LHV (MJ/kg)	Diesel fuel	Biodiesel (soybean)	Biodiesel (beef tallow)	Anhydrous ethanol	*n*-butanol	Castor Oil
Value	42.50	37.0	37.22	26.8	32.01	35.08
Source(s)	Qi, 2009; Yao, 2010	Castanheira, 2015	Tesfa, 2012	Yao, 2010; Gu, 2012	Szwaja, 2010	Mehta, 2009
Value	42.612	37.144	37.531	26.83	33.0	37.2-39.5
Source(s)	Boundy, 2011	Canakci, 2003	Yahya, 1994	Szwaja, 2010; Lapuerta, 2010a	Gu, 2012	Scholz, 2008
Value	42.640	37.2	39.858	26.860	34.366	-
Source(s)	Canakci, 2003	Castanheira, 2011	Öner, 2009	Wyman, 1990	Boundy, 2011	-
Value	42.692	37.68	-	26.952	35.1	-
Source(s)	Yahya, 1994	Mehta, 2009	-	Boundy, 2011	Yao, 2010	-
Value	42.700	37.75	-	-	-	-
Source(s)	Öner, 2009	Tesfa, 2012	-	-	-	-
Value	-	38.81	-	-	-	-
Source(s)	-	Qi. 2009	-	-	-	-
Average	42.61	37.60	38.20	26.85	33.62	37.26
Standard deviation	0.06 (0.14%)	0.48 (1.3%)	1.10 (2.9%)	0.05 (0.17%)	1.11 (3.3%)	1.49 (4.0%)

PUC-Rio - Certificação Digital Nº 1312923/CA

Table 35: Values available in literature of the specific gravity at 20°C of the different compounds.

Specific gravity (kg/m^3)	Diesel fuel	Biodiesel (soybean)	Biodiesel (beef tallow)	Anhydrous ethanol	*n*-butanol	Castor Oil
Value	820	870	874.3	789.4	809.7	950-974
Source(s)	Qi, 2009;	Qi, 2009	Tesfa, 2012	Szwaja, 2010	Szwaja, 2010	Scholz, 2008
Value	843.51	881.4	877	790	810	-
Source(s)	Öner, 2009	Canacki, 2003	Öner, 2009	Wyman, 1990; Yao, 2010; Gu, 2012	Yao, 2010; Gu, 2012	-
Value	851	882.9	878	-	-	-
Source(s)	Yahya, 1994	Tesfa, 2012	Yahya, 1994	-	-	-
Value	853.7	-	-	-		
Source(s)	Canacki, 2003	-	-	-		-
Value	860	-	-	-	-	-
Source(s)	Yao, 2010	-	-	-	-	-
Average	845.6	878.1	876.4	789.9	809.9	962.0
Standard deviation	11.1 (1.3%)	5.4 (0.61%)	1.4 (0.16%)	0.2 (0.03%)	0.1 (0.02%)	12.0 (1.3%)

As expected, normalized standard deviations of diesel fuel and anhydrous ethanol, studied for a longer period, were lower than the values found for castor oil, *n*-butanol and biodiesel, more recently studied. In all cases, the calculated normalized standard deviations were lower than 1.5%.

Calculated values of LHV of Brazilian typical biodiesel blends (mixtures of soybean FAME, with up to 35 vol% of beef tallow), diesel fuel with 7 and 15 vol% of biodiesel and additive are given in Table 36.

Table 36: Values of the lower heating value (LHV) of the different fuel.

Fuel	LHV (MJ/L)	Propagated uncertainty
Pure diesel fuel	36.03	0.95 MJ/L (2.6 %)
Biodiesel (100% soybean)	33.01	0.94 MJ/L (2.8 %)
Biodiesel (85% soybean + 15% beef tallow)	33.08	0.85 MJ/L (2.6 %)
Biodiesel (65% soybean + 35% beef tallow)	33.18	0.91 MJ/L (2.8 %)
Diesel B7 fuel (current blend)	35.82	0.89 MJ/L (2.5 %)
Diesel B15 fuel	35.59	0.82 MJ/L (2.3 %)
Additive	34.49	2.20 MJ/L (6.4 %)

PUC-Rio - Certificação Digital Nº 1312923/CA

All uncertainties, calculated by the Kline and McClintock formula, were lower than 3.0%, except for the additive, which uncertainty was governed by the high standard deviation for castor oil.

The variation of the beef tallow proportion influenced less than 0.5% the value of LHV. For this purpose, average value met for blends with 85 vol% of soybean and 15 vol % of beef tallow methyl ester can be used as a reference value for further investigations. The increase of the biodiesel incorporation from 7 to 15 vol% in diesel fuel reduced the LHV less than 0.7 %.

When compared to diesel B15 fuel, the anhydrous ethanol had a LHV 23% lower while the LHV of the additive was only 3% lower.

Figure 73 presents the values of the lower heating value (LHV) of the DBE blends, in function of additive content.

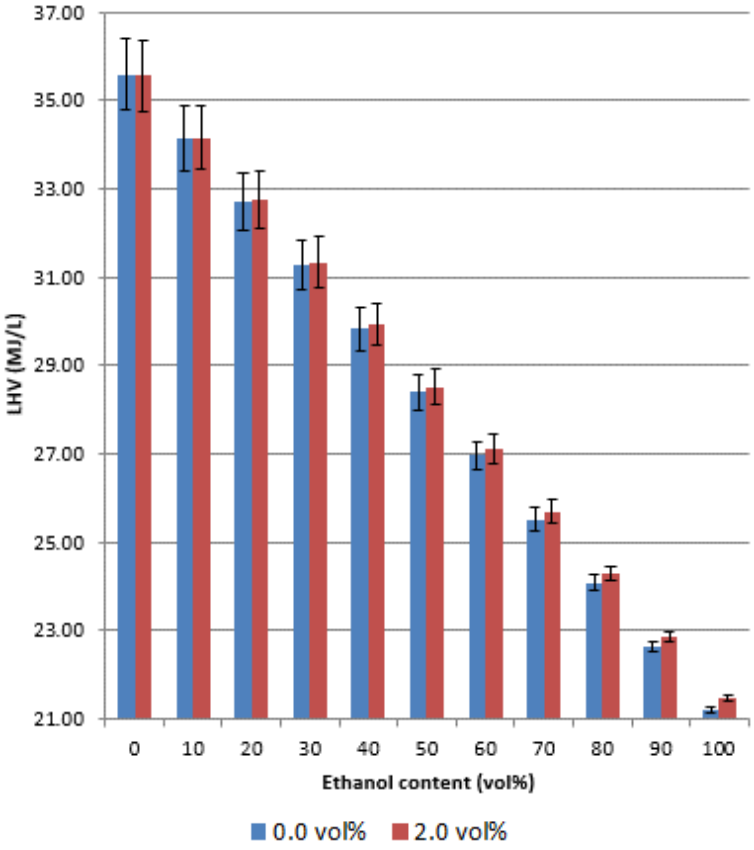

Figure 73: Values of the lower heating value (LHV) of the DBE blends, in function of additive content.

Except for very low ethanol content, the additive increased the LHV up to 1.25% in the case of additivated ethanol blend. Nevertheless, as the LHV enhancements were quite similar to the propagated uncertainties, regular and additivated blends with the same ethanol content can be considered having the

PUC-Rio - Certificação Digital Nº 1312923/CA

same LHV up to 90 vol% of ethanol. Each 10 vol% of ethanol into diesel B15 fuel reduced the LHV by approximately 4.0%.

5.3.11. Partial Conclusion

Regarding the impact of additive and ethanol content on some properties, the most restrictive property was the flash point, a property related to safety issues. A maximum of 5 vol% can be added to respect the Brazilian specification for diesel fuel. Nevertheless, new practices for storage and handling, inspired to current use of ethanol in gasoline, could be used to reduce the risks

The second more restrictive criterion was the cetane number, which implied a maximum ethanol content of 10 vol% to follow the current Brazilian legislation, regardless of the additivation. Considering the ASTM legislation for cetane number, the limit rose up to 20 vol%.

Kinematic viscosity and specific gravity allowed up to 40 vol% of anhydrous ethanol. Considering lubricity issue, results showed that additivated blends respected the Brazilian legislation up to 20 vol% (maximum tested ethanol content). Considering CFPP, blends with up to 60 vol% of anhydrous ethanol or at all concentrations can be used considering the Brazilian regional legislation. There is no restriction considering corrosiveness of the fuel at all ethanol proportions.

For all investigated properties, the sample with 1.0 vol% of additive always presented intermediate behavior to that observed for blends with 0.0 and 2.0 vol% of additive. All in all, based on the stability results and the physicochemical properties, we recommend using the additive in a current diesel engine at a concentration of 1.0 vol% in blends with up to 20 vol% of anhydrous ethanol for temperatures higher than 10°C. The impact of the additive on the properties is reduced, but they lead to a null or small improvement of the investigated properties, mainly lubricity, contact angle, cetane number and viscosity, with exception of surface tension. Modifications of the engine and expensive addition of additives (such as cetane improver or lubricity enhancer) are necessary to use blends with higher ethanol content.

PUC-Rio - Certificação Digital Nº 1312923/CA

5.4. Evaluation of the Engine Efficiency Running on Diesel B15 Blended with up to 20 vol% of Anhydrous Ethanol and 1.0 vol% of Additive.

As mentioned before, the experiments were conducted on a four-stroke compression ignition engine with four-cylinder, model 4.10 TCA by MWM. According to the manufacturer, the maximum power of 107 kW is measured at 2,600 rpm (maximum rotation) and the maximum torque of 430 Nm is observed at 1,800 rpm. The experimental points were determined for three engine speeds (1,500, 1,800 and 2,100 rpm), centered around 1,800 rpm, which is the current engine speed where the maximum torque was found.

All the details of the numerical data reduction and experimental results (average value and uncertainties) are given in the Appendix G and H, respectively.

5.4.1. Experimental Conditions: Limitation of Maximum Torque

The Figure 74 presents the observed maximum torque for each DBE blend and engine speed.

PUC-Rio - Certificação Digital Nº 1312923/CA

a) Maximum torque (N.m)

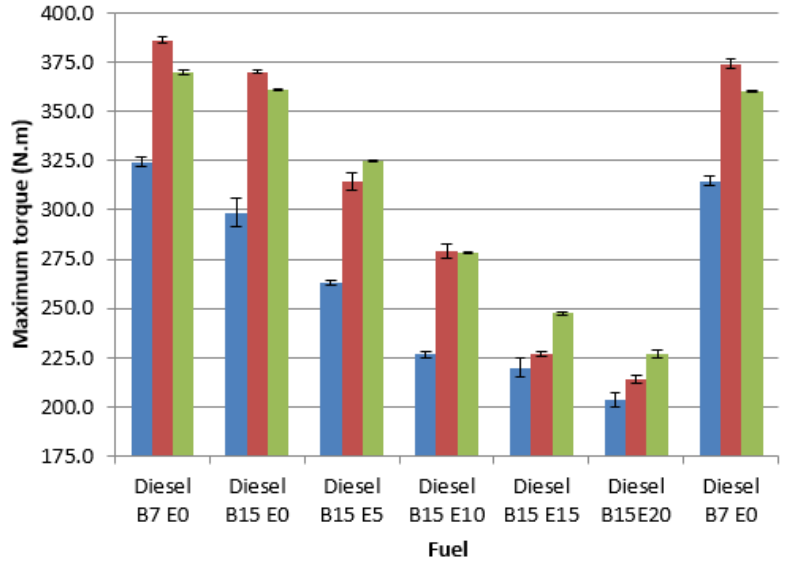

b) Fraction of B7 maximum torque (%)

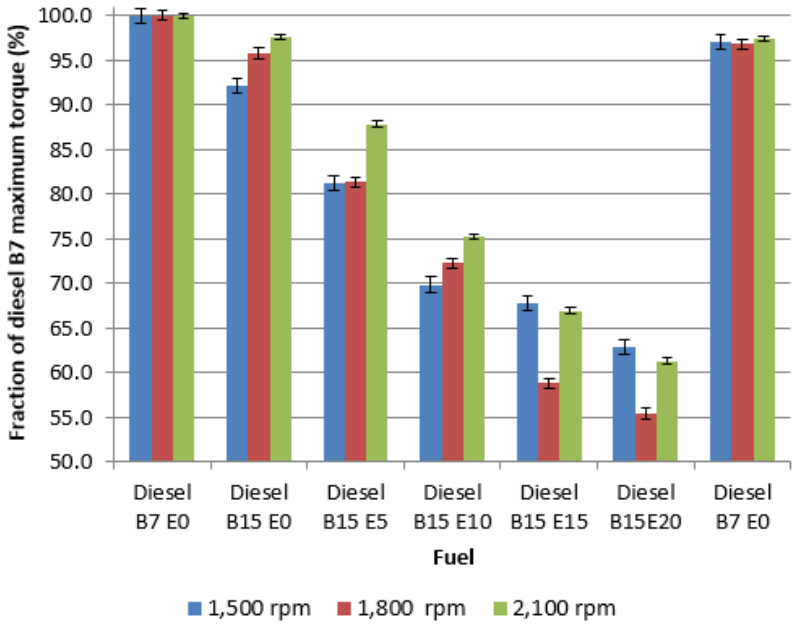

Figure 74: Observed maximum torque for each DBE blend and engine speed: a) absolute values (N.m) and b) fraction of B7 maximum torque (%).

It can be seen in this figure that the increase of biodiesel content reduced the maximum torque from 2.4 to 7.9%, mainly due to the reduction of the lower heating value of the blend (45.125 kJ/kg in diesel B7 E0 fuel and 44.379 kJ/kg in diesel B15 E0 fuel). Other factors are discussed in the next sections.

Moreover, the maximum value of torque also decreased with the increase of ethanol content in the blends. The diminution was function of the engine speed and the ethanol content. For some blends, this value was lower than 60% of the values measured for commercial diesel B7 fuel in the same conditions. One of the

PUC-Rio - Certificação Digital Nº 1312923/CA

reason is that the mixture with diesel B15 fuel did not use any additive, making the comparison quite unfair. The other reasons related to fuel injection and combustion of this reduction are further discussed.

It is also important to note that the second repetition of the commercial diesel B7 fuel showed values of maximum torque 3% lower than the initial value. These results showed that the engine did not suffer any change during the tests, since the observed difference was small, probably due to residual ethanol in the line and a variation on the chemical composition of the commercial fuel.

PUC-Rio - Certificação Digital Nº 1312923/CA

The position of the accelerator for each DBE blend and value of torque is given for different engine speeds in Figure 75.

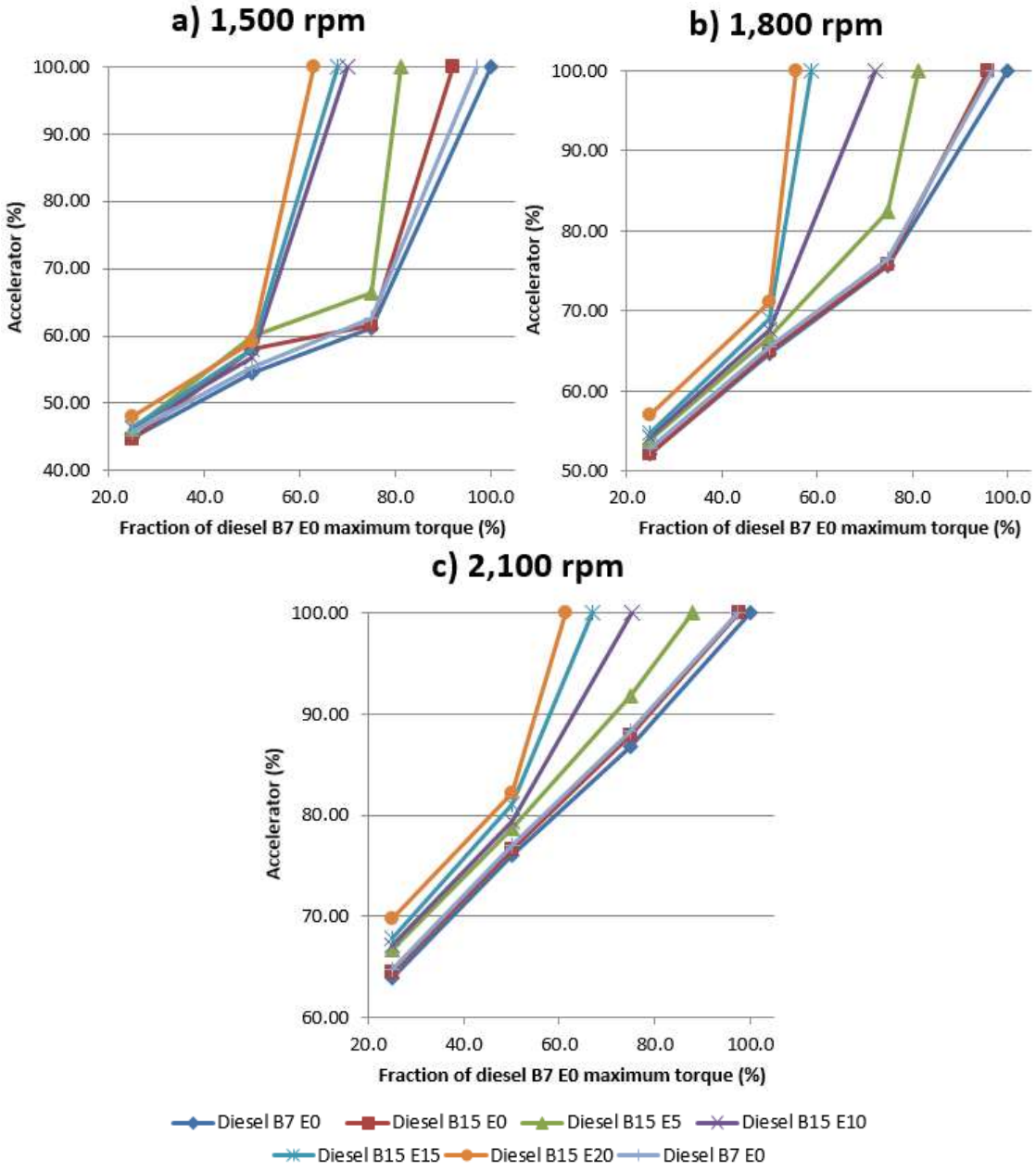

Figure 75: Position of the accelerator (%) for each DBE blend and value of torque at a) 1,500 rpm, b) 1,800 rpm and c) 2,100 rpm.

It can be seen in Figure 75 that, for 25 and 50% of the maximum diesel B7 fuel torque, the variation of the accelerator position increased with ethanol content and it was poorly impacted by the biodiesel concentration. Such behavior was mainly related to the lower energy content in the blends: the injection of more fuel was required to reach the torque.

PUC-Rio - Certificação Digital Nº 1312923/CA

Nevertheless, it was observed during the tests that the throttle position had few impact on the torque measured by the dynamometer for blends with more than 5 vol% of ethanol on the range 60 to 100% at 1,500 rpm (low engine speed), 70 to 100% at 1,800 rpm (medium engine speed) and 80 to 100% at 2,100 rpm (high engine speed). At least, two factors can explain this observation:

(i) The combustion was not optimized for these blends, in particular an earlier injection would be required to compensate the longer ignition delay. This fact affected the performance of the engine and the conversion of the chemical energy into useful work. An adequacy of the parameters of the engine is required to better recover the injected energy.

(ii) When ethanol content increased, the specific gravity and the lower heating value of the fuel decreased. Such properties have to be compensated injecting more fuel. For this reason, the capacity of the pump to reach the volume of fuel demand has to be considered.

For this purpose, the injected energy for each condition, shown in Figure 76, was calculated in function of fuel consumption ($\dot{m}_f$), engine speed (N) and lower heating value of the blends (LHV_f), as given in equation 61.

$$E_{inj} = \frac{\dot{m}_f . LHV_f}{N} \tag{61}$$

PUC-Rio - Certificação Digital Nº 1312923/CA

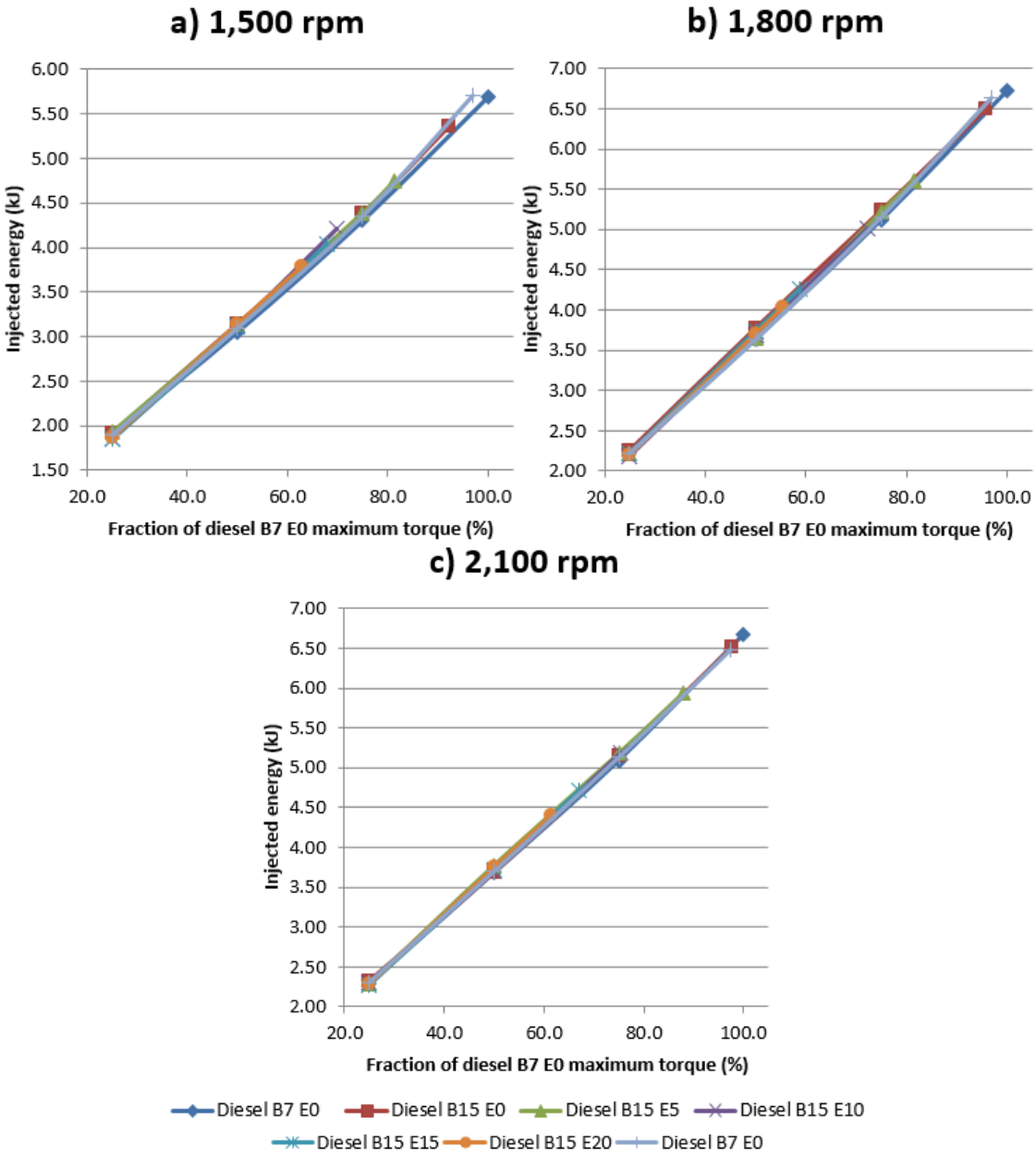

Figure 76: Injected energy (kJ) for each DBE blend and value of torque at a) 1,500 rpm, b) 1,800 rpm and c) 2,100 rpm.

It can be observed in Figure 76 that, for a determined blend and engine speed, the injected energy was almost a linear function of the torque. Moreover, as ethanol and biodiesel content increased, the curve slightly drifted to higher value of injected energy. This confirmed that it was necessary to inject a little more energy to have the same torque (and also brake power, since the engine speed was also determined). The optimization of combustion process was necessary to recover the chemical energy. Nevertheless, such variation was very small and did not justify on its own the significant reduction of torque.

PUC-Rio - Certificação Digital Nº 1312923/CA

Consequently, the injected volume for each condition was also calculated in function of fuel consumption ($\dot{m}_f$), engine speed (N) and specific gravity (ρ_f) of the blends to determine how the pump influenced the reduction of maximum torque, as given in equation 62:

$$V_{inj} = \frac{\dot{m}_f}{N.\rho_f} \tag{62}$$

The injected volume for each DBE blend and value of torque at different engine speeds is plotted in Figure 77.

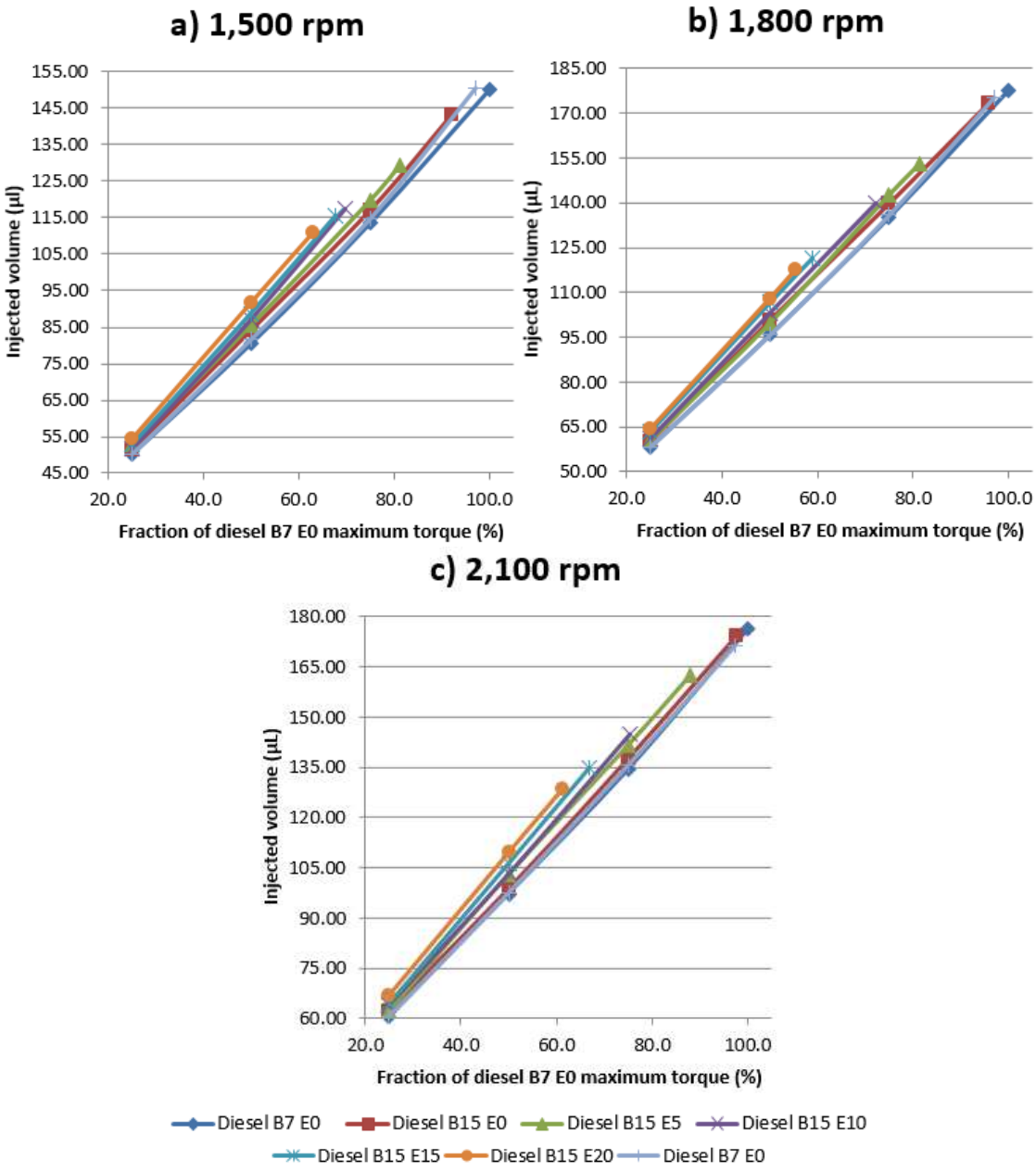

Figure 77: Injected volume (µL) for each DBE blend and value of torque at a) 1,500 rpm, b) 1,800 rpm and c) 2,100 rpm.

PUC-Rio - Certificação Digital Nº 1312923/CA

The Figure 77 showed that, for a determined blend and engine speed, the injected volume was, again, almost a crescent linear function of the torque. Again, as biodiesel and ethanol contents increased, the curve also drifted to increase the value of injected volume, but the variation was higher than for injected energy. This confirmed that it was necessary to inject a greater volume to have the same torque, due to the lower LHV and lower specific gravity.

Nevertheless, it also can be observed that a maximum volume of 178 μL was injected for commercial diesel B7 blend. When biodiesel content increased to 15 vol%, the maximum injected volume decreased by less than 5%. When ethanol was added to the blends, the injected volume at the maximum torque decreased for the maximum torque up to 30% in relation to the diesel B15 fuel. As commented by Hansen *et al.* (2001a), the reduction of the viscosity of the blend can interfere on the operation of the pump (leakage, lower pumping capacity) and explain the incapacity of the pump to reach the required volume.

PUC-Rio - Certificação Digital Nº 1312923/CA

Temperatures of lubricating oil (Figure 78), cooling water (Figure 79) and inlet air (Figure 80) and relative humidity (Figure 81) were recorded during the tests.

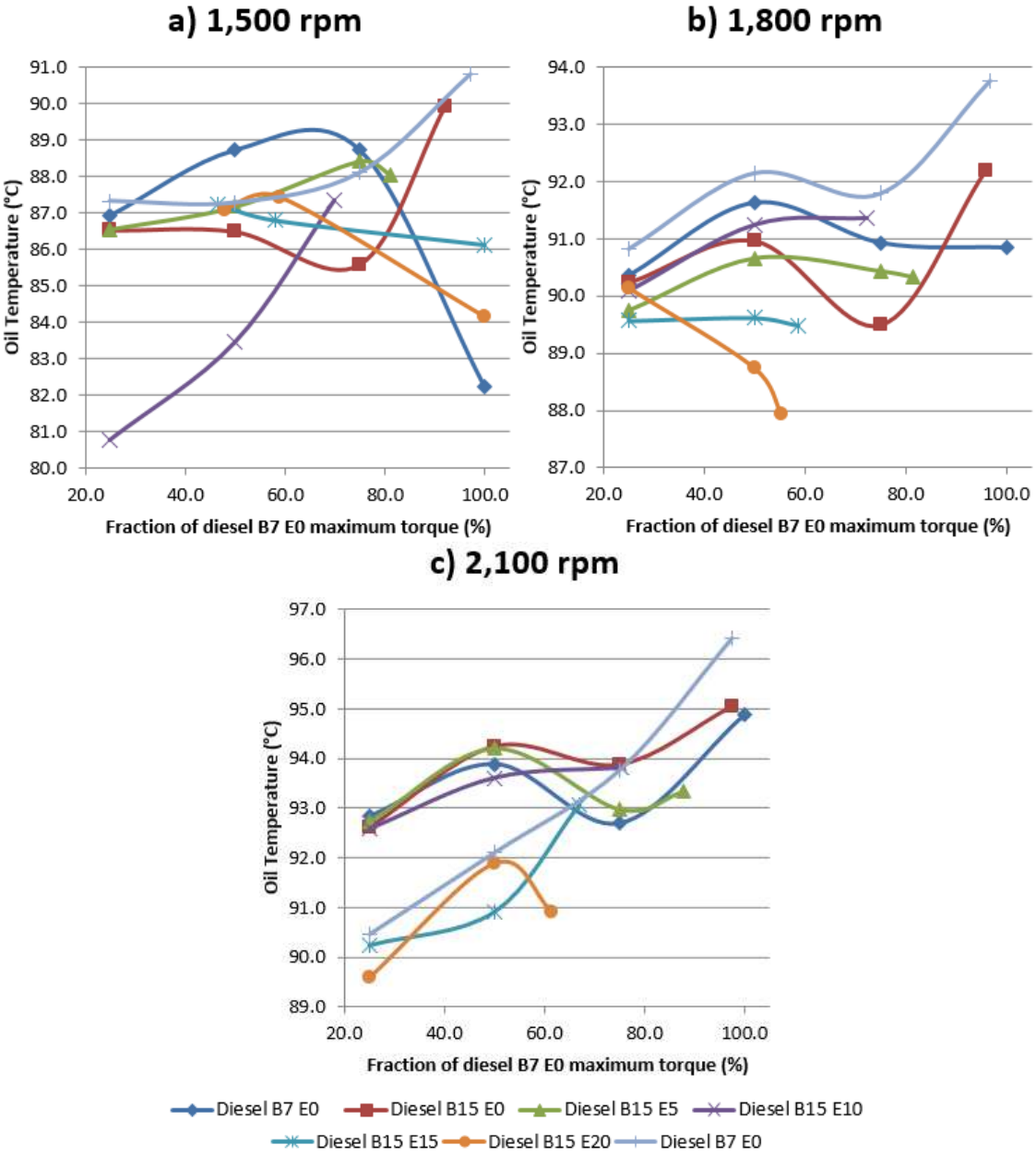

Figure 78: Lubricating oil temperature (°C) for each DBE blend and value of torque at a) 1,500 rpm, b) 1,800 rpm and c) 2,100 rpm.

PUC-Rio - Certificação Digital Nº 1312923/CA

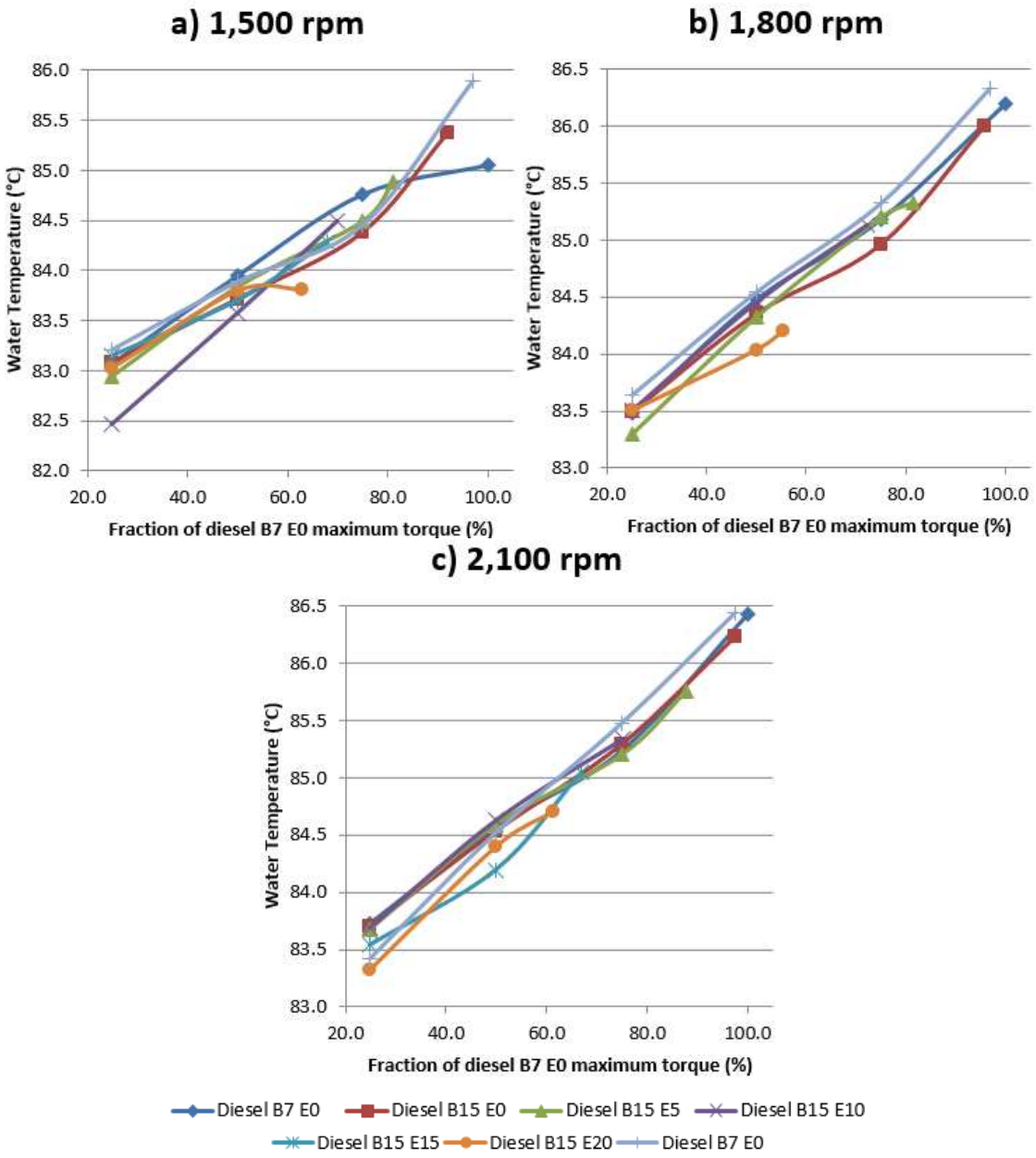

Figure 79: Water temperature (°C) for each DBE blend and value of torque at a) 1,500 rpm, b) 1,800 rpm and c) 2,100 rpm.

PUC-Rio - Certificação Digital Nº 1312923/CA

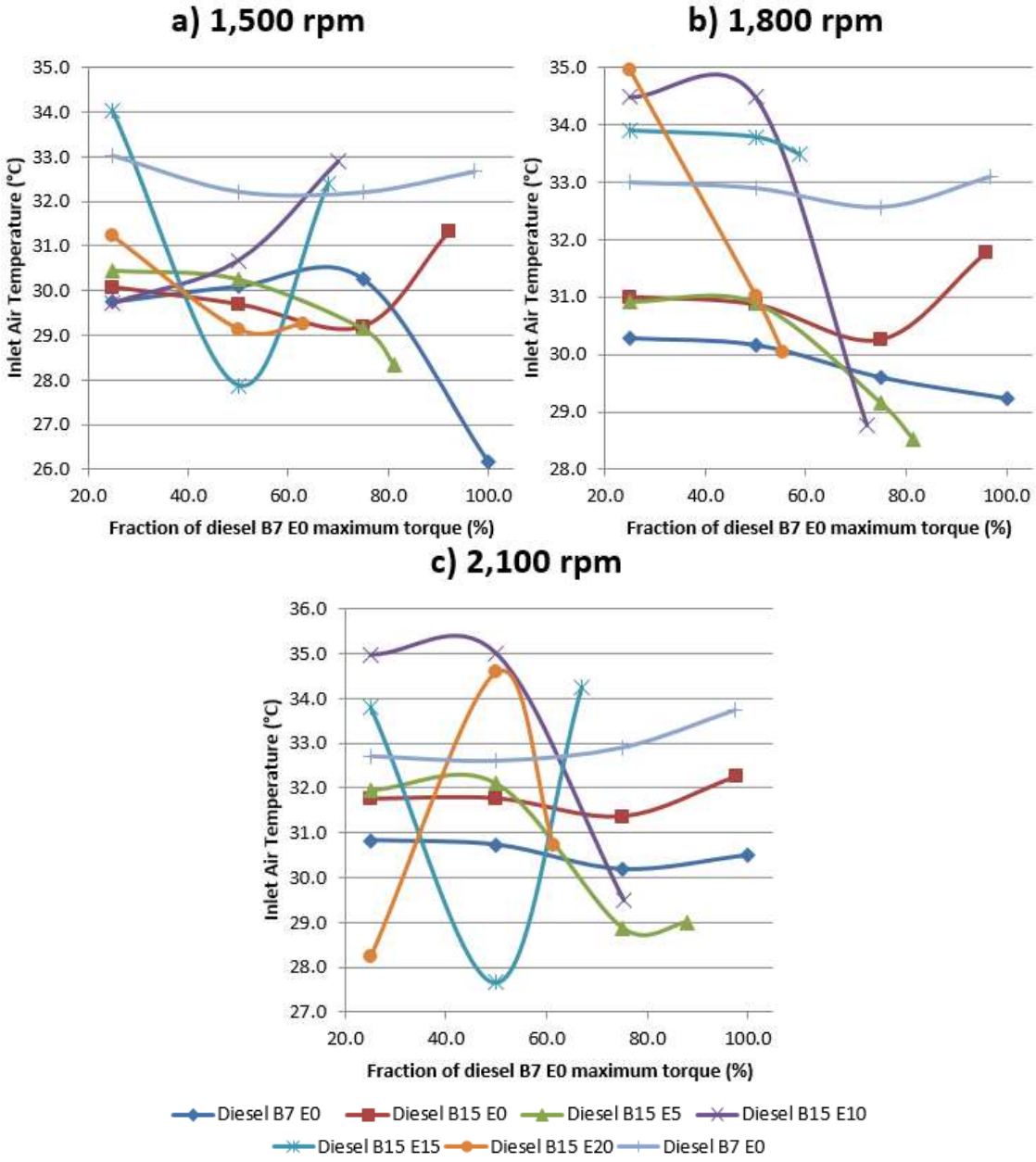

Figure 80: Inlet air temperature (°C) for each DBE blend and value of torque at a) 1,500 rpm, b) 1,800 rpm and c) 2,100 rpm.

PUC-Rio - Certificação Digital Nº 1312923/CA

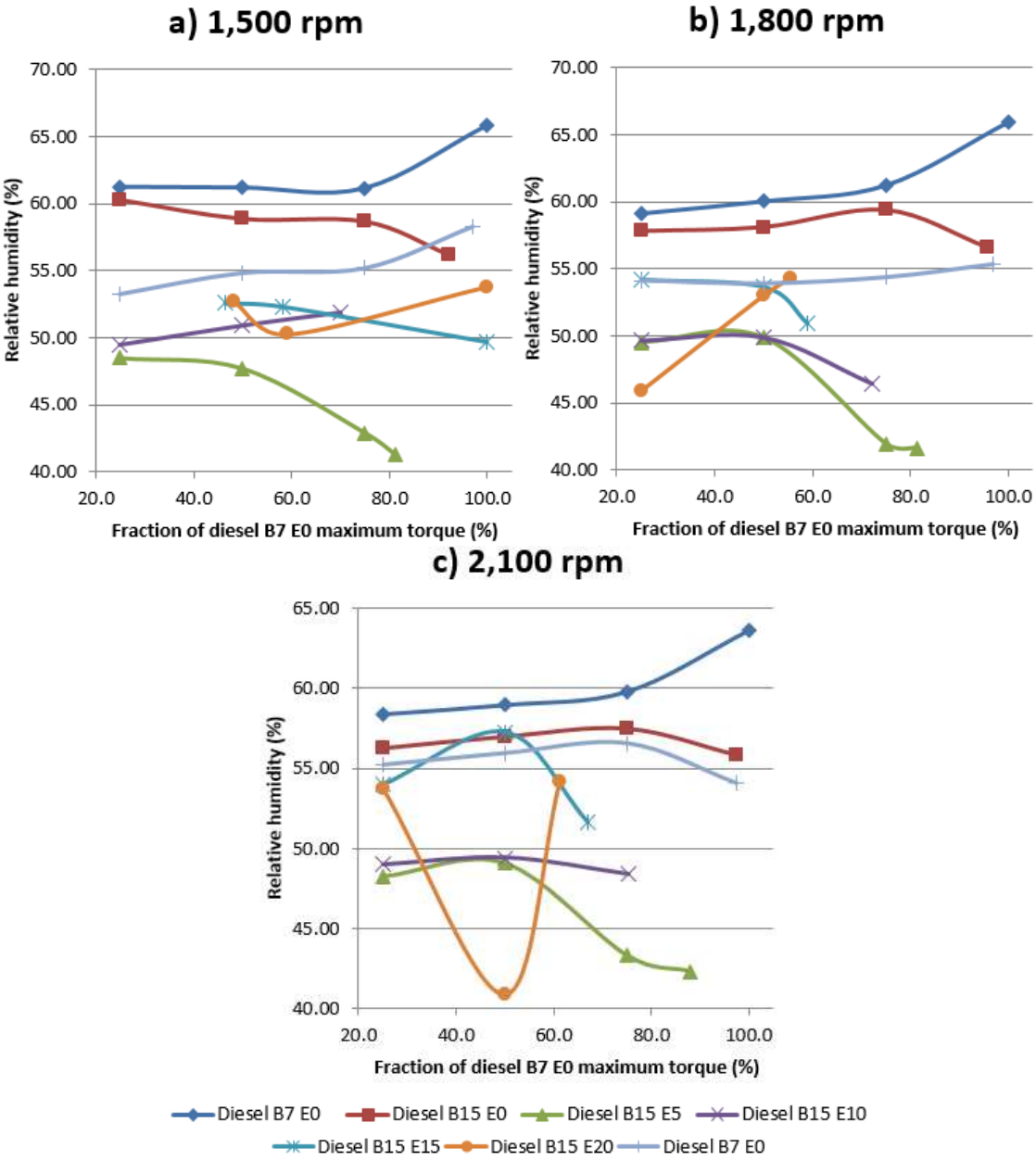

Figure 81: Relative humidity (%) for each DBE blend and value of torque at a) 1,500 rpm, b) 1,800 rpm and c) 2,100 rpm.

All values were comparable for same experimental conditions (engine speed and torque) and temperatures varied in the range of 90.0 ± 5.0°C, 84.4 ± 1.5°C and 31.3 ± 3.3°C, respectively. The relative humidity ranged from 40.8 to 60.0 %, with an average value of 53.6 %. The variations observed in inlet air temperature, in particular in diesel B15 E15 blends, could be explained by the necessity to repeat the experiments in different days, leading to the observed variation.

PUC-Rio - Certificação Digital Nº 1312923/CA

Temperature and pressure of exhaust gas were measured and plotted in Figures 82 and 83, respectively.

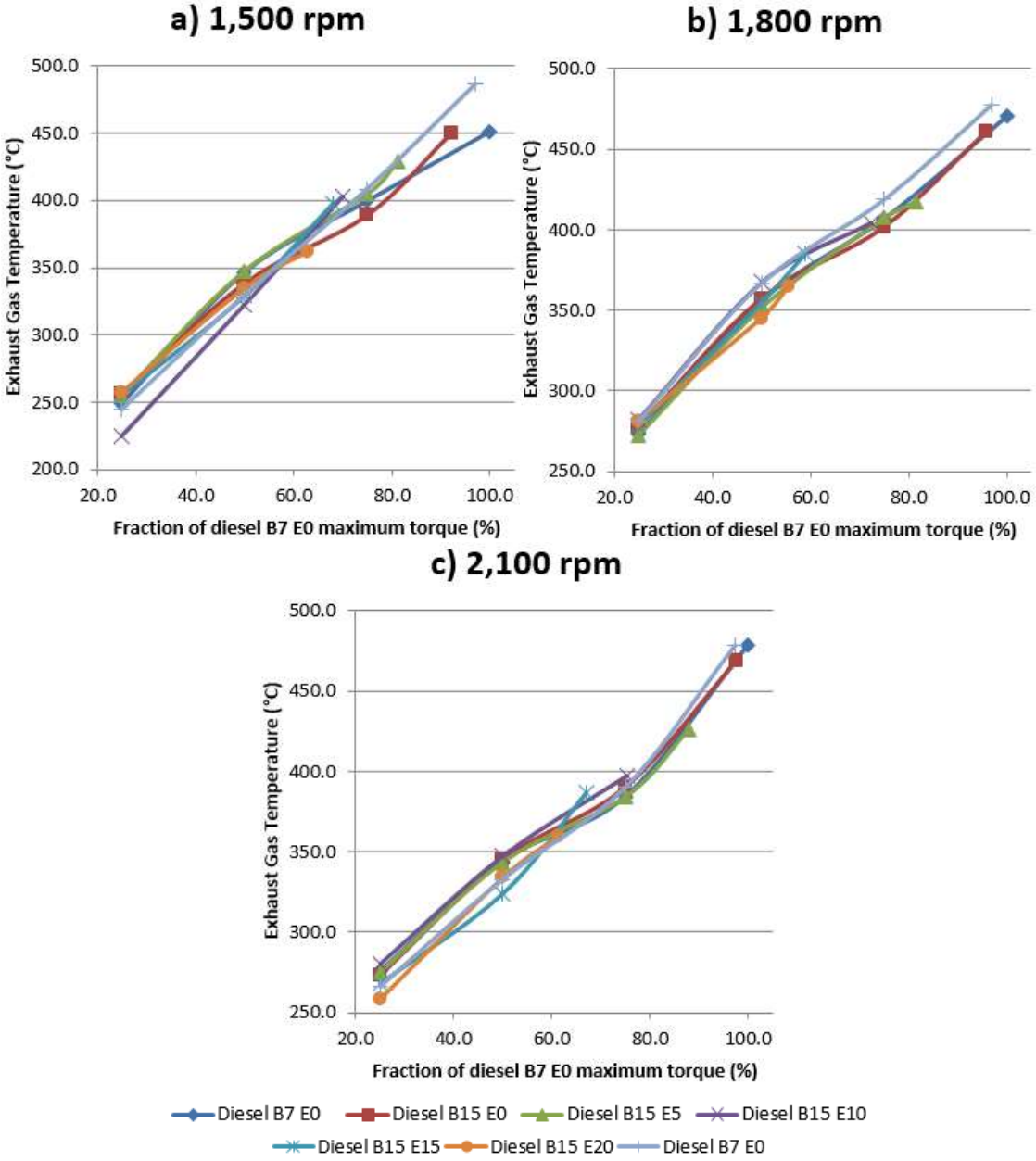

Figure 82: Exhaust gas temperature (°C) for each DBE blend and value of torque at a) 1,500 rpm, b) 1,800 rpm and c) 2,100 rpm.

PUC-Rio - Certificação Digital Nº 1312923/CA

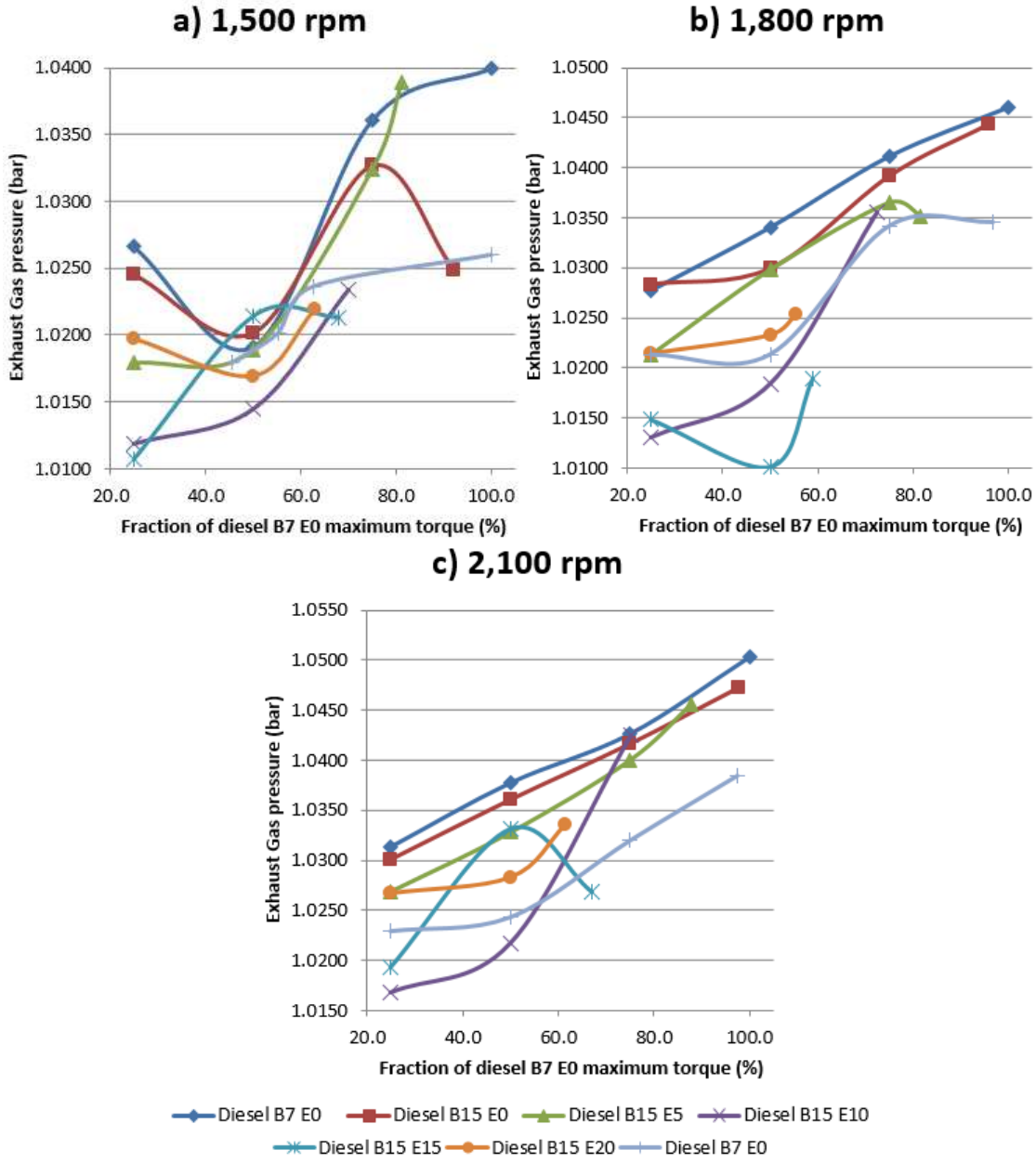

Figure 83: Exhaust gas pressure (bar) for each DBE blend and value of torque at a) 1,500 rpm, b) 1,800 rpm and c) 2,100 rpm.

It can be observed that, for a determined blend and engine speed, the temperature increased with the torque. The temperature was slightly influenced by the blend for a determined torque and engine speed, since the values were very close for a same condition (±10°C). Nevertheless, the exhaust gas temperature seemed to decrease slightly with the increase of the amount of ethanol existing in the blend. The lower cetane number of ethanol slowed the burning rate in the cylinder close to the TDC, which may cause a decrease in the exhaust gas temperature. Consequently, the rejected heat was almost the same. The comparison of the heat rejected through the exhausted gas did not go deeper

PUC-Rio - Certificação Digital Nº 1312923/CA

because the chemical composition of the combustion products was not defined in this work. The proper knowledge of the composition is necessary to determine their thermophysical properties and, consequently, the heat dissipated through the exhaustion.

Pressure also tended to increase with the torque for a determined blend and engine speed. All values of pressure were in the range of 1.01 to 1.05 bars. No further quantitative analysis of the absolute pressure was possible, since the comparison must be done considering the gauge pressure (acting as backpressure).

5.4.2. Fuel and Air Consumption

Fuel consumption for each condition was recorded as shown in Figure 84.

PUC-Rio - Certificação Digital Nº 1312923/CA

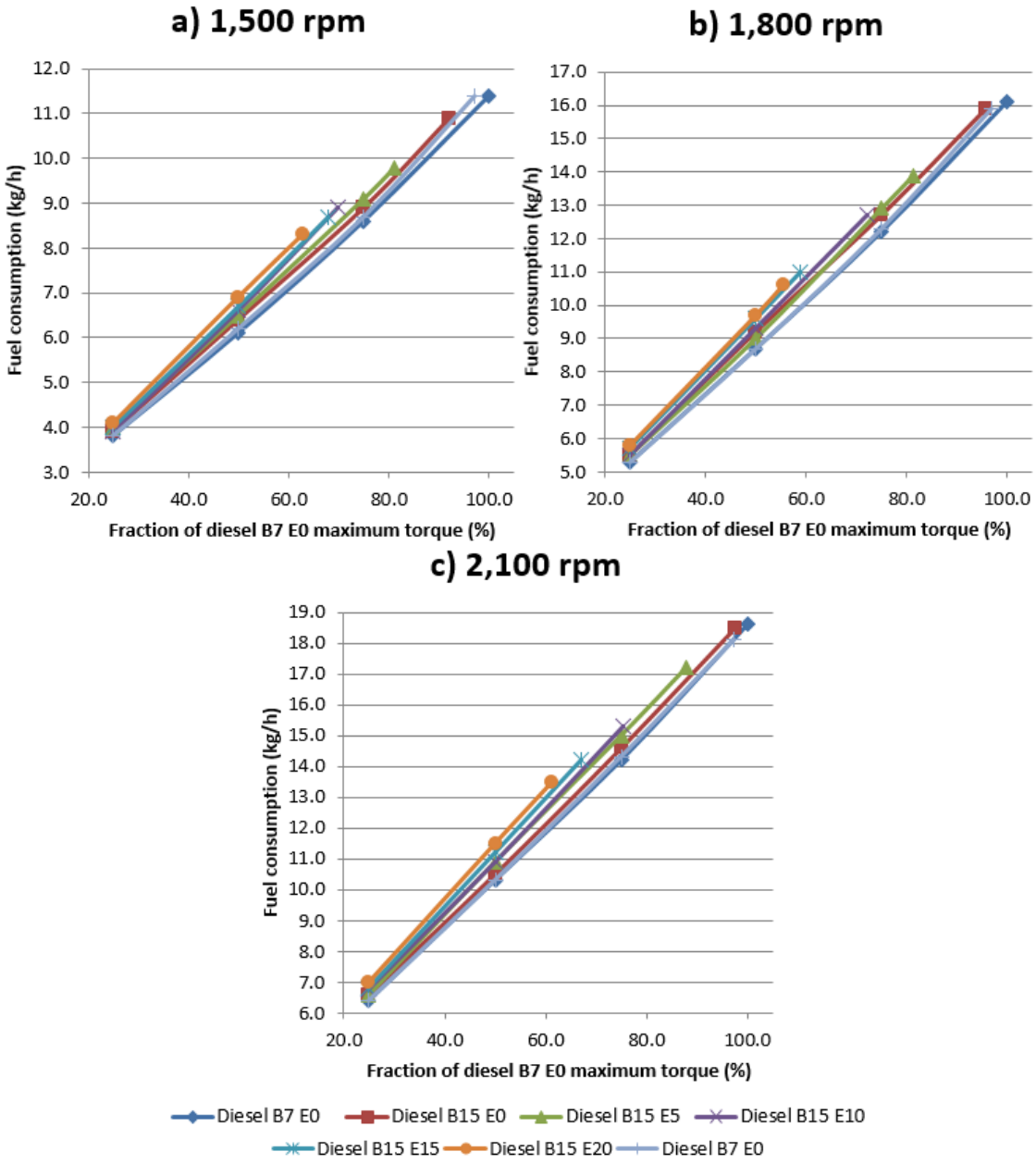

Figure 84: Fuel consumption (kg/h) for each DBE blend and value of torque at a) 1,500 rpm, b) 1,800 rpm and c) 2,100 rpm.

It can be observed that fuel consumption ranged from 3.5 to 11.5 kg/h at 1,500 rpm, 5.0 to 16.0 kg/h at 1,800 rpm and 6.0 to 19.0 kg/h at 2,100 rpm. For a determined blend and engine speed, the injected energy was almost a crescent linear function of the torque. Moreover, as biodiesel and ethanol contents increased, the curve slightly drifted to higher values. Again, this confirmed that it was necessary to inject more mass (and, consequently, more energy) to have the same torque to the lower LHV and specific gravity.

PUC-Rio - Certificação Digital Nº 1312923/CA

Air consumption was also recorded and the air / fuel ratio was calculated for each condition. The values are plotted in Figure 85.

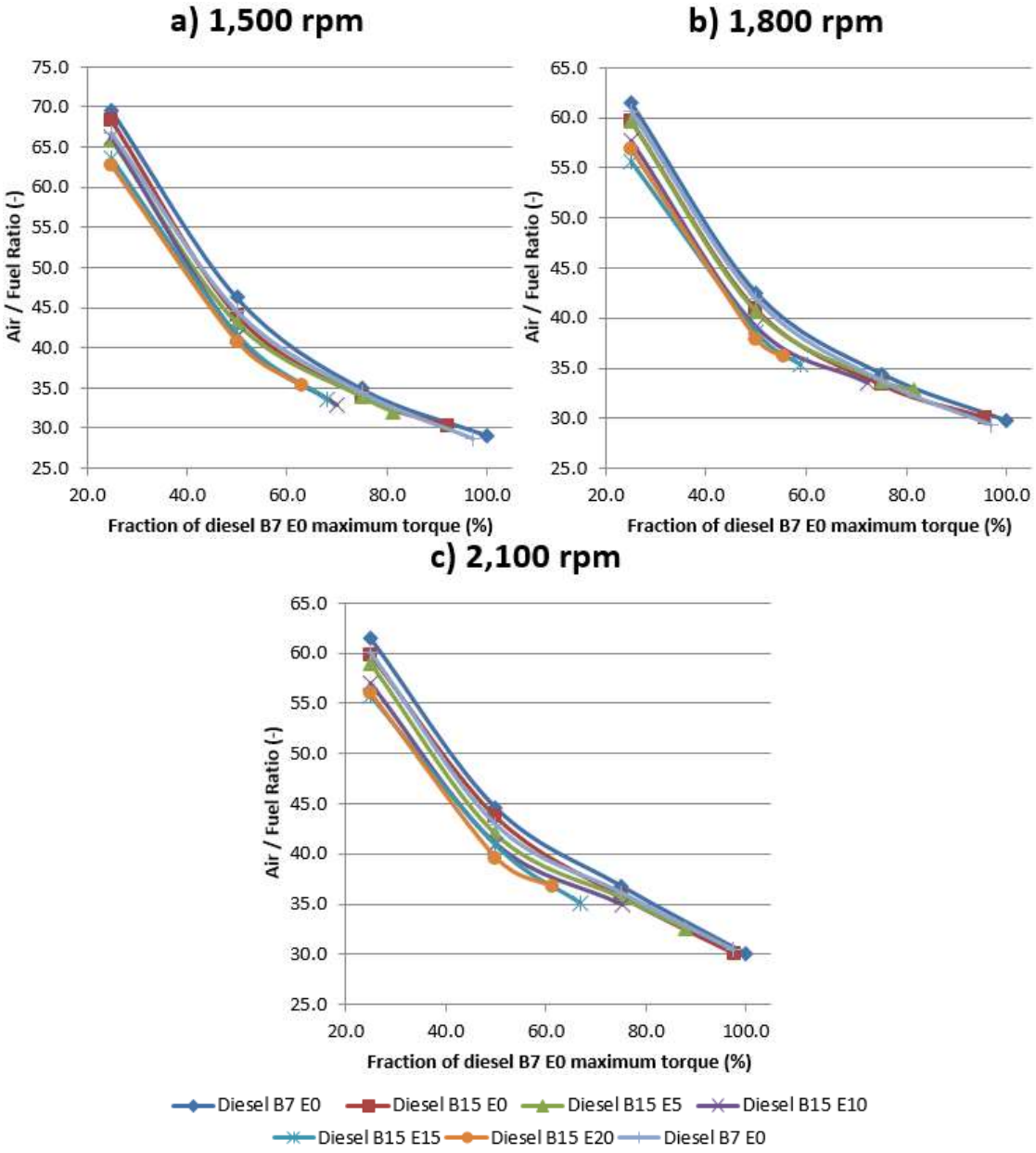

Figure 85: Air / fuel ratio (kg/kg) for each DBE blend and value of torque at a) 1,500 rpm, b) 1,800 rpm and c) 2,100 rpm.

It can be observed that, for a determined blend and engine speed, this parameter decreased with the torque. Moreover, as biodiesel and ethanol contents increased, the curve slightly drifted to lower values. Once more, this confirmed that it was necessary to inject more fuel and energy to have the same torque. The consumption of air, at these constant engine speeds, increased due to the performance of the turbocharger assembly.

PUC-Rio - Certificação Digital Nº 1312923/CA

From the air / fuel ratio for each condition, the lambda was calculated and the Figure 86 presents these values.

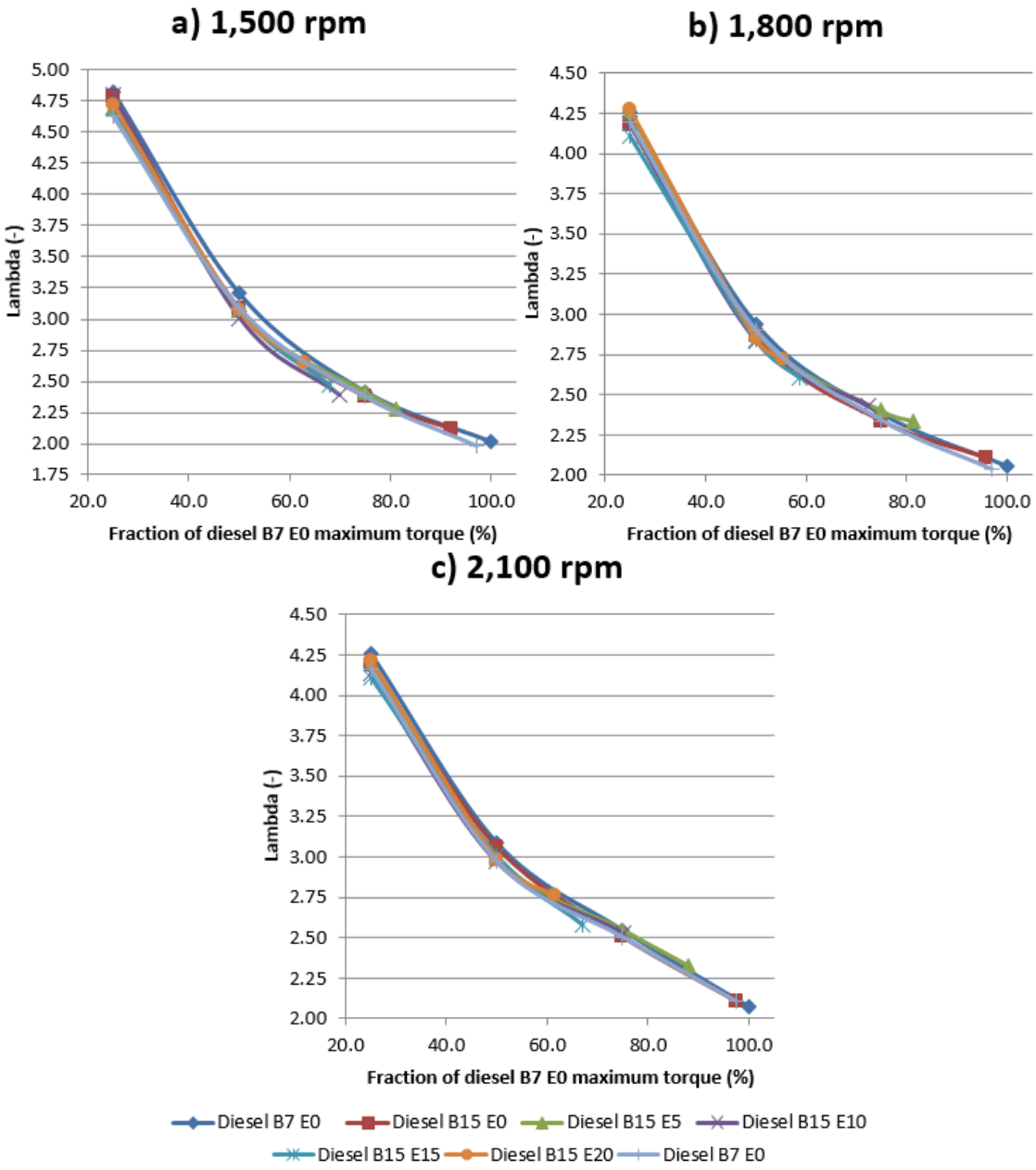

Figure 86: Lambda (-) for each DBE blend and value of torque at a) 1,500 rpm, b) 1,800 rpm and c) 2,100 rpm.

For a determined blend and engine speed, the lambda values decreased with the torque, from 4.75 (1,500 rpm) and 4.25 (1,800 and 2,100 rpm) for 25% of the maximum B7 torque to 2.00 for maximum torque with commercial diesel B7 fuel. All lambdas were characteristic of lean mixture, in the traditional range met for compression ignition engine. Moreover, the lambda seemed to be independent of the blends as the curves were almost overlaid.

PUC-Rio - Certificação Digital Nº 1312923/CA

Specific fuel consumption of the blend was determined for each condition and plotted in Figure 87.

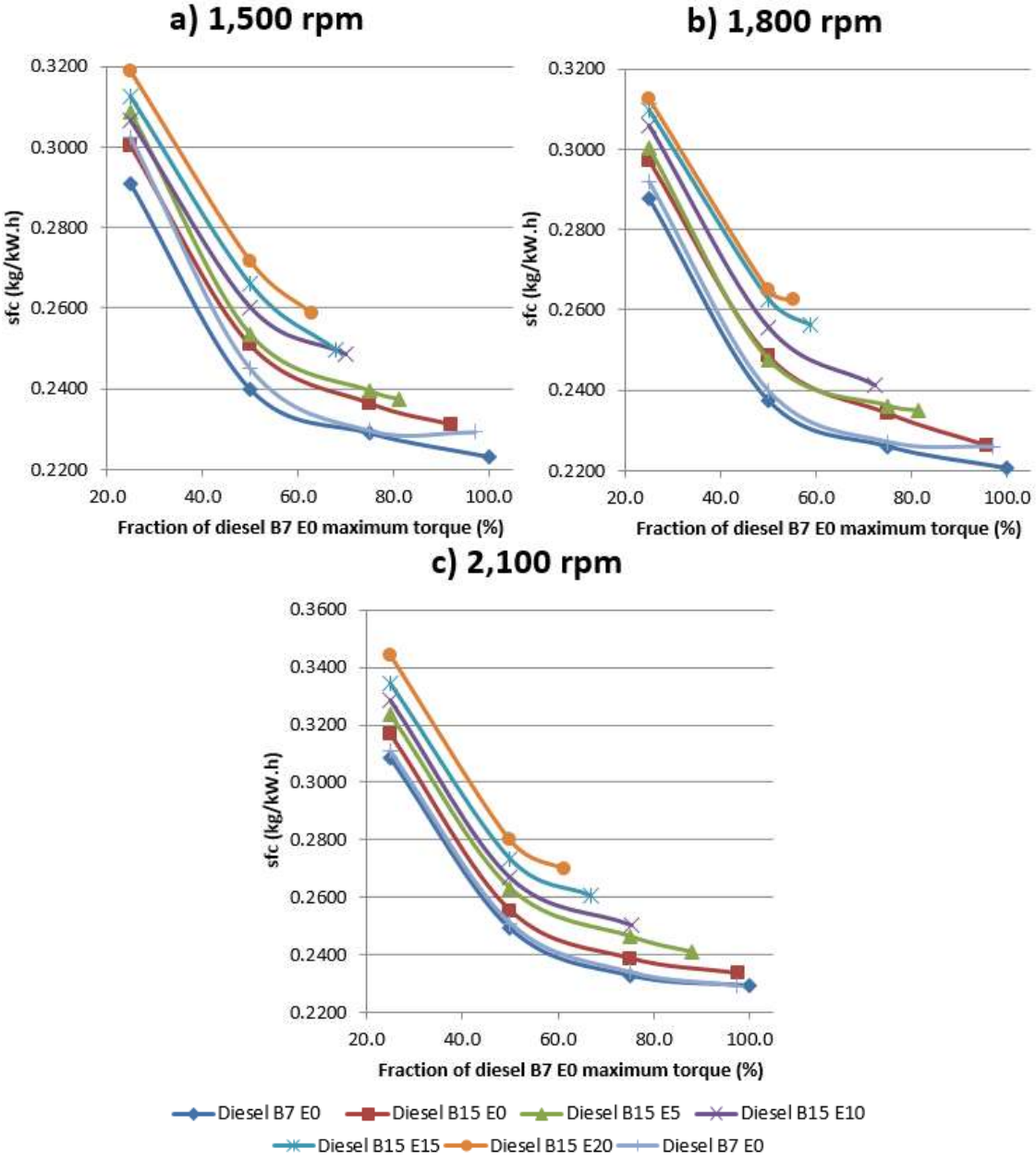

Figure 87: Specific fuel consumption (kg/(kW.h)) for each DBE blend and value of torque at a) 1,500 rpm, b) 1,800 rpm and c) 2,100 rpm.

It can be observed that, for a determined blend and engine speed, this parameter decreased with the torque. Moreover, as biodiesel and ethanol contents increased, the curve drifted to higher values. Values increased up to 4.7% when biodiesel content increased from 7 to 15 vol%. Specific fuel consumption increased almost 2% for each 5 vol% of anhydrous ethanol added in the blends, up to 9.6% for diesel B15 E20 fuel at 2,100 rpm and 50% of the maximum diesel B7

PUC-Rio - Certificação Digital Nº 1312923/CA

fuel torque. Again, this confirmed that it was necessary to inject more fuel to have the same torque.

For blends with ethanol, it was possible to extract the specific fuel consumption of ethanol. For this purpose, it was considered that the specific fuel consumption of the blend could be divided in two fractions, in function of the mass fraction of diesel B15 fuel and ethanol in the blends, as given in equation 37. Such values are plotted in Figure 88.

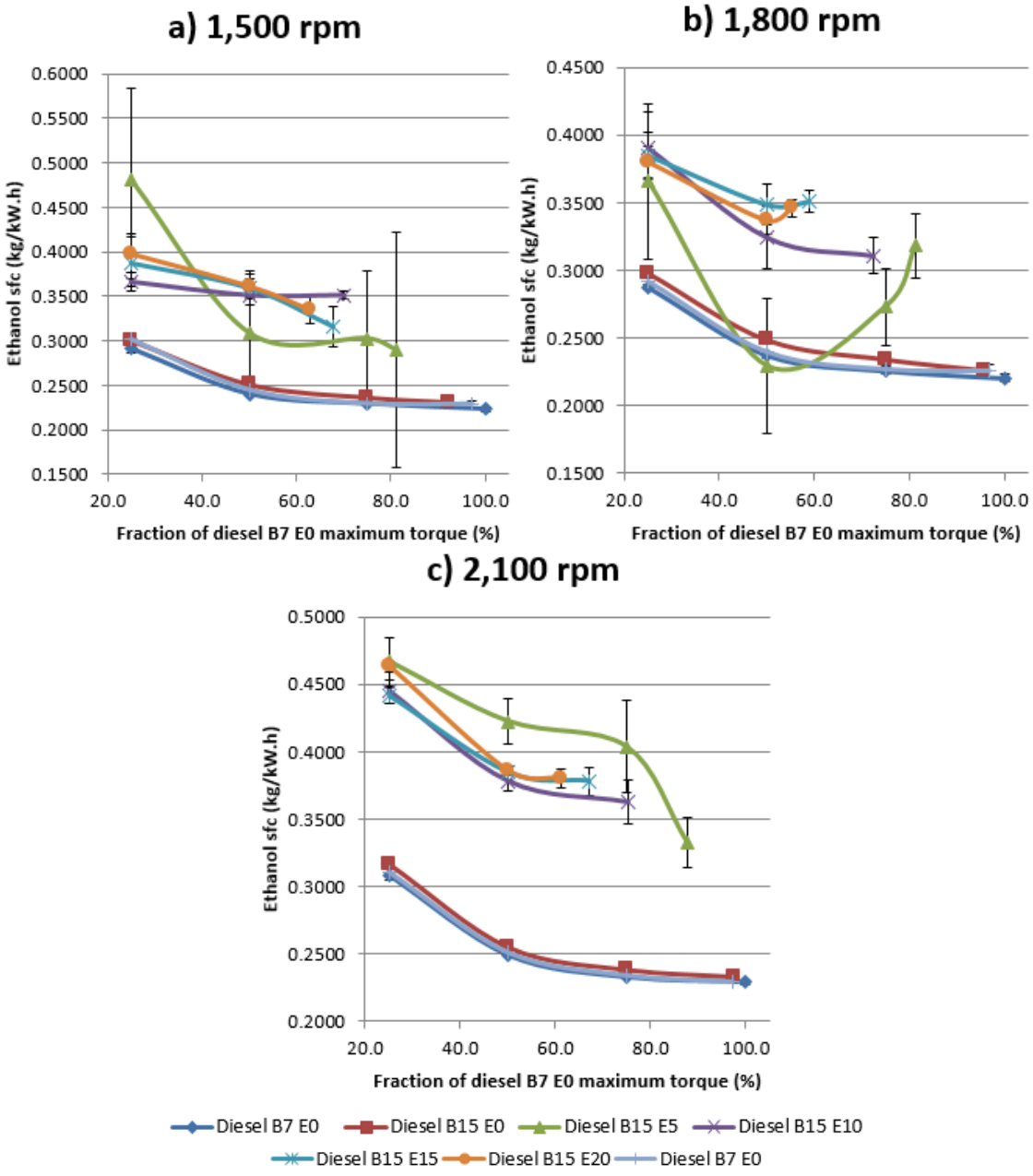

Figure 88: Specific fuel consumption due to ethanol (kg/(kW.h)) for each DBE blend and value of torque at a) 1,500 rpm, b) 1,800 rpm and c) 2,100 rpm. References of diesel B7 and B15 fuels are also given for each engine speed.

PUC-Rio - Certificação Digital Nº 1312923/CA

It can be observed that, for a determined blend and engine speed, this parameter decreased with the torque. Values were 25 to 55% higher than those of diesel B7 and B15 fuels were. This increase was expected since ethanol has a 40% lower LHV than diesel B7 and B15 fuels. At a determined engine speed, all results had the same order of magnitude. It was not possible to clearly define the impact of ethanol content in DBE blends in this parameter. It can be noticed that the results obtained for diesel B15 E5 blends were quite different. Indeed, such results must be considered carefully as the values of the specific fuel consumption of the blend were very close to those of the diesel B15 E0 fuel. Consequently, differences between both fuels were small and relative uncertainty was higher than for the other blends.

PUC-Rio - Certificação Digital Nº 1312923/CA

To compare the fuel on a same energy basis, the conversion of the injected energy (MJ) into useful power (kW.h), in the form of brake power, has to be considered. Values are plotted in Figure 89.

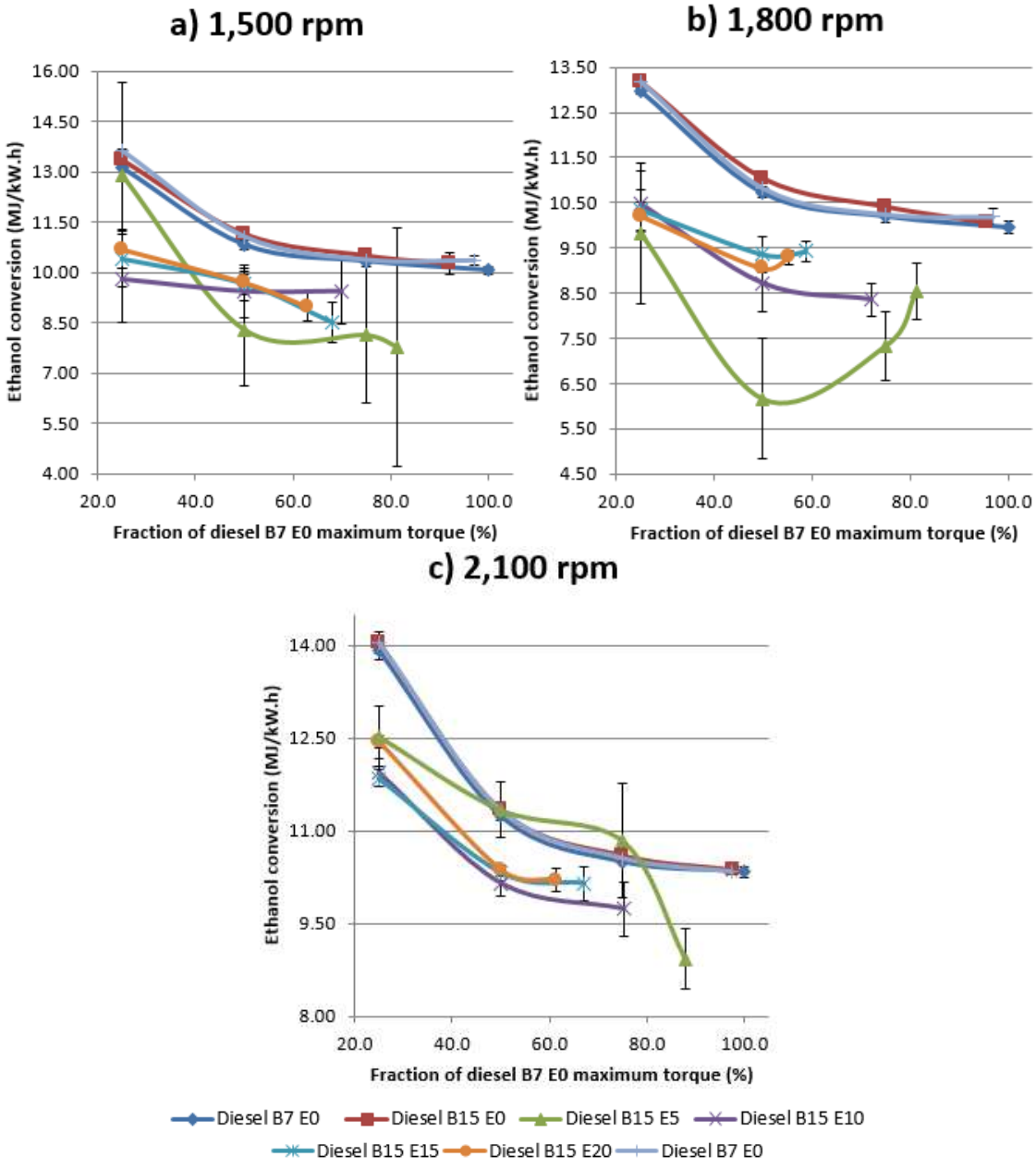

Figure 89: Conversion of ethanol (MJ/(kW.h)) for each DBE blend and value of torque at a) 1,500 rpm, b) 1,800 rpm and c) 2,100 rpm. References of diesel B7 and B15 fuels are also given for each engine speed.

At all engine speeds, this parameter decreased with the increase of load, showing that a better conversion of chemical energy was observed at high values of torque. Diesel B7 and B15 fuels had similar values and achieved the highest

PUC-Rio - Certificação Digital Nº 1312923/CA

values for conversion of chemical energy in the fuel. Again, results for diesel B15 E5 fuel have to be carefully considered, for the same formerly described reasons.

It can be observed that, in comparison with diesel B7 and B15 fuels, lower ethanol energy must be injected to produce useful work (difference of 1 or 2 MJ/(kW.h)). The economy made using ethanol was higher at low engine speeds than at high engine speeds and at low torque. This behavior was related to the combustion characteristics of the blends (see section 5.4.4).

To correlate these results with conversion of ethanol energy in useful power in spark ignition engine, these results were compared to those obtained by Villela (2010) with a Fiat 1.4 8v Fire tetrafuel fueled with anhydrous ethanol. This engine was projected to operate with gasoline A, gasoline C, hydrous ethanol, blends of gasoline C with hydrous ethanol at all proportions, and natural gas. Its electronic control unit (ECU) has specific calibration maps for the different fuels and strategies of interpolation between the maps that allow covering all the possibilities of blending between gasoline and ethanol. The compression ratio offers a compromise between the application gasoline and ethanol (10.35:1). Data were obtained for three conditions corresponding to conditions of maximum torque, maximum power and characteristic condition of a Siena vehicle, equipped with the same engine, at 60 km/h in the 5^{th} gear. Villela observed that values of conversion of ethanol energy varied from 10.90 to 13.83 MJ/(kW.h). These values were higher than those found in this study, with exception of results obtained with 25% of diesel B7 E0 fuel maximum torque at 2,100 rpm. Consequently, the chemical energy into the anhydrous ethanol was better converted into useful work in the investigated Diesel engine then in flex fuel gasoline vehicles.

PUC-Rio - Certificação Digital Nº 1312923/CA

5.4.3. Brake Mean Effective Pressure (BMEP) and Indicated Mean Effective Pressure (IMEP)

Figure 90 gives the brake mean effective pressure (BMEP) for each DBE blend and value of torque at different engine speeds.

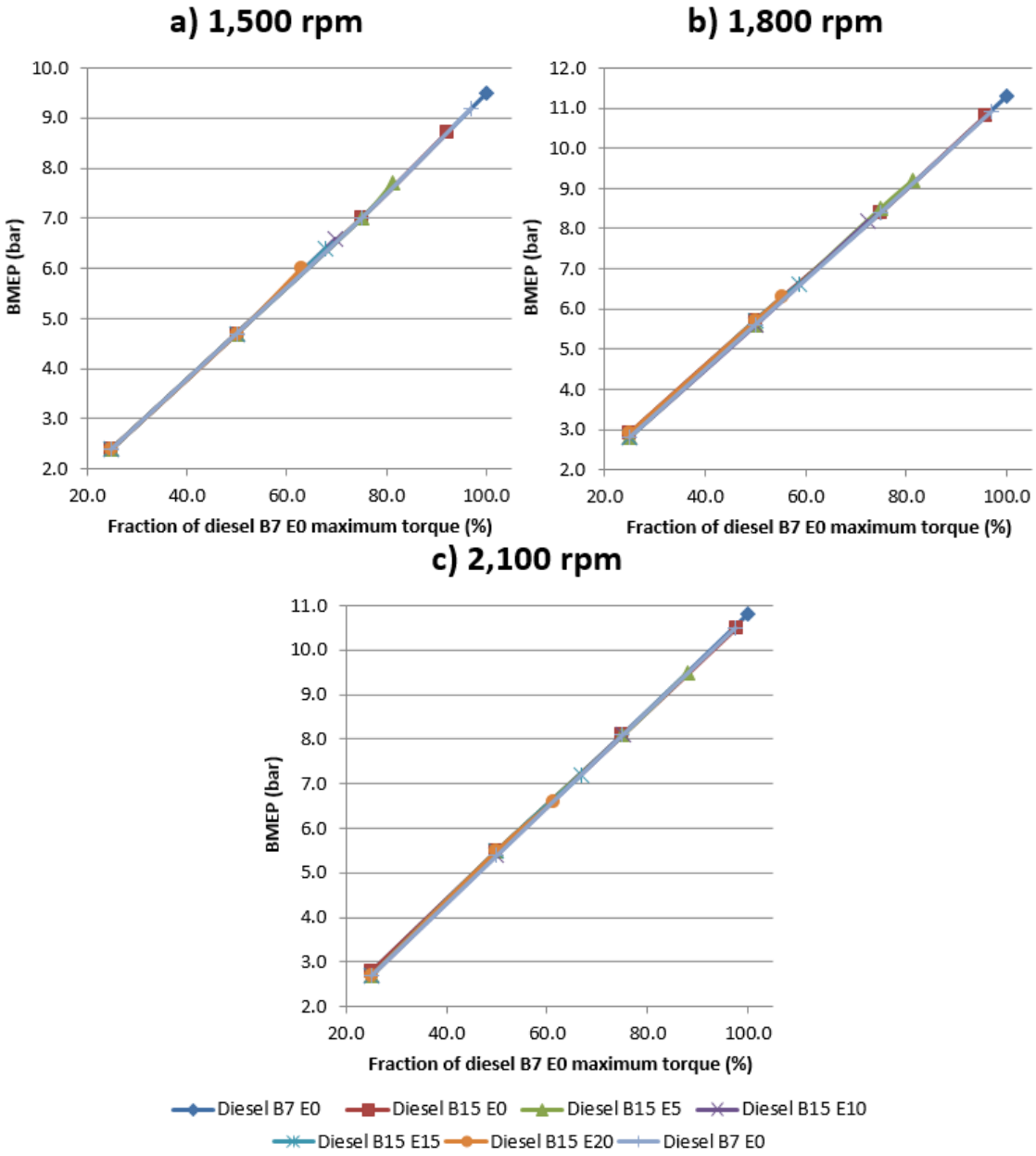

Figure 90: Brake Mean Effective Pressure (BMEP, bar) for each DBE blend and value of torque at a) 1,500 rpm, b) 1,800 rpm and c) 2,100 rpm.

As expected, it can be observed in Figure 90 that, for a determined engine speed, the BMEP was a crescent linear function of the torque and the curves were overlaid. Such observation confirmed the good execution of the experimental procedure since the value of brake power was determined through the conditions of engine speed and torque.

PUC-Rio - Certificação Digital Nº 1312923/CA

In Figure 91, the indicated mean effective pressure (IMEP) is plotted for each DBE blend and value of torque at different engine speeds.

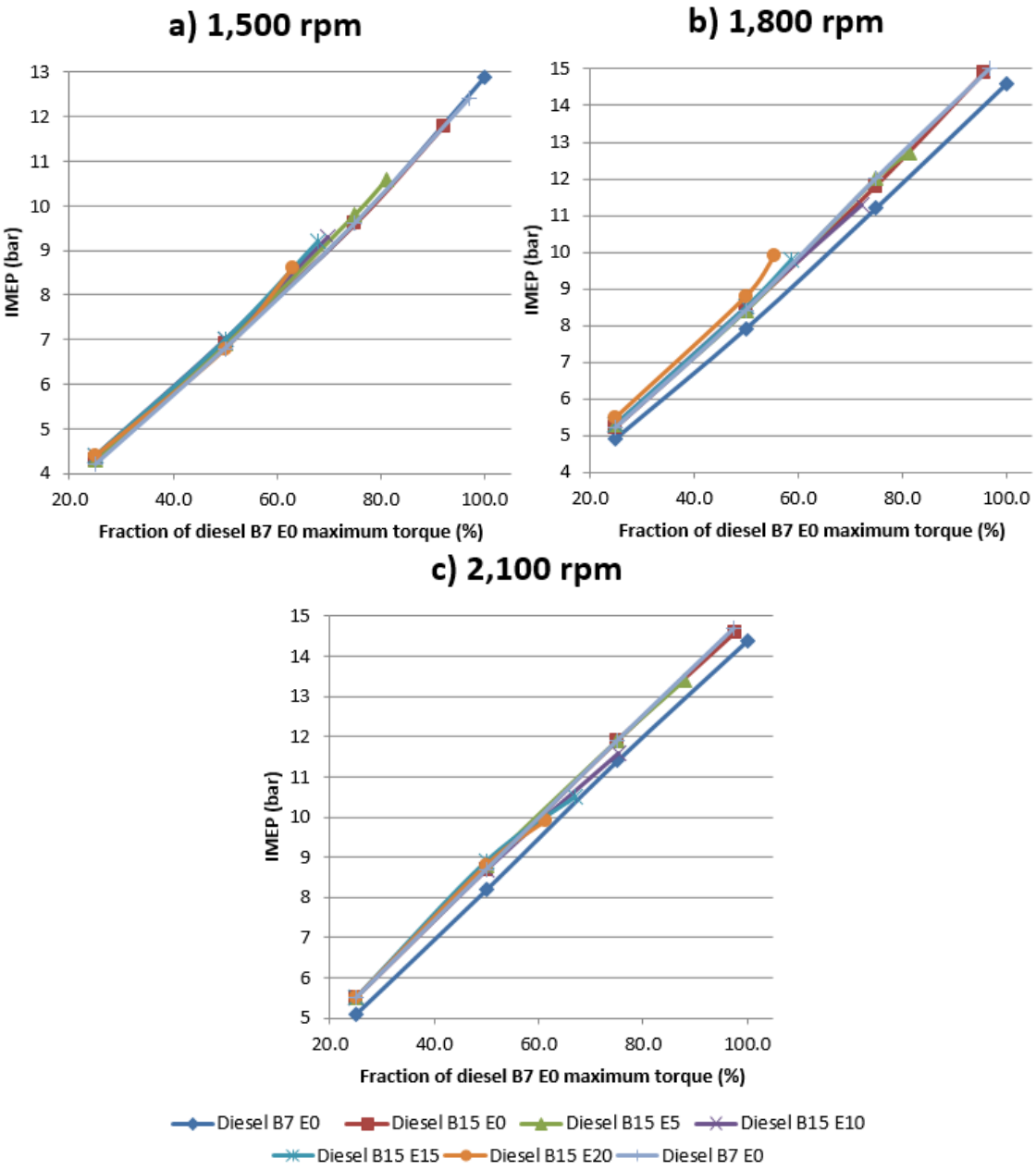

Figure 91: Indicated Mean Effective Pressure (IMEP, bar) for each DBE blend and value of torque at a) 1,500 rpm, b) 1,800 rpm and c) 2,100 rpm.

For a determined blend and engine speed, the IMEP was a crescent function of the torque. Such curves were almost linear function of torque. Moreover, as biodiesel and ethanol contents increased, the curve slightly drifted to higher values. This behavior can be explained by an increase of the friction power when ethanol content increased. At medium and high engine speeds, the first repetition

PUC-Rio - Certificação Digital Nº 1312923/CA

of diesel B7 fuel presented much lower values of IMEP. Again, this confirmed that it was necessary to inject more energy to compensate the friction power and to obtain the same torque.

5.4.4. Combustion Characteristics

For each blend and engine speed, the ignition delay determined from the heat liberation rate was plotted in Figure 92.

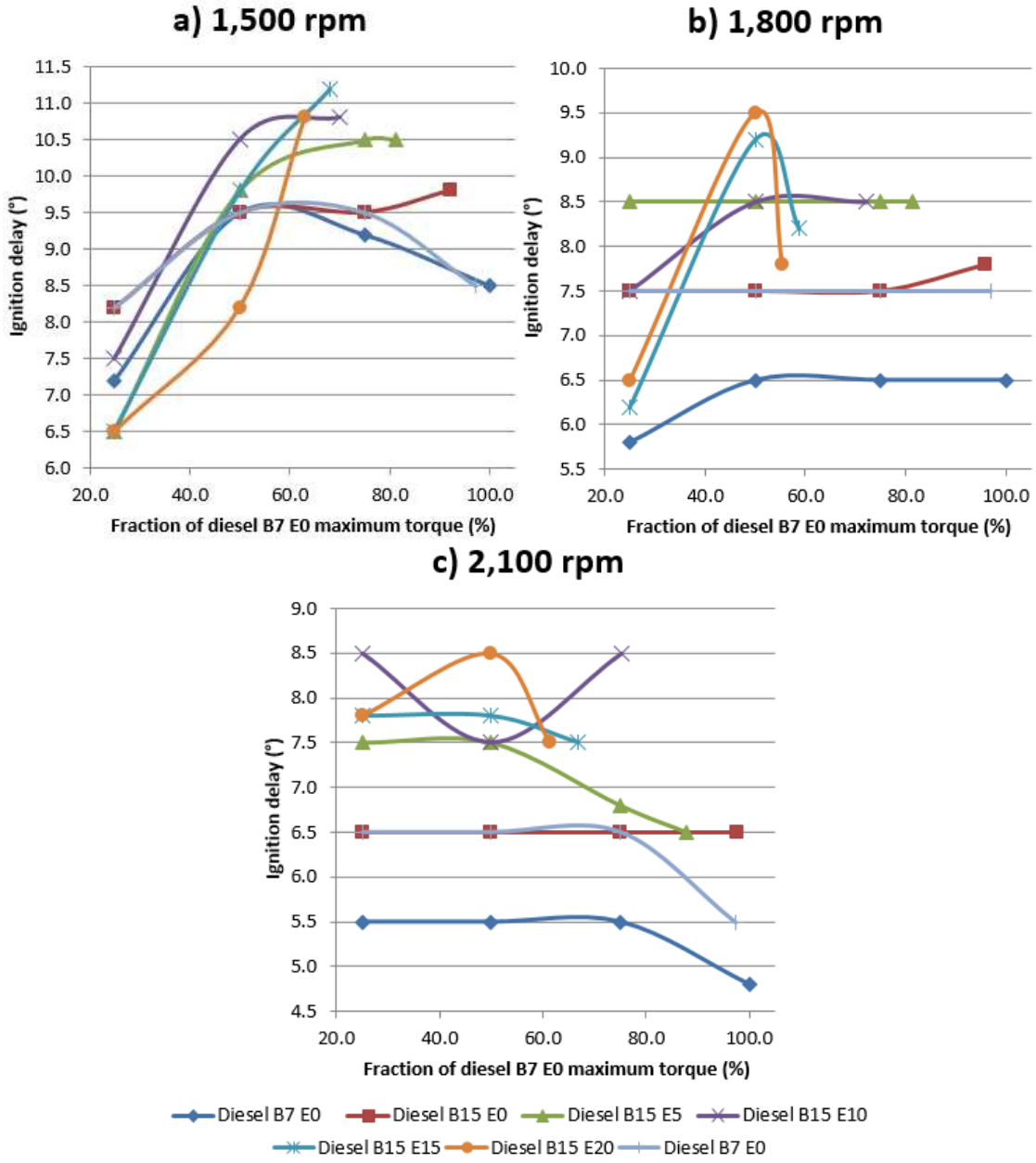

Figure 92: Ignition delay (°) for each DBE blend and value of torque at a) 1,500 rpm, b) 1,800 rpm and c) 2,100 rpm.

PUC-Rio - Certificação Digital Nº 1312923/CA

The ignition delay varied from 6.5 to 11.2° at 1,500 rpm, 5.7 to 9.5° at 1,800 rpm and 4.7 to 8.5° at 2,100 rpm. As observed by Hulwan *et al.* (2011), the ignition delay was higher when the engine was under low load at low and medium engine speeds since the fuel had more time to vaporize in a favorable situation of air excess. At high engine speed, this parameter looked constant. Time available for fuel vaporization was reduced and, as the load increased, the temperatures of the residual gas in the cylinder and that of cylinder walls contributed to early ignition of the blends.

Nevertheless, comparing diesel B7 and B15 fuels, it was expected to observe a reduction of ignition delay with the increase of biodiesel content as its cetane number was slightly higher than for pure diesel fuel. The opposite behavior was observed, since ignition delay slightly increased. The difference with the experimental behavior could be related to three main factors:

(i) The cetane number of the diesel fuel used in the diesel B7 and B15 blends could be different.

(ii) The cetane number of the biodiesel was function of its nature and its origin. Different compositions influenced differently the cetane number.

(iii) The uncertainty associated to the different calculation necessary to obtain the gross heat liberation rate could affect the results. However, such uncertainty was almost the same for all blends.

This increase of ignition delay was more evident at 1,800 rpm and 2,100 rpm due to the combustion characteristics of the blends.

As observed by Park *et al.* (2010 and 2012), Hulwan *et al.* (2011) and Kannan (2013), the ignition delay increased with the ethanol content, with exception of the lower investigated torque at 1,500 rpm (the fuel had more time to vaporize in a favorable situation of air excess). This tendency to present higher ignition delay values was related to the decrease of the pressure and temperature levels at the end of the compression because of the higher latent heat of vaporization (according to Zhu *et al.* (2011), $\Delta h_{Euro\ V\ diesel}$ = 250-290 kJ/kg; $\Delta h_{biodiesel}$ = 300 kJ/kg and $\Delta h_{anhydrous\ EtOH}$ = 840 kJ/kg) and specific heat at constant pressure of ethanol with respect to air (according to Sonntag *et al.* (2003), at 25°C and 100 kPa, $c_{p_{air,d}}$ = 1.004 kJ/(kg.K) and $c_{p_{EtOH}}$ = 2.46 kJ/(kg.K)). Moreover, the ethanol had a much lower cetane number than the diesel

PUC-Rio - Certificação Digital Nº 1312923/CA

fuel and biodiesel, influencing the values of the required pressure and temperature to ignite the air-fuel mixture.

This behavior can also be observed on the indicated pressure in function of crank angle, CA, shown in Figure 93, and recovered chemical energy (see Figure 102 discussed later).

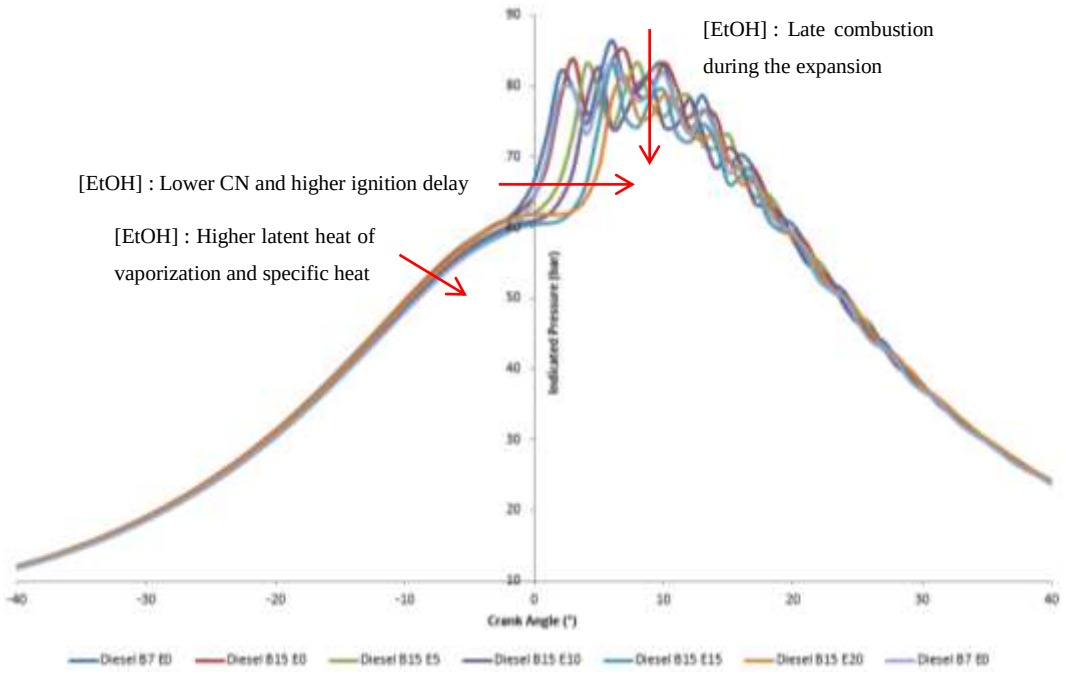

Figure 93: Indicated pressure (bar) for each DBE blend at 2,100 rpm and 25% of the maximum diesel B7 fuel maximum torque.

In Figure 93, all blends presents the same profile of indicated pressure. The chart also indicates that detonation occurred during the combustion process of all blends.

The CA10, CA50 and CA90 were also an indicator of the combustion process, since they represented the value of crank angle where 10%, 50% and 90% of the energy due to combustion has been released, respectively. They were respectively plotted in Figures 94, 95 and 96 for the different blends, engine speeds and torques.

PUC-Rio - Certificação Digital Nº 1312923/CA

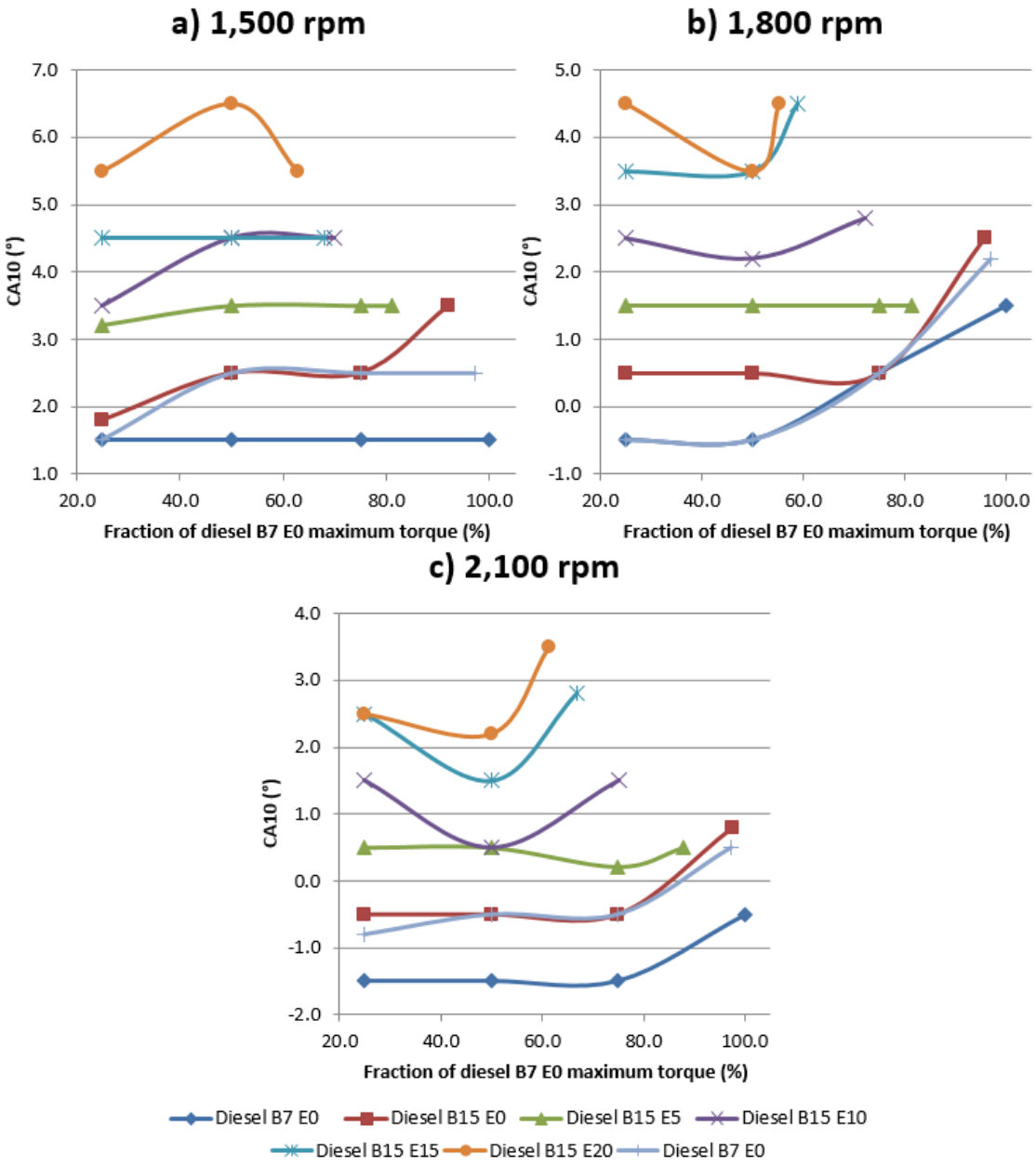

Figure 94: CA10 (°) for each DBE blend and value of torque at a) 1,500 rpm, b) 1,800 rpm and c) 2,100 rpm.

PUC-Rio - Certificação Digital Nº 1312923/CA

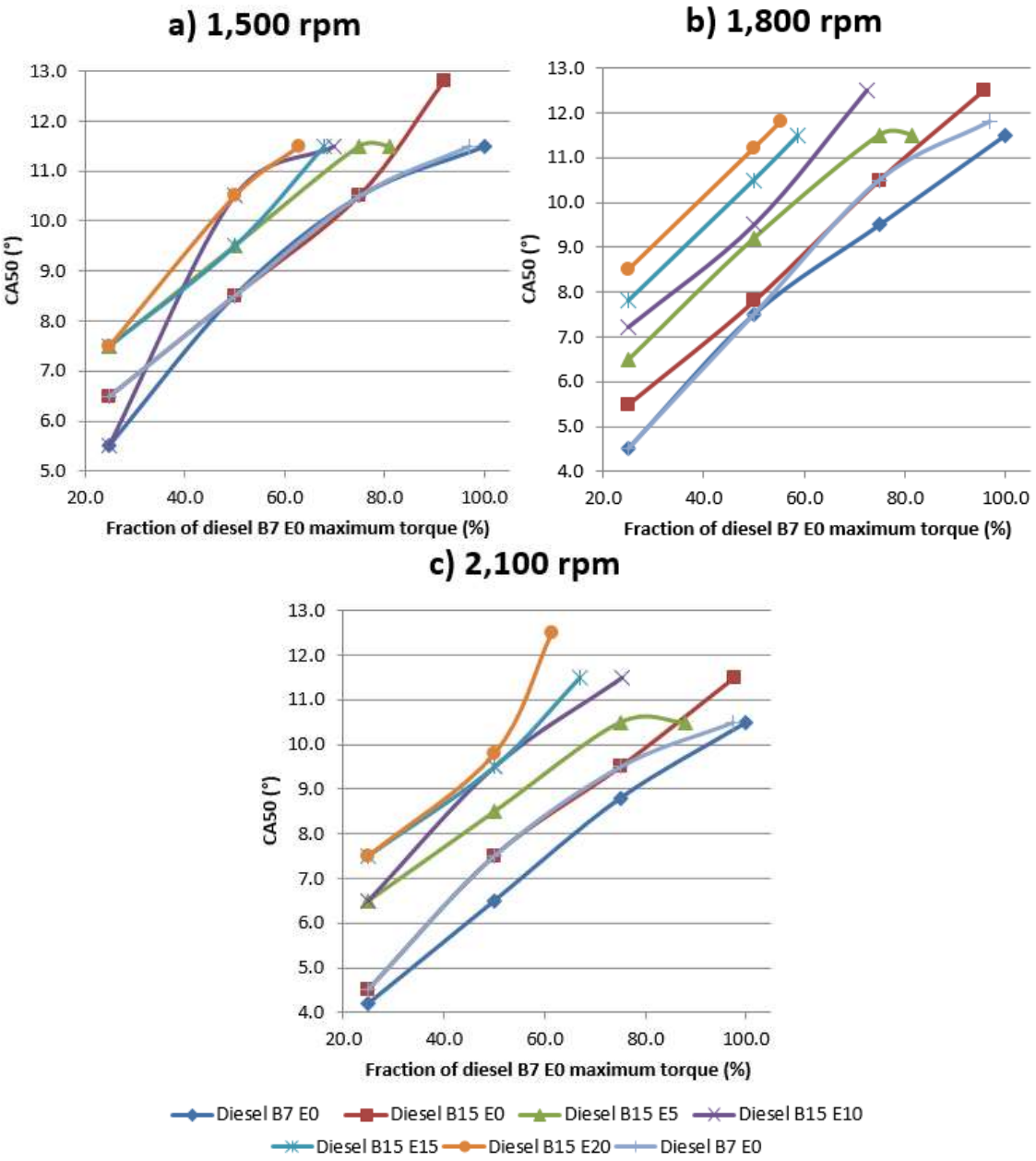

Figure 95: CA50 (°) for each DBE blend and value of torque at a) 1,500 rpm, b) 1,800 rpm and c) 2,100 rpm.

PUC-Rio - Certificação Digital Nº 1312923/CA

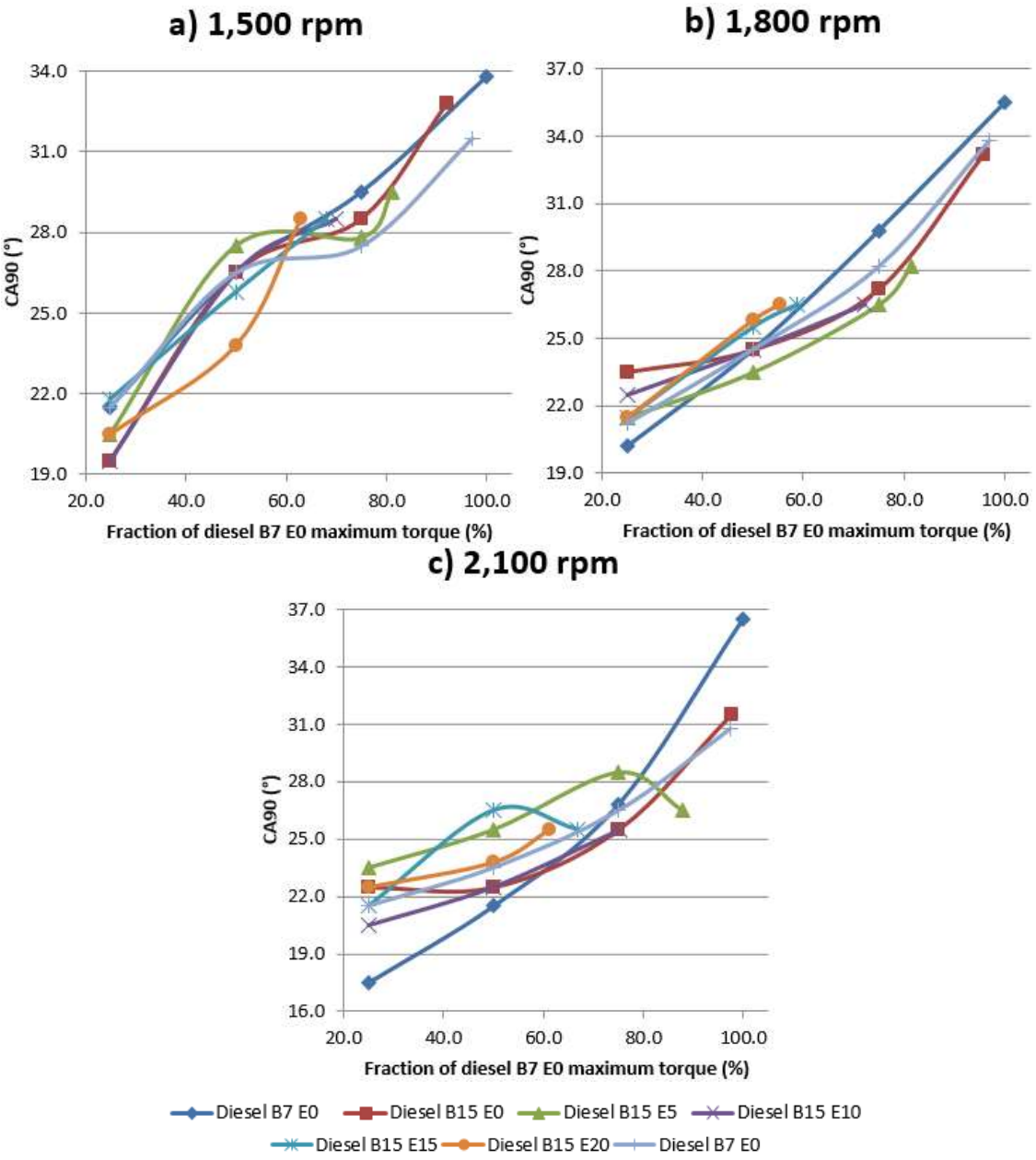

Figure 96: CA90 (°) for each DBE blend and value of torque at a) 1,500 rpm, b) 1,800 rpm and c) 2,100 rpm.

For a determined blend and engine speed, these parameters increased with the value of torque. The influence of torque increased during the combustion process. It can also be observed that the CA10 and CA50 increased with biodiesel and ethanol content. For the CA90 parameter, the situation was more complex: at 2,100 rpm, the previous tendency was also observed, while at 1,500 and 1,800 rpm, the CA90 decreased with biodiesel and ethanol content.

The determination of the parameter CA90-CA10 allowed assessing indirectly the duration of the combustion. Figure 97 gathers the values of this parameter.

PUC-Rio - Certificação Digital Nº 1312923/CA

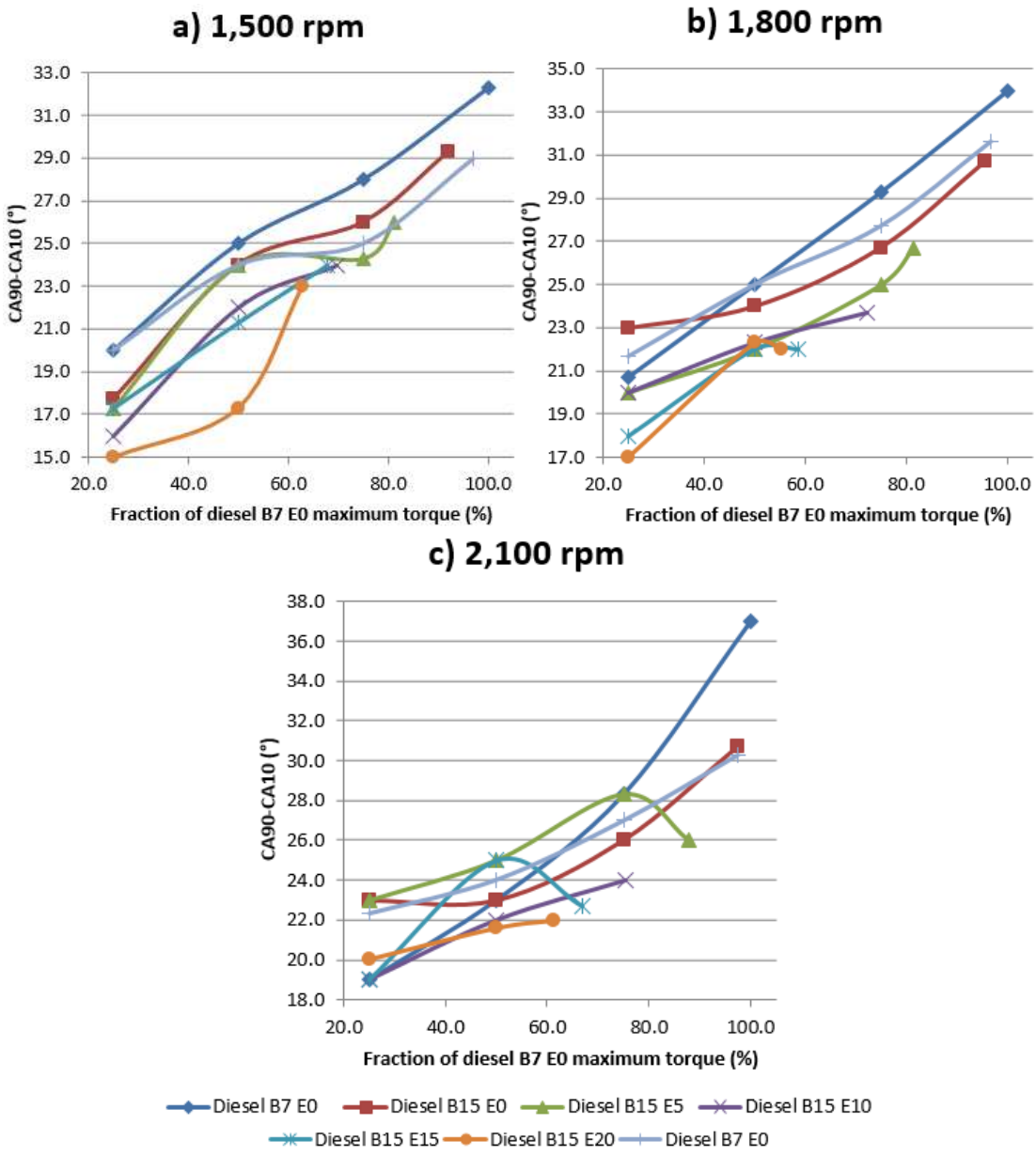

Figure 97: CA90 – CA10 (°) for each DBE blend and value of torque at a) 1,500 rpm, b) 1,800 rpm and c) 2,100 rpm.

At low engine speed, the combustion happened quicker when ethanol content increased. At medium and high engine speeds, the tendency was not so clear, but blends with ethanol had a shorter combustion process. This observation showed that the combustion process involving blends with ethanol started later and ended before the free-alcohol blends.

The former comments showed that the injected energy was slightly increasing with the biodiesel and ethanol content to compensate the lower energy content and the non-optimized combustion process. Moreover, the combustion process happened in a shorter time than for commercial diesel B7 fuel.

PUC-Rio - Certificação Digital Nº 1312923/CA

Consequently, it was expected that the heat was released at a higher rate, as observed by Hulwan *et al.* (2011). Such fact was confirmed in Figure 98 where the maximum gross heat liberation rate was plotted for each blend and engine speed.

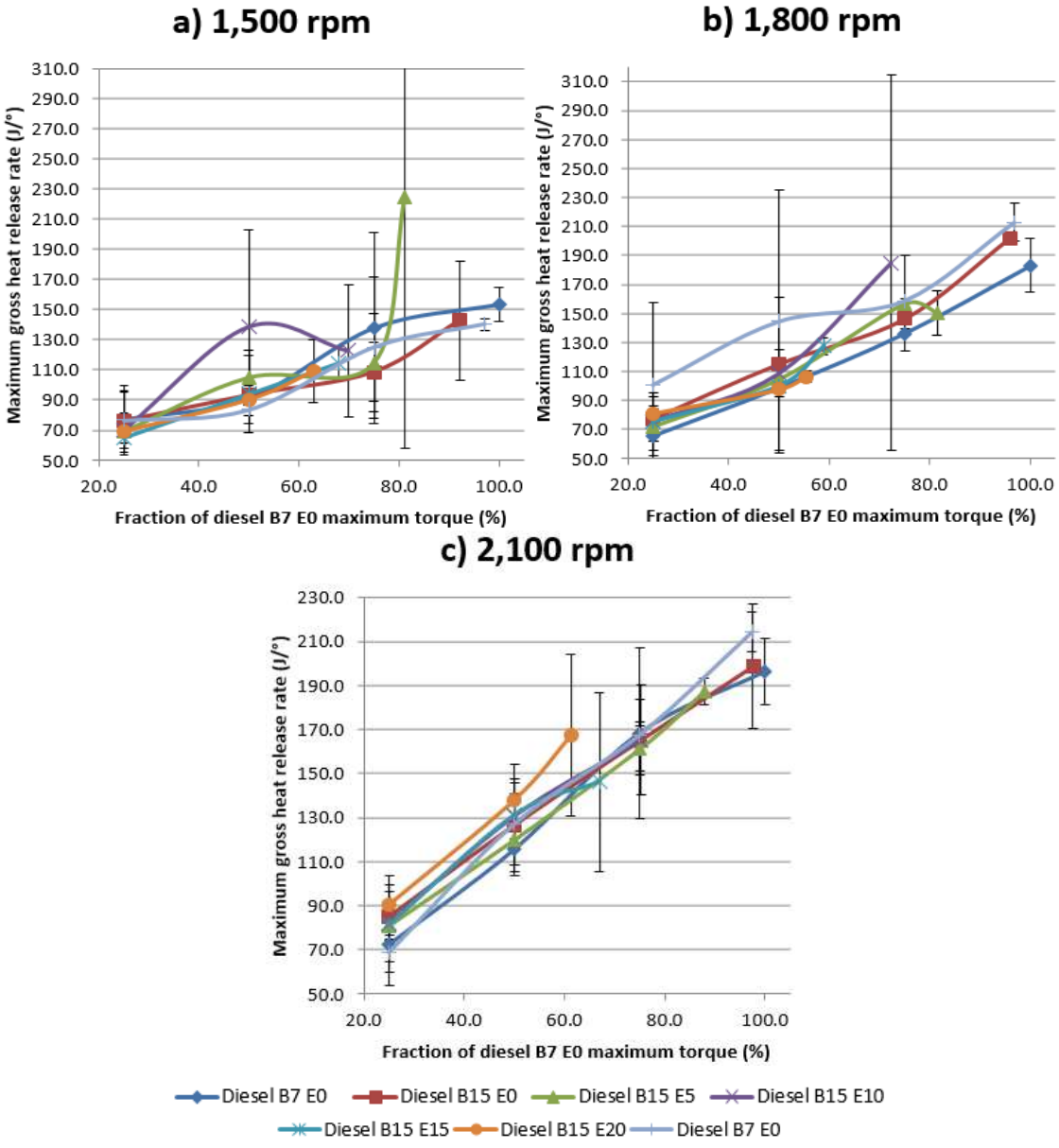

Figure 98: Maximum gross heat release rate (J/°) for each DBE blend and value of torque at a) 1,500 rpm, b) 1,800 rpm and c) 2,100 rpm.

As biodiesel and ethanol contents increased, the curve in Figure 98 drifted to the top. At medium and high engine speeds, the first repetition of diesel B7 fuel presented much lower values (the differentiated behavior observed for the second repetition of the diesel B7 fuel is probably due to the contamination of the fuel

PUC-Rio - Certificação Digital Nº 1312923/CA

with ethanol). Even if the heat release happened faster, such behavior seemed to be traduced in terms of the maximum pressure rate. The maximum pressure increase rate for each DBE blend and value of torque at the different investigated engine speeds is given in Figure 99.

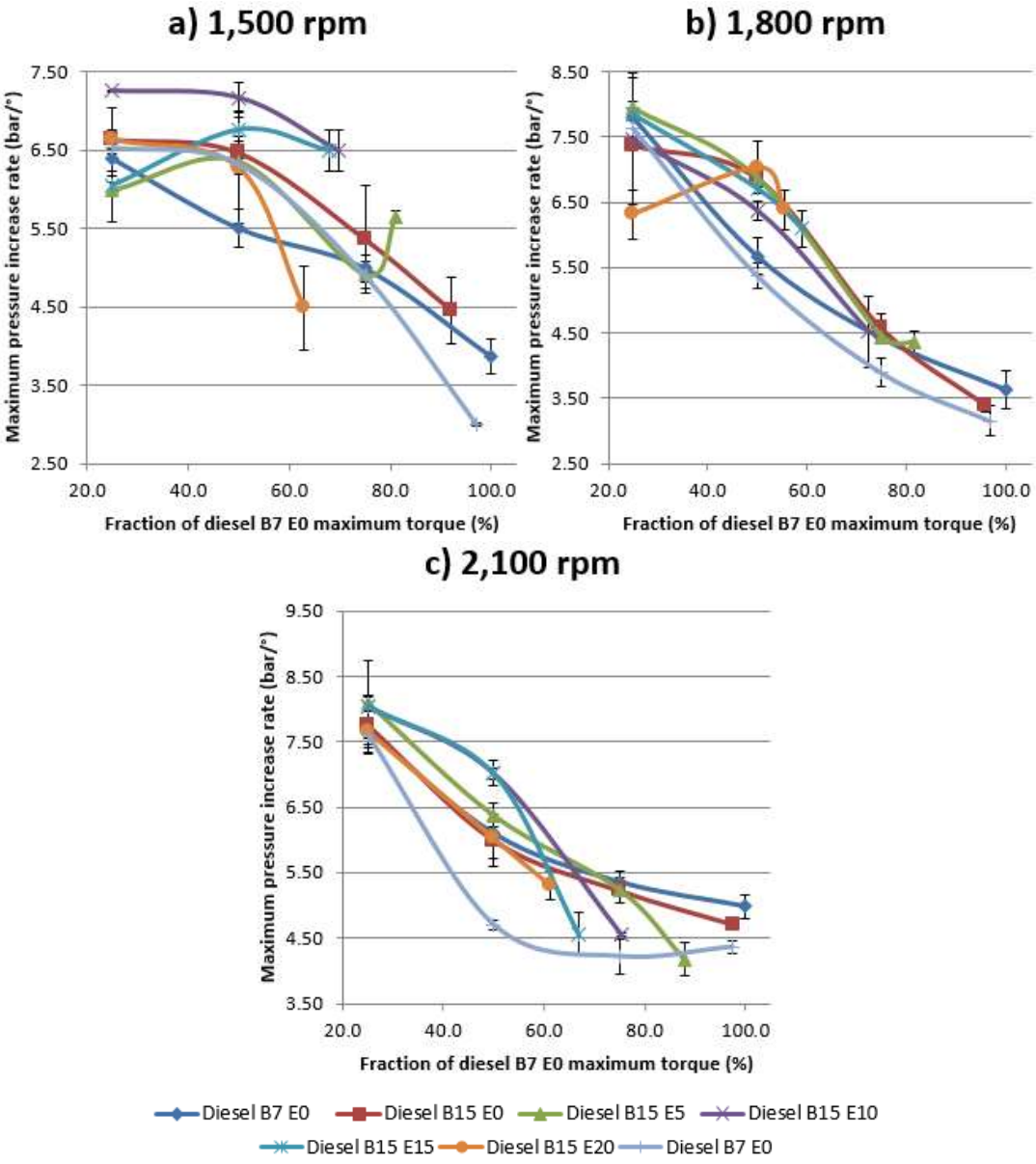

Figure 99: Maximum pressure increase rate (bar/°) for each DBE blend and value of torque at a) 1,500 rpm, b) 1,800 rpm and c) 2,100 rpm.

It can be seen in Figure 99 that the maximum pressure increase rate was higher in diesel B15 fuels than in the reference fuel. This behavior appeared clearly at low (1,500 rpm) and medium (1,800 rpm) engine speeds. At high engine speed (2,100 rpm), the behavior was more complex and all blends had similar values for a determined value of torque. This could be explained by the difficulty

PUC-Rio - Certificação Digital Nº 1312923/CA

met to define the maximum of the pressure increase rate (detonation). At all rotations, the maximum pressure increase rate decreased with the increase of torque. Indeed, due to the late combustion, the maximum pressure increase rate was met quite far from the TDC, as shown in Figure 100, where the crank angle of maximum pressure increase rate for each DBE blend, value of torque and engine speed is plotted.

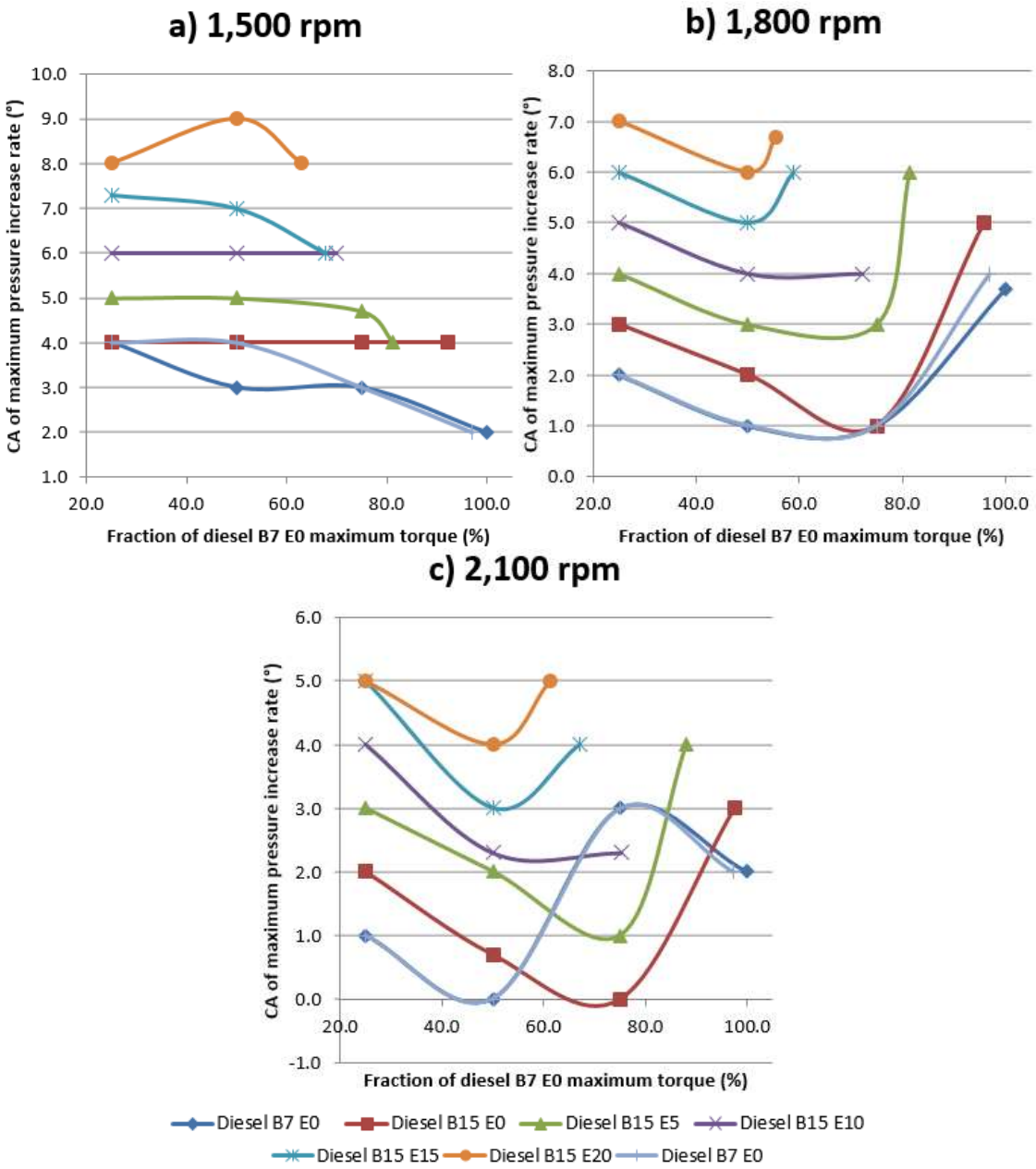

Figure 100: Crank angle of maximum pressure increase rate (°) for each DBE blend and value of torque at a) 1,500 rpm, b) 1,800 rpm and c) 2,100 rpm.

PUC-Rio - Certificação Digital Nº 1312923/CA

The value of crank angle increased with ethanol content, as observed by Hulwan *et al.* (2011). This fact implied that pressure increase due to combustion happened later during the expansion process, when pressure naturally decreased. Consequently, the value of maximum pressure increase rate was lower, as seen in Figure 99.

Figure 101 presents the maximum pressure for each DBE blend, value of torque and engine speeds.

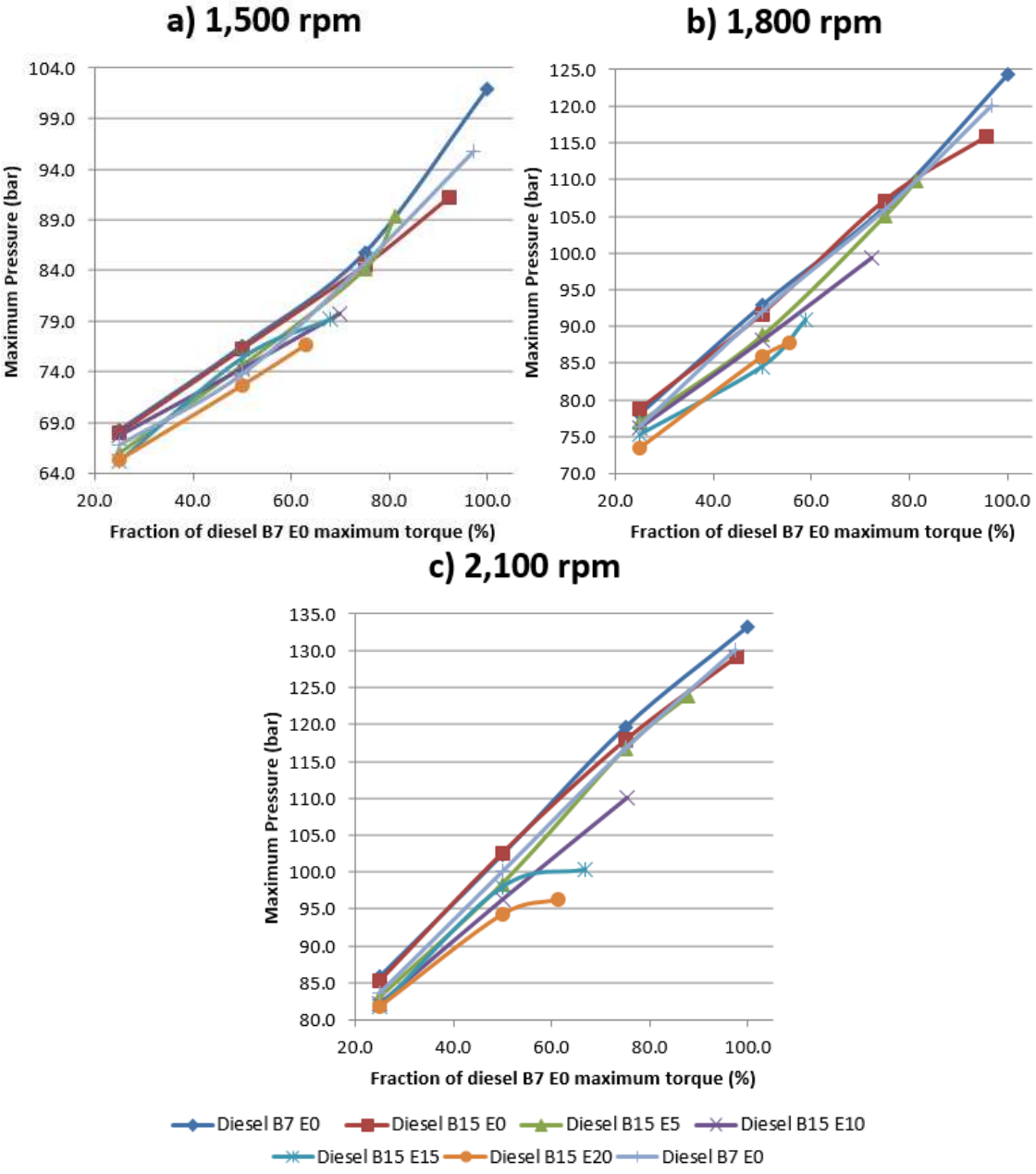

Figure 101: Maximum pressure (bar) for each DBE blend and value of torque at a) 1,500 rpm, b) 1,800 rpm and c) 2,100 rpm.

PUC-Rio - Certificação Digital Nº 1312923/CA

In terms of pressure, the addition of biodiesel seemed to have no impact on the value of the maximum pressure in the cylinder. For the other DBE blends, the higher was the ethanol content, the lower was the maximum pressure. Such behavior was related to:

(i) The higher latent heat of vaporization and specific heat of ethanol: More pressure energy was required to vaporize the ethanol in the blends. Consequently, the temperature and pressure before combustion were lower. This can be seen in the profile of indicated pressure (Figure 93).

(ii) The higher ignition delay values: The chemical energy in the fuel was converted into heat and pressure energy later (and faster) in the expansion phase, as shown in Figure 102.

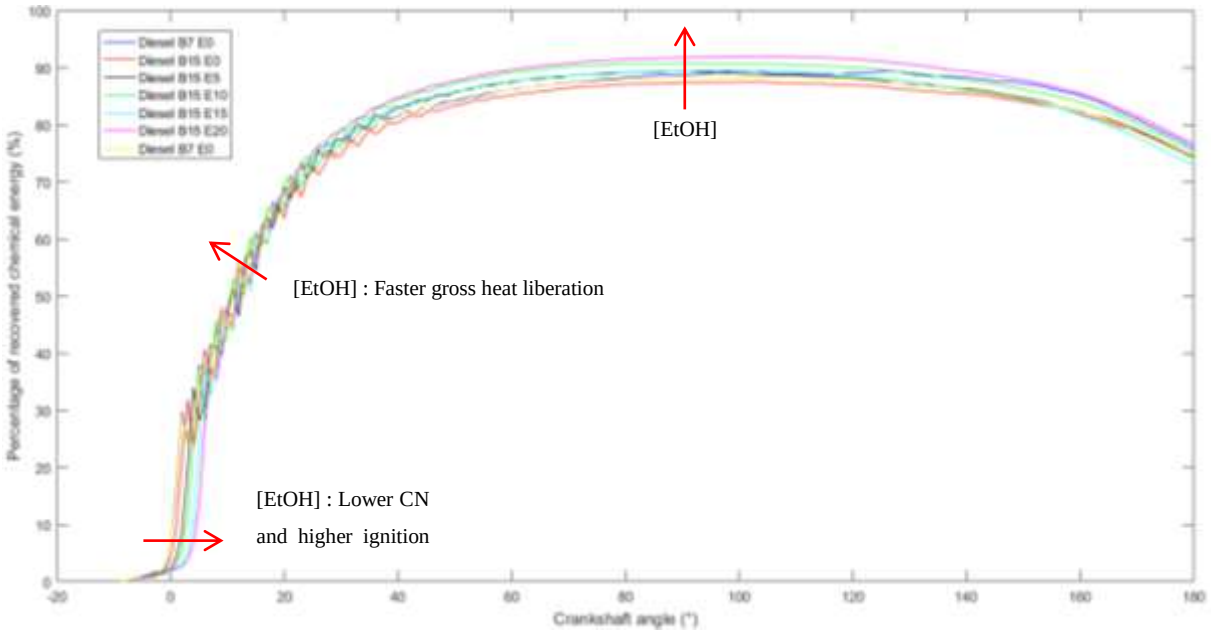

Figure 102: Percentage of recovered chemical energy (%) for each DBE blend at 1,800 rpm and 25% of the maximum diesel B7 fuel maximum torque.

This figure also clearly shows the impact of ignition delay on the left side of the graph and the higher liberation energy rate (higher inclination) when more ethanol was added.

The variation of crank angle position of the maximum pressure, shown in Figure 103, were also coherent with the former observations.

PUC-Rio - Certificação Digital Nº 1312923/CA

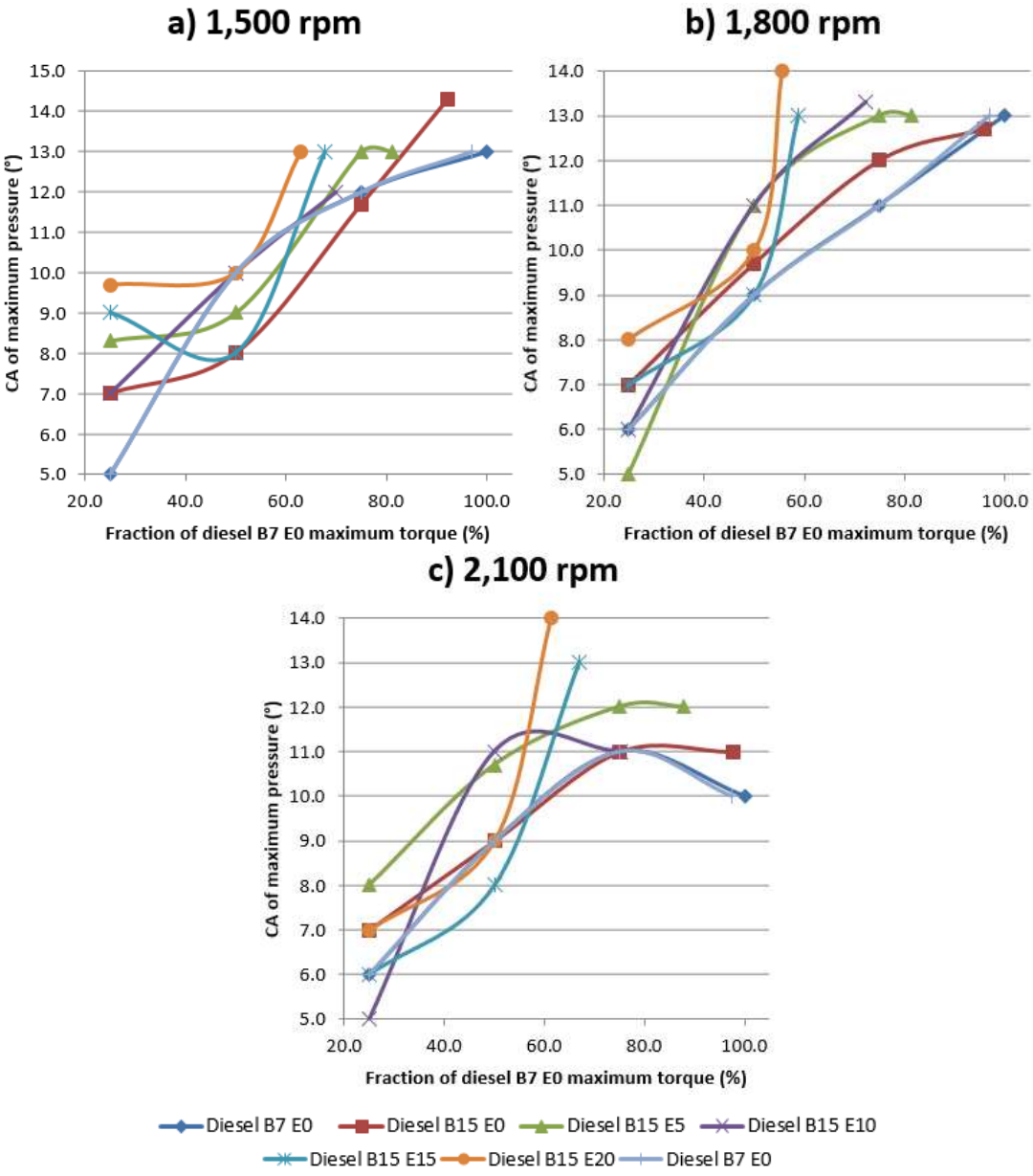

Figure 103: Crank angle of maximum pressure (°) for each DBE blend and value of torque at a) 1,500 rpm, b) 1,800 rpm and c) 2,100 rpm.

For all engine speeds, the observed tendency was to increase with torque and biofuels (biodiesel and ethanol). Values varied from 5° to 14.3° ATDC. To compensate the higher ignition delay values, a new strategy for injection was required, since it was necessary to inject the fuel earlier.

The other impact of the higher latent heat of vaporization of ethanol can be observed on the polytropic coefficient during compression, as the heat used to vaporize ethanol reduced the value of this parameter. Figure 104 gives the value of this parameter in function of blend composition, torque and rotation.

PUC-Rio - Certificação Digital Nº 1312923/CA

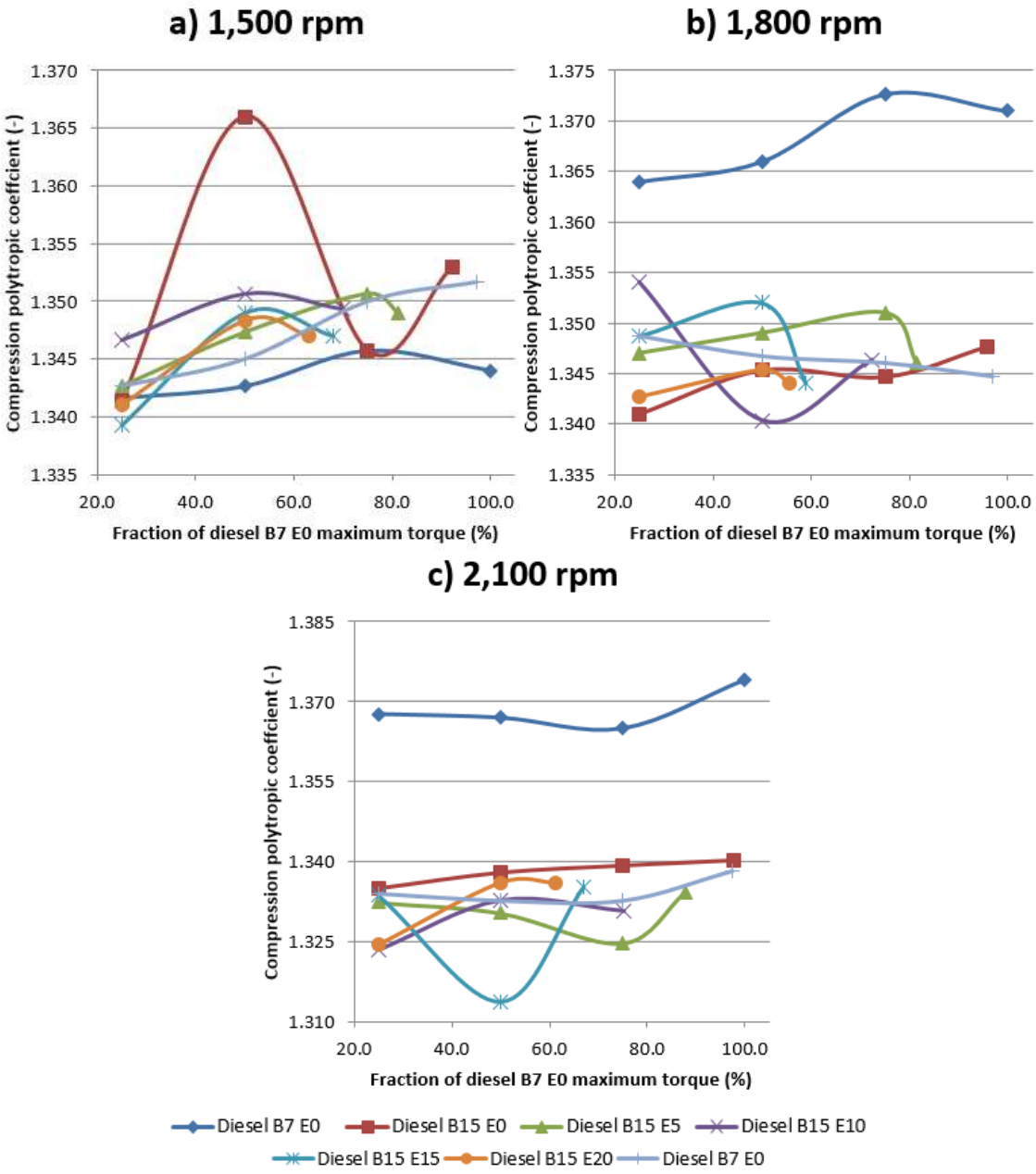

Figure 104: Polytropic coefficient during compression (-) for each DBE blend and value of torque at a) 1,500 rpm, b) 1,800 rpm and c) 2,100 rpm.

At medium (1,800 rpm) and high (2,100 rpm) engine speed, all blends with 15 vol% of biodiesel had lower polytropic coefficients when compared with the first repetition of commercial diesel B7 fuel (residual ethanol affected the results obtained during the second repetition). At low engine speed (1,500 rpm), all blends had similar values of the parameter. It can be observed that, when engine speed increased (medium and high engine speeds), the impact of ethanol was higher, since less time was available to proceed to ethanol vaporization and, consequently, more energy was required, so the polytropic coefficient was

PUC-Rio - Certificação Digital Nº 1312923/CA

reduced. At 2,100 rpm, blends with ethanol had lower values of polytropic coefficient during compression than the diesel B15 blends. The polytropic coefficients during compression process were similar to the values related by Heywood (1988) for conventional fuels in compression ignition engine: 1.3 ± 0.05.

The polytropic coefficient during the expansion was also calculated and their values are plotted in Figure 105.

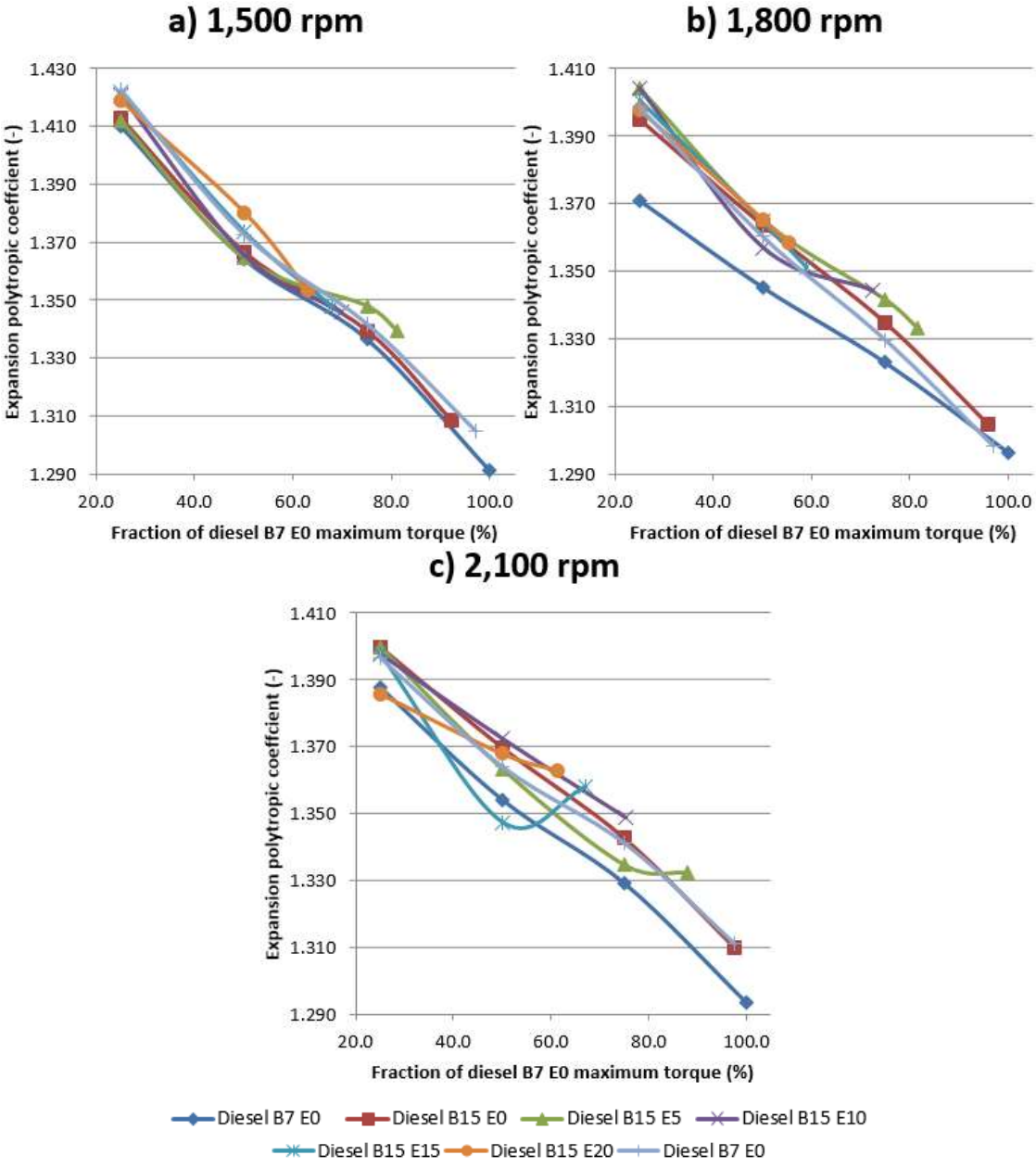

Figure 105: Polytropic coefficient during expansion (-) for each DBE blend and value of torque at a) 1,500 rpm, b) 1,800 rpm and c) 2,100 rpm.

PUC-Rio - Certificação Digital Nº 1312923/CA

During the expansion, the polytropic coefficient for a determined engine speed decreased with the torque and it did not vary significantly with the nature of the blends at low engine speed. At medium and high engine speeds, it seemed that the parameter increased with the biodiesel content. In all cases, the range variation was quite similar, from 1.400 (25% of maximum diesel B7 fuel torque) to 1.290 (100% of maximum diesel B7 fuel torque). Such variations had to be related to the composition, pressure and temperature of the exhaust gas.

5.4.5. Engine Efficiency

The first engine efficiency indicator is related to the recovered chemical energy (for instance, plotted in Figure 102). The maximum percentage of recovered chemical energy for each DBE blend, torque and engine speeds are shown in Figure 106.

PUC-Rio - Certificação Digital Nº 1312923/CA

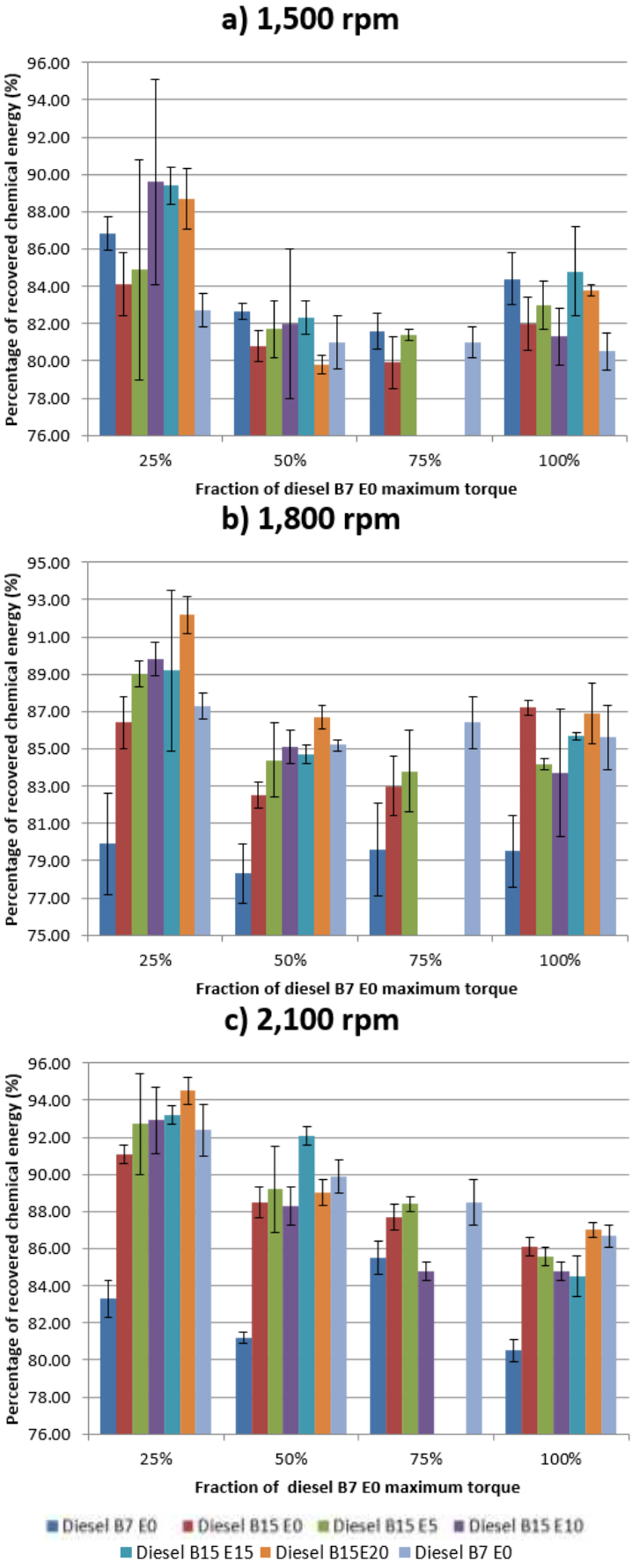

Figure 106: Maximum percentage of recovered chemical energy (%) for each DBE blend and value of torque at a) 1,500 rpm, b) 1,800 rpm and c) 2,100 rpm.

PUC-Rio - Certificação Digital Nº 1312923/CA

It can be observed some variations on the results, in particular for the second repetition of diesel B7 fuel (that seems to confirm a contamination with residual ethanol due to the variation of the experimental conditions). However, this property seemed to decrease when biodiesel content increased from 7 vol% to 15 vol% and tended to increase with the addition of ethanol. Moreover, as commented formerly, this released energy was not recovered at the best moment. Consequently, the fuel conversion efficiency was not following the same trend, which means it decreased. In extreme conditions, small portions of the fuel, negligible compared to the fuel consumption, were not completely burnt and formed particulate matters. This phenomenon occurred even with a poor air / fuel ratio and it was justified by the limited time available to the interaction of diesel fuel with the air admitted into the cylinders.

Figure 107 shows the variation of fuel conversion efficiency with engine speed, torque and blend composition.

PUC-Rio - Certificação Digital Nº 1312923/CA

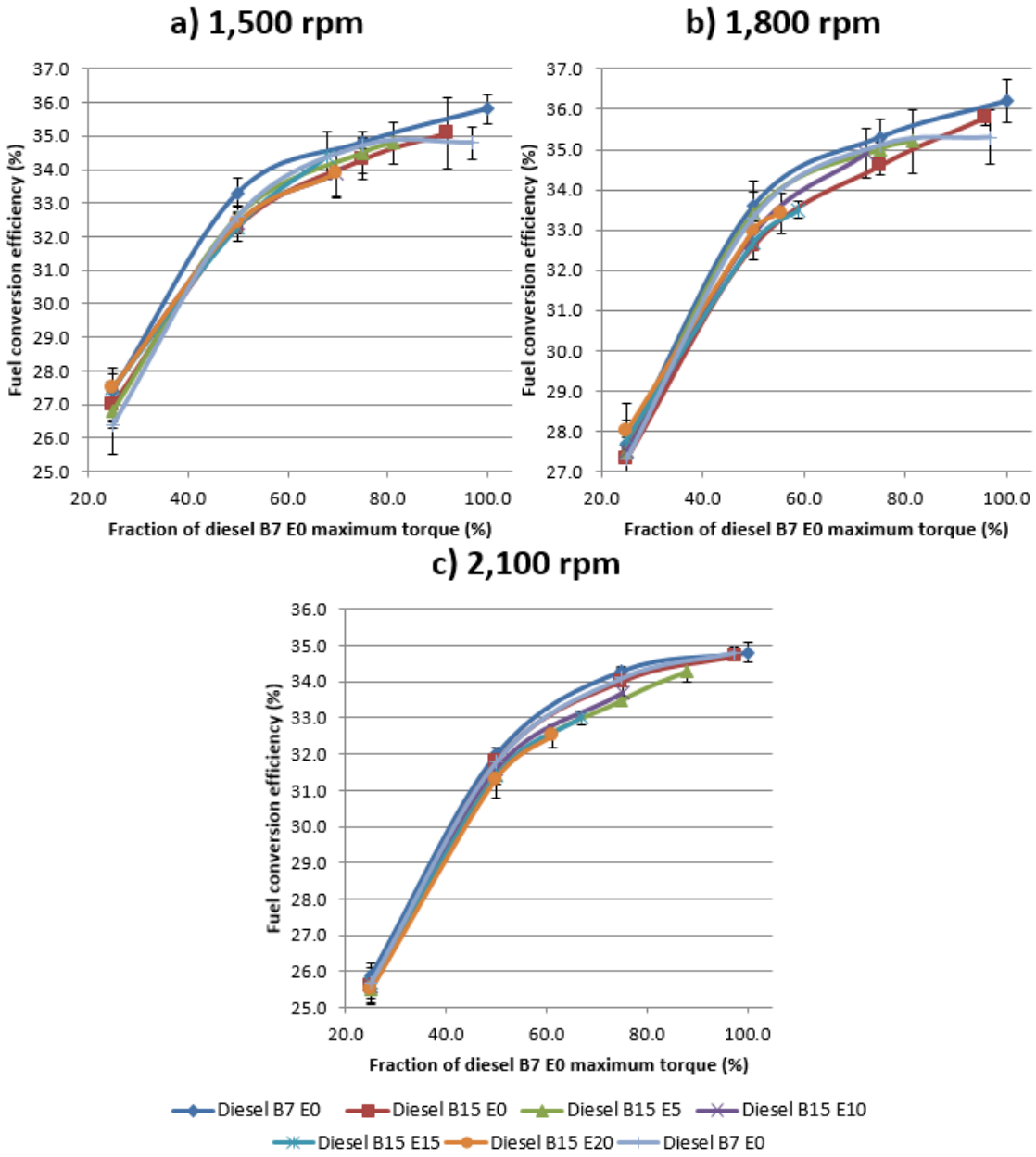

Figure 107: Fuel Conversion Efficiency η_f (%) for each DBE blend and value of torque at a) 1,500 rpm, b) 1,800 rpm and c) 2,100 rpm.

At all engine speeds, the parameter increased with torque, from 25.0-28.0 for 25% of the maximum diesel B7 fuel torque to 32.0-36.0 for the maximum torque. At all engine speeds, the maximum fuel conversion efficiency was observed for commercial diesel B7 blends. At low and medium engine speeds, it can be observed that blends with alcohol had intermediary results between diesel B15 and B7 fuels. For 25% of maximum diesel B7 torque, the fuel conversion efficiency increased with ethanol content, since vaporization was easier in presence of less fuel. At high engine speed, blends with alcohol had lower fuel conversion efficiency than alcohol-free blends due to the difficulty met to

PUC-Rio - Certificação Digital Nº 1312923/CA

vaporize the ethanol. Moreover, the fuel conversion efficiency decreased with ethanol content at all engine speeds.

The Figure 108 showed the evolution of indicated efficiency with the experimental conditions.

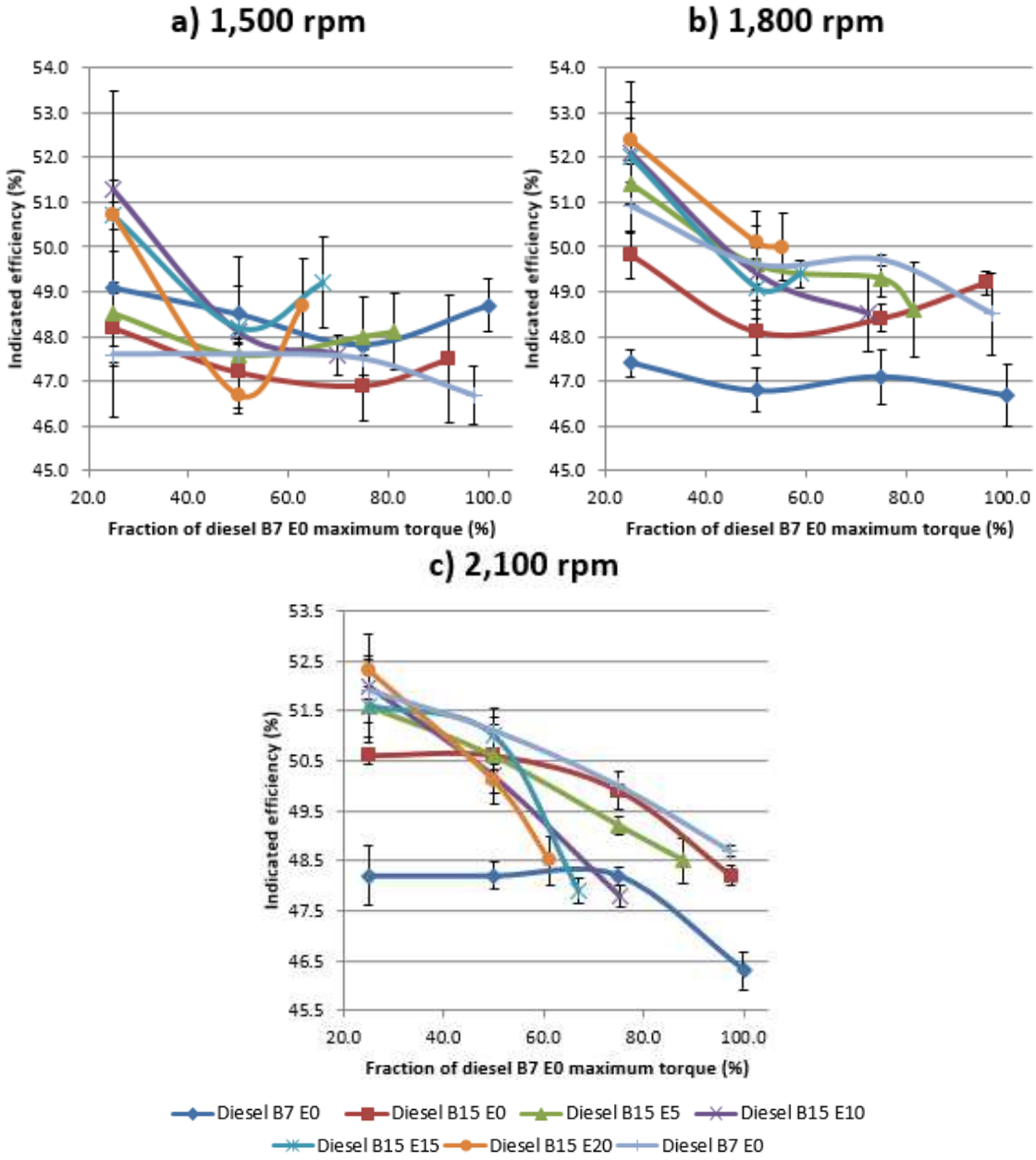

Figure 108: Indicated Efficiency η_i (%) for each DBE blend and value of torque at a) 1,500 rpm, b) 1,800 rpm and c) 2,100 rpm.

All values varied in the range from 46% to 53%. At all engine speeds, the indicated efficiency tended to decrease with torque and to increase with biodiesel (except at 1,500 rpm) and ethanol contents, up to 5.8%. At low engine speed, all blends had similar values, but, at medium and high engine speeds, the first test

PUC-Rio - Certificação Digital Nº 1312923/CA

with commercial diesel B7 fuel had a lower performance. At 2,100 rpm and full throttle, it can be observed that the indicated efficiency decreased significantly, showing the influence of non-optimized combustion and the friction loss, mainly in the pump.

The Figure 109 shows the volumetric efficiency for the different investigated values of engine speed, torque and blends composition.

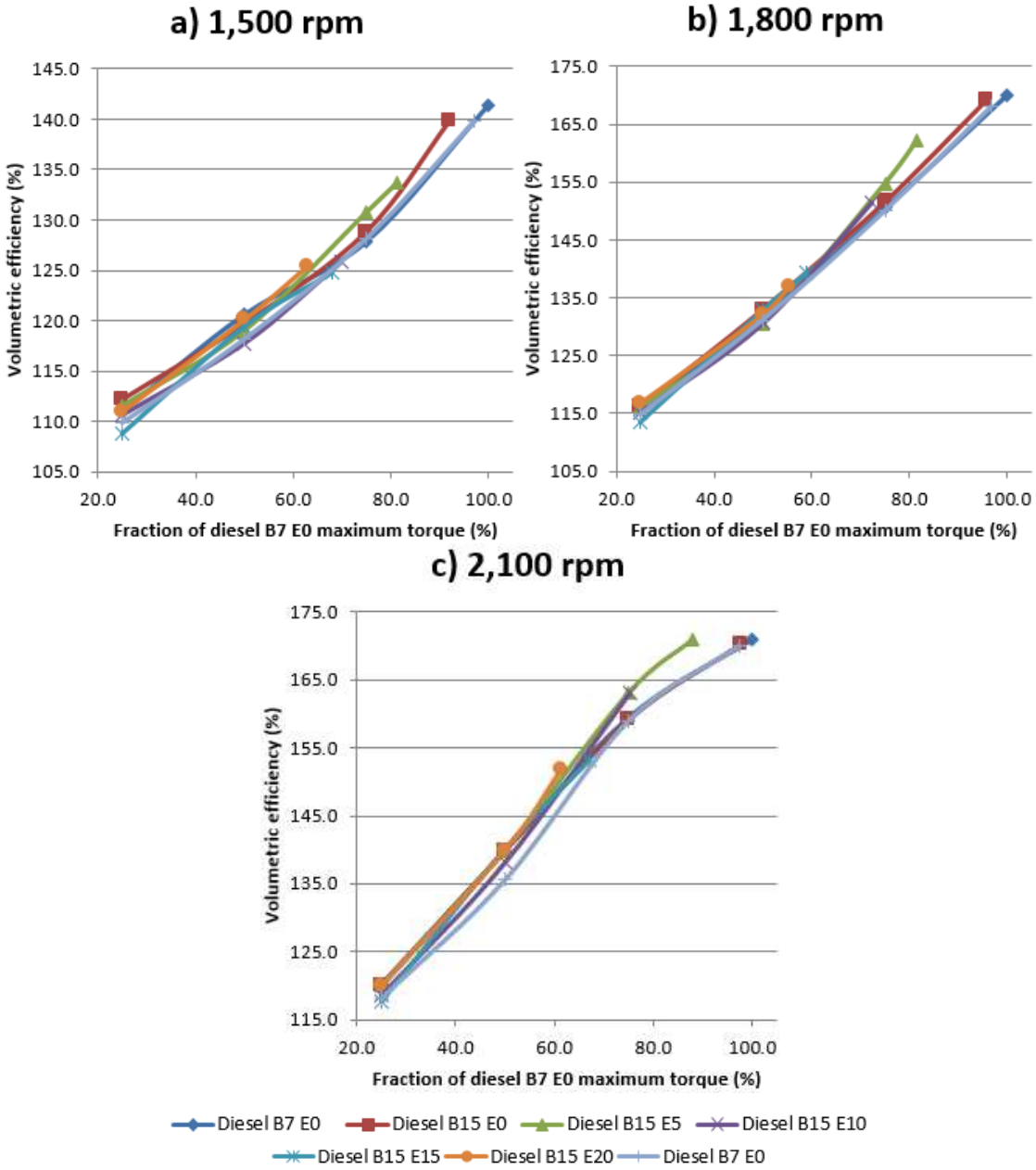

Figure 109: Volumetric Efficiency η_v (%) for each DBE blend and value of torque at a) 1,500 rpm, b) 1,800 rpm and c) 2,100 rpm.

PUC-Rio - Certificação Digital Nº 1312923/CA

For a turbocharged engine, the volumetric efficiency is higher than 100% because the engine's induction process is forced by the turbocharger. As it can be seen in Figure 109, the volumetric efficiency increased from 110-120% to 140-170% in function of the torque.

As biodiesel and ethanol contents increased, the curve slightly drifted to higher values. This variation can be related to the increase of fuel consumption and, consequently, the air consumption in order to maintain the same lambda. This process was ensured by the higher energy content in the exhaust gas that made the turbine rotate faster and, consequently, the capacity of the compressor increased. At 2,100 rpm and full throttle, for diesel B7, B15 E0 and E5 fuels, it can be observed that the linear character of volumetric efficiency was inflected and attained a maximum limit (171%).

PUC-Rio - Certificação Digital Nº 1312923/CA

Moreover, the mechanical efficiency for all tested conditions is plotted in Figure 110.

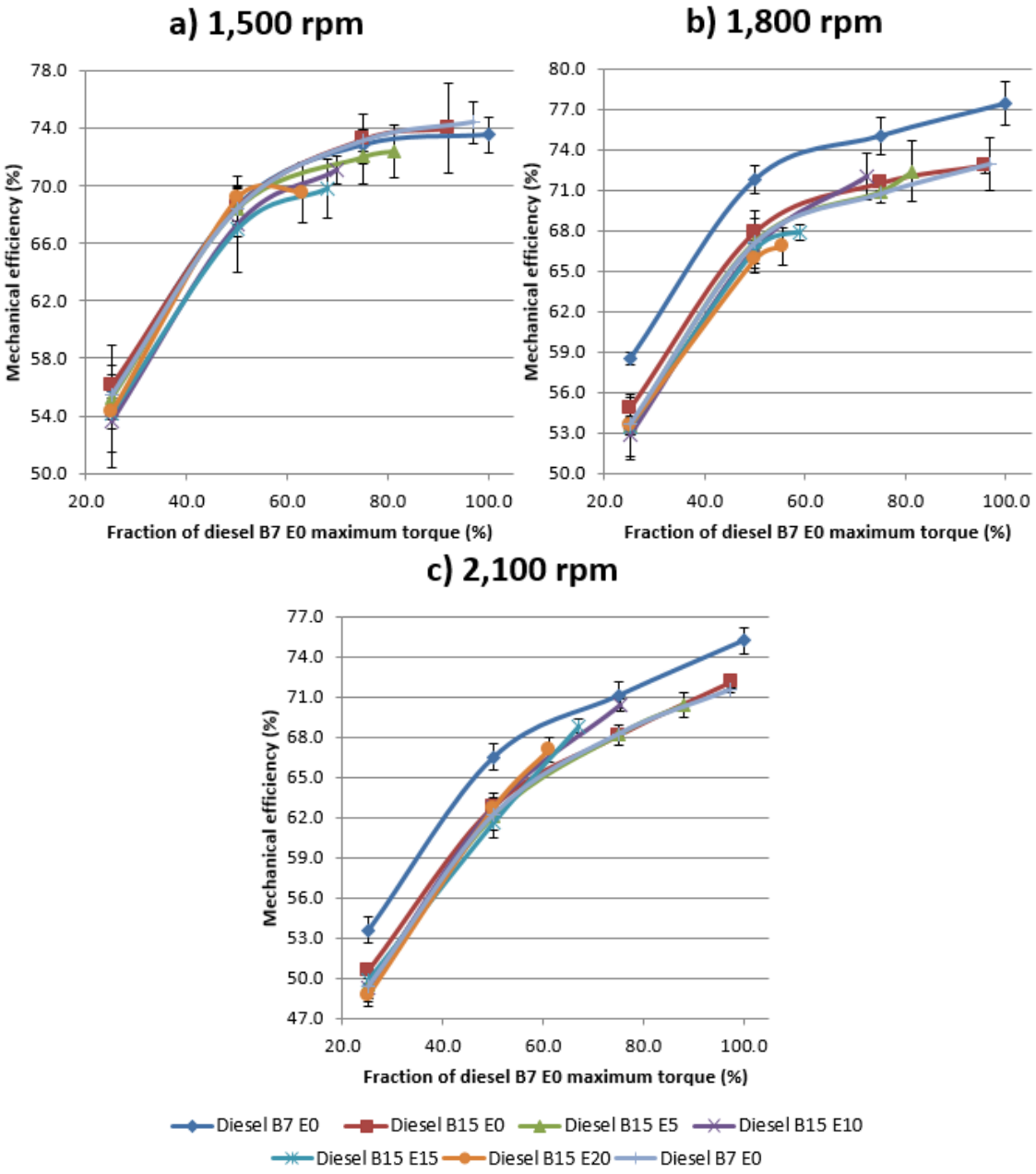

Figure 110: Mechanical Efficiency η_m (%) for each DBE blend and value of torque at a) 1,500 rpm, b) 1,800 rpm and c) 2,100 rpm.

At all engine speeds, the mechanical efficiency increased with torque and tended to decrease with biodiesel and ethanol content. Values varied from 50% (2,100 rpm) to 55% (1,500 and 1,800 rpm) up to 70 to 77% for maximum torque. These last values were coherent with the typical values of 75 to 90%, depending on the engine speed, for full throttle modern automotive engine supplied with

PUC-Rio - Certificação Digital Nº 1312923/CA

conventional fuels cited by Heywood (1988). At low engine speed, all blends had similar values, but, at medium and high engine speeds, the commercial diesel B7 fuel had a better performance. Again, the combustion characteristics of ethanol explained this behavior.

5.4.6. Partial Conclusion

Experimental limitations of the tested Euro III engine:

The initial analysis of the reduction of maximum torque showed that a strong limitation was related to the fuel injection. Despite a slightly higher requirement of injected energy when ethanol content increased (and, consequently, the higher requirement on the position of the accelerator), the main bottleneck was the reduction of the injected volume of fuel (up to 30% in diesel B15 E20 fuel) when compared to commercial diesel B7 fuel. Consequently, an adequacy of the injection pump to the low viscosity of the blends was required to obtain higher values of maximum torque.

Fuel consumption and conversion:

Specific fuel consumption increased almost 2% for each 5 vol% of anhydrous ethanol in the blends, due to the lower specific gravity and lower heating value of ethanol. Despite these non-optimized conditions for injection and combustion in the presence of ethanol, results showed a better conversion of ethanol chemical energy into brake power, in comparison to the values found for diesel B15 fuel. The observed improvement was around 15-20%. Furthermore, the observed values of ethanol conversion were lower than those observed in commercial flex fuel spark ignition engine.

Impact on combustion:

The results obtained showed that the diesel fuel substitution changed the characteristics of combustion. The increased ethanol content implied an increase of the ignition delay, due to the lower cetane number, the higher latent heat of vaporization and specific heat at constant pressure of ethanol, but the heat was released faster. As combustion began later, the maximum pressure was lower and observed lately in the expansion stroke. An optimization of the injection timing is required to fully harness the potential of these blends.

PUC-Rio - Certificação Digital Nº 1312923/CA

Engine efficiencies:

Despite of all these limitations, higher amount of thermal energy was recovered from the injected chemical energy when ethanol content increased, even if it was later in the expansion phase. This behavior lead to a small increase in the indicated efficiency of the engine, showing the high potential of the blends. Nevertheless, fuel conversion and mechanical efficiencies of DBE blends were similar to those of diesel B15 fuel, even if a slight decrease was observed. Again, the non-optimized combustion characteristics of ethanol and difficulty to pump the fuel explained this behavior.

PUC-Rio - Certificação Digital Nº 1312923/CA

6 Conclusion

6.1. Conclusion of the Present Work

In order to partially replace the demand of fossil diesel fuel, to reduce high import costs and to comply with environmental standards, sustainable policies have led to partially replace diesel fuel by biodiesel. However, other technologies, such as diesel-biodiesel-ethanol mixtures, are being investigated. A large literature is available, but there are still points to be further investigated and challenges to be overcome, like those that was studied in this thesis. The main results are gathers in the following items:

(i) **Formulation of an original additive for DBE blends with diesel B7 fuel**: Based on the literature data, a first set of additives was formulated to stabilize Brazilian diesel B7 S10 fuel blended with hydrous ethanol, both commercial. The tested additives were synthesized through a Doehlert design of experiments (DOE), considering all the possible combinations of biodiesel-vegetal oil from soybean and castor oil. As the blends presented high instability due to high moisture content, tests assessing the impact of temperature were done using anhydrous ethanol and the best additive for each combination of biodiesel-vegetal oil (4 additives). Stabilization impact was reduced, even with the best additive (78.9 vol% of soybean biodiesel, 9.4 vol% of castor oil and 11.7 vol of n-butanol).

(ii) **Formulation of an original additive for DBE blends with diesel B15 fuel**: Based on the former experimental results, additives with higher refined vegetal oil fraction were tested to increase the bridging power of the co-solvent. Ethanol with low moisture content was also chosen to be used to guarantee the stability. As biodiesel can be directly blended into diesel fuel and the tendency is to increase its concentration in commercial diesel fuel, different concentrations of biodiesel (B7, B15 and B30) were also investigated. For each concentration of biodiesel, the impact of 2

PUC-Rio - Certificação Digital Nº 1312923/CA

vol% of the additive to stabilize DBE blends was studied. Based on the experimental results, the best additive was defined as a mixture of 72.5 vol% of castor oil, 17.5 vol% of soybean biodiesel and 10 vol% of *n*-butanol in diesel B15 fuel. Its use is justified by the observed stability gain, in particular at 15°C and 10°C. The experimental results showed that a minimum addition of 1.0 vol% was required. However, when 2 vol% of additive was added, the short-term stability region was the same, but the separation ratio increased. Short and long-term tests showed stability for temperature higher than 10°C for additivated blends with up to 20 vol% of anhydrous ethanol.

(iii) **Assessment of several critical physicochemical properties involved in the proper operation of the fuel line**: The most restrictive property to respect the Brazilian specification for diesel fuel was the flash point (maximum concentration of ethanol that followed the specification: 5 vol%). Nevertheless, new practices for storage and handling, inspired in the current use of ethanol in gasoline, could be used to reduce the risks. The second more restrictive criterion was the cetane number, which implied a maximum ethanol content of 10 vol% to follow the current Brazilian legislation, regardless of the additivation. Nevertheless, the use of cetane improver could solve the issue. Other requirements are ethanol content up to 20 vol% in additivated blends for lubricity; up to 40 vol% for kinematic viscosity and specific gravity; and up to 60 vol% (most restrictive value of the Brazilian specification) for CFPP. There is no restriction considering corrosiveness of the fuel at all ethanol proportions. The impact of the additive on the properties is reduced, but they lead to a null or small improvement of the investigated properties, mainly lubricity, contact angle, cetane number and viscosity, with exception of surface tension. Modifications of the engine and expensive addition of additives (such as cetane improver or lubricity enhancer) are necessary to use blends with higher ethanol content.

(iv) **Experimental limitations on the tested Euro III engine**: The injection pump must be adequate to the low viscosity of the blends to manage to increase the injected fuel volume and recover the loss of maximum

PUC-Rio - Certificação Digital Nº 1312923/CA

torque. With the tested equipment, the injected volume of fuel was up to 30% lower than in commercial diesel B7 fuel for full load demand,

(v) **Fuel consumption and conversion**: The lower specific gravity and lower heating value of ethanol lead to an increase of the specific fuel consumption of almost 2% for each 5 vol% of anhydrous ethanol in the blends. Despite these non-optimized conditions for injection and combustion, the chemical energy of ethanol was better converted into brake power than the energy inside diesel B15 fuel (improvement of 15-20%). Furthermore, the observed values of ethanol conversion were lower than those observed in commercial flex fuel spark ignition engine.

(vi) **Impact on combustion**: The increased ethanol content implied an increase of the ignition delay due to the lower cetane number, the higher latent heat of vaporization and specific heat at constant pressure of ethanol. However, the heat was released faster. As combustion began later, the maximum pressure was lower and observed lately in the expansion stroke. An optimization of the injection timing is required to better recover the energy of these blends.

(vii) **Engine efficiencies**: Event tough the engine was use without adaptation, higher amount of thermal energy was recovered from the injected chemical energy when ethanol content increased. This behavior lead to a small increase in the indicated efficiency of the tested engine, showing the high potential of the blends. However, fuel conversion and mechanical efficiencies of DBE blends were similar to those of diesel B15 fuel, even if a slight decrease was observed when ethanol content increased. Again, the non-optimized combustion characteristics of ethanol and the difficulty to pump the fuel could explain this behavior.

These results showed the potential of such blends to be an alternative to current fuel for CI engine. The potential to reduce pollutants emission observed in literature is also an argument to keep on the research on these blends.

PUC-Rio - Certificação Digital Nº 1312923/CA

6.2. Perspectives

The present work gave an overview of the potential of DBE blends. Nevertheless, further investigations can be carried out to go further on some aspects of the investigated properties and to study new parameters. For instance, the following issues can be considered:

(i) **Additive formulation and blend stability**:

- **Full characterization of the physicochemical properties of the additive**: The variation of the additive characteristics should be described in order to assess the variability due to raw materials and blending, and consolidate the technical viability;
- **Impact of moisture content in ethanol**: In this work, we managed to stabilize DBE blends with anhydrous ethanol. Since ethanol is hygroscopic, moisture content naturally increased with time. An evaluation of the impact of moisture content is necessary to define the feasibility of such blends under wet climate and, eventually, to consider blends with all types of ethanol (premium hydrous ethanol or hydrous ethanol);
- **Influence of fuel tank on the observed stability**: Phase demixion is highly dependent on the interface available for the mass transfer process. The geometry of the tank is a crucial parameter to be assessed. Moreover, a new design should be interesting to reduce safety concerns due to ethanol volatility and flammability, to allow a quick mixing after a long time of parking at low temperatures or heating of the fuel to avoid phase separation.

(ii) **Physicochemical properties of the DBE blends**:

- **Investigation of other properties:** In this thesis, some of the main physicochemical properties involved in fuel storage, pumping and combustion were investigated. However, a broader characterization is necessary to fully understand the impact of DBE blends. Moreover, the impact on the other properties regulated by the ANP is necessary to adequate the legislation to this kind of blends;

PUC-Rio - Certificação Digital Nº 1312923/CA

- **Assessment of the lubricity at high alcohol concentration**: The impact of ethanol was not defined in this work at high concentration for safety concerns and partial evaporation of the alcohol. For this purpose, a procedure should be found to avoid ethanol vaporization;
- **Adjustment of the cetane number by addition of improvers**: The present work showed that cetane number decreases rapidly with ethanol content. The use of cetane improver is required to avoid misfire and/or detonation at high ethanol content. Such parameter must be considered simultaneously to the optimization of the engine parameters, the definition of standards for such kind of blends and the assessment of the economic viability.

(iii) **Tests in engine**:

- **Adequacy of the pump**: Lower viscosity leads to greater pump and injector leakage, reducing maximum fuel delivery. Hot start problems may also be encountered since insufficient fuel may be injected at cranking speed when fuel leakage in the high-pressure pump is amplified because of the reduced viscosity of the hot fuel. Consequently, a new design of the pump is required. The impact of injection pressure should also be assessed, in particular the vaporization of the fuel droplets;
- **Optimization of the engine parameters**: To better recover the injected energy, the combustion should be optimized by adjusting the start of injection and piston geometry (swirl, tumble, and squish). A strategy of air injection using EGR system can also be investigated to enhance fuel vaporization by increasing the temperature inside the piston. The compression ratio can also be slightly increased, allowing to have better efficiency;
- **Long term durability**: The long term impact of this alternative blends can be assessed, in particular the interaction with polymeric material and corrosion issues;
- **Assessment of pollutants emission**: The potential of such blends to reduce greenhouse gases emission is one of the advantages that promote the development of this technology. Nevertheless, the bibliographic

PUC-Rio - Certificação Digital Nº 1312923/CA

review showed that the reduction is closely related to the formulation of the blend, the engine speed, the load, and the engine technology. The impact of the additive on the emission profile of the studied Euro III engine can also be assessed.

- **Study of legislated and non-legislated gases**: New technologies were introduced in the vehicles to comply the Euro V (Brazil) and Euro VI (Europe) emission standards. It is necessary to study the emissions of the DBE blends and their adequacy to the modern technology. For instance, the compatibility with after-treatment system is a crucial point.

(iv) **Economic viability and social sustainability**:

- **Economic viability**: The technical gain in term of stability (ethanol content and duration before demixion) at a determined temperature must be balanced assessing the additional cost due to the use of additive. This aspect is a decision factor for the use of the additive at a commercial scale.
- **Social acceptation and sustainability**: To rapidly expanding the production of first generation of biofuels, new arable land were cultivated worldwide for this purpose. This represents a shift in land use away from food production and poses a global dilemma, namely the need to feed humanity. The development of second-generation biofuels and use of biomass growing in degraded areas are two options to improve the social acceptation of such technologies. A synergetic approach mixing a technical solution with strong ecological benefit and high economic return, under a clear sustainable policy coupled with a strong education program and culture, will allow the social sustainability of the technology.

PUC-Rio - Certificação Digital Nº 1312923/CA

6.3. Publications

The present work led to the publication of one article into the 23rd ABCM International Congress of Mechanical Engineering (COBEM 2015) in December 6th – 11th, 2015 (Rio de Janeiro, Brazil). The article was published under the title

"STUDY OF ETHANOL – DIESEL (E-DIESEL) BLENDS STABILITY USING A RENEWABLE TERNARY ADDITIVE", with the reference COB-2015-0633 [Pradelle, 2015].

A patent application was registered on March 9th, 2017, with Peugeot Citroën do Brasil Automóveis Ltda in the French *Institut National de la Propriété Industrielle* to protect the formulation of the additive [Pradelle, 2017]. The document gathers information relative to the compounds of the additive and its impact on the stability of the blends.

Furthermore, other articles should be published in international journal after patenting the additive (additive formulation, physicochemical properties, combustion and engine performance).

PUC-Rio - Certificação Digital Nº 1312923/CA

References

Abu-Qudais, M.; Haddad, O.; Qudaisat, M. **The effect of alcohol fumigation on diesel engine performance and emissions**. Energy Conversion & Management, v.11, p. 389-399, 2000.

Adhikesavan, C., Rajadurai, J. S. **Influence of B20 Biodiesel Blends on Diesel Engine Combustion**. Journal of the Japan Institute of Energy, v.93, p. 675-683, 2014.

Ahmed, I. **Oxygenated diesel: emissions and performance characteristics of ethanol–diesel blends in CI engines**. SAE Paper No. 2001-01-2475, 2001.

Ajav, E. A.; Singh, B.; Bhattacharya, T. K. **Experimental study of some performance parameters of a constant speed stationary diesel engine using ethanol-diesel blends as fuel**. Biomass and Bioenergy, v.17, p. 357-365, 1999.

Ajav, E. A.; Akingbehin, O. A. **A study of some fuel properties of local ethanol blended with diesel fuel**. Agricultural Engineering International: the CIGR Journal of Scientific Research and Development, v.4, 2002. 9 p.

Ali, Y.; Hanna, M. A.; Borg, J. E. **Optimization of diesel, methyl tallowate and ethanol blend for reducing emissions from diesel engine**. Bioresource Technology, v.52, p. 237–243, 1995.

Alptekin, E.; Canakci, M. **Characterization of the key fuel properties of methyl ester–diesel fuel blends**. Fuel, v.88, p. 75–80, 2009.

Anastopoulos, G.; Lois, E.; Zannikos, F.; Teas, C. **Influence of aceto acetic esters and dicarboxylic acid esters on diesel fuel lubricity**. Tribology International, v.34, p. 749-755, 2001.

Anastopoulos, G.; Lois, E.; Karonis, D.; Kalligeros, S.; Zannikos, F. **Impact of oxygen and nitrogen compounds on the lubrication properties of low sulfur diesel fuels**. Energy, v.30, p. 415-426, 2005.

Andablo-Reyes, E.; Hidalgo-Alvarez, R.; de Vicente, J. **Controlling friction using magnetic nanofluids**. Soft Matter, v.7, p. 880-883, 2011.

PUC-Rio - Certificação Digital Nº 1312923/CA

ASTM International. **ASTM D6079 - Standard Test Method for Evaluating Lubricity of Diesel Fuels by the High-Frequency Reciprocating Rig (HFRR)**. West Conshohocken, PA, 2011.

ASTM International. **ASTM D613 - Standard Test Method for Cetane Number of Diesel Fuel Oil**. West Conshohocken, PA, 2013.

Aydin, F.; Ögut, H. **Effects of using ethanol-biodiesel-diesel fuel in single cylinder diesel engine to engine performance and emissions**. Renewable Energy, v.103; p. 688–694, 2017.

Aydogan, H.; Acaroglu, M. **Determination of the effects of bioethanol-diesel fuel blends containing Beraid ED10 additive on engine performance and emissions in a diesel engine with a pump injection system**. Scientific Research and Essays, v.8 (37), p. 1741-1751, 2013.

Balat, M.; Balat, H. **A critical review of bio-diesel as a vehicular fuel**. Energy Conversion and Management, v.49, p. 2727–2741, 2008.

Ballerini, D. **Le plein de biocarburants ? – Enjeux et réalités**. Ed. Technip, 2007.

Bamgboye, A.; Hansen, A. **Prediction of cetane number of biodiesel fuel from the fatty acid methyl ester (FAME) composition**. International Agrophysics, v.22, p. 21-29, 2008.

Barabás, I.; Todoruţ, A. **Key fuel properties of biodiesel–diesel fuel–ethanol blends**. SAE paper No. 2009-01-1810, 2009.

Barabás, I.; Todoruţ, A.; Baldean, D. **Performance and emission characteristics of an CI engine fueled with diesel–biodiesel–bioethanol blends**. Fuel, v.89, p. 3827–3832, 2010.

Barabás, I.; Todoruţ, I.-A. Utilization of biodiesel-diesel-ethanol blends in CI engine. In: Montero, G.; Stoytcheva, M. **Biodiesel-quality, emissions and by-products**, Ed. InTech; 2011. p. 215–34.

Beer, T.; Grant, T.; Morgan, G.; Lapszewicz, J.; Anyon, P.; Edwards, J.; Nelson, P.; Watson, H.; Williams, D. **Final report to the Australian Greenhouse Office on the Stage 2 study of life-cycle emissions analysis of alternative fuels for heavy vehicles**. CSIRO, 2007.

Bergmann, J. C., Tupinambá, D. D.; Costa, O. Y. A.; Almeida, J. R. M., Barreto, C. C.; Quirino, B. F. **Biodiesel production in Brazil and alternative biomass feedstocks**. Renewable and Sustainable Energy Reviews, v. 21, p. 411-420, 2013.

PUC-Rio - Certificação Digital Nº 1312923/CA

Bhale P. V.; Deshpande, N. V.; Thombre, S.B. **Improving the low temperature properties of biodiesel fuel**. Renewable Energy, v.34, p. 794–800, 2009.

Bhide, S.; Morris, D.; Leroux, J.; Wian, K. S.; Perez, J. M.; Boehman, A. L. **Characterization of the Viscosity of Blends of Dimethyl Ether with Various Fuels and Additives**. Energy & Fuels, v.17, p. 1126-1132, 2003.

Boretti, A. **Advantages of converting Diesel engines to run as dual fuel ethanol-Diesel**. Applied Thermal Engineering, v.47, p. 1-9, 2012.

Boruff, P. A.; Schwab, W.; Goering, C. E.; Pryde, E. H. **Evaluation of Diesel Fuel – Ethanol Microemulsions**. Transactions of the ASAE, v.25 (1), p. 47-53, 1982.

Bosch, **Diesel distributor fuel-injection pumps.** Technical publications. 4th edition, 66 p. 1999

Boundy, B.; Diegel, S. W.; Wright, L.; Davis, S. C. **Biomass Energy Data Book: Edition 4**. Report to NREL/MP-540-32674, Oak Ridge National Laboratory, U.S. Department of Energy, 2001.

Brasil. ANP Resolution No. 50, December 23rd, 2013. Especificação do óleo diesel A e B. **Portaria Agência Nacional do Petróleo, Gás Natural e Biocombustíveis**, December 24th, 2013. Available from: <http://nxt.anp.gov.br/nxt/gateway.dll/leg/resolucoes_anp/2013/dezembro/ranp%2050%20-%202013.xml>. Accessed on October 5th, 2015.

Brasil. ANP Resolution No. 45, August 25th, 2014. Especificação do biodiesel. **Portaria Agência Nacional do Petróleo, Gás Natural e Biocombustíveis**, August 26th, 2014. Available from: <http://nxt.anp.gov.br/nxt/gateway.dll/leg/resolucoes_anp/2014/agosto/ranp%2045%20-%202014.xml>. Accessed on October 5th, 2015.

Brasil. Resolution No. 3, September 21st, 2015. Autoriza e define diretrizes para comercialização e uso voluntário de biodiesel. **Diário Oficial da República Federativa do Brasil**, Brasília, DF, October 14th, 2015a. Available from: <http://pesquisa.in.gov.br/imprensa/jsp/visualiza/index.jsp?jornal=1&pagina=2&data=14/10/2015>. Accessed on: October 15th, 2015.

PUC-Rio - Certificação Digital Nº 1312923/CA

Brasil. ANP Resolution No. 19, April 15th, 2015. Especificação do Etanol Anidro Combustível (EAC), ao Etanol Hidratado Combustível (EHC) e ao Etanol Hidratado Combustível Premium (EHCP). **Portaria Agência Nacional do Petróleo, Gás Natural e Biocombustíveis**, April 20th, 2015b. Available from: <http://nxt.anp.gov.br/nxt/gateway.dll/leg/resolucoes_anp/2015/abril/ranp%2019%20-%202015.xml>. Accessed on October 5th, 2015.

Brasil. Ordinary Law No. 13,263, March 23rd, 2016. Sobre os percentuais de adição de biodiesel ao óleo diesel comercializado no território nacional. **Diário Oficial da República Federativa do Brasil**, Brasília, DF, March 24th, 2016. Available from: <http://www.planalto.gov.br/ccivil_03/_Ato2015-2018/2016/Lei/L13263.htm>. Accessed on April 4th, 2015.

Brasil. Dados estatísticos - Importações & exportações. **Portaria Agência Nacional do Petróleo, Gás Natural e Biocombustíveis**, October 5th, 2016b. Available from: <http://www.anp.gov.br/wwwanp/dados-estatisticos>. Accessed on January 27th, 2017.

Caetano, T. **Estudo da miscibilidade de etanol com componentes do diesel e biodiesel**. Master dissertation submitted to the *Faculdade de Engenharia Química* of the *Universidade Estadual de Campinas*. Campinas, São Paulo, 2003.

Can, O.; Çelikten, I.; Usta, N. **Effects of ethanol addition on performance and emissions of a turbocharged indirect injection Diesel engine running at different injection pressures**. Energy Conversion and Management, v.45, p. 2429–2440, 2004.

Canakci, M.; Van Gerpen, J. H. **Comparison of Engine Performance and Emissions For Petroleum Diesel Fuel, Yellow Grease Biodiesel, and Soybean Oil Biodiesel**. Transactions of the ASAE, v.46 (4), p. 937-944, 2003.

Carneiro, M. L. N. M., Pradelle, F.; Braga, S. L.; Gomes, M. S. P., Martins, A. R. F. A.; Turkovics, F.; Pradelle, R. N. C. **Potential of biofuels from algae: Comparison with fossil fuels, ethanol and biodiesel in Europe and Brazil through life cycle assessment (LCA)**. Renewable and Sustainable Energy Reviews, v. 73, p. 632-653, 2017.

Castanheira, É. G.; Freire, F. GHG life-cycle assessment of soybean-based biodiesel: assessing the implications of alternative land use change scenarios. In **Workshop on land use impact of bioenergy - Quantifying and managing land use impacts of bioenergy** Campinas, São Paulo, 2011.

PUC-Rio - Certificação Digital Nº 1312923/CA

Castanheira, É. G.; Grisoli, R.; Coelho, S.; Silva, G. A.; Freire, F. **Life-cycle assessment of soybean-based biodiesel in Europe: comparing grain, oil and biodiesel import from Brazil**. Journal of Cleaner Production, v.102, p. 188-201, 2015.

Cheenkachorn, K.; Narasingha, M. H., Pupakornnopparut, J. **Biodiesel as an Additive for Diesohol**. Asian Journal on Energy and Environment, v.7 (1), p. 267-276, 2006.

Cheenkachorn, K.; Fungtammasan, B. **An Investigation of Diesel-Ethanol-Biodiesel Blends for Diesel Engine: Part 1. Emulsion Stability and Fuel Properties**. Energy Sources, Part A: Recovery, Utilization, and Environmental Effects, v.32 (7), p. 637–644, 2010a.

Chen, H.; Shuai, S. -J.; Wang, J. -X. **Study on combustion characteristics and PM emission of diesel engines using ester–ethanol–diesel blended fuels**. Proceedings of the Combustion Institute, v.31, p. 2981–2989, 2007.

Chen, H.; Wang, J.; Shuai, S.; Chen, W. **Study of oxygenated biomass fuel blends on a diesel engine**. Fuel, v.87, p. 3462–3468, 2008.

Chotwichien, A.; Luengnaruemitchai, A.; Jai-In, S. **Utilization of palm oil alkyl esters as an additive in ethanol–diesel and butanol–diesel blends**. Fuel, v.88, p. 1618–1624, 2009.

CIBSE. **Guide C: Reference Data 07**, Ed. Chartered Institution of Building Services Engineers (CIBSE), 2007.

Conservatoire National des Arts et Métiers (CNAM). Havet, J. - L. Apostille : **Notes de cours: Plan de Doehlert**, Paris, 2011, 132 p.

Corporan, E.; DeWitt, M.; Wagner, M. **Evaluation of soot particulate mitigation additives in a T63 engine**. Fuel Processing Technology, v.85, p. 727–742, 2004.

Cutrim, F. G. S. F.; de La Salles, W. F. **Avaliação de agentes estabilizantes para formulação de misturas combustíveis a base de álcool e diesel**. In: 7º Congresso Brasileiro de P&D em Petróleo e Gás, Aracaju, Sergipe, 2013.

Da Silva, E. J. **Equilíbrio líquido-líquido em misturas de hidrocarbonetos + alcoóis: Comportamento de fases e desenvolvimento de aditivos para aumentar a miscibilidade em misturas óleo diesel + etanol**. Doctorate thesis submitted to the Instituto de Química of the *Universidade Estadual de Campinas*. Campinas, São Paulo, 2005.

PUC-Rio - Certificação Digital Nº 1312923/CA

Demirbas, A. **Biofuels sources, biofuel policy, biofuel economy and global biofuel projections**. Energy Conversion and Management, v.49, p. 2106–2116, 2008.

Demirbas, A. **Progress and recent trends in biodiesel fuels**. Energy Conversion and Management, v.50, p. 14–34, 2009.

Di, Y.; Cheung, C. S.; Huang, Z. **Experimental study on particulate emission of a diesel engine fueled with blended ethanol–dodecanol–diesel**. Aerosol Science, v.40, p. 101–112, 2009.

Dmytryshyn, S. L.; Dalai, A. K.; Chaudhari, S. T.; Mishra, H. K.; Reaney, M. J. **Synthesis and characterization of vegetable oil derived esters: evaluation for their diesel additive properties**. Bioresource Technology, v.92, p. 55-64, 2004.

Duffield, J.; Shapouri, H.; Graboski, M.; McCormick, R.; Wilson, R. **U.S. Biodiesel Development: New Markets for Conventional and Genetically Modified Agricultural Products**, Agricultural economic report. Economic Research Service, US Department of Agriculture, 1998.

Duran, R. Importation of Oil in Brazil. The Brazil Business, 2013. Available from: <http://thebrazilbusiness.com/article/importation-of-oil-in-brazil 2013>. Accessed on June 6th, 2016.

Ecológica Mato Grosso Indústria e Comércio Ltda. (Ecomat). **AEP-102: Creator of the biodegradable ecological fuel**. 1999. 6 p.

Egúsquiza, J. C. C. **Avaliação Experimental de um Motor do Ciclo Diesel Operando no Modo Bicombustivel: Diesel/Etanol e Diesel/Gás**. Doctorate thesis submitted to the *Departamento de Engenharia Mecânica* of the *Pontifícia Universidade Católica do Rio de Janeiro*. Rio de Janeiro, Rio de Janeiro, 2011.

Ejim C. E.; Fleck, B. A.; Amirfazli, A. **Analytical study for atomization of biodiesels and their blends in a typical injector: surface tension and viscosity effects**. Fuel, v.86, p. 1534–1544, 2007.

El-Awad, M. M.; Yusaf, T. F. **Performance and exhaust emission of a diesel engine using crude palm oil as a fuel extender**. Journal of Energy & Environment, v.3, p. 61–68, 2004.

Empresa de Pesquisa Energética (EPE), **Brazilian Energy Balance 2016 Year 2015**. Rio de Janeiro, Rio de Janeiro, 2016.

PUC-Rio - Certificação Digital Nº 1312923/CA

Fang, Q.; Fang, J.; Zhuang, J.; Huang, Z. **Effects of ethanol-diesel-biodiesel blends on combustion and emissions in premixed low temperature combustion**. Applied Thermal Engineering, v.54, p.541-548, 2013.

Fazal, M. A.; Haseeb, A. S. M. A.; Masjuki, H. H**. Biodiesel feasibility study: An evaluation of material compatibility; performance; emission and engine durability**. Renewable and Sustainable Energy Reviews, v.15, p. 1314–1324, 2011.

Fernando, S.; Hanna, M. **Development of a Novel Biofuel Blend Using Ethanol-Biodiesel-Diesel Microemulsions: EB-Diesel**. Energy & Fuels, v.18, p. 1695-1703, 2004.

Ferreira, S. L. C.; dos Santos, H. C.; Fernandes, M. S.; de Carvalho, M. S. **Application of Doehlert matrix and factorial designs in optimization of experimental variables associated with preconcentration and determination of molybdenum in sea-water by inductively coupled plasma optical emission spectrometry**. Journal of Analytical Atomic Spectrometry; v.17, p. 115–120, 2002.

Fox, R. W.; McDonald, A. T.; Pritchard, P. J. **Introdução a Mecânica dos Fluidos**, 6th ed, Ed. LTC, 2006.

Geller, D. P.; Goodrum, J. W. **Effects of specific fatty acid methyl esters on diesel fuel lubricity**. Fuel, v.83, p. 2351-2356, 2004.

Gerdes, K. R.; Suppes, G. J. **Miscibility of Ethanol in Diesel Fuels**. Industrial & Engineering Chemistry Research, v.40, p. 949-956, 2001.

Ghobadian G.; Rahimi, H. M. K. **Evaluation of engine performance using net diesel fuel and biofuel blends**. In: Proceedings of the first combustion conference of Iran, Tehran, Iran, 2006.

Giakoumis, E. G.; Rakopoulos, C. D.; Dimaratos, A. M.; Rakopoulos, D. C. **Exhaust emissions with ethanol or n-butanol diesel fuel blends during transient operation: A review**. Renewable and Sustainable Energy Reviews, v.17, p. 170–190, 2013.

Goodrum, J. W.; Geller, D. P. **Influence of fatty acid methyl esters from hydroxylated vegetable oils on diesel fuel lubricity**. Bioresource Technology, v.96, p.851-855, 2005.

PUC-Rio - Certificação Digital Nº 1312923/CA

Gu, X.; Huang, Z.; Cai, J.; Gong, J.; Wu, X.; Lee, C. - F. **Emission characteristics of a spark-ignition engine fuelled with gasoline-n-butanol blends in combination with EGR**. Fuel, v.93, p. 611-617, 2012.

Guarieiro, L. L. N.; de Souza, A. F.; Torres, E. A.; de Andrade, J. B.; **Emission profile of 18 carbonyl compounds, CO, CO_2, and NOx emitted by a diesel engine fuelled with diesel and ternary blends containing diesel, ethanol and biodiesel or vegetable oils**. Atmospheric Environment, v.43, p. 2754–2761, 2009.

Hancsók J.; Eller Z.; Marsi G.; Nagy G. **Increasing the Stability of Bioethanol/Gas Oil Emulsions by a New Emulsion Additive**. Petroleum & Coal, v.53 (2), p. 106-114, 2011.

Hanna, M. A.; Ali, Y.; Cuppett, S. L.; Zheng, D. **Crystallization Characteristics of Methyl Tallowate and Its Blends with Ethanol and Diesel Fuel**. Journal of the American Oil Chemists' Society, v.73 (6), p.759-763, 1996.

Hansen, A. C.; Lyne, P. W. L.; Zhang, Q. **Ethanol–diesel fuel blends: a step towards a bio-based fuel for diesel engines**. In: 2001 ASAE Annual International Meeting, Sacramento, California, USA, 2001a.

Hansen, A. C.; Hornbaker, R. H.; Zhang, Q.; Lyne, P. W. L**. On-farm Evaluation of Diesel Fuel Oxygenated with Ethanol**. In: 2001 ASAE Annual International Meeting, Sacramento, California, USA, 2001b.

Hansen, A. C.; Zhang, Q.; Lyne, P. W. L. **Ethanol–diesel fuel blends – a review**. Bioresource Technology, v.96, p. 277–285, 2005.

Hardenberg, H.; Ehnert, E. R. **Ignition quality determination problems with alternative fuels for compression ignition engines**. SAE Paper No. 811212, 1981a.

Hardenberg, H. O.; Schaefer, A. J. **The use of ethanol as a fuel for compression–ignition engines**. SAE Paper No. 811211, 1981b.

He, B. - Q.; Shuai, S. - J.; Wang, J. - X.; He, H. **The effect of ethanol blended diesel fuels on emissions from a diesel engine**. Atmospheric Environment, v.37, p. 4965–4971, 2003.

Heywood, J. B. **Internal Combustion Engine Fundamentals**, Ed. McGraw-Hill, 1988.

Hu, J.; Du, Z.; Li, C.; Min, E. **Study on the lubrication properties of biodiesel as fuel lubricity enhancers**. Fuel, v.84, p. 1601-1606, 2005.

PUC-Rio - Certificação Digital Nº 1312923/CA

Huang, J.; Wang, Y.; Li, S.; Roskilly, A. P., Yu, H.; Li, H. **Experimental investigation on the performance and emissions of a diesel engine fuelled with ethanol–diesel blends**. Applied Thermal Engineering, v.29, p. 2484–2490, 2009.

Hulwan, D. B.; Joshi, S. V. **Performance, emission and combustion characteristic of a multicylinder DI diesel engine running on diesel–ethanol–biodiesel blends of high ethanol content**. Applied Energy, v.88, p. 5042–5055, 2011.

Hussan, M. J.; Hassan, M. H.; Kalam, M. A.; Memon, L. A. **Tailoring key fuel properties of diesel-biodiesel-ethanol blends for diesel engine**. Journal of Cleaner Production, v.51, p. 118-125, 2013.

Ikura, M.; Stanciulescu, M.; Hogan, E. **Low temperature stable diesel oil / alcohol mixtures**. US Patent No. 2002/0178650 A1, December 5th, 2002.

International Energy Agency (IEA). **World energy outlook**, 2014. Available from: <http://www.iea.org/publications/freepublications/publication/WEO_2014_ES_English_WEB.pdf>. Accessed on January 27th, 2015.

International Organization for Standardization (ISO). **EN ISO 12156-1:2006 - Diesel fuel — Assessment of lubricity using the high-frequency reciprocating rig (HFRR) — Part 1: Test method**. Geneva, Switzerland, 2006.

Jackson, M. M.; Corkwell, K. C.; DeGroote, C. C. **Study of Diesel and Ethanol Blends Stability**. SAE Paper No. 2003-01-3191, 2003.

Jain, S.; Sharma, M. P. **Prospects of biodiesel from Jatropha in India: A review**. Renewable and Sustainable Energy Reviews, v.14, p. 763–771, 2010.

Jayed, M. H.; Masjuki, H. H.; Kalam, M. A.; Mahlia, T. M. I.; Husnawan, M.; Liaquat, A. M. **Prospects of dedicated biodiesel engine vehicles in Malaysia and Indonesia**. Renewable and Sustainable Energy Reviews, v.15, p. 220–235, 2011.

Joaquim, C. R. O. **Verificação do comportamento da lubricidade do óleo diesel veicular com adição de etanol**. Master dissertation submitted to the *Ecola Politécnica* of the *Universidade de São Paulo*. São Paulo, São Paulo, 2007.

Kannan, G. R.; **Effect of injection pressures and timings on the performance emission and combustion characteristics of a direct injection diesel engine using biodiesel–diesel–ethanol blend**. SAE Paper No. 2013-01-1699, 2013.

PUC-Rio - Certificação Digital Nº 1312923/CA

Kenar, J. A.; Knothe, G.; Dunn, R. O.; Ryan, T. W.; Matheaus, A. **Physical Properties of Oleochemical Carbonates**. Journal of the American Oil Chemists' Society, v.82, p. 201-205, 2005.

Khoobbakht, G.; Najafi, G.; Karimi, M.; Akram, A. **Optimization of operating factors and blended levels of diesel, biodiesel and ethanol fuels to minimize exhaust emissions of diesel engine using response surface methodology**. Applied Thermal Engineering, v.99, p. 1006-1017, 2016.

Kim, H.; Choi, B. **Effect of ethanol–diesel blend fuels on emission and particle size distribution in a common-rail direct injection diesel engine with warm-up catalytic converter**. Renewable Energy, v.33; p. 2222–2228, 2008.

Kinney, A. J.; Clemente, T. E. **Modifying soybean oil for enhanced performance in biodiesel blends**. Fuel Processing Technology, v.86 (10), p. 1137-1147, 2005.

Knothe, G.; Steidley, K. R. **Lubricity of Components of Biodiesel and Petrodiesel. The Origin of Biodiesel Lubricity**. Energy & Fuels, v.19, p. 1192-1200, 2005a.

Knothe, G. **Dependence of biodiesel fuel properties on the structure of fatty acid alkyl esters**. Fuel Processing Technology, v.86, p. 1059– 1070, 2005b.

Knothe, G.; Steidley, K. R. **Kinematic viscosity of biodiesel fuel components and related compounds. Influence of compound structure and comparison to petrodiesel fuel components**. Fuel, v.84, p. 1059-1065, 2005c.

Koike, G. H. A.; Dal Bem, A. J.; Passarini, L. C. **Estudo da Utilização da Mistura de Etanol Anidro a 7% em Motores de Ciclo Diesel sem Adição de Aditivos**. Minerva, v.3 (1), p. 83-92, 2006.

Koike, G. H. A.; Dal Bem, A. J.; Passarini, L. C. **Utilização de Etanol em Motores de Ciclo Diesel**. Minerva, v.3 (2); p. 141-149, 2007.

Kremer, F. G.; Fachetti, A. **Alcohol as Automotive Fuel - Brazilian Experience**. SAE Paper No. 2000-01-1965, 2000.

Kruss, **Du Noüy ring method**, 2016. Available from: <http://www.kruss.de/fr/services/education-theory/glossary/du-nouey-ring-method/>. Accessed on February 6h, 2015.

Kwanchareon, P.; Luengnaruemitchai, A.; Jai-In, S. **Solubility of a diesel–biodiesel–ethanol blend, its fuel properties, and its emission characteristics from diesel engine**. Fuel, v.86, p.1053–1061, 2007.

PUC-Rio - Certificação Digital Nº 1312923/CA

Lapuerta, M.; Armas, O.; García-Contreras, R. **Stability of diesel–bioethanol blends for use in diesel engines**. Fuel, v.86 (10-11), p. 1351–1357, 2007.

Lapuerta, M.; Armas, O.; García-Contreras, R. **Effect of Ethanol on Blending Stability and Diesel Engine Emissions**. Energy & Fuels, v.23, p. 4343-4354, 2009.

Lapuerta M.; García-Contreras, R.; Campos-Fernández, J.; Dorado, M. P. **Stability, lubricity, viscosity, and cold-flow properties of alcohol-diesel blends**. Energy & Fuels, v.24, p. 4497–4502, 2010a.

Lapuerta, M.; García-Contreras, R.; Agudelo, J. R. **Lubricity of Ethanol-Biodiesel-Diesel Fuel Blends**. Energy & Fuels v.24, p. 1374-1379, 2010b.

Lapuerta, M.; Hernández, J. J.; Fernández-Rodríguez, D.; Cova-Bonillo, A. **Autoignition of blends of n-butanol and ethanol with diesel or biodiesel fuels in a constant-volume combustion chamber**. Energy, v.118, p. 613–621, 2017a.

Lapuerta, M.; Rodríguez-Fernández, J.; Fernández-Rodríguez, D.; Patiño-Camino, R. **Modeling viscosity of butanol and ethanol blends with diesel and biodiesel fuels**. Fuel, v.199, p. 332–338, 2017b.

Lebedevas, S.; Lebedeva, G.; Makareviciene, V.; Janulis, P.; Sendzikiene, E. **Usage of Fuel Mixtures Containing Ethanol and Rapeseed Oil Methyl Esters in a Diesel Engine**. Energy & Fuels, v. 23, p. 217–223, 2009.

Lei, J.; Bi, Y.; Shen, L. **Performance and Emission Characteristics of Diesel Engine Fueled with ethanol-Diesel Blends in Different Altitude Regions**. Journal of Biomedicine and Biotechnology, p. 1-10, 2011.

Lei, J.; Shen, L.; Bi, Y.; Chen, H. **A novel emulsifier for ethanol–diesel blends and its effect on performance and emissions of diesel engine**. Fuel, v.93, p. 305–311, 2012.

Li, D. - G.; Zhen, H.; Xingcai, L.; Wu-gao, Z.; Jian-guang, Y. **Physicochemical properties of ethanol–diesel blend fuel and its effect on performance and emissions of diesel engines**. Renewable Energy, v.30; p. 967–976, 2005.

Lin, J.; Gaustad, G.; Trabold, T. A. **Profit and policy implications of producing biodiesel–ethanol–diesel fuel blends to specification**. Applied Energy, v.104, p. 936–944, 2013.

PUC-Rio - Certificação Digital Nº 1312923/CA

Loaiza, J. C. V. **Ignição por Compressão com Ratividade Controlada de Óleo Diesel e Etanol em Máquina de Compressão Rápida**. Doctorate thesis submitted to the *Departamento de Engenharia Mecânica* of the *Pontifícia Universidade Católica do Rio de Janeiro*. Rio de Janeiro, Rio de Janeiro, 2014.

Makareviciene, V.; Sendzikiene, E.; Janulis, P. **Solubility of multi-component biodiesel fuel systems**. Bioresource Technology, v.96, p. 611–616, 2005.

Marsi, G.; Nagy, G.; Hancsók, J. **Investigation and Production of Bioethanol/Gas Oil Emulsions**. Hungarian Journal of Industrial Chemistry Veszprém 2008; v.36 (1-2), p. 83-88, 2008

McCormick, R. L.; Parish, R. **Advanced Petroleum Based Fuels Program and Renewable Diesel Program - Milestone Report: Technical Barriers to the Use of Ethanol in Diesel Fuel**. National Renewable Energy Laboratory, U.S. Department of Energy, 2001.

Ministério da Ciência e Tecnologia - Conselho Interministerial do Açúcar e do Álcool (MCT-CIMA). *Sumário Executivo da Mistura de 3% de álcool ao Diesel (MAD3)*. Brasília, December 2000. 31 p.

Mehta, P. S.; Anand, K. **Estimation of a Lower Heating Value of Vegetable Oil and Biodiesel Fuel**. Energy & Fuels, v.23, p. 3893–3898, 2009.

Mehta, R. N.; Chakraborty, M.; Parikh, P. A. **Comparative study of stability and properties of alcohol-diesel blends**. Indian Journal of Chemical Technology, v.19, p. 134-139, 2012.

Merker, P. M.; Schwartz, C.; Stiesch, G.; Otto, F. **Simulating Combustion - Simulation of combustion and pollutant formation for engine-development**, Springer, 2006.

Ministério de Minas e Energia / Empresa de Pesquisa Energética (MME/EPE), **Plano Decenal de Expansão de Energia 2024**. Brasília, Distrito Federal, 2015.

Mofijur M.; Masjuki, H. H.; Kalam, M. A.; Hazrat, M. A.; Liaquat, A. M.; Shahabuddin, M. **Prospects of biodiesel from Jatropha in Malaysia**. Renewable and Sustainable Energy Reviews, v.16, p. 5007–5020, 2012.

Mofijur, M., Rasul, M. G.; Hyde, J.; Azad, A. K.; Mamat, R.; Bhuiya, M. M. K. **Role of biofuel and their binary (diesel–biodiesel) and ternary (ethanol–biodiesel–diesel) blends on internal combustion engines emission reduction**. Renewable and Sustainable Energy Reviews, v. 53, p. 265-278, 2016.

PUC-Rio - Certificação Digital Nº 1312923/CA

Moretti, R. R. **Mistura Diesel, Biodiesel e Etanol Anidro: uma Possibilidade para Reduzir o Custo de Produção da Cadeia da Cana-de-Açúcar**. Master dissertation submitted to the *Faculdade de Engenharia Mecânica* of the *Universidade Estadual de Campinas*. Campinas, São Paulo, 2013.

Murayama, T.; Miyamoto, N.; Yamada, T.; Kawashima, J.; Kawashima, J. - I.; Itow, K. **A Method to Improve the Solubility and Combustion Characteristics of Alcohol-Diesel Fuel Blends**. SAE Paper No. 821113, 1982.

Murugesan, A.; Umarani, C.; Subramanian, R.; Nedunchezhian, N. **Bio-diesel as an alternative fuel for diesel engines – A review**. Renewable and Sustainable Energy Reviews, v.13, p. 653–662, 2009.

MWM International. **Manual de Oficina – Série 10.** ASC Comunicação Técnica, 2007.

Nagy, G.; Marsi, G.; Hancsók, J. **Study on Stability of Ethanol/Diesel Fuel Blend**. In: Proceedings of European Congress of Chemical Engineering (ECCE-6), Copenhagen, Denmark, 2007.

National Fire Protection Association (NFPA), **NFPA 497: Recommended Practice for the Classification of Flammable Liquids, Gases, or Vapors and of Hazardous (Classified) Locations for Electrical Installations in Chemical Process Areas**, Quincy, Massachussetts, 2009

National Fire Protection Association (NFPA), **NFPA 921: Guide for Fire and Explosion Investigations**, Quincy, Massachussetts, 2014

National Renewable Energy Laboratory (NREL), **Handbook for Handling, Storing, and Dispensing E85 and Other Ethanol-Gasoline Blends**. Golden, Colorado, 2016.

Odziemkowska, M.; Matuszewska, A.; Czarnocka, J. **Diesel oil with bioethanol as a fuel for compression-ignition engines**. Applied Energy, v.184, p. 1264-1272, 2016.

Olivares, V. M. **Estudo experimental do uso de misturas de biocombustíveis em um motor CFR/ASTM**. Research monograph submitted to the *Departamento de Engenharia Mecânica* of the *Escola Politécnica of the Universidade Federal do Rio de Janeiro*. Rio de Janeiro, Rio de Janeiro, 2012.

PUC-Rio - Certificação Digital Nº 1312923/CA

Oliveira, H. R. **Estudo de Viabilidade Técnica e Ambiental para utilizar Álcool Anidro / Diesel / Aditivo em Frota de Ônibus Urbanos**. Master dissertation submitted to the *Programa Interunidades de Pós-graduação em Energia* of the *Universidade de São Paulo*. São Paulo, São Paulo, 2003.

Öner, C.; Altun, S. **Biodiesel production from inedible animal tallow and an experimental investigation of its use as alternative fuel in a direct injection diesel engine**. Applied Energy, v.86, p. 2114–2120, 2009.

Ong, H. C.; Mahlia, T. M. I.; Masjuki, H. H.; Norhasyima, R. S. **Comparison of palm oil, Jatropha curcas and Calophyllum inophyllum for biodiesel: A review.** Renewable and Sustainable Energy Reviews, v.15, p. 3501–3515, 2011.

Oxiteno, **ALKEST® SP/ ALKEST® TW - Sorbitan Esters and Ethoxylated Sorbitan Esters**. 5 p. Available from: <http://www.univar.com/US/Industries/~/media/PDFs/US%20Corp%20Region%20PDFs/PC/Naturals/Oxiteno%20Alkest%20SP%20and%20TW%20from%20Univar.ashx>. Accessed on January 24th, 2015.

Oxiteno S.A Indústria e Comércio. Altair de Oliveira Lima; Amadeu Nunes. **Formulação de aditivos e álcool carburante aditivo para uso em motores diesel**. Brazilian Patent No. 8502824, June 10th, 1985.

Pang, X.; Shi, X.; Mu, Y.; He, H.; Shuai, S.; Chen, H.; Li, R. **Characteristics of carbonyl compounds emission from a diesel-engine using biodiesel–ethanol–diesel as fuel**. Atmospheric Environment, v.40, p. 7057–7065, 2006.

Pang, X.; Mu, Y.; Yuan, J.; He, H. **Carbonyls emission from ethanol-blended gasoline and biodiesel-ethanol-diesel used in engines**. Atmospheric Environment, v.42, p. 1349–1358, 2008.

Park, S. H.; Kim, S. H.; Lee, C. S. **Mixing Stability and Spray Behavior Characteristics of Diesel-Ethanol-Methyl Ester Blended Fuels in a Common-Rail Diesel Injection System**. Energy & Fuels, v.23, p. 5228–5235, 2009.

Park, S. H.; Cha, J.; Lee, C. S. **Effects of Bioethanol-Blended Diesel Fuel on Combustion and Emission Reduction Characteristics in a Direct-Injection Diesel Engine with Exhaust Gas Recirculation (EGR)**. Energy & Fuels, v.24, p. 3872–3883, 2010.

Park, S. H.; Cha, J.; Lee, C. S. **Impact of biodiesel in bioethanol blended diesel on the engine performance and emissions characteristics in compression ignition engine**. Applied Energy, v.99, p. 334–343, 2012.

PUC-Rio - Certificação Digital Nº 1312923/CA

Park, S. H.; Yoon, S. H.; Lee, C. S. **HC and CO emissions reduction by early injection strategy in a bioethanol blended diesel-fueled engine with an arrow angle injection system**. Applied Energy, v.107, p. 81–88, 2013.

Pauferro, M. T. O. **Uso do Etanol como Combustível para Motores Diesel: uma Discussão sobre a Viabilidade**. Research monograph submitted to the *MBA-Gestão Ambiental e Práticas de Sustentabilidade* of the *Escola de Engenharia Mauá* of the *Instituto Mauá de Tecnologia*. São Caetano do Sul, São Paulo, 2012.

Peeples, J. **Summary of Oxydiesel™ technology**. 2015. 2 p. Available from: <http://infohouse.p2ric.org/ref/35/34340.pdf>. Accessed on February 19th, 2015.

Pereira, R. H. **Avaliação Experimental e Previsão de Desempenho de Motores Diesel Consumindo Gás Natural**. Doctorate thesis submitted to the *Departamento de Engenharia Mecânica* of the *Pontifícia Universidade Católica do Rio de Janeiro*. Rio de Janeiro, Rio de Janeiro, 2006.

Pidol, L.; Lecointe, B.; Starck, L.; Jeuland, N. **Ethanol–biodiesel–Diesel fuel blends: Performances and emissions in conventional Diesel and advanced Low Temperature Combustions**. Fuel, v.93, p. 329–338, 2012.

Pottmaier, D.; Melo, C. R.; Sartor, M. N.; Kuester, S.; Amadio, T. M.; Fernandes, C. A. H.; Marinha, D.; Alarcon, O. E. **The Brazilian energy matrix: From a materials Science and engineering perspective**. Renewable and Sustainable Energy Reviews, v.19, p. 678–691, 2013

Pousa, G. P. A. G; Santos, A. L. F; Suarez, P. A. Z. **History and policy of biodiesel in Brazil**. Energy Policy, v.35, p. 5393–5398, 2007.

Pradelle, F. A. Y.; Braga, S. L.; Martins, A. R. F. A.; Turkovics, F.; Souza, R. N. C. **Study of ethanol-diesel (E-diesel) blends stability using a renewable ternary additive**. In: 23rd ABCM International Congress of Mechanical Engineering, Rio de Janeiro, Brazil, 2015.

Pradelle, R. N. C, Turkovics, F., Airoldi, M. L., Serralvo Neto, R., Braga, S. L., Pradelle, F., Martins, A. R. F. A., **Additif pour carburant comprenant un mélange de gazole et d'au moins un alcool de type éthanol**. Patent application registered to the Institut National de la Propriété Industrielle (INPI, França) under the application number: 1000393998, 2017.

Pure Energy Corporation. Irshad Ahmed. **Diesel fuel composition**. US Patent No. 6,017,369, January 25th, 2000.

PUC-Rio - Certificação Digital Nº 1312923/CA

Pure Energy Corporation. Irshad Ahmed. **Diesel fuel composition**. US Patent No. 6,190,427, February 20th, 2001a.

Pure Energy Corporation. Irshad Ahmed. **Diesel fuel composition**. US Patent No. 6,306,184 B2, October 23th, 2001b.

Pure Energy. **PURANOL® for Ethanol-Diesel Blends**. 2015. 4 p. Available from: <http://www.pure-energy.com/products/Puranol%20Brochure.pdf>. Accessed on February 14th, 2015.

Putrasari, Y.; Nur, A.; Muharam, A. **Performance and emission characteristic on a two cylinder DI diesel engine fuelled with ethanol-diesel blends**. Energy Procedia, v.32, p. 21-30, 2013.

Qi, D. H.; Geng, L. M.; Chen, H.; Bian, Y. Z.; Liu, J.; Ren, X. C. **Combustion and performance evaluation of a diesel engine fueled with biodiesel produced from soybean crude oil**. Renewable Energy, v.34, p. 2706–2713, 2009.

Qi, D. H.; Chen, H.; Lee, C. F.; Geng, L. M.; Bian, Y. Z. **Experimental studies of a naturally aspirated DI diesel engine fuelled with ethanol–biodiesel–water microemulsions**. Energy & Fuels, v.24, p. 652–663, 2010.

Química Fina. **Misturas álcool Diesel MAD-10 - OCTIMISE D 7001**, 2005. 4 p.

Rahimi, H.; Ghobadian, B.; Yusaf, T.; Najafi, G.; Khatamifar, M. **Diesterol: an environment-friendly IC engine fuel**. Renewable Energy, v.34, p. 335–342, 2009.

Rahnejat, H. **Tribology and Dynamics of Engine and Powertrain - Fundamentals, Applications and Future Trends**. Woodhead Publishing Ltd, 2010.

Rajasekar E.; Murugesan, A.; Subramanian, R., Nedunchezhian N. **Review of NOx reduction technologies in CI engines fuelled with oxygenated biomass fuels**. Renewable and Sustainable Energy Reviews, v.14, p.2113–2121, 2010.

Rakopoulos, C. D.; Antonopoulos, K. A.; Rakopoulos, D. C. **Experimental heat release analysis and emissions of a HSDI diesel engine fueled with ethanol–diesel fuel blends**. Energy, v.32, p. 1791–1808, 2007.

Rakopoulos, D. C.; Rakopoulos, C. D.; Papagiannakis, R. G; Kyritsis, D. C. **Combustion heat release analysis of ethanol or n-butanol diesel fuel blends in heavy-duty DI diesel engine**. Fuel, v.90, p. 1855–1867, 2011.

PUC-Rio - Certificação Digital Nº 1312923/CA

Randazzo, M. L.; Sodré, J. R. **Cold start and fuel consumption of a vehicle fuelled with blends of diesel oil–soybean biodiesel–ethanol**. Fuel, v.90: p. 3291-3294, 2011a.

Randazzo, M. L.; Sodré, J. R. **Exhaust emissions from a diesel powered vehicle fuelled by soybean biodiesel blends (B3–B20) with ethanol as an additive (B20E2–B20E5)**. Fuel, v.90: p. 98-103, 2011b.

Rangel, I. R.; Pereira, R. G. **Análise da variação dos parâmetros de desempenho de um motor de ignição por compressão utilizando misturas álcool-diesel**. In: Proceedings of the 4º Encontro de Energia no Meio Rural, Campinas, São Paulo, 2002.

Reyes, Y. **Combustíveis Alternativos: Mistura de Etanol Anidro ao Óleo Diesel para Motores de Ciclo Diesel com Sistema de Injeção de Bomba Rotativa**. Doctorate thesis submitted to the *Pós-graduação em Tecnologia de Processos Químicos e Bioquímicos* of the *Escola de Química* of the *Universidade Federal do Rio de Janeiro*. Rio de Janeiro, Rio de Janeiro, 2009a.

Reyes, Y.; Aranda, D. A. G.; Santander, L. A. M.; Cavado, A.; Belchior, C .R. P. **Action Principles of Co-solvent Additives in Ethanol-Diesel Blends: Stability Studies**. Energy & Fuels, v.23, p. 2731–2735, 2009b.

Ribeiro, N. M.; Pinto, A. C; Quintella, C. M.; da Rocha, G. O.; Teixeira, L. S. G.; Guarieiro, L. L. N.; Rangel, M. C.; Veloso, M. C. C.; Rezende, M. J. C.; da Cruz, R. S.; de Oliveira, A. M.; Torres, E. A.; de Andrade, J. B. **The Role of Additives for Diesel and Diesel Blended (Ethanol or Biodiesel) Fuels: A Review**. Energy & Fuels, v.21, p. 2433-2445, 2007.

Rocha, H. L. **Estudo experimental do uso de misturas combustíveis ternárias em um motor CFR/ASTM-cetano**. Research monograph submitted to the *Curso de Engenharia Mecânica* of the *Escola Politécnica* of the *Universidade Federal do Rio de Janeiro*. Rio de Janeiro, Rio de Janeiro, 2014.

Roy, M. M.; Calder, J.; Wang, W.; Mangad, A.; Diniz, F. C. M. **Cold start idle emissions from a modern Tier-4 turbo-charged diesel engine fueled with diesel-biodiesel, diesel-biodiesel-ethanol, and diesel-biodiesel-diethyl ether blends**. Applied Energy, v.180, p. 52–65, 2016.

SAGA Fuel Systems, Inc. Deborah Wenzel. **Composition as an additive to create clear stable solutions and microemulsions with a combustible liquid fuel to improve combustion**. US Patent No. 6,348,074 B2, February 19th, 2002.

PUC-Rio - Certificação Digital Nº 1312923/CA

Santos, A. S.; Valle, M. L. M.; Giannini, R. G. **The Brazilian Experience on Developing a Alcohol Diesel Binary Fuel**. Economia & Energia, v.20, p. 1-6, 2000.

Satgé de Caro, P.; Mouloungui, Z.; Gaset, A. **Synthesis of Alkyloxy (di)Alkylamino Propanols, Hydroxy Alkyloxy (di)Alkylamino Propanols, and the Dimer Compounds for Use as Fuel Additives**. Journal of the American Oil Chemists' Society, v.74 (3), p. 235-240, 1997a.

Satgé de Caro, P.; Mouloungui, Z.; Gaset, A. **Synthesis of Derivatives of Alkylamino Alkyloxy Propanol Structures by N-alkylation, Acylation, and Nitration. Application as Fuel Additives**. Journal of the American Oil Chemists' Society, v.74 (3), p. 241-247, 1997b.

Satgé de Caro, P.; Mouloungui, Z.; Vaitilingom, G.; Berge, J. C. **Interest of combining an additive with diesel–ethanol blends for use in diesel engines**. Fuel, v.80; p. 565–574, 2001.

Sayin, C. **Engine performance and exhaust gas emissions of methanol and ethanol–diesel blends**. Fuel, v.89, p. 3410-3415, 2010.

Scholz, V.; da Silva, J. N. **Prospects and risks of the use of castor oil as a fuel**. Biomass and Bioenergy, v.32 (2), p. 95-100, 2008.

Serdari, A.; Lois, E.; Stournas, S. **Tertiary fatty amides as diesel fuel substitutes**. International Journal of Energy Research, v.24, p. 455-466, 2000.

Shahir, S. A.; Masjuki, H. H.; Kalam, M. A.; Imran, A.; Fattah, I. M. R.; Sanjid, A. **Feasibility of diesel–biodiesel–ethanol/bioethanol blend as existing CI engine fuel: An assessment of properties, material compatibility, safety and combustion**. Renewable and Sustainable Energy Reviews, v.32, p. 379–395, 2014.

Shi, X.; Yu, Y.; He, H.; Shuai, S.; Wang, J.; Li, R. **Emission characteristics using methyl soyate–ethanol–diesel fuel blends on a diesel engine**. Fuel, v.84, p. 1543-1549, 2005.

Shi, X.; Pang, X.; Mu, Y.; He, H.; Shuai, S.; Wang, J.; Chen, H.; Li, R. **Emission reduction potential of using ethanol–biodiesel–diesel fuel blend on a heavy-duty diesel engine**. Atmospheric Environment, v.40, p. 2567–2574, 2006.

Shu Q.; Wang, J.; Peng, B.; Wang, D.; Wang, G. **Predicting the surface tension of biodiesel fuels by a mixture topological index method, at 313K**. Fuel, v.87, p. 3586–3890, 2008.

PUC-Rio - Certificação Digital Nº 1312923/CA

Shudo, T.; Nakajima, T.; Hiraga, K. **Simultaneous reduction in cloud point, smoke, and NOx emissions by blending bioethanol into biodiesel fuels and exhaust gas recirculation**. International Journal of Engine Research, v.10, p. 15–26, 2009.

Silveira, M. B. **Estudo do Sistema Álcool + Biodiesel + Diesel (AB-Diesel): Equilíbrio e Propriedades Termofluidodinâmicas**. Master dissertation submitted to the *Pós-graduação em Engenharia Química* of the *Universidade Federal do Ceará*. Fortaleza, Ceará, 2013.

Sinterface, Methods for surface and interfacial tension measurements, 2016. Available from: <http://www.sinterface.com/service/fundamentals/methods/index.html>.

Accessed on February 6h, 2015.

Sonntag, R. E.; Borgnakke, C., Van Wylen, G. J. **Fundamentals of Thermodynamics**, 6th edition, Ed. Wiley, 2003.

Strapasson, A. B.; Job, L. C. M. A. **Etanol, meio ambiente e tecnologia - Reflexões sobre a experiência brasileira**. Revista de Política Agrícola, Brasilia, Ano XV (3), p. 51-63, 2006.

Subbaiah, G. V.; Gopal, K. R.; Hussain, S. A. **The Effect of Biodiesel and Bioethanol Blended Diesel Fuel on the Performance and Emission Characteristics of a Direct Injection Diesel Engine**. Iranica Journal of Energy & Environment, v.1 (3), p. 211-221, 2010a.

Subbaiah, G. V.; Gopal, K. R.; Hussain, S. A.; Prasad, B. D., Reddy, K. T.

Rice bran oil biodiesel as an additive in diesel-ethanol blends for diesel engines. International Journal of Research and Reviews in Applied Sciences, v.3 (3), p. 334-342, 2010b.

Suppes, G. J. **Past mistakes and future opportunities of ethanol in diesel**. Buffalo, Bioenergy; 2000.

Surisetty, V. R.; Dalai, A. K.; Kozinski, J. **Alcohols as alternative fuels: An overview**, Applied Catalysis A: General, v.404, p. 1– 11, 2011.

Szwaja, S.; Naber, J. D. **Combustion of n-butanol in a spark-ignition IC engine**. Fuel, v.89, p. 1573-1582, 2010.

PUC-Rio - Certificação Digital Nº 1312923/CA

Tan, Y. H; Abdullah, M. O.; Nolasco-Hipolito, C.; Zauzi, N. S. A.; Abdullah, G. W. **Engine performance and emissions characteristics of a diesel engine fueled with diesel-biodiesel-bioethanol emulsions**. Energy Conversion & Management, v.132, p. 54-64, 2017.

Tesfa, B.; Gu, F.; Mishra, R.; Ball, A. D. **LHV predication models and LHV effect on the performance of CI engine running with biodiesel blends**. Energy Conversion and Management,v.71; p. 217–226, 2003.

Thangavelu, S. K.; Ahmed, A. S.; Ani, F. N. **Impact of metals on corrosive behavior of biodiesel-diesel-ethanol (BDE) alternative fuel**. Renewable Energy, v.94; p. 1–9, 2016.

Török, Á. **Theoretical estimation of the environmental impact of biofuel mixtures**. Transport, v.24 (1), p. 26–29, 2009.

Torres-Jimenez, E.; Jerman, M. S.; Gregorc, A.; Lisec, I.; Dorado, M. P.; Kegl, B. **Physical and chemical properties of ethanol–diesel fuel blends**. Fuel, v.90, p. 795–802, 2011.

Villela, A. C. S. **Desempenho e Combustão de Etanol Anidro e Hidratado em Motor Multicombustível**. Master dissertation submitted to the *Departamento de Engenharia Mecânica* of the *Pontifícia Universidade Católica do Rio de Janeiro*. Rio de Janeiro, Rio de Janeiro, 2010.

Weber de Menezes, E.; da Silva, R.; Cataluña, R.; Ortega, R. J. C. **Effect of ethers and ether/ethanol additives on the physicochemical properties of diesel fuel and on engine tests**. Fuel, v.85, p. 815–822, 2006.

Wyman, C. E.; Hinman, N. D. **Ethanol: Fundamentals of Production from Renewable Feedstocks and Use as a Transportation Fuel**. Applied Biochemistry and Biotechnology, v.24-25(1), p. 735-753, 1990.

Xing-cai, L.; Jian-guang, Y.; Wu-gao, Z.; Zhen, H. **Effect of cetane number improver on heat release rate and emissions of high speed diesel engine fueled with ethanol–diesel blend fuel**. Fuel, v.83, p. 2013–2020, 2004.

Xu, Q.; Nakajima, M.; Nabetani, H.; Iwamoto, S.; Liu, X. **The Effects of Ethanol Content and Emulsifying Agent Concentration on the Stability of Vegetable Oil–Ethanol Emulsions**. Journal of the American Oil Chemists' Society, v.78 (12), p. 1185-1190, 2001.

PUC-Rio - Certificação Digital Nº 1312923/CA

Xue, J.; Grift, T. E.; Hansen, A. C. **Effect of biodiesel on engine performances and emissions**. Renewable and Sustainable Energy Reviews, v.15, p. 1098–1116, 2011.

Yaginuma, R.; Moriya, S.; Sato, Y.; Sako, T.; Kodama, D.; Tanaka, H.; Kato, M. **Homogenizing Effect of Addition of Ethers to Immiscible Binary Fuels of Ethanol and Oil**. Sekiyu Gakkaishi, v.42 (3), p. 173-177, 1999.

Yahya, A.; Marley, S. J. **Physical and Chemical Characterization of Methyl Soyoil and Methyl Tallow Esters as CI Engine Fuels**. Biomass and Bioenergy. v.6 (4), p. 321-328, 1994.

Yao, M.; Wang, H.; Zheng, Z.; Yue, Y. **Experimental study of n-butanol additive and multi-injection on HD diesel engine performance and emissions**. Fuel, v.89, p. 2191-2201, 2010.

Yilmaz, N. **Comparative analysis of biodiesel-ethanol-diesel and biodiesel-methanol-diesel blends in a diesel engine**. Energy, v.40, p. 210-213, 2012.

Yilmaz, N.; Vigil, F. M.; Donaldson, A. B.; Darabseh, T. **Investigation of CI engine emissions in biodiesel–ethanol–diesel blends as a function of ethanol concentration**. Fuel, v.115, p. 790–793, 2014.

Yuan, Y.; Lee, T. R. Chapter 1 - Contact Angle and Wetting Properties. In: **Surface Science Techniques**. Springer Science & Business Media, 2013, p. 3-34.

Zhu, L.; Cheung, C. S.; Zhang, W. G.; Huang, Z. **Combustion, performance and emission characteristics of a DI diesel engine fueled with ethanol–biodiesel blends**. Fuel, v.90, p. 1743-1750, 2011.

Zöldy, M.; Emöd, I.; Oláh, Z. **Lubrication and Viscosity of the Bioethanol-Biodiesel-Bioethanol Blends**, In: 11th EAEC European Automotive Congress, Budapest, Hungary, 2007.

Zöldy, M. **Ethanol–biodiesel–diesel blends as a diesel extender option on compression ignition engines**. Transport v.26, p. 303–309, 2011.

PUC-Rio - Certificação Digital Nº 1312923/CA

Appendixes

Appendix A: Comparative Study of Stability and Physicochemical Properties of Different DBE Blends

This Appendix contains tables with typical values of stability and physicochemical properties available in literature for diesel-biodiesel-ethanol. Such table was adapted from [Shahir, 2014] and additional data was added from other articles.

PUC-Rio - Certificação Digital Nº 1312923/CA

Table A1: Comparative study of stability and physicochemical properties of different DBE blends (Part 1 of 2).

Reference	D:B:EtOH (vol%)	Biodiesel source	EtOH purity	Miscibility and stability of blends	Specific gravity (kg/m^3)	Viscosity (mm^2/s)	Cetane number (-)	Lubricity (µm)
Brazilian specification* (in bold) or data from literature** (in italic)	Diesel fuel				**815 - 850**	**2.0 - 4.5 (40°C)**	**> 48**	**< 460**
	Biodiesel				**850 - 900**	**3.0 - 6.0 (40°C)**	*48 - 67*	*218 - 257*
	Etanol		99.7%		**< 791.5**	*1.07-1.13 (40°C)*	*5 - 15*	*842 - 1057*
Hulwan, 2011	70:10:20	JSO (methyl ester)	99.7%		832.87 (15°C)	2.380 (40°C)	50 (I)	
Hulwan, 2011	50:20:30	JSO (methyl ester)	99.7%		834.55 (15°C)	2.401 (40°C)	50 (I)	
Hulwan, 2011	50:10:40	JSO (methyl ester)	99.7%		820.42 (15°C)	2.018 (40°C)	41 (I)	
Cheenkachorn, 2010a	82.5:12.5:05	PO	99.5% (90%) + Hydrous (10%)	1 phase after 2 months at RT	829 (15°C)	2.82 (40°C)	56.20	
Cheenkachorn, 2010a	82.5:12.5:05	PO	99.5% (95%) + Hydrous (5%)	1 phase after 2 months at RT	829 (15°C)	2.78 (40°C)	57.60	
Cheenkachorn, 2010a	84:11:05	PO	99.5% (95%) + Hydrous (5%)	1 phase after 2 months at RT	828 (15°C)	2.69 (40°C)	57.91	
Cheenkachorn, 2010a	80:15:05	PO	99.5% (90%) + Hydrous (10%)	1 phase after 2 months at RT	830 (15°C)	2.97 (40°C)	56.32	
Chotwichien, 2009	85:10:05	PO (butyl ester)	99.5%	1 phase after 2 months at RT	835.4 (15°C)	2.65 (40°C)		
Chotwichien, 2009	80:15:05	PO (butyl ester)	99.5%	1 phase after 2 months at RT	837 (15°C)	2.73 (40°C)		
Chotwichien, 2009	85:10:05	PO (ethyl ester)	99.5%	1 phase after 2 months at RT	835.9 (15°C)	2.63 (40°C)		
Chotwichien, 2009	80:15:05	PO (ethyl ester)	99.5%	1 phase after 2 months at RT	837.8 (15°C)	2.72 (40°C)		
Chotwichien, 2009	85:10:05	PO (methyl ester)	99.5%	1 phase after 2 months at RT	836.1 (15°C)	2.57 (40°C)	52 (I)	
Chotwichien, 2009	80:15:05	PO (methyl ester)	99.5%	1 phase after 2 months at RT	838.3 (15°C)	2.63 (40°C)	53.2 (I)	
Kwanchareon, 2007	90:05:05	PO (methyl ester)	99.5%	1 phase after 3 months at RT	831.3 (15°C)		47.31 (I)	
Kwanchareon, 2007	85:10:05	PO (methyl ester)	99.5%	1 phase after 3 months at RT	833.4 (15°C)		47.7 (I)	
Kwanchareon, 2007	85:05:10	PO (methyl ester)	99.5%	1 phase after 3 months at RT	831.3 (15°C)		46.67 (I)	
Kwanchareon, 2007	80:15:05	PO (methyl ester)	99.5%	1 phase after 3 months at RT	837.5 (15°C)		48.66 (I)	
Kwanchareon, 2007	80:10:10	PO (methyl ester)	99.5%	1 phase after 3 months at RT	833.1 (15°C)		46.85 (I)	
Kwanchareon, 2007	80:05:15	PO (methyl ester)	99.5%	1 phase after 3 months at RT	829 (15°C)		46.25 (I)	
Barabás, 2009	90:05:05	RO (methyl ester)	99.3%		841.3 (15°C)	2.44		272
Barabás, 2009	85:15:05	RO (methyl ester)	99.3%		843 (15°C)	2.28		252
Barabás, 2009	85:10:10	RO (methyl ester)	99.3%		847.1 (15°C)	2.54		279
Barabás, 2009	85:10:05	RO (methyl ester)	99.3%		845.1 (15°C)	2.42		276
Barabás, 2009	85:05:10	RO (methyl ester)	99.3%		843.2 (15°C)	2.18		243
Barabás, 2009	75:20:05	RO (methyl ester)	99.3%		845.4 (15°C)	2.38		306
Barabás, 2009	75:15:10	RO (methyl ester)	99.3%		850.4 (15°C)	2.65		309
Barabás, 2009	70:25:05	RO (methyl ester)	99.3%		847.3 (15°C)	2.49		232
Barabás, 2009	70:20:10	RO (methyl ester)	99.3%		852.4 (15°C)	2.77		264
Barabás, 2010	85:10:05	RO (methyl ester)	99.3%		845 (15°C)	2.421 (40°C)	51 / 47.7 (I)	
Barabás, 2010	80:10:10	RO (methyl ester)	99.3%		843 (15°C)	2.275 (40°C)	51 /46.85 (I)	
Barabás, 2010	70:25:05	RO (methyl ester)	99.3%		852 (15°C)	2.756 (40°C)	52 / 48.66 (I)	
Barabás, 2011	90:05:05	RO (methyl ester)	99.3%	1 phase after 30 h at 20 and 0°C 2 phases after 30 h at -8°C	843.7 (15°C)	2.435 (40°C)	51.04	305
Barabás, 2011	85:10:05	RO (methyl ester)	99.3%	1 phase after 30 h at 20 and 0°C 2 phases after 30 h at -8°C	845 (15°C)	2.421 (40°C)	51.20	232
Barabás, 2011	80:15:05	RO (methyl ester)	99.3%	1 phase after 30 h at 20 and 0°C Clear with sediments after 30 h at -8°C	847.2 (15°C)	2.527 (40°C)	51.36	276
Barabás, 2011	75:20:05	RO (methyl ester)	99.3%	1 phase after 30 h at 20 and 0°C Clear with sediments after 30 h at -8°C	849.6 (15°C)	2.645 (40°C)	51.52	243
Barabás, 2011	75:15:10	RO (methyl ester)	99.3%	1 phase after 30 h at 20 and 0°C Clear with sediments after 30 h at -8°C	844.7 (15°C)	2.374 (40°C)	49.24	272
Barabás, 2011	70:25:05	RO (methyl ester)	99.3%	1 phase after 30 h at 20, 0 and -8°C	851.9 (15°C)	2.756 (40°C)	51.68	252
Barabás, 2011	70:20:10	RO (methyl ester)	99.3%	1 phase after 30 h at 20 and 0°C Clear with sediments after 30 h at -8°C	846.8 (15°C)	2.48 (40°C)	49.41	264
Randazzo, 2011a	78:20:02	SO	99.5%		861.4 (20°C)	3.59 (40°C)	48.7 (I)	
Randazzo, 2011a	75:20:05	SO	99.5%		859.6 (20°C)	3.31 (40°C)	48.4 (I)	
Lapuerta, 2009	63.3:30:7.7	SO (methyl ester)	99.7%		827 (15°C)	2.12 (40°C)		
Pang, 2006	75:20:05	SO (methyl ester)	99.3%		845 (20°C)	3.04 (40°C)	45	
Shi, 2005	85:12:03	SO (methyl ester)	99.7%	1 phase after 3 months at NAC	840 (20°C)	3.01 (40°C)		
Shi, 2005	80:16:04	SO (methyl ester)	99.7%	1 phase after 3 months at NAC	840 (20°C)	3.03 (40°C)		
Shi, 2006	75:20:05	SO (methyl ester)	99.7%		845 (20°C)	3.04 (40°C)	45	
Kannan, 2013	60:30:10	WCO (methyl ester)	99.9%	1 phase after 1 month at 30°C	826 (27°C)	2.44 (27°C)	47.3	
Kannan, 2013	50:40:10	WCO (methyl ester)	99.9%	1 phase after 1 month at 30°C	831 (27°C)	2.60 (27°C)	47.2	
Kannan, 2013	50:30:20	WCO (methyl ester)	99.9%	1 phase after 1 month at 30°C	821 (27°C)	2.14 (27°C)	47.2	

Legend: B: Biodiesel; D: Diesel fuel; EtOH: Ethanol; I: Cetane Index; JS: Jatropha Seed Oil; NAC: Normal Ambient Condition; PO: Palm Oil; RO: Rapeseed Oil; RT: Room Temperature; SO: Soybean Oil; WCO: Waste Cooking Oil.

* Data obtained from [Brasil, 2013; Brasil, 2014; Brasil, 2015]; ** Data obtained from [Barabás, 2009; Chotwichien, 2009; Demirbas, 2009; Rahimi, 2009; Lapuerta, 2010a; Lapuerta, 2010b; Barabás, 2011; Kannan, 2013; Park, 2013; Shahir, 2014].

PUC-Rio - Certificação Digital Nº 1312923/CA

Table A1: Comparative study of stability and physicochemical properties of different DBE blends (Part 2 of 2).

Reference	D:B:EtOH (vol%)	Biodiesel source	Surface tension (mN/m)	Flash point (°C)	Cloud point (°C)	CFPP (°C)	Pour point (°C)	Calorific value (MJ/kg)	C content (wt%)	O content (wt%)
Brazilian specification* (in bold) or data from literature** (in italic)	Diesel fuel		*26.9 (15°C) / 29.0 (20°C)*	**> 38**	*0 - 5*	**< 0-12**	*-19 - 6*	*42.5 - 45.7*	*85.21 - 86.13*	*0.00*
	Biodiesel		*31.1 (15°C) / 38.6 (20°C)*	**> 100**	*13*	**< 5-14**	*-11 - 12*	*37.0 - 39.9*	*52.14*	*34.73*
	Etanol		*21.7 (15°C) / 19.2 (20°C)*	*12 - 17*	*-7*	*< -51*	*-117.3*	*26.8 - 27.0*	*76.74 - 76.97*	*10.79 - 11.09*
Hulwan, 2011	70:10:20	JSO (methyl ester)		14			-3	39.930	78.69	7.77
Hulwan, 2011	50:20:30	JSO (methyl ester)		12.5			-9	38.965	74.49	12.21
Hulwan, 2011	50:10:40	JSO (methyl ester)		12			-12	36.338	72.07	14.53
Cheenkachorn, 2010a	82.5:12.5:05	PO						44.430		
Cheenkachorn, 2010a	82.5:12.5:05	PO						44.490		
Cheenkachorn, 2010a	84:11:05	PO						44.560		
Cheenkachorn, 2010a	80:15:05	PO						44.210		
Chotwichien, 2009	85:10:05	PO (butyl ester)		16			3	44.000		
Chotwichien, 2009	80:15:05	PO (butyl ester)		15			3	43.700		
Chotwichien, 2009	85:10:05	PO (ethyl ester)		15			3	43.900		
Chotwichien, 2009	80:15:05	PO (ethyl ester)		15.7			3	39.300		
Chotwichien, 2009	85:10:05	PO (methyl ester)		15			3	43.700		
Chotwichien, 2009	80:15:05	PO (methyl ester)		17			3	43.800		
Kwanchareon, 2007	90:05:05	PO (methyl ester)		17.5			3	44.5		
Kwanchareon, 2007	85:10:05	PO (methyl ester)		14.0			3	43.7		
Kwanchareon, 2007	85:05:10	PO (methyl ester)		13.5			3	43.6		
Kwanchareon, 2007	80:15:05	PO (methyl ester)		16.0			3	43.3		
Kwanchareon, 2007	80:10:10	PO (methyl ester)		15.0			3	43.5		
Kwanchareon, 2007	80:05:15	PO (methyl ester)		13.0			3	42.8		
Barabás, 2009	90:05:05	RO (methyl ester)	30.7	17		-18				
Barabás, 2009	85:15:05	RO (methyl ester)	34.9	16		-13				
Barabás, 2009	85:10:10	RO (methyl ester)	29.3	15		-6				
Barabás, 2009	85:10:05	RO (methyl ester)	34.6	14		-17				
Barabás, 2009	85:05:10	RO (methyl ester)	28.5	15		-14				
Barabás, 2009	75:20:05	RO (methyl ester)	32.8	17		-17				
Barabás, 2009	75:15:10	RO (methyl ester)	30.6	15		-4				
Barabás, 2009	70:25:05	RO (methyl ester)	34.9	18		-16				
Barabás, 2009	70:20:10	RO (methyl ester)	31.7	16		-7				
Barabás, 2010	85:10:05	RO (methyl ester)		14		-17			82.73	2.82
Barabás, 2010	80:10:10	RO (methyl ester)		15		-6			81.08	4.55
Barabás, 2010	70:25:05	RO (methyl ester)		18		-17			81.50	4.43
Barabás, 2011	90:05:05	RO (methyl ester)	30.79 (20°C)	17.5		-18		41.707	83.22	2.2
Barabás, 2011	85:10:05	RO (methyl ester)	34.62 (20°C)	14		-17		41.560	82.79	2.76
Barabás, 2011	80:15:05	RO (methyl ester)	34.66 (20°C)	16		-13		41.414	82.37	3.32
Barabás, 2011	75:20:05	RO (methyl ester)	32.86 (20°C)	17		-17		41.269	81.94	3.88
Barabás, 2011	75:15:10	RO (methyl ester)	30.66 (20°C)	15.5		-4		40.668	80.8	4.96
Barabás, 2011	70:25:05	RO (methyl ester)	34.83 (20°C)	18		-16		41.124	81.52	4.43
Barabás, 2011	70:20:10	RO (methyl ester)	31.77 (20°C)	16		-7		40.524	80.38	5.52
Randazzo, 2011a	78:20:02	SO				-7				
Randazzo, 2011a	75:20:05	SO				-7				
Lapuerta, 2009	63.3:30:7.7	SO (methyl ester)				-18.0		39.0	80.6	5.65
Pang, 2006	75:20:05	SO (methyl ester)						40.900	83	3.9
Shi, 2005	85:12:03	SO (methyl ester)						41.500		2.3
Shi, 2005	80:16:04	SO (methyl ester)						41.200		3.1
Shi, 2006	75:20:05	SO (methyl ester)			-5			40.9	83	3.9
Kannan, 2013	60:30:10	WCO (methyl ester)		18.5	-1		-3	39.100		
Kannan, 2013	50:40:10	WCO (methyl ester)		19	3		-3	38.700		
Kannan, 2013	50:30:20	WCO (methyl ester)		15	4		-6	37.850		

Legend: B: Biodiesel; D: Diesel fuel; EtOH: Ethanol; I: Cetane Index; JS: Jatropha Seed Oil; NAC: Normal Ambient Condition; PO: Palm Oil; RO: Rapeseed Oil; RT: Room Temperature; SO: Soybean Oil; WCO: Waste Cooking Oil.

* Data obtained from [Brasil, 2013; Brasil, 2014; Brasil, 2015]; ** Data obtained from [Barabás, 2009; Chotwichien, 2009; Demirbas, 2009; Rahimi, 2009; Lapuerta, 2010a; Lapuerta, 2010b; Barabás, 2011; Kannan, 2013; Park, 2013; Shahir, 2014].

PUC-Rio - Certificação Digital Nº 1312923/CA

Appendix B: Comparative Study of Emissions Tendencies of Different DBE Blends during Engine Tests

This Appendix contains tables with typical values of emissions tendency available in literature for diesel-biodiesel-ethanol for soot, PM and smoke; NOx; CO; CO_2; unburned HC and others pollutants, such as SO_2 and carbonyls. Such table was adapted from [Mofijur, 2016] and additional data was added from other articles.

PUC-Rio - Certificação Digital Nº 1312923/CA

Table B1: Summary of the emission studies using diesel-biodiesel-ethanol blends in diesel engines, compared to fossil diesel fuel (adapted from Mofijur *et al.* (2016)) (Part 1 of 2).

D:B:EtOH	Engine / Vehicles	Exhaust emissions						Reference
		Soot, PM and smoke	NO_x	CO	CO_2	HC	Other	
70:10:20 50:20:30	3-cylinder diesel engine	↓	Low loads: ↓ Higher loads: ↑	Low loads:↓ Higher loads: ↑	Low loads: ↑ Higher loads: =			Hulwan, 2011
94.95:03:2.05 89.90:06:4.10 84.85:09:6.15 79.80:12:8.20	Ruggerini RD 270 2-cylinder diesel engine	↓		↓	↓	↓		Rahimi, 2009
80:05:15 90:03:07	Agrale M 790 2-cylinder diesel engine		↓	Low and medium rpm: = High rpm: ↓	Low and medium rpm: = High rpm: ↓		Ketones and aldehydes: ↑	Guarieiro, 2009
40:40:20	PSA Peugeot Citroën DV6 4-cylinder diesel engine (Euro IV)	↓	↓	↑		↑		Pidol, 2012
75:05:20 70:10:20 60:20:20	Modified single cylinder from Hyundai U1.5 (D4FA) 4-cylinder diesel engine	↓	↓	↓		↓		Park, 2012
78:20:02 75:20:05	Isuzu 4HF1 4-cylinder diesel engine		↓	↑	↓	↑		Zhu, 2011
75:20:05	Cummins 4B 4-cylinder diesel engine		↑	Low and medium rpm: ↑ High rpm: ↓	↑	↓	Ketones and aldehydes: ↑	Shi, 2006
85:12:03 80:16:04	Sofim 8140.43C 4-cylinder diesel engine (Euro II)	↓	↑	↓		↑		Shi, 2005
10:80:10	Kirloskar TV1 single cylinder diesel engine	↓	=	↓		Low loads: ↓ Higher loads: =		Bhale, 2009
70:20:10 60:20:20 50:20:30	Kirloskar model AV1 single cylinder diesel engine		↑		↑	↑		Subbaiah, 2010a
85:10:05 80:10:10 75:10:05	Kirloskar model AV1 single cylinder diesel engine	85:10:05: ↑ Other blends: ↓	Low loads: ↓ Higher loads: ↑	Low loads: = Higher loads: ↓	↑	Low and medium loads: ↑ High loads: ↓		Subbaiah, 2010b
80:13:07 70:19.5:10.5 60:26:14	Cummins NTA-855-C 4-cylinder diesel engine	↑	=	↓		↓	SO_2: =	Ali, 1995
48.5:48.5:03 47.5:47.5:05 42.5:42.5:15 37.5:37.5:25	Kubota GL7000 2-cylinder diesel engine		↓	↑		Up to 5 vol%: ↓ Other blends: ↑		Yilmaz, 2014
80:10:10 70:10:20	4-cylinder heavy-duty diesel engine	↓	↓	↑		↑		Fang, 2013
45:45:10 40:40:20	Kubota GL7000 2-cylinder diesel engine	↓	↓	↑		↑		Yilmaz, 2012
78.4:19.6:02 76:19:05	Vehicle with a 4-cylinder diesel engine	↑	↓	↓	↓	↓		Randazzo, 2011b
85:10:05 70:25:05 80:10:10	D-2402.000 4-cylinder diesel engine	↓	↑	Low loads: = Higher loads: ↓	↑	↓		Barabás, 2010
95:2.5:2.5 90:05:05 92.5:05:2.5 92.5:2.5:05	Super Star Engine single cylinder diesel engine		↑	Low rpm: ↑ High rpm: ↓	↑	↑	SO_2: ↓	Aydin and Ogut, 2017
78:15:07 67:13:20 60:35:05 54:31:15 84:00:16 50:40:10 56:22:22 62.5:25:12.5	Mercedes-Benz OM 314 4-cylinder diesel engine (Euro II)	↓	↓	↓	↑	↓		Khoobbakht, 2016
76:19:05 62:17:15 47.5:47.5:05 42.5:42.5:15	Cummins QSB 4.5 T4L 4-cylinder diesel engine (Tier-4)		Low rpm: ↓ Higher rpm: ↑	62:17:15 : ↑ Other blends: ↓		↓		Roy, 2016
80:15:05 80:10:10 80:05:15	Kubota RK95-1-NB-RDK single cylinder diesel engine		Medium rpm: ↓ Other rpm: ↑	High rpm: ↑ Lower rpm: ↓	↓			Tan, 2017

Legend: B: Biodiesel; D: Diesel fuel; EtOH: Ethanol; SOF: Soluble organic fraction; VOF: Volatile organic fraction; ↓: Reduced emission; ↑: Increased emission; =: No impact.

PUC-Rio - Certificação Digital Nº 1312923/CA

Table B1: Summary of the emission studies using diesel-biodiesel-ethanol blends in diesel engines, compared to fossil diesel fuel (adapted from Mofijur *et al.* (2016)) (Part 2 of 2).

D:B:EtOH	Engine / Vehicles	Exhaust emissions						Reference
		Soot, PM and smoke	NO_x	CO	CO_2	HC	Other	
90:00:10 70:00:30	4-cylinder diesel engine	↓	↓	↑	↓	↑	Acetaldehyde : ↑	He, 2003
85:05:10 70:10:20 60:10:30	Cummins 4B 4-cylinder diesel engine	↓ (Dry soot : ↓; SOF: ↓ (except high loads: ↑); Sulfate: =)				↓		Chen, 2007
85:05:10 70:10:20 60:10:30	Cummins 4B 4-cylinder diesel engine	↓ (Dry soot: ↓; SOF: ↑; Sulfate: ↑)	↑	High loads: ↓ Lower loads: ↑		Medium rpm: ↓ Other rpm: ↑		Chen, 2008
85:00:15	4-cylinder diesel engine	↓	↑	↑		↑		Kim, 2008
95:00:05 90:00:10	Super Star 7710 single cylinder diesel engine	↓	↑	↓		↓		Sayin, 2010
75:20:05	Cummins 4B 4-cylinder diesel engine	↓	↑	=	=	↓	Ketones and aldehydes: ↑ (Formaldehyde: ↓; Acetaldehyde: ↑)	Pang, 2006; Pang 2008
95:00:05 90:00:10 85:00:15	Ricardo–Cussons Hydra single cylinder diesel engine	↓	↓	↓		↑		Rakopoulos, 2007
95:00:05 90:00:10	Mercedes-Benz OM 366 LA 6-cylinder diesel engine	↓	↓					Rakopoulos, 2011
95:00:05 90:00:10 85:00:15 80:00:20 75:00:25	4-cylinder diesel engine	↓	↓	↑		↓		Lei, 2011
95:00:05 90:00:10 85:00:15	4-cylinder diesel engine	↓	↓	Low loads: ↑ Higher loads: ↓		↑		Lei, 2012
90:00:10 80:00:20 75:00:25 70:00:30	Nanji Machinery S195 single-cylinder diesel engine	↓	Low rpm: ↓ High rpm: no tendency	Low loads: ↑ Higher loads: ↓		High rpm and loads: ↑ Other cases: ↓		Huang, 2009
40:02:58 35:09:56 16:07:77 11:31:58 21:46:33 06:65:29	JSC "Altaiskij motornij zavod" 1A41 single-cylinder diesel engine		↓	↓				Lebedevas, 2009
90:00:10 80:00:20 70:00:30	Single-cylinder diesel engine	↓	↓	Late injection: ↓ Early injection: ↑		Late injection: ↑ Early injection: ↓		Park, 2010
92.3:00.0:7.7 64.6:27.7:7.7 58.1:24.9:17	Nissan 4-cylinder diesel engine	↓ (VOF: ↑)	↓			↑		Lapuerta, 2009
95:00:05 90:00:10 85:00:15 80:00:20	ZS1100 single cylinder diesel engine	High rpm and low loads for 95:00:05 and 90:00:10 : ↑ Other conditions: ↓	High loads: ↑ Lower loads: ↓	High loads: ↓ Lower loads: ↑		↑		Li, 2005

Legend: B: Biodiesel; D: Diesel fuel; EtOH: Ethanol; SOF: Soluble organic fraction; VOF: Volatile organic fraction; ↓: Reduced emission; ↑: Increased emission; =: No impact.

PUC-Rio - Certificação Digital Nº 1312923/CA

Appendix C: Mass Flow Rate of Moist Air

The variables related to the correction factors for viscosity, temperature, pressure and specific gravity needed to calculate the volumetric flow of moist air are presented in this Appendix.

PUC-Rio - Certificação Digital Nº 1312923/CA

Correction factor for dynamic viscosity:

The correction factor for dynamic viscosity $\frac{\mu_r}{\mu_{air,w}}$ is given by:

$$\frac{\mu_r}{\mu_{air,w}} = \frac{1.84\ 10^{-5}}{\mu_{air,w}} \qquad (C1)$$

where μ_r is the dynamic viscosity of dry air in the reference atmospheric conditions (25°C and 101,325 Pa) and $\mu_{air,w}$ is the dynamic viscosity of moist air determined by:

$$\mu_{air,w} = \frac{\mu_w}{1 + \frac{Y_{air,d}}{Y_w}\frac{\left[1 + \sqrt{\frac{\mu_w}{\mu_{air,d}}}\left(\frac{M_w}{M_{air,d}}\right)^{1/4}\right]^2}{2.83\sqrt{1 + \frac{M_w}{M_{air,d}}}}} + \frac{\mu_{air,d}}{1 + \frac{Y_w}{Y_{air,d}}\frac{\left[1 + \sqrt{\frac{\mu_{air,d}}{\mu_w}}\left(\frac{M_{air,d}}{M_w}\right)^{1/4}\right]^2}{2.83\sqrt{1 + \frac{M_{air,d}}{M_w}}}} \qquad (C2)$$

where μ_w and $\mu_{air,d}$ are the viscosity of water vapour and dry air; Y_w and $Y_{air,d}$ are the molar fractions of the water and dry air; M_w and $M_{air,d}$ represent the molecular mass of water and dry air, respectively.

The equation (C3) is used to determine μ_w [Fox, 2006]

$$\mu_w\left(\frac{kg}{m.s}\right) = 2.414\ 10^{-5} 10^{\frac{247.8}{T_{amb}(K)-140}} \qquad (C3)$$

where T_{amb} is the room temperature of the atmospheric air.

For the calculation of $\mu_{air,d}$, the empirical correlation of Sutherland was used [Fox, 2006]:

$$\mu_{air,d}\left(\frac{kg}{m.s}\right) = 1.458\ 10^{-6}\frac{T_{amb}^{3/2}}{110.4 + T_{amb}(K)} \qquad (C4)$$

The molar fraction of dry air is calculated by the following relationship:

$$Y_{air,d} = \frac{p_{air,d}}{p_{air,w}} \qquad (C5)$$

where $p_{air,d}$ and $p_{air,w}$ correspond to dry and moist air pressure, respectively.

The molar fraction of water is calculated by difference:

$$Y_w = 1 - Y_{air,d} \qquad (C6)$$

PUC-Rio - Certificação Digital Nº 1312923/CA

Correction factors for temperature and pressure:

Moreover, the correction factors for temperature $\frac{T_r}{T_{air,w}}$ and pressure $\frac{p_{air,w}}{p_r}$ are given by:

$$\frac{T_r}{T_{air,w}} = \frac{298.15}{T_{air,w}} \; and \; \frac{p_{air,w}}{p_r} = \frac{p_{air,w}}{101{,}325} \qquad (C7)$$

where T_r and p_r are the dry air temperature and pressure in the reference atmospheric conditions (298.15 K and 101,325 Pa), while $T_{air,w} = T_{amb}$ and $p_{air,w}$ is the moist air pressure.

Correction factor for specific gravity:

The correction factor for specific gravity $\frac{\rho_{air,w}}{\rho_r}$ is given by:

$$\frac{\rho_{air,w}}{\rho_r} = \frac{\rho_{air,w}}{1.19} \qquad (C8)$$

where ρ_r is the dry air specific gravity in the reference atmospheric conditions.

To determine the specific gravity of moist air $\rho_{air,w}$, the following expression is used:

$$\rho_{air,w} = \frac{p_{air,w}}{R_{air,w}.T_{air,w}} \qquad (C9)$$

The value of $R_{air,w}$ is defined in function of the absolute humidity ω as:

$$R_{air,w} = \frac{R_{air,d} + R_w.\omega}{1+\omega} \qquad (C10)$$

where $R_{air,d}$ and R_w are the constants for dry air and water vapor, respectively. According to Sonntag *et al.* (2003), the absolute humidity is calculated as:

$$\omega = \frac{0.622 U_r.p_{sat}}{p_{air,w} - U_r.p_{sat}} \qquad (C11)$$

where U_r is the relative humidity and p_{sat} is the vapor pressure of water at room temperature $T_{air,w}(K)$, which is given in kPa by CIBSE (2007):

$$log(p_{sat}) = 30.59 - 8.2log\left(T_{air,w}\right) + 0.0024804 T_{air,w} - \frac{3142.31}{T_{air,w}} \qquad (C12)$$

PUC-Rio - Certificação Digital Nº 1312923/CA

Appendix D: Air-Fuel Equivalence Ratios

This Appendix D gives the air-fuel ratio (A/F) for diesel fuel, biodiesel, ethanol and DBE blends.

PUC-Rio - Certificação Digital Nº 1312923/CA

The complete combustion of the fuel is performed when the amount of dry air, or oxygen content, verified the stoichiometric principles.

In that case, the resulting are carbon dioxide and water. Thus, the general equation for the combustion of a generic hydrocarbon C_xH_y with dry air is given by Sonntag *et al.* (2003):

$$C_xH_y + \left(x + \frac{y}{4}\right)(O_2 + 3.76N_2) \rightarrow xCO_2 + \frac{y}{2}H_2O + 3.76\left(x + \frac{y}{4}\right)N_2 \quad (D1)$$

where the stoichiometric coefficients where defined through the conservation of the chemical species.

The air-fuel ratio (A/F) can be calculated on a mass $((A/F)_m)$ or molar $((A/F)_n)$ basis, both related through the molecular weight of dry air (M_{air}) and fuel (M_f):

$$(A/F)_m = \frac{m_{air}}{m_f} = \frac{n_{air}}{n_f}\frac{M_{air}}{M_f} = (A/F)_n\frac{M_{air}}{M_f} \quad (D2)$$

For an ideal or stoichiometric combustion, the index "s" is used. In the next paragraphs, the stoichiometric combustion equations and the reasons (A/F) are determined for the fuel used for engine testing: diesel fuel, biodiesel and ethanol.

PUC-Rio - Certificação Digital Nº 1312923/CA

Diesel fuel

According to Egúsquiza (2011), the average representation of diesel fuel is given by $C_{12}H_{23}$. Therefore, the balanced equation is:

$$C_{12}H_{23} + 17.75O_2 + 66.74N_2 \rightarrow 12CO_2 + 11.5H_2O + 66.74N_2 \quad (D3)$$

Then, the stoichiometric molar air-fuel ratio is:

$$(A/F_D)_n^s = \frac{17.75 + 66.74}{1} = 84.49\ \frac{mol_{air}}{mol_D} \quad (D4)$$

Consequently, the stoichiometric mass air-fuel ratio is:

$$(A/F_D)_m^s = (A/F_D)_n^s\frac{M_{air}}{M_D} = 84.49\frac{28.97}{167.18} = 14.6\ \frac{kg_{air}}{kg_D} \quad (D5)$$

Biodiesel

Considering that biodiesel is mostly composed of methyl esters from soybean, the average representation of biodiesel can be represented by its main compound, the linoleic acid ($C_{18}H_{32}$). Therefore, the balanced equation is:

$$C_{18}H_{32}O_2 + 25O_2 + 94N_2 \rightarrow 18CO_2 + 16H_2O + 94N_2 \quad (D6)$$

Then, the stoichiometric molar air-fuel ratio is:

$$(A/F_B)_n^s = \frac{25+94}{1} = 119\ \frac{mol_{air}}{mol_B} \quad (D7)$$

Consequently, the stoichiometric mass air-fuel ratio is:

$$(A/F_B)_m^s = (A/F_B)_n^s \frac{M_{air}}{M_B} = 119 \frac{28.97}{280.45} = 12.3\ \frac{kg_{air}}{kg_B} \quad (D8)$$

Ethanol

The balanced equation is given in equation (D9):

$$C_2H_6O + 3O_2 + 11.28N_2 \rightarrow 2CO_2 + 3H_2O + 11.26N_2 \quad (D9)$$

Then, the stoichiometric molar air-fuel ratio is:

$$(A/F_{EtOH})_n^s = \frac{3+11.28}{1} = 14.28\ \frac{mol_{air}}{mol_{EtOH}} \quad (D10)$$

Consequently, the stoichiometric mass air-fuel ratio is:

$$(A/F_{EtOH})_m^s = (A/F_{EtOH})_n^s \frac{M_{air}}{M_{EtOH}} = 14.28 \frac{28.97}{46.07} = 9.0\ \frac{kg_{air}}{kg_{EtOH}} \quad (D11)$$

DBE blends

The required stoichiometric mass air-fuel ratio for DBE blends can be calculated in function of the respective mass fraction and stoichiometric mass air-fuel ratio by equation (D12):

$$(A/F_{DBE})_m^s = \%_D\,(A/F_D)_m^s + \%_B\,(A/F_B)_m^s + \%_{EtOH}(A/F_{EtOH})_n^s \quad (D12)$$

PUC-Rio - Certificação Digital Nº 1312923/CA

Appendix E: Results of the Doehlert Design of Experiments

This appendix presents the results of the Doehlert design of experiments performed in sections 5.1.3 and 5.2.1.

PUC-Rio - Certificação Digital Nº 1312923/CA

$$Y = b_0 + b_1X_1 + b_2X_2 + b_{11}X_1^2 + b_{22}X_2^2 + b_{12}X_1X_2 + \varepsilon_{X_1,X_2} \quad (D1)$$

where Y is the experimental response, X_1 and X_2 represents the variables to be optimized.

Table E1: Parameters of the Doehlert design of experiments obtained for maximum volumetric fraction (%) of ethanol in 100 mL of diesel fuel with 4 vol% of additive until phase separation after 15 min of decantation in Section 5.1.3.

Parameters	BO: Soybean - Soybean	BO: Soybean-Castor oil	BO: Castor oil-Soybean	BO: Castor oil-Castor oil
b_0	14,286 ± 0.018	14,286 ± 0.515	15,789 ± 0.007	17,241 ± 0.005
b_{11}	-0,109 ± 0.002	-0,109 ± 0.091	-0,912 ± 0.001	-0,878 ± 0.0003
b_{22}	-0,539 ± 0.002	0,431 ± 0.068	1,238 ± 0.001	0,210 ± 0.001
b_1	3,334 ± 0.005	3,299 ± 0.106	3,479 ± 0.001	3,852 ± 0.002
b_2	0,467 ± 0.002	2,175 ± 0.037	0,839 ± 0.001	0,826 ± 0.001
b_{12}	-0,933 ± 0.001	0,683 ± 0.053	-0,058 ± 0.001	-0,085 ± 0.001

Legend: X_1: biodiesel concentration and X_2: vegetal oil concentration.

Table E2: Parameters of the Doehlert design of experiments obtained for separation ratio (SR) after 2 hours of decantation in Section 5.2.1.

Parameters	BO: Soybean-Castor oil Diesel B15 fuel at 10°C	BO: Soybean-Castor oil Diesel B7 fuel at 25°C
b_0	1.554 ± 0.107	1.550 ± 0.108
b_{11}	-0.091 ± 0.015	-0.075 ± 0.015
b_{22}	0.008 ± 0.020	0.042 ± 0.020
b_1	-0.088 ± 0.017	-0.100 ± 0.017
b_2	-0.046 ± 0.010	-0.029 ± 0.010
b_{12}	0.013 ± 0.014	0.029 ± 0.014

Legend: X_1: vegetal oil concentration and X_2: *n*-butanol concentration.

PUC-Rio - Certificação Digital Nº 1312923/CA

Appendix F: Physicochemical Properties of the Blends

This Appendix F contains the tables with experimental physicochemical properties of diesel–biodiesel–ethanol.

PUC-Rio - Certificação Digital Nº 1312923/CA

Table F1: Kinematic viscosity (mm²/s) at 40°C of the DBE blends.

Ethanol content (vol%)		0	10	20	30	40	50	60	70	80	90	100
Additive content (vol%)	**0.0**	3.164 ± 0.012	2.636 ± 0.012	2.347 ± 0.009	2.162 ± 0.010	1.958 ± 0.008	1.828 ± 0.008	1.518 ± 0.006	1.405 ± 0.005	1.301 ± 0.005	1.178 ± 0.004	1.098 ± 0.004
	1.0	-	-	2.395 ± 0.009	-	-	-	-	-	-	-	-
	2.0	3.350 ± 0.012	2.785 ± 0.012	2.431 ± 0.009	2.254 ± 0.010	2.083 ± 0.007	1.907 ± 0.008	1.641 ± 0.006	1.500 ± 0.005	1.362 ± 0.005	1.256 ± 0.005	1.176 ± 0.004

Table F2: Specific gravity (kg/m³) at 25°C of the DBE blends.

Ethanol content (vol%)		0	10	20	30	40	50	60	70	80	90	100
Additive content (vol%)	**0.0**	828.8 ± 0.4	828.7 ± 0.4	822.0 ± 0.4	818.4 ± 0.4	813.1 ± 0.4	809.3 ± 0.4	801.2 ± 0.4	800.3 ± 0.4	795.0 ± 0.4	789.1 ± 0.4	786.5 ± 0.4
	1.0	-	-	823.7 ± 0.4	-	-	-	-	-	-	-	-
	2.0	836.2 ± 0.4	830.3 ± 0.4	826.8 ± 0.4	821.0 ± 0.4	817.1 ± 0.4	811.3 ± 0.4	806.5 ± 0.4	803.4 ± 0.4	798.4 ± 0.4	794.2 ± 0.4	789.4 ± 0.4

Table F3: Specific gravity (kg/m³) at 20°C of the DBE blends.

Ethanol content (vol%)			0	10	20	30	40	50	60	70	80	90	100
Additive content	**0.0**	Blend	837.4 ± 0.4	831.8 ± 0.4	826.7 ± 0.4	821.8 ± 0.4	***817.5*** ± 0.4	***814.5*** ± 0.4	***809.0*** ± 0.4	803.3 ± 0.4	798.4 ± 0.4	793.6 ± 0.4	791.0 ± 0.4
		Sup. phase	-	-	-	-	813.0 ± 0.4	811.0 ± 0.4	807.2 ± 0.4	802.6 ± 0.4	-	-	-
		Inf. phase					823.6 ± 0.4	824.8 ± 0.4	825.8 ± 0.4	***836.9*** ± 0.4			
	1.0	Blend	-	-	826.1 ± 0.4	-	-	-	-	-	-	-	-
	2.0	Blend	839.3 ± 0.4	834.5 ± 0.4	830.8 ± 0.4	825.1 ± 0.4	820.6 ± 0.4	***815.9*** ± 0.4	***811.0*** ± 0.4	807.1 ± 0.4	803.2 ± 0.4	797.4 ± 0.4	794.4 ± 0.4
		Sup. phase	-	-	-	-	-	815.1 ± 0.4	810.5 ± 0.4	-	-	-	-
		Inf. phase	-	-	-	-	-	823.9 ± 0.4	826.2 ± 0.4	-	-	-	-

In **italic**: Calculated Value

PUC-Rio - Certificação Digital Nº 1312923/CA

Table F4: Surface tension (mN/m) at 25°C of the DBE blends.

Ethanol content (vol%)		0	10	20	30	40	50	60	70	80	90	100
Additive content (vol%)	0.0	27.4 ± 0.5	25.2 ± 0.5	24.4 ± 0.5	24.2 ± 0.5	24.0 ± 0.5	23.9 ± 0.5	23.7 ± 0.5	23.5 ± 0.5	23.3 ± 0.5	23.2 ± 0.5	22.7 ± 0.5
	1.0	-	-	24.2 ± 0.5	-	-	-	-	-	-	-	-
	2.0	28.6 ± 0.5	26.0 ± 0.5	24.8 ± 0.5	24.5 ± 0.5	24.2 ± 0.5	24.1 ± 0.5	24.0 ± 0.5	23.8 ± 0.5	23.5 ± 0.5	23.3 ± 0.5	23.1 ± 0.5

Table F5: Contact angle properties at 25°C of the DBE blends without additive.

Ethanol content (vol%)	0		5		10	
Measure	1	2	1	2	1	2
Area (mm^2)	10.376	10.394	10.728	12.757	19.204	22.856
Volume (mm^3)	0.822	0.855	0.832	1.051	1.481	1.599
Diameter (mm)	3.530	3.516	3.618	3.967	4.922	5.214
Apex radius (mm)	9.537	8.527	9.882	12.565	17.754	23.748
Temperature (°C)	20.7	20.7	20.9	20.7	20.9	20.7
Contact angle (°)	9.4	9.0	7.4	7.9	5.6	5.8

Table F6: Contact angle properties at 25°C of the DBE blends with 2.0 vol% of additive.

Ethanol content (vol%)	0		5		10		15		20	
Measure	1	2	1	2	1	2	1	2	1	2
Area (mm^2)	11.945	11.636	15.417	19.362	14.043	15.671	8.817	9.484	18.479	15.883
Volume (mm^3)	0.880	0.955	1.286	1.530	0.958	1.076	0.740	0.817	1.922	1.746
Diameter (mm)	3.889	3.749	4.284	4.734	4.065	4.234	3.279	3.411	4.832	4.401
Apex radius (mm)	12.524	9.461	13.850	16.879	11.644	13.620	7.027	7.344	17.375	19.958
Temperature (°C)	20.4	20.9	20.1	20.6	20.6	20.7	20.6	20.6	20.7	21.6
Contact angle (°)	8.6	8.1	6.6	6.3	5.4	5.4	9.8	10.1	10.9	11.2

PUC-Rio - Certificação Digital Nº 1312923/CA

Table F7: Flash point (°C) of the DBE blends.

Ethanol content (vol%)		0	10	20	30	40	50	60	70	80	90	100
Additive content (vol%)	0.0	64.7 ± 1.2	12.3 ± 1.2	11.3 ± 1.2	11.3 ± 1.2	11.0 ± 1.2	11.8 ± 1.2	11.6 ± 1.2	11.6 ± 1.2	12.3 ± 1.2	11.8 ± 1.2	12.6 ± 1.2
	1.0	-	-	11.8 ± 1.2	-	-	-	-	-	-	-	-
	2.0	52.3 ± 1.2	14.4 ± 1.2	11.3 ± 1.2	10.3 ± 1.2	9.8 ± 1.2	11.3 ± 1.2	11.8 ± 1.2	11.3 ± 1.2	11.3 ± 1.2	12.1 ± 1.2	12.3 ± 1.2

Table F8: Cold Filter Plugging Point (CFPP) (°C) of the DBE blends.

Ethanol content (vol%)		0	10	20	30	40	50	60	70	80	90	100
Additive content (vol%)	0.0	-5.0 ± 1.8	-5.0 ± 1.8	-5.0 ± 1.8	-3.0 ± 1.8	-3.0 ± 1.8	-1.0 ± 1.8	0.0 ± 1.8	3.0 ± 1.8	7.0 ± 1.8	9.0 ± 1.8	ND
	1.0	-	-	-4.0 ± 1.8	-	-	-	-	-	-	-	-
	2.0	-6.0 ± 1.8	-4.0 ± 1.8	-4.0 ± 1.8	-3.0 ± 1.8	-3.0 ± 1.8	-2.0 ± 1.8	1.0 ± 1.8	3.0 ± 1.8	7.0 ± 1.8	7.0 ± 1.8	ND

ND: Not Determined

Table F9: Corrosiveness to Copper at 50°C of the DBE blends.

Ethanol content (vol%)		0	10	20	30	40	50	60	70	80	90	100
Additive content (vol%)	0.0	1a	1a	1a	1a	1a	1a	1a	1a	1a	1a	1a
	1.0	-	-	1a	-	-	-	-	-	-	-	-
	2.0	1a	1a	1a	1a	1a	1a	1a	1a	1a	1a	1a

Table F10: Cetane number (CN) of the DBE blends.

Ethanol content (vol%)		0	5	10	20	40
Additive content (vol%)	0.0	54.9 ± 1.0	51.5 ± 0.9		40.0 ± 0.8	26.2 ± 0.8
	1.0	-	-	-		-
	2.0	56.6 ± 1.0	52.9 ± 0.9		40.0 ± 0.8	25.2 ± 0.8

PUC-Rio - Certificação Digital Nº 1312923/CA

Table F11: Lubricity properties of the DBE blends without additive at 60°C.

Ethanol content (vol%)	X (µm)	Y (µm)	MWSD (µm)	T (°C)	Film (%)	Friction coefficient
0	244	189	216.5 ± 80.0	59.9	95	0.125
5	-	-	-	-	-	-
20	-	-	-	-	-	-

Table F12: Lubricity properties of the DBE blends with 2 vol% of additive at 60°C.

Ethanol content (vol%)	X (µm)	Y (µm)	MWSD (µm)	T (°C)	Film (%)	Friction coefficient
0	211	169	190 ± 80.0	59.9	95	0.128
5	230	179	204.5 ± 80.0	59.9	92	0.125
20	208	138	173 ± 80.0	59.9	92	0.118

Table F13: Lubricity properties of the DBE blends without additive at 25°C.

Ethanol content (vol%)	Measure 1			Measure 2			Conditions		
	X (µm)	Y (µm)	MWSD (µm)	X (µm)	Y (µm)	MWSD (µm)	T (°C)	Film (%)	Friction coefficient
0	260	222	241 ± 80.0	248	208	228 ± 80.0	25.9	94	0.146
5	307	214	260.5 ± 80.0	297	207	252 ± 80.0	25.0	67	0.144
20	372	326	349 ± 80.0	362	319	340.5 ± 80.0	25.0	57	0.151
40	354	257	305.5 ± 80.0	349	254	301.5 ± 80.0	25.0	47	0.166

Table F14: Lubricity properties of the DBE blends with 2.0 vol% of additive at 25°C.

Ethanol content (vol%)	Measure 1			Measure 2			Measure 3			Conditions		
	X (µm)	Y (µm)	MWSD (µm)	X (µm)	Y (µm)	MWSD (µm)	X (µm)	Y (µm)	MWSD (µm)	T (°C)	Film (%)	Friction coefficient
0	198	173	185.5 ± 80.0	243	133	188 ± 80.0	-	-	-	25.8	95	0.108
5	261	184	222.5 ± 80.0	252	187	219.5 ± 80.0	254	190	222 ± 80.0	25.0	73	0.131
20	321	258	289.5 ± 80.0	301	241	271 ± 80.0	-	-	-	25.0	62	0.152
40	298	223	260.5 ± 80.0	365	310	337.5 ± 80.0	364	298	331 ± 80.0	25.0	47	0.141

PUC-Rio - Certificação Digital Nº 1312923/CA

Table F15: Lubricity properties of the DBE blends with 1.0 vol% of additive at 25°C.

Ethanol content (vol%)	Measure 1			Measure 2			Conditions		
	X (μm)	Y (μm)	MWSD (μm)	X (μm)	Y (μm)	MWSD (μm)	T (°C)	Film (%)	Friction coefficient
20	362	266	314 ± 80.0	356	238	297 ± 80.0	25.0	71	0.148

Table F16: Calculated lower heating value (LHV) at 20°C of the DBE blends.

Ethanol content (vol%)		0	10	20	30	40	50	60	70	80	90	100
Additive content (vol%)	**0.0**	35.59 ± 0.82	34.15 ± 0.74	32.71 ± 0.66	31.27 ± 0.58	29.84 ± 0.49	28.40 ± 0.41	26.96 ± 0.33	25.52 ± 0.25	24.08 ± 0.17	22.64 ± 0.11	21.21 ± 0.07
	1.0	35.58 ± 0.82	34.15 ± 0.74	32.73 ± 0.66	-	-	-	-	-	-	-	-
	2.0	35.57 ± 0.81	34.16 ± 0.73	32.75 ± 0.65	31.34 ± 0.57	29.93 ± 0.49	28.52 ± 0.41	27.11 ± 0.33	25.70 ± 0.25	24.29 ± 0.18	22.88 ± 0.11	21.47 ± 0.08

PUC-Rio - Certificação Digital Nº 1312923/CA

Appendix G: Matlab Code to Analyze the Experimental Data

This Appendix G gives the Matlab® code used to analyze the experimental data available in Excel table. The results were obtained for the version 2016b of the software.

PUC-Rio - Certificação Digital Nº 1312923/CA

```
clc
clear all
close all

% ENGINE TECHNICAL DATA
rc = 15.8;                  % Compression ratio
dia = 0.103;                % Bore (m)
L_pistao = 0.129;           % Stroke (m)
l_biela = 0.207;            % Connecting rod length (m)
a = L_pistao/2;             % Crank radius (m)
V_d = 4.3/4*1e-3;           % Displaced or swept volume (m^3)
V_c = V_d/(rc-1);           % Clearance volume (m^3)
M_wat = 18.015;             % Molar weight of water (g/mol)
M_air_d = 28.9645;          % Molar weight of dry air (g/mol)
R_wat = 0.4615;             % Gas constant of water (kJ/(kg.K))
R_air_d = 0.287;            % Gas constant of dry air (kJ/(kg.K))

% TEST DESCRIPTION
LHV = 45.125;               % Lower Heating Value (MJ/kg)

% DATA COLLECTION
% Accelerator(%)
Acc_1 = xlsread('Teste_MWM_040716.xlsx','Médias','C18');
Acc_2 = xlsread('Teste_MWM_040716.xlsx','Médias','C19');
Acc_3 = xlsread('Teste_MWM_040716.xlsx','Médias','C20');

% Piston speed (rpm)
rpm_1 = xlsread('Teste_MWM_040716.xlsx','Médias','G18');
rpm_2 = xlsread('Teste_MWM_040716.xlsx','Médias','G19');
rpm_3 = xlsread('Teste_MWM_040716.xlsx','Médias','G20');

% Torque (N.m)
torque_1 = xlsread('Teste_MWM_040716.xlsx','Médias','B18');
torque_2 = xlsread('Teste_MWM_040716.xlsx','Médias','B19');
torque_3 = xlsread('Teste_MWM_040716.xlsx','Médias','B20');

% Fuel consumption (kg/h)
m_f_1 = xlsread('Teste_MWM_040716.xlsx','Médias','J18');
m_f_2 = xlsread('Teste_MWM_040716.xlsx','Médias','J19');
m_f_3 = xlsread('Teste_MWM_040716.xlsx','Médias','J20');

% Wet air temperature (°C)
T_air_w_1 = xlsread('Teste_MWM_040716.xlsx','Médias','M18');
T_air_w_2 = xlsread('Teste_MWM_040716.xlsx','Médias','M19');
T_air_w_3 = xlsread('Teste_MWM_040716.xlsx','Médias','M20');

% Measured pressure diference(in H20)
delta_p_1 = xlsread('Teste_MWM_040716.xlsx','Médias','H18');
delta_p_2 = xlsread('Teste_MWM_040716.xlsx','Médias','H19');
delta_p_3 = xlsread('Teste_MWM_040716.xlsx','Médias','H20');

% Volumetric air flow (ft^3/min)
V_r_1_in = 54.1288*delta_p_1-0.200199*delta_p_1*delta_p_1;
V_r_2_in = 54.1288*delta_p_2-0.200199*delta_p_2*delta_p_2;
V_r_3_in = 54.1288*delta_p_3-0.200199*delta_p_3*delta_p_3;

% Volumetric air flow (m^3/s)
V_r_1 = 0.0004719474*V_r_1_in;
V_r_2 = 0.0004719474*V_r_2_in;
V_r_3 = 0.0004719474*V_r_3_in;

% Relative moisture(%)
Ur_1 = xlsread('Teste_MWM_040716.xlsx','Médias','L18');
Ur_2 = xlsread('Teste_MWM_040716.xlsx','Médias','L19');
Ur_3 = xlsread('Teste_MWM_040716.xlsx','Médias','L20');

% Air pressure (Pa)
p_air_w_1 = 6894.76*xlsread('Teste_MWM_040716.xlsx','Médias','I18');
```

PUC-Rio - Certificação Digital Nº 1312923/CA

```
p_air_w_2 = 6894.76*xlsread('Teste_MWM_040716.xlsx','Médias','I19');
p_air_w_3 = 6894.76*xlsread('Teste_MWM_040716.xlsx','Médias','I20');

% Room temperature (°C)
T_room_1 = xlsread('Teste_MWM_040716.xlsx','Médias','K18');
T_room_2 = xlsread('Teste_MWM_040716.xlsx','Médias','K19');
T_room_3 = xlsread('Teste_MWM_040716.xlsx','Médias','K20');

% Exhaust gas pressure (Pa)
p_exh_1 = 6894.76*xlsread('Teste_MWM_040716.xlsx','Médias','M18');
p_exh_2 = 6894.76*xlsread('Teste_MWM_040716.xlsx','Médias','M19');
p_exh_3 = 6894.76*xlsread('Teste_MWM_040716.xlsx','Médias','M20');

% Exhaust gas temperature (°C)
T_exh_1 = xlsread('Teste_MWM_040716.xlsx','Médias','O18');
T_exh_2 = xlsread('Teste_MWM_040716.xlsx','Médias','O19');
T_exh_3 = xlsread('Teste_MWM_040716.xlsx','Médias','O20');

% Water temperature (°C)
T_w_1 = xlsread('Teste_MWM_040716.xlsx','Médias','E18');
T_w_2 = xlsread('Teste_MWM_040716.xlsx','Médias','E19');
T_w_3 = xlsread('Teste_MWM_040716.xlsx','Médias','E20');

% Oil temperature (°C)
T_oil_1 = xlsread('Teste_MWM_040716.xlsx','Médias','F18');
T_oil_2 = xlsread('Teste_MWM_040716.xlsx','Médias','F19');
T_oil_3 = xlsread('Teste_MWM_040716.xlsx','Médias','F20');

% Power (W)
Power_1 = xlsread('Teste_MWM_040716.xlsx','Médias','P18');
Power_2 = xlsread('Teste_MWM_040716.xlsx','Médias','P19');
Power_3 = xlsread('Teste_MWM_040716.xlsx','Médias','P20');

% Correction factor) dynamic viscosity (
mu_air_d_1 =
1.458/1000000*(T_room_1+273.15)^1.5*1/(110.4+273.15+T_room_1);
mu_air_d_2 =
1.458/1000000*(T_room_2+273.15)^1.5*1/(110.4+273.15+T_room_2);
mu_air_d_3 =
1.458/1000000*(T_room_3+273.15)^1.5*1/(110.4+273.15+T_room_3);

mu_w_1 = 2.414/100000*10^(247.8/(T_room_1+273.15-140));
mu_w_2 = 2.414/100000*10^(247.8/(T_room_2+273.15-140));
mu_w_3 = 2.414/100000*10^(247.8/(T_room_3+273.15-140));

p_sat_1 = 10^(30.59-8.2*log10(T_air_w_1+273.15)
+0.0024804*(T_air_w_1+273.15)-3142.31/(T_air_w_1+273.15))*1000;
p_sat_2 = 10^(30.59-8.2*log10(T_air_w_2+273.15)
+0.0024804*(T_air_w_2+273.15)-3142.31/(T_air_w_2+273.15))*1000;
p_sat_3 = 10^(30.59-8.2*log10(T_air_w_3+273.15)
+0.0024804*(T_air_w_3+273.15)-3142.31/(T_air_w_3+273.15))*1000;

w_1 = 0.622*Ur_1/100*p_sat_1/(p_air_w_1-Ur_1/100*p_sat_1);
w_2 = 0.622*Ur_2/100*p_sat_1/(p_air_w_2-Ur_1/100*p_sat_2);
w_3 = 0.622*Ur_3/100*p_sat_1/(p_air_w_3-Ur_1/100*p_sat_3);

Y_w_1 = M_air_d*w_1/(M_wat+w_1*M_air_d);
Y_w_2 = M_air_d*w_2/(M_wat+w_2*M_air_d);
Y_w_3 = M_air_d*w_3/(M_wat+w_3*M_air_d);


Y_air_d_1 = 1-Y_w_1;
Y_air_d_2 = 1-Y_w_2;
Y_air_d_3 = 1-Y_w_3;

p_air_d_1 = Y_air_d_1*p_air_w_1;
p_air_d_2 = Y_air_d_2*p_air_w_2;
p_air_d_3 = Y_air_d_3*p_air_w_3;
```

PUC-Rio - Certificação Digital Nº 1312923/CA

```
mu_air_w_1 =
mu_w_1/(1+Y_air_d_1/Y_w_1*(1+sqrt(mu_w_1/mu_air_d_1)*(M_wat/M_air_d)^0.25
)^2*1/(2.83*sqrt(1+M_wat/M_air_d)))+
mu_air_d_1/(1+Y_w_1/Y_air_d_1*(1+sqrt(mu_air_d_1/mu_w_1)*(M_air_d/M_wat)^
0.25)^2*1/(2.83*sqrt(1+M_air_d/M_wat)));
mu_air_w_2 =
mu_w_2/(1+Y_air_d_2/Y_w_2*(1+sqrt(mu_w_2/mu_air_d_2)*(M_wat/M_air_d)^0.25
)^2*1/(2.83*sqrt(1+M_wat/M_air_d)))+
mu_air_d_2/(1+Y_w_2/Y_air_d_2*(1+sqrt(mu_air_d_2/mu_w_2)*(M_air_d/M_wat)^
0.25)^2*1/(2.83*sqrt(1+M_air_d/M_wat)));
mu_air_w_3 =
mu_w_3/(1+Y_air_d_3/Y_w_3*(1+sqrt(mu_w_3/mu_air_d_3)*(M_wat/M_air_d)^0.25
)^2*1/(2.83*sqrt(1+M_wat/M_air_d)))+
mu_air_d_3/(1+Y_w_3/Y_air_d_3*(1+sqrt(mu_air_d_3/mu_w_3)*(M_air_d/M_wat)^
0.25)^2*1/(2.83*sqrt(1+M_air_d/M_wat)));

R_air_w_1 = (R_air_d + R_wat*w_1)/(1+w_1);
R_air_w_2 = (R_air_d + R_wat*w_2)/(1+w_2);
R_air_w_3 = (R_air_d + R_wat*w_3)/(1+w_3);

rho_air_w_1 = p_air_w_1/(1000*R_air_w_1*(T_air_w_1+273.15));
rho_air_w_2 = p_air_w_2/(1000*R_air_w_2*(T_air_w_2+273.15));
rho_air_w_3 = p_air_w_3/(1000*R_air_w_3*(T_air_w_3+273.15));

% Wet air consumption (kg/h)
m_air_w_1 = 3600*V_r_1*rho_air_w_1*(1.84/(100000*mu_air_w_1))
*(298.15/(273.15+T_air_w_1))*(p_air_w_1/101325)*(rho_air_w_1/1.19);
m_air_w_2 = 3600*V_r_2*rho_air_w_2*(1.84/(100000*mu_air_w_2))
*(298.15/(273.15+T_air_w_2))*(p_air_w_2/101325)*(rho_air_w_2/1.19);
m_air_w_3 = 3600*V_r_3*rho_air_w_3*(1.84/(100000*mu_air_w_3))
*(298.15/(273.15+T_air_w_3))*(p_air_w_3/101325)*(rho_air_w_3/1.19);

% Dry air consumption (kg/h)
m_air_d_1 = m_air_w_1/(1+w_1/100);
m_air_d_2 = m_air_w_2/(1+w_2/100);
m_air_d_3 = m_air_w_3/(1+w_3/100);

% Air / Fuel Ratio
Phi_1 = m_air_d_1/m_f_1;
Phi_2 = m_air_d_2/m_f_2;
Phi_3 = m_air_d_3/m_f_3;

% Crank angle (°)
Grau = xlsread('MWM-B7-1500-25-1.xlsx','A3:A722');
Grau_rad = pi/180*Grau;

% Pressure (Pa)
P_1 = 1e5*xlsread('MWM-B7-1500-25-1.xlsx','B3:B722');
P_2 = 1e5*xlsread('MWM-B7-1500-25-2.xlsx','B3:B722');
P_3 = 1e5*xlsread('MWM-B7-1500-25-3.xlsx','B3:B722');

figure(1)
plot(Grau,P_1,'blue',Grau,P_2,'red',Grau,P_3,'black')
set(gca,'FontSize',12);
xlabel('Crank angle (°)')
ylabel('Pressure (Pa)')
title('Pressure in function of crank angle')
hold on


% CLAPEYRON DIAGRAM
for i = 1:720
    % Distance between the crank axis and the piston pin axis
    s(i) = a*cos(Grau_rad(i))+(l_biela^2-a^2*sin(Grau_rad(i))^2)^0.5;

    % Cylinder volume
    V(i) = V_c+pi*dia^2/4*(l_biela+a-s(i));
```

PUC-Rio - Certificação Digital Nº 1312923/CA

```
end

figure(2)
plot(V,P_1,'blue',V,P_2,'red',V,P_3,'black')
set(gca,'FontSize',12);
xlabel('Volume (m^3)')
ylabel('Pressure (Pa)')
title('Clapeyron Diagram for one cylinder')
hold on

% MEAN EFFECTIVE PRESSURES, POWERS AND EFFICIENCY
% Indicated mean effective pressure - IMEP (Pa)
    IMEP_1 = 0;
    IMEP_2 = 0;
    IMEP_3 = 0;

for i=1:719;
    IMEP_1 = IMEP_1+1/V_d*(P_1(i)+P_1(i+1))/2*(V(i+1)-V(i));
    IMEP_2 = IMEP_2+1/V_d*(P_2(i)+P_2(i+1))/2*(V(i+1)-V(i));
    IMEP_3 = IMEP_3+1/V_d*(P_3(i)+P_3(i+1))/2*(V(i+1)-V(i));
end

% IMEP (bar)
    IMEP_1_bar = IMEP_1*1e-5;
    IMEP_2_bar = IMEP_2*1e-5;
    IMEP_3_bar = IMEP_3*1e-5;

% Brake Power (kW)
    P_b_1 = 2*pi*rpm_1/60*torque_1/1000;
    P_b_2 = 2*pi*rpm_2/60*torque_2/1000;
    P_b_3 = 2*pi*rpm_3/60*torque_3/1000;

% Specific Fuel Consumption (kg/(kW.h))
    sfc_1 = m_f_1/P_b_1;
    sfc_2 = m_f_2/P_b_2;
    sfc_3 = m_f_3/P_b_3;

% Brake mean eflective pressure - BMEP (bar)
    BMEP_1 = 12.56*torque_1/(V_d*1000)*1/100;
    BMEP_2 = 12.56*torque_2/(V_d*1000)*1/100;
    BMEP_3 = 12.56*torque_3/(V_d*1000)*1/100;

% Indicated Power (kW)
    P_i_1 = 4*V_d*IMEP_1*rpm_1/60*1/2000;
    P_i_2 = 4*V_d*IMEP_2*rpm_2/60*1/2000;
    P_i_3 = 4*V_d*IMEP_3*rpm_3/60*1/2000;

% Fuel conversion efficiency
    Nu_f_1 = P_b_1/(m_f_1/3.6*LHV);
    Nu_f_2 = P_b_2/(m_f_2/3.6*LHV);
    Nu_f_3 = P_b_3/(m_f_3/3.6*LHV);

% Volumetric efficiency
    rho_air_d_1 = p_air_d_1/100000*28.96/(8.2057/100*(T_air_w_1+273.15));
    rho_air_d_2 = p_air_d_2/100000*28.96/(8.2057/100*(T_air_w_2+273.15));
    rho_air_d_3 = p_air_d_3/100000*28.96/(8.2057/100*(T_air_w_3+273.15));

    Nu_v_1 = 2*m_air_d_1/(rho_air_d_1*4*V_d*rpm_1*60);
    Nu_v_2 = 2*m_air_d_2/(rho_air_d_2*4*V_d*rpm_2*60);
    Nu_v_3 = 2*m_air_d_3/(rho_air_d_3*4*V_d*rpm_3*60);

% Indicated efficiency
    Nu_i_1 = 3.6*P_i_1/(m_f_1*LHV);
    Nu_i_2 = 3.6*P_i_2/(m_f_2*LHV);
    Nu_i_3 = 3.6*P_i_3/(m_f_3*LHV);

% Mechanical efficiency
    Nu_m_1 = P_b_1/P_i_1;
```

PUC-Rio - Certificação Digital Nº 1312923/CA

```
    Nu_m_2 = P_b_2/P_i_2;
    Nu_m_3 = P_b_3/P_i_3;


% PRESSURE DERIVATIVE
% Calculus of pressure derivative (Pa/°)
d_P_1(1) = (P_1(2)-P_1(1))/(Grau(2)-Grau(1));
for i=2:719
    d_P_1(i) = (P_1(i+1)-P_1(i-1))/(Grau(i+1)-Grau(i-1));
end
d_P_1(720) = (P_1(720)-P_1(719))/(Grau(720)-Grau(719));

d_P_2(1) = (P_2(2)-P_2(1))/(Grau(2)-Grau(1));
for i=2:719
    d_P_2(i) = (P_2(i+1)-P_2(i-1))/(Grau(i+1)-Grau(i-1));
end
d_P_2(720) = (P_2(720)-P_2(719))/(Grau(720)-Grau(719));

d_P_3(1) = (P_3(2)-P_3(1))/(Grau(2)-Grau(1));
for i=2:719
    d_P_3(i) = (P_3(i+1)-P_3(i-1))/(Grau(i+1)-Grau(i-1));
end
d_P_3(720) = (P_3(720)-P_3(719))/(Grau(720)-Grau(719));

% Smoothed pressure derivative (Pa/°)
ds_P_1 = smooth(Grau,d_P_1,0.035,'rloess');
ds_P_2 = smooth(Grau,d_P_2,0.035,'rloess');
ds_P_3 = smooth(Grau,d_P_3,0.035,'rloess');

% Max pressure derivative (Pa/°)

dP_p_1= ds_P_1(360:720);
dP_p_2= ds_P_2(360:720);
dP_p_3= ds_P_3(360:720);

[Max_d_P_1,pos_1]= max(dP_p_1);
[Max_d_P_2,pos_2]= max(dP_p_2);
[Max_d_P_3,pos_3]= max(dP_p_3);

Grau_dPmax_1 = Grau(pos_1+359);
Grau_dPmax_2 = Grau(pos_2+359);
Grau_dPmax_3 = Grau(pos_3+359);

Max_d_P_1;
Max_d_P_2;
Max_d_P_3;

% Max pressure (Pa)

[Max_P_1,pos_1]= max(P_1);
[Max_P_2,pos_2]= max(P_2);
[Max_P_3,pos_3]= max(P_3);

Grau_Pmax_1 = pos_1-361;
Grau_Pmax_2 = pos_2-361;
Grau_Pmax_3 = pos_3-361;

Max_P_1;
Max_P_2;
Max_P_3;

figure(3)
plot(Grau,d_P_1,'blue',Grau,d_P_2,'red',Grau,d_P_3,'black')
set(gca,'FontSize',12);
xlabel('Crank angle (°)')
ylabel('Smoothed pressure derivative (Pa/°)')
title('Smoothed pressure derivative in function of crank angle')
hold on
```

PUC-Rio - Certificação Digital Nº 1312923/CA

```
% OBTENCÃO DO PERFIL DE VELOCIDADE DO PISTÃO
% Derivada do volume (em m^3/grau)
d_V(1) = V(2)-V(1);
for i=2:717
    d_V(i) = V(i+1)-V(i-1);
end
d_V(720) = V(720)-V(719);

% GROSS HEAT RELEASE
% Gross heat release rate (J/°)

T_1 = zeros(720,1);
T_2 = zeros(720,1);
T_3 = zeros(720,1);

gamma_1 = zeros(720,1);
gamma_2 = zeros(720,1);
gamma_3 = zeros(720,1);

d_Q_1 = zeros(720,1);
d_Q_2 = zeros(720,1);
d_Q_3 = zeros(720,1);

for i=1:720
    T_1(i) = P_1(i)*V(i)*60*rpm_1/(1000*m_air_w_1*R_air_w_1);
    T_2(i) = P_2(i)*V(i)*60*rpm_2/(1000*m_air_w_2*R_air_w_2);
    T_3(i) = P_3(i)*V(i)*60*rpm_3/(1000*m_air_w_3*R_air_w_3);

    gamma_1(i) = 1/(1-1/(3.04473+1.33805e-3*T_1(i)-4.88256e-7*T_1(i)^2
+8.55475e-11*T_1(i)^3-5.70132e-15*T_1(i)^4));
    gamma_2(i) = 1/(1-1/(3.04473+1.33805e-3*T_2(i)-4.88256e-7*T_2(i)^2
+8.55475e-11*T_2(i)^3-5.70132e-15*T_2(i)^4));
    gamma_3(i) = 1/(1-1/(3.04473+1.33805e-3*T_3(i)-4.88256e-7*T_3(i)^2
+8.55475e-11*T_3(i)^3-5.70132e-15*T_3(i)^4));

    d_Q_1(i) = gamma_1(i)/(gamma_1(i)-1)*P_1(i)*d_V(i)+1/(gamma_1(i)-
1)*V(i)*d_P_1(i);
    d_Q_2(i) = gamma_2(i)/(gamma_2(i)-1)*P_2(i)*d_V(i)+1/(gamma_2(i)-
1)*V(i)*d_P_2(i);
    d_Q_3(i) = gamma_3(i)/(gamma_3(i)-1)*P_3(i)*d_V(i)+1/(gamma_3(i)-
1)*V(i)*d_P_3(i);
end

% Smoothed gross heat release rate (J/°)
ds_Q_1 = smooth(Grau,d_Q_1,0.02,'rloess');
ds_Q_2 = smooth(Grau,d_Q_2,0.02,'rloess');
ds_Q_3 = smooth(Grau,d_Q_3,0.02,'rloess');

% Max gross heat release rate (J/°)
Max_dQ_s_1 = max(ds_Q_1);
Max_dQ_s_2 = max(ds_Q_2);
Max_dQ_s_3 = max(ds_Q_3);

figure(4)
set(gca,'FontSize',12);
plot(Grau,T_1,'blue',Grau,T_2,'red',Grau,T_3,'black')
xlabel('Crank angle (°)')
ylabel('Temperature (K)')
title('Gamma in function of crank angle')
hold on

figure(5)
set(gca,'FontSize',12);
plot(Grau,gamma_1,'blue',Grau,gamma_2,'red',Grau,gamma_3,'black')
xlabel('Crank angle (°)')
ylabel('Gamma (-)')
```

PUC-Rio - Certificação Digital Nº 1312923/CA

```
title('Gamma in function of crank angle')
hold on

figure(6)
set(gca,'FontSize',12);
plot(Grau,ds_Q_1,'blue',Grau,ds_Q_2,'red',Grau,ds_Q_3,'black')
xlabel('Crank angle (°)')
ylabel('Smoothed gross heat release rate (J/°)')
title('Smoothed gross heat release rate in function of crank angle')
hold on

% Gross heat release (J)
Q_1 = zeros(190,1);
Q_2 = zeros(190,1);
Q_3 = zeros(190,1);

for i=2:190
    Q_1(i) = Q_1(i-1) + gamma_1(351+i)/(gamma_1(351+i)-1)*(P_1(351+i)
+P_1(351+i+1))/2*(V(351+i+1)-V(351+i))+1/(gamma_1(351+i)-1)*(V(351+i)
+V(351+i+1))/2*(P_1(351+i+1)-P_1(351+i));
    Q_2(i) = Q_2(i-1) + gamma_2(351+i)/(gamma_1(351+i)-1)*(P_2(351+i)
+P_2(351+i+1))/2*(V(351+i+1)-V(351+i))+1/(gamma_2(351+i)-1)*(V(351+i)
+V(351+i+1))/2*(P_2(351+i+1)-P_2(351+i));
    Q_3(i) = Q_3(i-1) + gamma_3(351+i)/(gamma_1(351+i)-1)*(P_3(351+i)
+P_3(351+i+1))/2*(V(351+i+1)-V(351+i))+1/(gamma_3(351+i)-1)*(V(351+i)
+V(351+i+1))/2*(P_3(351+i+1)-P_3(351+i));
end

for i=1:190
    Grau_Q(i) = Grau(351+i);
end

Q_1_s = smooth(Grau_Q,Q_1,0.02,'rloess');
Q_2_s = smooth(Grau_Q,Q_2,0.02,'rloess');
Q_3_s = smooth(Grau_Q,Q_3,0.02,'rloess');

% Fraction of gross heat release (%)
for i=1:190
    Per_Q_1_s(i) = Q_1_s(i)/max(Q_1_s)*100;
    Per_Q_2_s(i) = Q_2_s(i)/max(Q_2_s)*100;
    Per_Q_3_s(i) = Q_3_s(i)/max(Q_3_s)*100;
end

figure(7)
set(gca,'FontSize',12);
plot(Grau_Q,Per_Q_1_s,'blue',Grau_Q,Per_Q_2_s,'red',Grau_Q,Per_Q_3_s,'bla
ck')
xlabel('Crank angle (°)')
ylabel('Percentage of gross heat release (%)')
title('Percentage of gross heat release in function of crank angle')
hold on

% CA10, CA50 and CA90 (°)
for i=1:50
    if (Per_Q_1_s(i)<3) Ignition_Delay_1 = Grau(351+i)+9.5;
    else if (Per_Q_1_s(i)<10) CA10_1=Grau_Q(i)+0.5;
        else if (Per_Q_1_s(i)<50) CA50_1=Grau_Q(i)+0.5;
            else if (Per_Q_1_s(i)<90) CA90_1=Grau_Q(i)+0.5;
                end
            end
        end
    end
end
Ignition_Delay_1;
CA10_1;
CA50_1;
CA90_1;
```

PUC-Rio - Certificação Digital Nº 1312923/CA

```
for i=1:50
    if (Per_Q_2_s(i)<3) Ignition_Delay_2 = Grau(351+i)+9.5;
    else if (Per_Q_2_s(i)<10) CA10_2=Grau_Q(i)+0.5;
        else if (Per_Q_2_s(i)<50) CA50_2=Grau_Q(i)+0.5;
            else if (Per_Q_2_s(i)<90) CA90_2=Grau_Q(i)+0.5;
                end
            end
        end
    end
end
Ignition_Delay_2;
CA10_2;
CA50_2;
CA90_2;

for i=1:50
    if (Per_Q_3_s(i)<3) Ignition_Delay_3 = Grau(351+i)+9.5;
    else if (Per_Q_3_s(i)<10) CA10_3=Grau_Q(i)+0.5;
        else if (Per_Q_3_s(i)<50) CA50_3=Grau_Q(i)+0.5;
            else if (Per_Q_3_s(i)<90) CA90_3=Grau_Q(i)+0.5;
                end
            end
        end
    end
end
Ignition_Delay_3;
CA10_3;
CA50_3;
CA90_3;


% POLYTROPIC COEFFICIENT
% Smoothed logarithm of pressure
log_P_1 = log(P_1);
log_P_2 = log(P_2);
log_P_3 = log(P_3);

log_P_1_s = smooth(Grau,log_P_1,0.015,'rloess');
log_P_2_s = smooth(Grau,log_P_2,0.015,'rloess');
log_P_3_s = smooth(Grau,log_P_3,0.015,'rloess');

% Logarithm of volume
log_V = log(V);

% Polytropic coefficient
% Compression
X_1_1 = zeros(70,1);
Y_1_1 = zeros(70,1);
X_2_1 = zeros(70,1);
Y_2_1 = zeros(70,1);
X_3_1 = zeros(70,1);
Y_3_1 = zeros(70,1);

f_1 = fittype({'-x','1'},'coefficients',{'n_1','p_1'});
f_2 = fittype({'-x','1'},'coefficients',{'n_2','p_2'});

for i=1:70
    X_1_1(i) = log_V(i+281);
    Y_1_1(i) = log_P_1_s(i+281);
end
[cfun_1_1,gof_1_1] = fit(X_1_1,Y_1_1,f_1)
for i=1:110
    x_1_1(i) = log_V(i+271);
    y_1_1(i) = -1.342*x_1_1(i)+2.614;
end

for i=1:70
    X_2_1(i) = log_V(i+281);
```

PUC-Rio - Certificação Digital Nº 1312923/CA

```
    Y_2_1(i) = log_P_2_s(i+281);
end
[cfun_2_1,gof_2_1] = fit(X_2_1,Y_2_1,f_1)
for i=1:110
    x_2_1(i) = log_V(i+271);
    y_2_1(i) = -1.341*x_2_1(i)+2.619;
end

for i=1:70
    X_3_1(i) = log_V(i+281);
    Y_3_1(i) = log_P_3_s(i+281);
end
[cfun_3_1,gof_3_1] = fit(X_3_1,Y_3_1,f_1)
for i=1:110
    x_3_1(i) = log_V(i+271);
    y_3_1(i) = -1.341*x_3_1(i)+2.622;
end

% Expansion
X_1_2 = zeros(70,1);
Y_1_2 = zeros(70,1);
X_2_2 = zeros(70,1);
Y_2_2 = zeros(70,1);
X_3_2 = zeros(70,1);
Y_3_2 = zeros(70,1);

for i=1:70
    X_1_2(i) = log_V(396+i);
    Y_1_2(i) = log_P_1_s(396+i);
end
[cfun_1_2,gof_1_2] = fit(X_1_2,Y_1_2,f_2)
for i=1:110
    x_1_2(i) = log_V(376+i);
    y_1_2(i) = -1.411*x_1_2(i)+2.672;
end

for i=1:70
    X_2_2(i) = log_V(396+i);
    Y_2_2(i) = log_P_2_s(396+i);
end
[cfun_2_2,gof_2_2] = fit(X_2_2,Y_2_2,f_2)
for i=1:110
    x_2_2(i) = log_V(376+i);
    y_2_2(i) = -1.408*x_2_2(i)+2.695;
end

for i=1:70
    X_3_2(i) = log_V(396+i);
    Y_3_2(i) = log_P_3_s(396+i);
end
[cfun_3_2,gof_3_2] = fit(X_3_2,Y_3_2,f_2)
for i=1:110
    x_3_2(i) = log_V(376+i);
    y_3_2(i) = -1.411*x_3_2(i)+2.669;
end

figure(8)
set(gca,'FontSize',12);
plot(log_V,log_P_1_s,'red', x_1_1,y_1_1,'blue', x_1_2,y_1_2,'blue')
xlabel('Ln(v)')
ylabel('Ln(p)')
title('Test1 - ln(v) versus ln(p)')
hold on

figure(9)
set(gca,'FontSize',12);
plot(log_V,log_P_2_s,'red', x_2_1,y_2_1,'blue', x_2_2,y_2_2,'blue')
xlabel('Ln(v)')
```

PUC-Rio - Certificação Digital Nº 1312923/CA

```
ylabel('Ln(p)')
title('Test2 - ln(v) versus ln(p)')
hold on

figure(10)
set(gca,'FontSize',12);
plot(log_V,log_P_3_s,'red', x_3_1,y_3_1,'blue', x_3_2,y_3_2,'blue')
xlabel('Ln(v)')
ylabel('Ln(p)')
title('Test3 - ln(v) versus ln(p)')
hold on

Acc = (Acc_1+Acc_2+Acc_3)/3;
rpm = (rpm_1+rpm_2+rpm_3)/3;
torque = (torque_1+torque_2+torque_3)/3;
m_f = (m_f_1+m_f_2+m_f_3)/3;
Ur = (Ur_1+Ur_2+Ur_3)/3;
p_air_w = (p_air_w_1+p_air_w_2+p_air_w_3)/3;
p_air_d = (p_air_d_1+p_air_d_2+p_air_d_3)/3;
p_exh = (p_exh_1+p_exh_2+p_exh_3)/3;
T_exh = (T_exh_1+T_exh_2+T_exh_3)/3;
T_air_w =(T_air_w_1+T_air_w_2+T_air_w_3)/3;
T_room = (T_room_1+T_room_2+T_room_3)/3;
T_w = (T_w_1+T_w_2+T_w_3)/3;
T_oil = (T_oil_1+T_oil_2+T_oil_3)/3;
IMEP = (IMEP_1+IMEP_2+IMEP_3)/3*1e-5;
BMEP = 0.25*(BMEP_1+BMEP_2+BMEP_3)/3;
P_b = (P_b_1+P_b_2+P_b_3)/3;
P_i = (P_i_1+P_i_2+P_i_3)/3;
Nu_f = 100*(Nu_f_1+Nu_f_2+Nu_f_3)/3;
Nu_i = 100*(Nu_i_1+Nu_i_2+Nu_i_3)/3;
Nu_m = 100*(Nu_m_1+Nu_m_2+Nu_m_3)/3;
Nu_v = 100*(Nu_v_1+Nu_v_2+Nu_v_3)/3;
Ur = (Ur_1+Ur_2+Ur_3)/3;
Ignition_Delay = (Ignition_Delay_1+Ignition_Delay_2+Ignition_Delay_3)/3;
CA10 = (CA10_1+CA10_2+CA10_3)/3;
CA50 = (CA50_1+CA50_2+CA50_3)/3;
CA90 = (CA90_1+CA90_2+CA90_3)/3;
Grau_dPmax = (Grau_dPmax_1+Grau_dPmax_2+Grau_dPmax_3)/3;
Grau_Pmax = (Grau_Pmax_1+ Grau_Pmax_2+ Grau_Pmax_3)/3;
Max_dQ_s = (Max_dQ_s_1+Max_dQ_s_2+Max_dQ_s_3)/3;
Max_d_P = (Max_d_P_1+Max_d_P_2+Max_d_P_3)/3;
Max_P = 1e-5*(Max_P_1+Max_P_2+Max_P_3)/3;
Phi = (Phi_1+Phi_2+Phi_3)/3;
m_air_w =(m_air_w_1+m_air_w_2+m_air_w_3)/3;
m_air_d =(m_air_d_1+m_air_d_2+m_air_d_3)/3;
sfc = (sfc_1+sfc_2+sfc_3)/3;
```

PUC-Rio - Certificação Digital Nº 1312923/CA

Appendix H: Experimental Results of the Engine Tests

This Appendix H contains tables with typical experimental results obtained during engine tests with diesel-biodiesel-ethanol. Given the large number of quantities measured and calculated, they present only the average value obtained for each experimental condition and their respective uncertainty.

In this section, pressure data in the cylinder were not included, because of the large volume of information available. However, this information can be accessed contacting the author (or advisors) by e-mail.

PUC-Rio - Certificação Digital Nº 1312923/CA

Table H1: Experimental results of engine tests for each blend (Part 1 of 8).

Biodiesel content (%)	Ethanol content (%)	Lower Heating Value (kJ/kg)	Specific gravity (kg/m³)	Engine speed (rpm)	Torque (N.m)	Fraction of B7 maximum torque (%)	Accelerator (%)	Brake Power (kW)	Lubricating oil temperature (°C)	Water temperature (°C)	Inlet air temperature (°C)	Relative humidity (%)	Fuel consumption (kg/h)	Dry air consumption (kg/h)	Air / Fuel Ratio (-)	Lambda (-)
7	0	45.125	0.8395	1,505 ± 2.8	81.8 ± 0.1	25.0	44.80 ± 0.23	12.9 ± 0.0	86.93 ± 0.53	83.07 ± 0.05	29.75 ± 0.14	61.25 ± 0.04	3.8 ± 0.0	261.2 ± 3.2	69.6 ± 0.9	4.82 ± 0.06
				1,504 ± 3.6	162.0 ± 0.3	50.0	54.38 ± 0.11	25.5 ± 0.1	88.74 ± 0.32	83.95 ± 0.23	30.10 ± 0.00	61.20 ± 0.12	6.1 ± 0.1	283.2 ± 2.3	46.3 ± 0.4	3.20 ± 0.03
				1,503 ± 5.6	238.5 ± 0.2	75.0	61.20 ± 0.09	37.5 ± 0.1	88.75 ± 0.07	84.76 ± 0.04	30.27 ± 0.07	61.15 ± 0.11	8.6 ± 0.0	299.7 ± 3.7	34.9 ± 0.4	2.42 ± 0.03
				1,507 ± 3.1	324.3 ± 2.7	100.0	100.00 ± 0.00	51.2 ± 0.4	82.23 ± 0.88	85.05 ± 0.18	26.17 ± 0.22	65.87 ± 0.15	11.4 ± 0.1	331.7 ± 2.1	29.1 ± 0.2	2.01 ± 0.01
				1,801 ± 6.2	98.1 ± 0.1	25.0	52.12 ± 0.03	18.5 ± 0.1	90.36 ± 0.57	83.49 ± 0.13	30.28 ± 0.04	59.12 ± 0.15	5.3 ± 0.0	327.6 ± 1.7	61.5 ± 0.3	4.26 ± 0.02
				1,802 ± 0.8	195.0 ± 0.1	50.0	64.60 ± 0.06	36.8 ± 0.0	91.62 ± 0.10	84.48 ± 0.06	30.17 ± 0.09	60.02 ± 0.13	8.7 ± 0.1	371.3 ± 2.6	42.5 ± 0.3	2.94 ± 0.02
				1,792 ± 1.5	288.1 ± 0.2	75.0	75.62 ± 0.37	54.1 ± 0.1	90.93 ± 0.65	85.18 ± 0.04	29.60 ± 0.13	61.22 ± 0.49	12.2 ± 0.2	420.7 ± 12.4	34.4 ± 1.0	2.38 ± 0.07
				1,800 ± 11.2	386.1 ± 1.8	100.0	100.00 ± 0.00	72.8 ± 0.6	90.85 ± 1.09	86.20 ± 0.20	29.23 ± 0.33	65.92 ± 0.41	16.1 ± 0.2	476.8 ± 11.7	29.7 ± 0.7	2.06 ± 0.05
				2,102 ± 5.2	94.2 ± 0.1	25.0	63.95 ± 0.37	20.7 ± 0.1	92.84 ± 0.57	83.73 ± 0.02	30.83 ± 0.09	58.39 ± 0.11	6.4 ± 0.1	393.9 ± 3.0	61.5 ± 0.5	4.26 ± 0.04
				2,104 ± 4.9	187.6 ± 0.0	50.0	75.99 ± 0.23	41.3 ± 0.1	93.89 ± 0.12	84.57 ± 0.17	30.73 ± 0.09	58.96 ± 0.27	10.3 ± 0.1	458.9 ± 3.0	44.6 ± 0.3	3.09 ± 0.02
				2,098 ± 2.1	277.2 ± 0.1	75.0	86.71 ± 0.20	60.9 ± 0.1	92.70 ± 0.68	85.24 ± 0.07	30.20 ± 0.14	59.80 ± 0.04	14.2 ± 0.1	521.6 ± 2.0	36.8 ± 0.1	2.55 ± 0.01
				2,096 ± 3.1	369.7 ± 1.0	100.0	100.00 ± 0.00	81.1 ± 0.2	94.88 ± 0.56	86.43 ± 0.05	30.50 ± 0.26	63.62 ± 0.40	18.6 ± 0.1	558.1 ± 4.3	30.0 ± 0.2	2.08 ± 0.02
15	0	44.379	0.8437	1,503 ± 16.7	81.7 ± 0.4	25.0	44.73 ± 0.07	12.9 ± 0.2	86.54 ± 0.35	83.08 ± 0.30	30.08 ± 0.06	60.30 ± 0.22	3.9 ± 0.1	263.9 ± 3.1	68.3 ± 0.8	4.78 ± 0.06
				1,504 ± 3.0	162.0 ± 0.3	50.0	54.36 ± 0.04	25.5 ± 0.1	86.51 ± 0.12	83.71 ± 0.07	29.70 ± 0.13	58.89 ± 0.26	6.4 ± 0.1	281.5 ± 0.8	44.0 ± 0.2	3.08 ± 0.01
				1,504 ± 1.7	240.1 ± 0.6	75.0	61.47 ± 0.09	37.8 ± 0.1	85.60 ± 0.71	84.38 ± 0.00	29.20 ± 0.27	58.69 ± 0.26	8.9 ± 0.1	302.8 ± 2.3	33.9 ± 0.3	2.37 ± 0.02
				1,506 ± 5.6	298.7 ± 7.3	92.1	100.00 ± 0.00	47.1 ± 1.2	89.95 ± 0.41	85.37 ± 0.39	31.33 ± 0.09	56.22 ± 0.10	10.9 ± 0.2	329.1 ± 10.5	30.2 ± 1.0	2.12 ± 0.07
				1,802 ± 1.5	97.7 ± 0.1	25.0	52.09 ± 0.04	18.4 ± 0.0	90.24 ± 0.42	83.50 ± 0.11	31.00 ± 0.00	57.82 ± 0.09	5.5 ± 0.1	327.1 ± 2.5	59.7 ± 0.5	4.18 ± 0.03
				1,804 ± 1.0	195.3 ± 0.3	50.0	65.01 ± 0.15	36.9 ± 0.1	90.97 ± 0.05	84.36 ± 0.04	30.87 ± 0.21	58.12 ± 0.57	9.2 ± 0.1	375.0 ± 2.4	40.9 ± 0.3	2.86 ± 0.02
				1,794 ± 2.4	289.0 ± 0.1	75.0	75.77 ± 0.04	54.3 ± 0.1	89.50 ± 1.44	84.97 ± 0.20	30.27 ± 0.31	59.41 ± 0.52	12.7 ± 0.1	424.8 ± 9.7	33.4 ± 0.8	2.34 ± 0.05
				1,811 ± 4.1	369.9 ± 0.9	95.8	100.00 ± 0.00	70.2 ± 0.2	92.20 ± 0.71	86.01 ± 0.12	31.77 ± 0.13	56.59 ± 0.06	15.9 ± 0.1	478.1 ± 3.1	30.1 ± 0.2	2.11 ± 0.01
				2,101 ± 2.8	94.6 ± 0.0	25.0	64.55 ± 0.09	20.8 ± 0.0	92.62 ± 0.30	83.70 ± 0.00	31.77 ± 0.09	56.27 ± 0.17	6.6 ± 0.0	393.9 ± 1.8	59.8 ± 0.3	4.19 ± 0.02
				2,104 ± 5.7	187.4 ± 0.1	50.0	76.63 ± 0.31	41.3 ± 0.1	94.24 ± 0.24	84.53 ± 0.22	31.77 ± 0.07	56.97 ± 0.14	10.5 ± 0.0	460.1 ± 2.5	43.7 ± 0.2	3.06 ± 0.02
				2,098 ± 2.5	277.5 ± 0.3	75.0	87.83 ± 0.12	61.0 ± 0.1	93.87 ± 0.75	85.29 ± 0.05	31.37 ± 0.22	57.47 ± 0.26	14.6 ± 0.1	520.6 ± 2.4	35.8 ± 0.2	2.51 ± 0.01
				2,099 ± 1.5	360.8 ± 0.3	97.6	100.00 ± 0.00	79.3 ± 0.1	95.04 ± 0.37	86.23 ± 0.09	32.27 ± 0.09	55.85 ± 0.18	18.5 ± 0.1	556.9 ± 2.0	30.1 ± 0.1	2.11 ± 0.01
15	5	43.560	0.8411	1,501 ± 4.4	81.6 ± 0.1	25.0	46.02 ± 0.14	12.8 ± 0.0	86.57 ± 0.42	82.95 ± 0.12	30.46 ± 0.08	48.51 ± 0.68	4.0 ± 0.2	260.8 ± 7.4	65.9 ± 2.1	4.70 ± 0.15
				1,504 ± 1.5	161.8 ± 0.5	50.0	59.93 ± 0.05	25.5 ± 0.1	87.18 ± 0.19	83.83 ± 0.19	30.27 ± 0.36	47.73 ± 0.38	6.5 ± 0.1	278.6 ± 2.8	43.1 ± 0.4	3.07 ± 0.03
				1,505 ± 9.6	240.9 ± 0.2	75.0	66.45 ± 0.06	38.0 ± 0.2	88.43 ± 0.08	84.49 ± 0.05	29.14 ± 0.06	42.88 ± 0.07	9.1 ± 0.2	307.9 ± 4.9	33.9 ± 0.6	2.42 ± 0.04
				1,501 ± 8.7	263.3 ± 1.2	81.2	100.00 ± 0.00	41.4 ± 0.3	88.06 ± 0.05	84.88 ± 0.08	28.34 ± 0.05	41.25 ± 0.05	9.8 ± 0.2	314.0 ± 6.8	32.0 ± 0.7	2.28 ± 0.05
				1,802 ± 3.5	96.8 ± 0.5	25.0	53.80 ± 0.04	18.3 ± 0.1	89.74 ± 0.25	83.30 ± 0.14	30.92 ± 0.06	49.51 ± 0.21	5.5 ± 0.0	325.8 ± 2.3	59.7 ± 0.4	4.25 ± 0.03
				1,792 ± 2.5	192.9 ± 0.2	50.0	66.73 ± 0.07	36.2 ± 0.1	90.66 ± 0.08	84.33 ± 0.07	30.90 ± 0.00	49.86 ± 0.13	9.0 ± 0.2	364.3 ± 3.7	40.6 ± 0.5	2.89 ± 0.03
				1,794 ± 7.3	290.2 ± 0.5	75.0	82.46 ± 0.14	54.5 ± 0.2	90.43 ± 0.29	85.20 ± 0.05	29.15 ± 0.07	41.97 ± 0.46	12.9 ± 0.1	433.9 ± 12.5	33.7 ± 1.0	2.40 ± 0.07
				1,801 ± 14.5	314.3 ± 4.3	81.4	100.00 ± 0.00	59.3 ± 0.9	90.33 ± 0.20	85.33 ± 0.02	28.51 ± 0.04	41.66 ± 0.34	13.9 ± 0.2	456.7 ± 5.7	32.8 ± 0.4	2.34 ± 0.03
				2,100 ± 4.7	93.4 ± 0.1	25.0	66.65 ± 0.23	20.5 ± 0.0	92.73 ± 0.50	83.68 ± 0.06	31.95 ± 0.07	48.29 ± 0.37	6.6 ± 0.1	392.0 ± 4.9	59.0 ± 0.8	4.20 ± 0.06
				2,097 ± 1.3	188.1 ± 0.5	50.0	78.63 ± 0.06	41.3 ± 0.1	94.20 ± 0.26	84.59 ± 0.08	32.10 ± 0.00	49.12 ± 0.21	10.9 ± 0.2	456.1 ± 1.9	42.0 ± 0.3	2.99 ± 0.02
				2,099 ± 1.7	277.4 ± 0.1	75.0	91.73 ± 0.14	61.0 ± 0.1	92.97 ± 0.30	85.20 ± 0.07	28.88 ± 0.11	43.32 ± 0.23	15.0 ± 0.1	535.4 ± 4.0	35.7 ± 0.3	2.54 ± 0.02
				2,100 ± 3.3	324.9 ± 0.6	87.9	100.00 ± 0.00	71.4 ± 0.2	93.33 ± 0.45	85.76 ± 0.02	29.00 ± 0.12	42.35 ± 0.06	17.2 ± 0.1	560.2 ± 1.6	32.6 ± 0.1	2.32 ± 0.01

PUC-Rio - Certificação Digital Nº 1312923/CA

PUC-Rio - Certificação Digital Nº 1312923/CA

Table H1: Experimental results of engine tests for each blend (Part 2 of 8).

Biodiesel content (%)	Ethanol content (%)	Lower Heating Value (kJ/kg)	Specific gravity (kg/m³)	Sfc (kg/(kW.h))	Ethanol sfc (kg/(kW.h))	Ethanol conversion (MJ/(kW.h))	Exhaust Gas Temperature (°C)	Exhaust Gas pressure (bar)	BMEP (bar)	IMEP (bar)	Indicated efficiency (%)	Fuel conversion efficiency (%)	Volumetric efficiency (%)	Mechanical efficiency (%)
7	0	45.125	0.8395	0.291 ± 0.001	[redacted]	13.12 ± 0.03	249.1 ± 9.0	1.0266 ± 0.0347	2.4 ± 0.00	4.3 ± 0.00	49.1 ± 0.1	27.4 ± 0.1	111.0 ± 1.5	55.9 ± 0.2
				0.240 ± 0.003		10.82 ± 0.14	346.4 ± 5.7	1.0191 ± 0.1422	4.7 ± 0.01	6.9 ± 0.01	48.5 ± 0.6	33.3 ± 0.4	120.6 ± 1.1	68.6 ± 1.3
				0.229 ± 0.001		10.33 ± 0.05	399.3 ± 3.5	1.0361 ± 0.2333	7.0 ± 0.01	9.6 ± 0.01	47.8 ± 0.2	34.8 ± 0.2	127.8 ± 1.7	72.8 ± 0.5
				0.223 ± 0.003		10.06 ± 0.12	450.8 ± 8.0	1.0400 ± 0.1182	9.5 ± 0.08	12.9 ± 0.11	48.7 ± 0.6	35.8 ± 0.4	141.3 ± 1.5	73.5 ± 1.3
				0.288 ± 0.002		12.98 ± 0.08	273.6 ± 5.8	1.0277 ± 0.0596	2.9 ± 0.00	4.9 ± 0.00	47.4 ± 0.3	27.7 ± 0.2	116.3 ± 0.8	58.5 ± 0.5
				0.237 ± 0.002		10.71 ± 0.11	356.4 ± 1.9	1.0340 ± 0.1213	5.7 ± 0.00	7.9 ± 0.00	46.8 ± 0.5	33.6 ± 0.3	132.0 ± 1.0	71.8 ± 1.1
				0.226 ± 0.003		10.20 ± 0.13	407.1 ± 3.9	1.0411 ± 0.3707	8.4 ± 0.01	11.2 ± 0.01	47.1 ± 0.6	35.3 ± 0.5	150.5 ± 4.5	75.0 ± 1.4
				0.221 ± 0.003		9.95 ± 0.15	470.8 ± 6.6	1.0460 ± 0.1338	11.3 ± 0.05	14.6 ± 0.07	46.7 ± 0.7	36.2 ± 0.5	170.1 ± 4.7	77.4 ± 1.6
				0.309 ± 0.004		13.93 ± 0.17	275.4 ± 6.9	1.0313 ± 0.0329	2.8 ± 0.00	5.1 ± 0.00	48.2 ± 0.6	25.9 ± 0.3	120.1 ± 1.0	53.6 ± 0.9
				0.249 ± 0.001		11.24 ± 0.06	344.1 ± 3.3	1.0377 ± 0.0560	5.5 ± 0.00	8.2 ± 0.00	48.2 ± 0.3	32.0 ± 0.2	139.8 ± 1.1	66.5 ± 0.5
				0.233 ± 0.001		10.50 ± 0.04	384.3 ± 3.2	1.0426 ± 0.0293	8.1 ± 0.00	11.4 ± 0.00	48.2 ± 0.2	34.3 ± 0.1	159.4 ± 1.0	71.1 ± 0.4
				0.229 ± 0.002		10.34 ± 0.08	478.6 ± 1.5	1.0503 ± 0.0391	10.8 ± 0.03	14.4 ± 0.04	46.3 ± 0.4	34.8 ± 0.3	170.9 ± 2.0	75.2 ± 0.9
15	0	44.379	0.8437	0.300 ± 0.005		13.33 ± 0.24	256.5 ± 13.2	1.0245 ± 0.0667	2.4 ± 0.01	4.3 ± 0.02	48.2 ± 0.9	27.0 ± 0.5	112.2 ± 1.8	56.1 ± 1.4
				0.251 ± 0.003		11.13 ± 0.14	338.5 ± 3.2	1.0201 ± 0.5316	4.7 ± 0.01	6.9 ± 0.01	47.2 ± 0.6	32.3 ± 0.4	119.7 ± 0.7	68.5 ± 1.3
				0.236 ± 0.004		10.49 ± 0.18	389.1 ± 9.7	1.0327 ± 0.2511	7.0 ± 0.02	9.6 ± 0.02	46.9 ± 0.8	34.3 ± 0.6	128.8 ± 1.5	73.2 ± 1.7
				0.231 ± 0.007		10.26 ± 0.31	450.0 ± 16.4	1.0249 ± 0.5196	8.7 ± 0.21	11.8 ± 0.29	47.5 ± 1.4	35.1 ± 1.1	139.8 ± 4.5	74.0 ± 3.1
				0.297 ± 0.003		13.19 ± 0.13	277.2 ± 6.8	1.0283 ± 0.0951	2.9 ± 0.00	5.2 ± 0.00	49.8 ± 0.5	27.3 ± 0.3	116.1 ± 0.9	54.8 ± 0.8
				0.249 ± 0.003		11.03 ± 0.12	357.0 ± 5.0	1.0299 ± 0.1093	5.7 ± 0.01	8.4 ± 0.01	48.1 ± 0.5	32.6 ± 0.3	132.9 ± 1.3	67.9 ± 1.0
				0.234 ± 0.001		10.40 ± 0.07	401.6 ± 9.0	1.0392 ± 0.0844	8.4 ± 0.00	11.8 ± 0.00	48.4 ± 0.3	34.6 ± 0.2	151.6 ± 3.8	71.5 ± 0.6
				0.226 ± 0.001		10.05 ± 0.06	461.1 ± 6.0	1.0444 ± 0.0462	10.8 ± 0.03	14.9 ± 0.03	49.2 ± 0.3	35.8 ± 0.2	169.3 ± 1.4	72.8 ± 0.6
				0.317 ± 0.001		14.05 ± 0.04	273.0 ± 3.0	1.0301 ± 0.0364	2.8 ± 0.00	5.5 ± 0.00	50.6 ± 0.2	25.6 ± 0.1	120.0 ± 0.7	50.6 ± 0.2
				0.255 ± 0.001		11.33 ± 0.04	345.0 ± 4.2	1.0361 ± 0.0298	5.5 ± 0.00	8.7 ± 0.00	50.6 ± 0.2	31.8 ± 0.1	139.9 ± 0.9	62.8 ± 0.3
				0.239 ± 0.002		10.59 ± 0.08	390.1 ± 4.2	1.0417 ± 0.0022	8.1 ± 0.01	11.9 ± 0.01	49.9 ± 0.4	34.0 ± 0.3	159.2 ± 1.4	68.1 ± 0.7
				0.234 ± 0.001		10.36 ± 0.04	468.6 ± 1.4	1.0473 ± 0.0693	10.5 ± 0.01	14.6 ± 0.01	48.2 ± 0.2	34.7 ± 0.1	170.3 ± 0.8	72.1 ± 0.4
15	5	43.560	0.8411	0.309 ± 0.015	0.480 ± 0.103	12.90 ± 2.76	254.6 ± 9.9	1.0179 ± 0.2004	2.4 ± 0.00	4.3 ± 0.01	48.5 ± 2.3	26.8 ± 1.3	111.5 ± 3.2	55.2 ± 3.7
				0.254 ± 0.002	0.309 ± 0.062	8.29 ± 1.66	347.5 ± 15.2	1.0189 ± 0.1809	4.7 ± 0.01	6.9 ± 0.02	47.6 ± 0.5	32.6 ± 0.3	119.0 ± 1.8	68.4 ± 0.9
				0.240 ± 0.004	0.303 ± 0.076	8.13 ± 2.03	404.9 ± 0.5	1.0324 ± 0.1062	7.0 ± 0.01	9.8 ± 0.01	48.0 ± 0.9	34.5 ± 0.6	130.8 ± 2.3	72.0 ± 1.9
				0.237 ± 0.004	0.290 ± 0.132	7.78 ± 3.54	429.4 ± 0.2	1.0389 ± 0.0898	7.7 ± 0.04	10.6 ± 0.05	48.1 ± 0.9	34.8 ± 0.6	133.7 ± 3.0	72.4 ± 1.8
				0.300 ± 0.003	0.366 ± 0.057	9.82 ± 1.54	272.1 ± 3.5	1.0213 ± 0.0489	2.8 ± 0.02	5.3 ± 0.03	51.4 ± 0.4	27.5 ± 0.2	116.1 ± 0.9	53.5 ± 0.7
				0.248 ± 0.006	0.229 ± 0.050	6.16 ± 1.34	351.6 ± 0.1	1.0298 ± 0.0236	5.6 ± 0.01	8.4 ± 0.01	49.6 ± 1.2	33.4 ± 0.8	130.5 ± 1.3	67.2 ± 2.3
				0.236 ± 0.002	0.273 ± 0.028	7.33 ± 0.76	407.4 ± 2.0	1.0365 ± 0.3093	8.5 ± 0.01	12.0 ± 0.02	49.3 ± 0.4	35.0 ± 0.3	154.8 ± 4.5	70.9 ± 0.9
				0.235 ± 0.005	0.318 ± 0.024	8.54 ± 0.63	417.6 ± 1.4	1.0352 ± 0.1524	9.2 ± 0.13	12.7 ± 0.18	48.6 ± 1.1	35.2 ± 0.8	162.1 ± 2.4	72.4 ± 2.3
				0.324 ± 0.005	0.467 ± 0.018	12.53 ± 0.49	274.6 ± 4.7	1.0269 ± 0.0716	2.7 ± 0.00	5.5 ± 0.00	51.6 ± 0.7	25.5 ± 0.4	119.9 ± 1.6	49.5 ± 1.0
				0.263 ± 0.005	0.422 ± 0.016	11.34 ± 0.44	343.4 ± 2.4	1.0328 ± 0.0200	5.5 ± 0.01	8.8 ± 0.02	50.6 ± 1.0	31.4 ± 0.6	139.9 ± 0.6	62.1 ± 1.7
				0.246 ± 0.001	0.404 ± 0.034	10.84 ± 0.92	384.0 ± 2.5	1.0400 ± 0.0062	8.1 ± 0.00	11.9 ± 0.01	49.2 ± 0.2	33.5 ± 0.1	163.1 ± 1.4	68.2 ± 0.4
				0.241 ± 0.002	0.332 ± 0.018	8.93 ± 0.49	425.9 ± 1.6	1.0456 ± 0.0618	9.5 ± 0.02	13.4 ± 0.02	48.5 ± 0.4	34.3 ± 0.3	170.9 ± 0.9	70.4 ± 0.9

PUC-Rio - Certificação Digital Nº 1312923/CA

Table H1: Experimental results of engine tests for each blend (Part 3 of 8).

Biodiesel content (%)	Ethanol content (%)	Lower Heating Value (kJ/kg)	Specific gravity (kg/ m³)	Maximum Pressure (bar)	CA of maximum pressure (°)	Maximum pressure increase rate (bar/°)	CA of maximum pressure increase rate (°)	Maximum gross heat release rate (J/°)	Ignition delay (°)	CA10 (°)	CA50 (°)	CA90 (°)	CA10 - CA90 (°)	Gross heat/Injected energy (%)
7	0	45.125	0.8395	68.20 ± 0.10	5.0 ± 0.0	6.4 ± 0.3	4.0 ± 0.0	76.8 ± 18.7	7.2 ± 0.9	1.5 ± 0.0	5.50 ± 0.0	21.50 ± 0.0	20.0 ± 0.0	86.8 ± 0.89
				76.50 ± 0.20	10.0 ± 0.0	5.5 ± 0.2	3.0 ± 0.0	90.8 ± 6.5	9.5 ± 0.0	1.5 ± 0.0	8.50 ± 0.0	26.50 ± 2.8	25.0 ± 0.0	82.7 ± 0.41
				85.70 ± 0.50	12.0 ± 0.0	5.0 ± 0.2	3.0 ± 0.0	137.9 ± 63.7	9.2 ± 0.9	1.5 ± 0.0	10.50 ± 0.0	29.50 ± 0.9	28.0 ± 2.8	81.6 ± 0.96
				101.90 ± 0.30	13.0 ± 0.0	3.9 ± 0.2	2.0 ± 0.0	153.6 ± 11.5	8.5 ± 0.0	1.5 ± 0.0	11.50 ± 0.0	33.80 ± 5.0	32.3 ± 0.9	84.4 ± 1.40
				78.00 ± 0.50	6.0 ± 0.0	7.8 ± 0.0	2.0 ± 0.0	65.5 ± 13.5	5.8 ± 0.9	-0.5 ± 0.0	4.50 ± 0.0	20.20 ± 0.0	20.7 ± 5.0	79.9 ± 2.70
				92.90 ± 0.30	9.0 ± 0.0	5.7 ± 0.3	1.0 ± 0.0	98.7 ± 1.8	6.5 ± 0.0	-0.5 ± 0.0	7.50 ± 0.0	24.50 ± 4.1	25.0 ± 0.0	78.3 ± 1.60
				106.30 ± 0.80	11.0 ± 0.0	4.4 ± 0.1	1.0 ± 0.0	136.2 ± 1.5	6.5 ± 0.0	0.5 ± 0.0	9.50 ± 0.0	29.80 ± 2.8	29.3 ± 4.1	79.6 ± 2.50
				124.30 ± 0.90	13.0 ± 0.0	3.6 ± 0.3	3.7 ± 0.9	183.1 ± 18.4	6.5 ± 0.0	1.5 ± 0.0	11.50 ± 0.0	35.50 ± 0.0	34.0 ± 2.8	79.5 ± 1.90
				85.90 ± 0.70	6.0 ± 0.0	7.7 ± 0.1	1.0 ± 0.0	72.5 ± 19.0	5.5 ± 0.0	-1.5 ± 0.0	4.20 ± 0.9	17.50 ± 2.8	19.0 ± 0.0	83.3 ± 1.00
				102.40 ± 0.20	9.0 ± 0.0	6.1 ± 0.1	0.0 ± 0.0	115.5 ± 10.2	5.5 ± 0.0	-1.5 ± 0.0	6.50 ± 0.9	21.50 ± 2.5	23.0 ± 2.8	81.2 ± 0.30
				119.60 ± 0.40	11.0 ± 0.0	5.3 ± 0.2	3.0 ± 0.0	168.2 ± 38.7	5.5 ± 0.0	-1.5 ± 0.0	8.80 ± 0.9	26.80 ± 2.8	28.3 ± 2.5	85.5 ± 0.90
				133.20 ± 0.60	10.0 ± 0.0	5.0 ± 0.2	2.0 ± 0.0	196.1 ± 15.1	4.8 ± 0.9	-0.5 ± 0.0	10.50 ± 0.0	36.50 ± 0.0	37.0 ± 2.8	80.5 ± 0.60
15	0	44.379	0.8437	67.90 ± 0.80	7.0 ± 2.8	6.6 ± 0.1	4.0 ± 0.0	76.0 ± 20.6	8.2 ± 0.9	1.8 ± 0.9	6.50 ± 0.0	19.50 ± 0.0	17.7 ± 0.9	84.1 ± 1.70
				76.20 ± 0.30	8.0 ± 0.0	6.5 ± 0.2	4.0 ± 0.0	93.3 ± 6.2	9.5 ± 0.0	2.5 ± 0.0	8.50 ± 0.0	26.50 ± 0.0	24.0 ± 0.0	80.8 ± 0.80
				84.50 ± 0.20	11.7 ± 2.5	5.4 ± 0.7	4.0 ± 0.0	108.6 ± 19.6	9.5 ± 0.0	2.5 ± 0.0	10.50 ± 0.0	28.50 ± 1.9	26.0 ± 0.0	79.9 ± 1.40
				91.20 ± 1.80	14.3 ± 1.9	4.5 ± 0.4	4.0 ± 0.0	142.8 ± 39.6	9.8 ± 0.9	3.5 ± 0.0	12.80 ± 0.9	32.80 ± 0.0	29.3 ± 1.9	82.0 ± 1.40
				78.70 ± 0.20	7.0 ± 0.0	7.4 ± 1.0	3.0 ± 0.0	77.3 ± 15.6	7.5 ± 0.0	0.5 ± 0.0	5.50 ± 0.0	23.50 ± 2.8	23.0 ± 0.0	86.4 ± 1.40
				91.70 ± 0.70	9.7 ± 0.9	6.9 ± 0.1	2.0 ± 0.0	115.1 ± 9.8	7.5 ± 0.0	0.5 ± 0.0	7.80 ± 0.9	24.50 ± 0.9	24.0 ± 2.8	82.5 ± 0.70
				107.10 ± 0.50	12.0 ± 0.0	4.6 ± 0.2	1.0 ± 0.0	146.4 ± 7.1	7.5 ± 0.0	0.5 ± 0.0	10.50 ± 0.0	27.20 ± 0.9	26.7 ± 0.9	83.0 ± 1.60
				115.80 ± 0.50	12.7 ± 1.9	3.4 ± 0.1	5.0 ± 0.0	202.0 ± 3.4	7.8 ± 0.9	2.5 ± 0.0	12.50 ± 0.0	33.20 ± 0.0	30.7 ± 0.9	87.2 ± 0.40
				85.20 ± 0.20	7.0 ± 0.0	7.7 ± 0.4	2.0 ± 0.0	85.2 ± 11.3	6.5 ± 0.0	-0.5 ± 0.0	4.50 ± 0.0	22.50 ± 2.8	23.0 ± 0.0	91.1 ± 0.50
				102.60 ± 0.70	9.0 ± 0.0	6.0 ± 0.4	0.7 ± 0.9	126.8 ± 10.5	6.5 ± 0.0	-0.5 ± 0.0	7.50 ± 0.0	22.50 ± 0.0	23.0 ± 2.8	88.5 ± 0.80
				117.90 ± 0.30	11.0 ± 0.0	5.2 ± 0.1	0.0 ± 0.0	165.0 ± 6.7	6.5 ± 0.0	-0.5 ± 0.0	9.50 ± 0.0	25.50 ± 0.0	26.0 ± 0.0	87.7 ± 0.70
				129.20 ± 0.40	11.0 ± 0.0	4.7 ± 0.0	3.0 ± 0.0	198.8 ± 28.4	6.5 ± 0.0	0.8 ± 0.9	11.50 ± 0.0	31.50 ± 0.0	30.7 ± 0.9	86.1 ± 0.50
15	5	43.560	0.8411	66.00 ± 0.50	8.3 ± 1.9	6.0 ± 0.4	5.0 ± 0.0	69.7 ± 5.0	6.5 ± 0.0	3.2 ± 0.9	7.50 ± 0.0	20.50 ± 0.0	17.3 ± 0.9	84.9 ± 5.90
				74.60 ± 0.20	9.0 ± 0.0	6.4 ± 0.0	5.0 ± 0.0	105.2 ± 17.6	9.8 ± 0.9	3.5 ± 0.0	9.50 ± 0.0	27.50 ± 2.5	24.0 ± 0.0	81.7 ± 1.50
				84.10 ± 0.80	13.0 ± 0.0	4.9 ± 0.2	4.7 ± 0.9	114.6 ± 32.6	10.5 ± 0.0	3.5 ± 0.0	11.50 ± 0.0	27.80 ± 2.8	24.3 ± 2.5	81.4 ± 0.30
				89.30 ± 0.60	13.0 ± 0.0	5.6 ± 0.1	4.0 ± 0.0	224.4 ± 166.6	10.5 ± 0.0	3.5 ± 0.0	11.50 ± 0.0	29.50 ± 0.0	26.0 ± 2.8	83.0 ± 1.30
				77.00 ± 0.30	5.0 ± 0.0	7.9 ± 0.1	4.0 ± 0.0	72.3 ± 10.4	8.5 ± 0.0	1.5 ± 0.0	6.50 ± 0.0	21.50 ± 0.0	20.0 ± 0.0	89.0 ± 0.70
				88.80 ± 0.30	11.0 ± 0.0	6.9 ± 0.1	3.0 ± 0.0	104.9 ± 1.1	8.5 ± 0.0	1.5 ± 0.0	9.20 ± 0.9	23.50 ± 2.8	22.0 ± 0.0	84.4 ± 2.00
				105.10 ± 0.60	13.0 ± 0.0	4.4 ± 0.1	3.0 ± 0.0	156.9 ± 32.7	8.5 ± 0.0	1.5 ± 0.0	11.50 ± 0.0	26.50 ± 0.9	25.0 ± 2.8	83.8 ± 2.20
				109.90 ± 0.40	13.0 ± 0.0	4.4 ± 0.2	6.0 ± 0.0	150.5 ± 15.3	8.5 ± 0.0	1.5 ± 0.0	11.50 ± 0.0	28.20 ± 0.0	26.7 ± 0.9	84.2 ± 0.30
				83.00 ± 0.50	8.0 ± 0.0	8.1 ± 0.1	3.0 ± 0.0	81.0 ± 6.0	7.5 ± 0.0	0.5 ± 0.0	6.50 ± 0.0	23.50 ± 0.0	23.0 ± 0.0	92.7 ± 2.70
				98.40 ± 0.60	10.7 ± 0.9	6.4 ± 0.2	2.0 ± 0.0	120.0 ± 16.3	7.5 ± 0.0	0.5 ± 0.0	8.50 ± 0.0	25.50 ± 2.8	25.0 ± 0.0	89.2 ± 2.30
				116.70 ± 0.20	12.0 ± 0.0	5.2 ± 0.2	1.0 ± 0.0	161.2 ± 12.1	6.8 ± 0.9	0.2 ± 0.9	10.50 ± 0.0	28.50 ± 0.0	28.3 ± 2.9	88.4 ± 0.40
				123.90 ± 0.20	12.0 ± 0.0	4.2 ± 0.3	4.0 ± 0.0	187.4 ± 5.9	6.5 ± 0.0	0.5 ± 0.0	10.50 ± 0.0	26.50 ± 0.0	26.0 ± 0.0	85.6 ± 0.50

PUC-Rio - Certificação Digital Nº 1312923/CA

Table H1: Experimental results of engine tests for each blend (Part 4 of 8).

Biodiesel content (%)	Ethanol content (%)	Lower Heating Value (kJ/kg)	Specific gravity (kg/m³)	Compression polytropic coefficient (-)	Expansion polytropic coefficient (-)	Injected energy (kJ)	Injected volume (μL)
7	0	45.125	0.8395	1.342 ± 0.001	1.410 ± 0.003	1.899 ± 0.004	50.1 ± 0.1
				1.343 ± 0.002	1.364 ± 0.004	3.050 ± 0.012	80.5 ± 0.3
				1.346 ± 0.001	1.337 ± 0.004	4.303 ± 0.016	113.6 ± 0.4
				1.344 ± 0.001	1.291 ± 0.002	5.689 ± 0.016	150.2 ± 0.4
				1.364 ± 0.008	1.371 ± 0.019	2.213 ± 0.008	58.4 ± 0.2
				1.366 ± 0.004	1.345 ± 0.004	3.631 ± 0.009	95.9 ± 0.2
				1.373 ± 0.001	1.323 ± 0.001	5.120 ± 0.015	135.2 ± 0.4
				1.371 ± 0.005	1.296 ± 0.010	6.727 ± 0.046	177.6 ± 1.2
				1.368 ± 0.002	1.388 ± 0.001	2.290 ± 0.010	60.4 ± 0.3
				1.367 ± 0.001	1.354 ± 0.000	3.682 ± 0.010	97.2 ± 0.3
				1.365 ± 0.001	1.329 ± 0.004	5.090 ± 0.007	134.4 ± 0.2
				1.374 ± 0.004	1.293 ± 0.003	6.674 ± 0.015	176.2 ± 0.4
15	0	44.379	0.8437	1.341 ± 0.001	1.413 ± 0.001	1.919 ± 0.023	51.3 ± 0.6
				1.366 ± 0.001	1.367 ± 0.003	3.147 ± 0.012	84.1 ± 0.3
				1.346 ± 0.002	1.339 ± 0.005	4.377 ± 0.018	116.9 ± 0.5
				1.353 ± 0.001	1.308 ± 0.003	5.353 ± 0.029	143.0 ± 0.8
				1.341 ± 0.004	1.395 ± 0.007	2.258 ± 0.007	60.3 ± 0.2
				1.345 ± 0.005	1.364 ± 0.006	3.772 ± 0.010	100.7 ± 0.3
				1.345 ± 0.004	1.335 ± 0.002	5.236 ± 0.010	139.8 ± 0.3
				1.348 ± 0.004	1.305 ± 0.002	6.494 ± 0.016	173.4 ± 0.4
				1.335 ± 0.001	1.400 ± 0.004	2.324 ± 0.004	62.1 ± 0.1
				1.338 ± 0.001	1.370 ± 0.003	3.691 ± 0.010	98.6 ± 0.3
				1.339 ± 0.001	1.343 ± 0.004	5.147 ± 0.011	137.5 ± 0.3
				1.340 ± 0.002	1.310 ± 0.001	6.519 ± 0.008	174.1 ± 0.2
15	5	43.560	0.8411	1.343 ± 0.001	1.412 ± 0.001	1.935 ± 0.029	52.8 ± 0.8
				1.347 ± 0.001	1.365 ± 0.001	3.138 ± 0.008	85.6 ± 0.2
				1.351 ± 0.001	1.348 ± 0.001	4.390 ± 0.033	119.8 ± 0.9
				1.349 ± 0.001	1.339 ± 0.002	4.740 ± 0.033	129.4 ± 0.9
				1.347 ± 0.003	1.404 ± 0.006	2.216 ± 0.006	60.5 ± 0.2
				1.349 ± 0.001	1.365 ± 0.002	3.646 ± 0.022	99.5 ± 0.6
				1.351 ± 0.000	1.342 ± 0.001	5.220 ± 0.023	142.5 ± 0.6
				1.346 ± 0.000	1.333 ± 0.001	5.603 ± 0.049	152.9 ± 1.3
				1.332 ± 0.001	1.400 ± 0.003	2.282 ± 0.012	62.3 ± 0.3
				1.330 ± 0.003	1.363 ± 0.004	3.774 ± 0.019	103.0 ± 0.5
				1.325 ± 0.005	1.335 ± 0.003	5.188 ± 0.006	141.6 ± 0.2
				1.334 ± 0.001	1.332 ± 0.001	5.946 ± 0.016	162.3 ± 0.4

Table H1: Experimental results of engine tests for each blend (Part 5 of 8).

(%)	Ethanol content (%)	Lower Heating Value (kJ/kg)	Specific gravity (kg/m³)	Engine speed (rpm)	Torque (N.m)	Fraction of B7 maximum torque (%)	Accelerator (%)	Brake Power (kW)	Lubricating oil temperature (°C)	Water temperature (°C)	Inlet air temperature (°C)	Relative humidity (%)	Fuel consumption (kg/h)	Dry air consumption (kg/h)	Air / Fuel Ratio (-)	Lambda (-)
PUC-Rio - Certificação Digital Nº 1312923/CA	10	42,736	0,8384	1,499 ± 5.3	80.6 ± 0.1	25.0	46.32 ± 0.18	12.7 ± 0.0	80.80 ± 1.16	82.47 ± 0.18	29.72 ± 0.37	49.47 ± 0.75	3.9 ± 0.2	256.6 ± 3.5	66.2 ± 1.3	4.80 ± 0.09
				1,506 ± 4.3	161.2 ± 0.2	50.0	56.83 ± 0.07	25.4 ± 0.1	83.46 ± 0.69	83.58 ± 0.08	30.67 ± 0.24	50.94 ± 0.09	6.6 ± 0.2	274.2 ± 3.4	41.5 ± 0.6	3.01 ± 0.05
				1,505 ± 6.0	226.6 ± 1.7	69.9	100.00 ± 0.00	35.7 ± 0.3	87.34 ± 0.32	84.50 ± 0.03	32.90 ± 0.14	51.94 ± 0.32	8.9 ± 0.0	292.4 ± 3.4	32.9 ± 0.4	2.39 ± 0.03
				1,797 ± 8.9	96.4 ± 1.6	25.0	54.22 ± 0.45	18.1 ± 0.3	90.10 ± 0.62	83.51 ± 0.04	34.48 ± 0.05	49.65 ± 0.11	5.5 ± 0.1	320.1 ± 2.8	57.7 ± 0.5	4.18 ± 0.04
				1,796 ± 2.5	192.9 ± 0.1	50.0	67.58 ± 0.09	36.3 ± 0.1	91.25 ± 0.07	84.46 ± 0.09	34.49 ± 0.03	49.90 ± 0.28	9.3 ± 0.1	362.4 ± 4.5	39.1 ± 0.5	2.84 ± 0.04
				1,804 ± 9.5	279.1 ± 3.6	72.3	100.00 ± 0.00	52.7 ± 0.7	91.37 ± 0.22	85.14 ± 0.05	28.77 ± 0.09	46.43 ± 0.86	12.7 ± 0.1	426.2 ± 7.4	33.5 ± 0.6	2.43 ± 0.04
				2,098 ± 1.6	93.3 ± 0.6	25.0	67.20 ± 0.01	20.5 ± 0.1	92.58 ± 0.30	83.69 ± 0.05	34.97 ± 0.07	49.00 ± 0.34	6.8 ± 0.1	384.1 ± 2.2	57.0 ± 0.5	4.13 ± 0.03
				2,100 ± 0.2	186.4 ± 0.6	50.0	79.43 ± 0.01	41.0 ± 0.1	93.60 ± 0.01	84.63 ± 0.06	35.00 ± 0.01	49.42 ± 0.34	10.9 ± 0.1	447.8 ± 2.0	41.0 ± 0.2	2.97 ± 0.01
				2,102 ± 1.9	278.3 ± 0.3	75.3	100.00 ± 0.00	61.2 ± 0.1	93.81 ± 0.14	85.34 ± 0.04	29.50 ± 0.00	48.42 ± 0.11	15.3 ± 0.1	534.4 ± 1.9	34.9 ± 0.1	2.53 ± 0.01
	15	41,906	0,8358	1,506 ± 1.8	80.8 ± 0.0	25.0	46.40 ± 0.15	12.7 ± 0.0	87.26 ± 0.30	83.15 ± 0.02	34.02 ± 0.10	52.58 ± 0.63	4.0 ± 0.0	253.2 ± 3.5	63.6 ± 0.9	4.70 ± 0.07
				1,505 ± 4.5	160.4 ± 0.4	50.0	58.07 ± 0.02	25.3 ± 0.1	86.80 ± 0.00	83.70 ± 0.04	27.88 ± 0.05	52.33 ± 0.50	6.7 ± 0.0	280.1 ± 4.9	41.6 ± 0.7	3.07 ± 0.05
				1,503 ± 4.6	220.1 ± 0.7	67.9	100.00 ± 0.00	34.6 ± 0.1	86.11 ± 0.98	84.28 ± 0.15	32.40 ± 0.40	49.66 ± 1.09	8.7 ± 0.2	289.8 ± 8.1	33.5 ± 1.0	2.47 ± 0.07
				1,793 ± 0.7	97.3 ± 0.0	25.0	54.80 ± 0.11	18.3 ± 0.0	89.57 ± 0.29	83.51 ± 0.13	33.90 ± 0.00	54.19 ± 0.20	5.7 ± 0.2	314.4 ± 8.0	55.6 ± 1.5	4.10 ± 0.11
				1,794 ± 2.3	193.8 ± 0.1	50.0	69.01 ± 0.17	36.4 ± 0.0	89.62 ± 0.38	84.23 ± 0.39	33.79 ± 0.02	53.64 ± 0.23	9.6 ± 0.0	368.0 ± 1.9	38.5 ± 0.2	2.84 ± 0.01
				1,804 ± 1.9	227.1 ± 1.3	58.8	100.00 ± 0.00	42.9 ± 0.2	89.49 ± 0.53	84.60 ± 0.02	33.50 ± 0.13	50.97 ± 0.06	11.0 ± 0.0	388.0 ± 1.1	35.3 ± 0.1	2.61 ± 0.01
				2,100 ± 3.6	93.1 ± 0.1	25.0	67.88 ± 0.13	20.5 ± 0.0	90.24 ± 0.19	83.54 ± 0.04	33.80 ± 0.00	53.97 ± 0.23	6.8 ± 0.0	381.1 ± 1.7	55.7 ± 0.2	4.11 ± 0.02
				2,101 ± 1.1	186.6 ± 0.4	50.0	81.04 ± 0.00	41.1 ± 0.1	90.91 ± 0.31	84.19 ± 0.04	27.67 ± 0.09	57.25 ± 0.12	11.2 ± 0.1	457.6 ± 1.6	40.8 ± 0.2	3.01 ± 0.01
				2,101 ± 0.9	247.5 ± 0.6	66.9	100.00 ± 0.00	54.5 ± 0.1	93.06 ± 0.31	85.05 ± 0.07	34.25 ± 0.07	51.63 ± 0.14	14.2 ± 0.1	496.1 ± 4.7	35.0 ± 0.3	2.58 ± 0.02
15	20	41,072	0,8332	1,503 ± 4.9	82.3 ± 0.1	25.0	48.02 ± 0.02	13.0 ± 0.0	87.09 ± 0.15	83.03 ± 0.03	31.24 ± 0.07	52.69 ± 0.09	4.1 ± 0.1	259.2 ± 0.5	62.8 ± 0.3	4.72 ± 0.02
				1,504 ± 1.0	161.2 ± 0.3	50.0	59.00 ± 0.01	25.4 ± 0.1	87.43 ± 0.23	83.79 ± 0.05	29.14 ± 0.35	50.26 ± 1.38	6.9 ± 0.1	281.6 ± 1.4	40.8 ± 0.2	3.07 ± 0.02
				1,499 ± 7.1	204.0 ± 3.6	62.9	100.00 ± 0.00	32.0 ± 0.6	84.15 ± 1.10	83.81 ± 0.12	29.25 ± 0.23	53.75 ± 0.51	8.3 ± 0.1	292.2 ± 4.1	35.3 ± 0.5	2.65 ± 0.04
				1,805 ± 1.4	97.7 ± 0.1	25.0	56.96 ± 0.12	18.5 ± 0.0	90.13 ± 0.45	83.51 ± 0.09	34.94 ± 0.58	45.96 ± 1.19	5.8 ± 0.1	328.0 ± 1.4	56.8 ± 0.3	4.27 ± 0.02
				1,797 ± 3.6	194.7 ± 0.1	50.0	71.03 ± 0.08	36.6 ± 0.1	88.74 ± 0.73	84.04 ± 0.05	31.03 ± 0.15	53.00 ± 0.03	9.7 ± 0.1	368.6 ± 1.8	37.9 ± 0.2	2.85 ± 0.01
				1,801 ± 2.3	214.0 ± 2.3	55.4	100.00 ± 0.00	40.4 ± 0.4	87.93 ± 1.33	84.20 ± 0.15	30.04 ± 0.32	54.27 ± 0.34	10.6 ± 0.1	382.9 ± 4.8	36.2 ± 0.5	2.72 ± 0.04
				2,098 ± 2.6	92.5 ± 0.4	25.0	69.72 ± 0.03	20.3 ± 0.1	89.60 ± 0.05	83.33 ± 0.05	28.23 ± 0.07	53.79 ± 0.10	7.0 ± 0.0	392.1 ± 0.2	56.0 ± 0.1	4.21 ± 0.01
				2,100 ± 1.8	187.6 ± 0.1	50.0	82.12 ± 0.06	41.2 ± 0.0	91.88 ± 0.36	84.40 ± 0.10	34.58 ± 0.37	40.88 ± 0.80	11.5 ± 0.1	456.9 ± 2.5	39.6 ± 0.2	2.98 ± 0.02
				2,100 ± 6.0	226.7 ± 1.9	61.3	100.00 ± 0.00	49.9 ± 0.4	90.92 ± 0.35	84.70 ± 0.00	30.73 ± 0.09	54.23 ± 0.18	13.5 ± 0.1	493.8 ± 2.2	36.7 ± 0.2	2.76 ± 0.01
7	0	45,125	0,8395	1,504 ± 2.2	80.5 ± 0.1	25.0	45.66 ± 0.02	12.7 ± 0.0	87.34 ± 0.09	83.21 ± 0.04	33.03 ± 0.09	53.25 ± 0.23	3.8 ± 0.0	256.2 ± 1.8	66.8 ± 0.5	4.62 ± 0.03
				1,508 ± 1.6	160.0 ± 0.1	50.0	55.20 ± 0.05	25.3 ± 0.0	87.29 ± 0.10	83.89 ± 0.04	32.21 ± 0.04	54.84 ± 0.16	6.2 ± 0.1	276.5 ± 1.7	44.6 ± 0.3	3.09 ± 0.02
				1,506 ± 3.9	240.5 ± 0.1	75.0	62.54 ± 0.02	37.9 ± 0.1	88.12 ± 0.16	84.45 ± 0.18	32.20 ± 0.00	55.20 ± 0.05	8.7 ± 0.1	299.3 ± 1.0	34.4 ± 0.1	2.38 ± 0.01
				1,504 ± 7.2	314.8 ± 2.5	97.1	100.00 ± 0.00	49.6 ± 0.5	90.80 ± 0.01	85.89 ± 0.05	32.67 ± 0.09	58.32 ± 0.07	11.4 ± 0.1	325.8 ± 3.3	28.7 ± 0.3	1.99 ± 0.02
				1,801 ± 1.5	96.0 ± 0.1	25.0	52.79 ± 0.03	18.1 ± 0.0	90.83 ± 0.17	83.64 ± 0.06	33.00 ± 0.00	54.14 ± 0.18	5.3 ± 0.1	320.3 ± 2.8	60.6 ± 0.6	4.19 ± 0.04
				1,803 ± 0.6	193.2 ± 0.1	50.0	65.48 ± 0.02	36.5 ± 0.0	92.15 ± 0.09	84.55 ± 0.04	32.90 ± 0.00	53.93 ± 0.04	8.7 ± 0.0	366.2 ± 1.7	41.9 ± 0.2	2.90 ± 0.01
				1,795 ± 0.9	289.1 ± 0.1	75.0	76.50 ± 0.02	54.3 ± 0.0	91.79 ± 0.15	85.33 ± 0.11	32.57 ± 0.08	54.37 ± 0.07	12.3 ± 0.0	416.7 ± 4.7	33.8 ± 0.4	2.34 ± 0.03
				1,801 ± 12.3	374.0 ± 2.5	96.9	100.00 ± 0.00	70.6 ± 0.7	93.76 ± 0.19	86.33 ± 0.07	33.10 ± 0.00	55.30 ± 0.23	15.9 ± 0.3	468.7 ± 7.9	29.4 ± 0.5	2.03 ± 0.04
				2,094 ± 1.7	93.5 ± 0.0	25.0	64.83 ± 0.09	20.5 ± 0.0	90.46 ± 0.02	83.42 ± 0.23	32.70 ± 0.01	55.25 ± 0.08	6.4 ± 0.1	383.2 ± 1.8	60.1 ± 0.4	4.16 ± 0.03
				2,097 ± 0.7	186.0 ± 0.0	50.0	77.00 ± 0.02	40.8 ± 0.0	92.11 ± 0.13	84.52 ± 0.01	32.60 ± 0.00	55.97 ± 0.08	10.3 ± 0.0	439.8 ± 2.4	42.9 ± 0.2	2.97 ± 0.02
				2,095 ± 1.1	278.2 ± 0.0	75.0	88.31 ± 0.09	61.0 ± 0.0	93.78 ± 0.24	85.48 ± 0.02	32.90 ± 0.00	56.59 ± 0.12	14.3 ± 0.0	514.9 ± 3.2	36.1 ± 0.2	2.50 ± 0.02
				2,099 ± 1.7	360.0 ± 0.5	97.4	100.00 ± 0.00	79.1 ± 0.1	96.43 ± 0.15	86.44 ± 0.01	33.75 ± 0.07	54.11 ± 0.20	18.1 ± 0.0	551.6 ± 2.8	30.4 ± 0.2	2.10 ± 0.01

PUC-Rio - Certificação Digital Nº 1312923/CA

Table H1: Experimental results of engine tests for each blend (Part 6 of 8).

Biodiesel content (%)	Ethanol content (%)	Lower Heating Value (kJ/kg)	Specific gravity (kg/m³)	Specific Fuel Consumption (kg/(kW.h))	Ethanol sfc (kg/(kW.h))	Ethanol Conversion (MJ/(kW.h))	Exhaust Gas Temperature (°C)	Exhaust Gas pressure (bar)	BMEP (bar)	IMEP (bar)	Indicated efficiency (%)	Fuel conversion efficiency (%)	Volumetric efficiency (%)	Mechanical efficiency (%)
15	10	42,736	0,8384	0.307 ± 0.013	0.366 ± 0.049	9.81 ± 1.31	224.3 ± 7.1	1.0119 ± 0.1578	2.4 ± 0.00	4.4 ± 0.01	51.3 ± 2.2	27.5 ± 1.2	110.6 ± 2.1	53.6 ± 3.2
				0.260 ± 0.009	0.351 ± 0.029	9.43 ± 0.79	322.3 ± 8.0	1.0145 ± 0.0249	4.7 ± 0.01	7.0 ± 0.01	48.1 ± 1.7	32.4 ± 1.1	117.7 ± 1.8	67.3 ± 3.4
				0.249 ± 0.002	0.351 ± 0.036	9.43 ± 0.96	402.4 ± 5.4	1.0234 ± 0.0844	6.6 ± 0.05	9.3 ± 0.07	47.6 ± 0.4	33.9 ± 0.3	125.8 ± 1.7	71.1 ± 0.9
				0.306 ± 0.007	0.390 ± 0.027	10.47 ± 0.73	282.0 ± 10.8	1.0130 ± 0.0493	2.8 ± 0.05	5.3 ± 0.09	52.1 ± 1.1	27.5 ± 0.6	115.2 ± 1.2	52.9 ± 1.6
				0.256 ± 0.003	0.324 ± 0.024	8.71 ± 0.63	367.3 ± 1.5	1.0184 ± 0.0667	5.6 ± 0.00	8.5 ± 0.01	49.4 ± 0.6	32.9 ± 0.4	130.6 ± 1.6	66.7 ± 1.1
				0.241 ± 0.004	0.311 ± 0.013	8.35 ± 0.36	404.6 ± 1.6	1.0355 ± 0.1169	8.2 ± 0.11	11.3 ± 0.15	48.5 ± 0.8	34.9 ± 0.6	151.5 ± 2.8	72.0 ± 1.8
				0.329 ± 0.006	0.445 ± 0.009	11.94 ± 0.23	280.5 ± 3.1	1.0168 ± 0.0556	2.7 ± 0.02	5.5 ± 0.04	52.0 ± 1.0	25.6 ± 0.5	118.5 ± 0.7	49.3 ± 1.4
				0.267 ± 0.002	0.378 ± 0.008	10.15 ± 0.21	347.5 ± 0.6	1.0217 ± 0.0218	5.4 ± 0.02	8.7 ± 0.03	50.2 ± 0.3	31.6 ± 0.2	138.1 ± 0.7	62.8 ± 0.6
				0.250 ± 0.001	0.363 ± 0.016	9.74 ± 0.43	397.2 ± 0.5	1.0425 ± 0.0178	8.1 ± 0.01	11.6 ± 0.01	47.8 ± 0.2	33.7 ± 0.1	163.2 ± 0.6	70.4 ± 0.4
15	15	41,906	0,8358	0.313 ± 0.002	0.387 ± 0.031	10.39 ± 0.82	255.1 ± 6.4	1.0107 ± 0.0142	2.4 ± 0.00	4.4 ± 0.00	50.7 ± 0.3	27.5 ± 0.2	108.8 ± 1.6	54.2 ± 0.5
				0.266 ± 0.001	0.359 ± 0.018	9.65 ± 0.49	329.2 ± 0.7	1.0214 ± 0.1951	4.7 ± 0.01	7.0 ± 0.02	48.2 ± 0.3	32.3 ± 0.2	119.4 ± 2.1	67.0 ± 0.5
				0.250 ± 0.005	0.317 ± 0.023	8.50 ± 0.61	397.8 ± 5.1	1.0213 ± 0.1507	6.4 ± 0.02	9.2 ± 0.03	49.2 ± 1.0	34.4 ± 0.7	124.7 ± 3.8	69.8 ± 2.1
				0.310 ± 0.010	0.385 ± 0.017	10.34 ± 0.46	278.0 ± 5.2	1.0148 ± 0.1213	2.8 ± 0.00	5.3 ± 0.00	52.0 ± 1.7	27.8 ± 0.9	113.6 ± 2.9	53.4 ± 2.4
				0.263 ± 0.000	0.349 ± 0.015	9.36 ± 0.40	354.5 ± 2.2	1.0101 ± 0.1231	5.7 ± 0.00	8.5 ± 0.00	49.1 ± 0.1	32.7 ± 0.0	132.8 ± 0.7	66.6 ± 0.1
				0.256 ± 0.002	0.351 ± 0.008	9.42 ± 0.23	384.6 ± 0.7	1.0189 ± 0.0182	6.6 ± 0.04	9.8 ± 0.06	49.4 ± 0.3	33.5 ± 0.2	139.2 ± 0.7	67.9 ± 0.6
				0.334 ± 0.001	0.441 ± 0.005	11.85 ± 0.14	267.6 ± 0.4	1.0193 ± 0.0071	2.7 ± 0.00	5.5 ± 0.01	51.6 ± 0.1	25.7 ± 0.1	117.6 ± 0.6	49.8 ± 0.2
				0.274 ± 0.002	0.384 ± 0.005	10.32 ± 0.13	323.9 ± 2.1	1.0331 ± 0.0378	5.5 ± 0.01	8.9 ± 0.02	51.0 ± 0.4	31.4 ± 0.2	140.1 ± 0.7	61.6 ± 0.6
				0.261 ± 0.001	0.378 ± 0.010	10.15 ± 0.27	386.7 ± 0.1	1.0268 ± 0.0636	7.2 ± 0.02	10.5 ± 0.02	47.9 ± 0.3	33.0 ± 0.2	153.1 ± 1.6	68.8 ± 0.5
15	20	41,072	0,8332	0.319 ± 0.005	0.398 ± 0.022	10.69 ± 0.58	257.0 ± 4.0	1.0197 ± 0.1084	2.4 ± 0.00	4.4 ± 0.01	50.7 ± 0.8	27.5 ± 0.4	111.0 ± 0.5	54.3 ± 1.2
				0.272 ± 0.003	0.361 ± 0.013	9.70 ± 0.35	335.0 ± 3.0	1.0169 ± 0.1102	4.7 ± 0.01	6.8 ± 0.01	46.7 ± 0.4	32.3 ± 0.3	120.1 ± 1.6	69.1 ± 0.9
				0.259 ± 0.006	0.335 ± 0.016	8.99 ± 0.43	362.4 ± 11.2	1.0219 ± 0.2253	6.0 ± 0.11	8.6 ± 0.15	48.7 ± 1.0	33.9 ± 0.7	125.4 ± 2.1	69.5 ± 2.1
				0.313 ± 0.003	0.380 ± 0.012	10.19 ± 0.32	280.6 ± 7.5	1.0214 ± 0.0471	2.9 ± 0.00	5.3 ± 0.00	52.4 ± 0.5	28.0 ± 0.3	116.7 ± 2.0	53.5 ± 0.7
				0.265 ± 0.002	0.337 ± 0.010	9.04 ± 0.28	345.1 ± 7.0	1.0233 ± 0.0516	5.7 ± 0.00	8.6 ± 0.00	50.1 ± 0.4	33.0 ± 0.2	132.1 ± 1.0	65.9 ± 0.7
				0.263 ± 0.004	0.346 ± 0.006	9.29 ± 0.16	364.7 ± 3.2	1.0254 ± 0.0724	6.3 ± 0.07	9.4 ± 0.10	50.0 ± 0.7	33.4 ± 0.5	137.0 ± 2.3	66.8 ± 1.4
				0.344 ± 0.002	0.463 ± 0.004	12.44 ± 0.10	258.3 ± 0.1	1.0267 ± 0.0031	2.7 ± 0.01	5.5 ± 0.03	52.3 ± 0.3	25.5 ± 0.2	119.9 ± 0.3	48.7 ± 0.4
				0.280 ± 0.001	0.386 ± 0.003	10.36 ± 0.09	334.0 ± 2.4	1.0283 ± 0.0511	5.5 ± 0.00	8.8 ± 0.00	50.1 ± 0.2	31.3 ± 0.2	139.9 ± 1.7	62.6 ± 0.4
				0.270 ± 0.003	0.380 ± 0.007	10.20 ± 0.19	359.9 ± 1.1	1.0335 ± 0.0267	6.6 ± 0.05	9.9 ± 0.08	48.5 ± 0.5	32.5 ± 0.3	151.8 ± 0.9	67.0 ± 0.9
7	0	45,125	0,8395	0.302 ± 0.001	[redacted]	13.64 ± 0.05	244.4 ± 0.1	1.0179 ± 0.0991	2.4 ± 0.00	4.2 ± 0.00	47.6 ± 0.2	26.4 ± 0.1	109.9 ± 0.9	55.5 ± 0.3
				0.245 ± 0.002		11.06 ± 0.11	329.4 ± 1.1	1.0201 ± 0.0151	4.7 ± 0.00	6.8 ± 0.01	47.6 ± 0.5	32.6 ± 0.3	118.2 ± 0.8	68.4 ± 0.9
				0.230 ± 0.002		10.37 ± 0.08	408.2 ± 2.2	1.0236 ± 0.1315	7.0 ± 0.00	9.6 ± 0.01	47.5 ± 0.3	34.7 ± 0.3	128.2 ± 0.6	73.1 ± 0.8
				0.229 ± 0.003		10.35 ± 0.14	486.3 ± 1.0	1.0260 ± 0.3298	9.2 ± 0.07	12.4 ± 0.10	46.7 ± 0.6	34.8 ± 0.5	139.9 ± 1.6	74.4 ± 1.5
				0.292 ± 0.003		13.17 ± 0.15	281.3 ± 2.3	1.0213 ± 0.0800	2.8 ± 0.00	5.2 ± 0.00	50.9 ± 0.6	27.3 ± 0.3	114.8 ± 1.0	53.7 ± 0.8
				0.240 ± 0.001		10.82 ± 0.02	366.8 ± 1.8	1.0213 ± 0.0973	5.6 ± 0.00	8.4 ± 0.00	49.6 ± 0.1	33.3 ± 0.1	131.1 ± 0.7	67.1 ± 0.2
				0.227 ± 0.001		10.25 ± 0.03	418.7 ± 0.3	1.0342 ± 0.1929	8.4 ± 0.00	12.0 ± 0.00	49.7 ± 0.1	35.1 ± 0.1	150.0 ± 1.8	70.7 ± 0.3
				0.226 ± 0.004		10.19 ± 0.20	477.6 ± 2.1	1.0346 ± 0.0920	10.9 ± 0.07	15.0 ± 0.10	48.5 ± 0.9	35.3 ± 0.7	168.1 ± 3.1	72.9 ± 2.0
				0.311 ± 0.004		14.03 ± 0.17	266.1 ± 0.2	1.0229 ± 0.0253	2.7 ± 0.00	5.5 ± 0.00	51.9 ± 0.6	25.7 ± 0.3	118.2 ± 0.6	49.4 ± 0.9
				0.251 ± 0.001		11.33 ± 0.03	332.9 ± 0.9	1.0243 ± 0.0284	5.4 ± 0.00	8.7 ± 0.00	51.1 ± 0.1	31.8 ± 0.1	135.6 ± 0.8	62.2 ± 0.2
				0.234 ± 0.000		10.55 ± 0.01	390.0 ± 2.2	1.0320 ± 0.0369	8.1 ± 0.00	11.9 ± 0.00	50.0 ± 0.1	34.1 ± 0.0	159.0 ± 1.0	68.2 ± 0.1
				0.229 ± 0.001		10.34 ± 0.02	478.5 ± 0.2	1.0385 ± 0.1324	10.5 ± 0.01	14.7 ± 0.02	48.7 ± 0.1	34.8 ± 0.1	170.0 ± 1.0	71.5 ± 0.2

PUC-Rio - Certificação Digital Nº 1312923/CA

Table H1: Experimental results of engine tests for each blend (Part 7 of 8).

Biodiesel content (%)	Ethanol content (%)	Lower Heating Value (kJ/kg)	Specific gravity (kg/m³)	Maximum Pressure (bar)	CA of maximum pressure (°)	Maximum pressure increase rate (bar/°)	CA of maximum pressure increase rate (°)	Maximum gross heat release rate (J/°)	Ignition delay (°)	CA10 (°)	CA50 (°)	CA90 (°)	CA90 – CA10 (°)	Q/Injected energy (%)
15	10	42,736	0,8384	67.70 ± 0.50	7.0 ± 0.0	7.3 ± 0.0	6.0 ± 0.0	69.9 ± 11.9	7.5 ± 0.0	3.5 ± 0.0	5.5 ± 0.0	19.5 ± 2.8	16.0 ± 2.8	89.6 ± 5.50
				74.30 ± 0.00	10.0 ± 0.0	7.2 ± 0.2	6.0 ± 0.0	139.0 ± 64.5	10.5 ± 0.0	4.5 ± 0.0	10.5 ± 0.0	26.5 ± 0.0	22.0 ± 0.0	82.0 ± 4.00
				79.70 ± 1.00	12.0 ± 0.0	6.5 ± 0.3	6.0 ± 0.0	122.8 ± 44.1	10.8 ± 0.9	4.5 ± 0.0	11.5 ± 0.0	28.5 ± 0.0	24.0 ± 0.0	81.3 ± 1.50
				76.20 ± 0.40	6.0 ± 0.0	7.5 ± 1.0	5.0 ± 0.0	75.6 ± 20.0	7.5 ± 0.0	2.5 ± 0.0	7.2 ± 0.9	22.5 ± 0.0	20.0 ± 0.0	89.8 ± 0.90
				88.10 ± 0.50	11.0 ± 0.0	6.4 ± 0.1	4.0 ± 0.0	108.7 ± 52.9	8.5 ± 0.0	2.2 ± 0.9	9.5 ± 0.0	24.5 ± 0.0	22.3 ± 0.9	85.1 ± 0.90
				99.30 ± 1.30	13.3 ± 0.0	4.5 ± 0.5	4.0 ± 0.0	184.9 ± 129.7	8.5 ± 0.0	2.8 ± 0.9	12.5 ± 0.0	26.5 ± 0.0	23.7 ± 0.9	83.7 ± 3.40
				82.20 ± 0.80	5.0 ± 0.0	7.3 ± 0.2	4.0 ± 0.0	82.1 ± 5.8	8.5 ± 0.0	1.5 ± 0.0	6.5 ± 0.0	20.5 ± 0.0	19.0 ± 0.0	92.9 ± 1.80
				96.30 ± 0.50	11.0 ± 0.0	5.4 ± 0.1	2.3 ± 0.9	130.8 ± 10.3	7.5 ± 0.0	0.5 ± 0.0	9.5 ± 0.0	22.5 ± 0.0	22.0 ± 0.0	88.3 ± 1.00
				110.00 ± 0.80	11.0 ± 0.0	3.8 ± 0.0	2.3 ± 0.9	165.3 ± 24.8	8.5 ± 0.0	1.5 ± 0.0	11.5 ± 0.0	25.5 ± 0.0	24.0 ± 0.0	84.8 ± 0.50
15	15	41,906	0,8358	65.20 ± 0.60	9.0 ± 0.0	6.0 ± 0.1	7.3 ± 0.9	65.2 ± 4.1	6.5 ± 0.0	4.5 ± 0.0	7.5 ± 0.0	21.8 ± 1.9	17.3 ± 1.9	89.4 ± 1.00
				75.40 ± 0.30	8.0 ± 0.0	6.8 ± 0.2	7.0 ± 0.0	94.1 ± 25.6	9.8 ± 0.9	4.5 ± 0.0	9.5 ± 0.0	25.8 ± 1.9	21.3 ± 1.9	82.3 ± 0.90
				79.20 ± 0.40	13.0 ± 0.0	6.5 ± 0.3	6.0 ± 0.0	114.5 ± 11.4	11.2 ± 0.9	4.5 ± 0.0	11.5 ± 0.0	28.5 ± 0.0	24.0 ± 0.0	84.8 ± 2.40
				75.20 ± 0.90	7.0 ± 0.0	7.8 ± 0.1	6.0 ± 0.0	75.5 ± 10.7	6.2 ± 0.9	3.5 ± 0.0	7.8 ± 0.9	21.5 ± 2.8	18.0 ± 2.8	89.2 ± 4.30
				84.50 ± 0.20	9.0 ± 0.0	6.7 ± 0.1	5.0 ± 0.0	100.2 ± 4.6	9.2 ± 0.9	3.5 ± 0.0	10.5 ± 0.0	25.5 ± 0.0	22.0 ± 0.0	84.7 ± 0.50
				90.80 ± 0.50	13.0 ± 0.0	6.1 ± 0.3	6.0 ± 0.0	127.7 ± 5.8	8.2 ± 0.9	4.5 ± 0.0	11.5 ± 0.0	26.5 ± 0.0	22.0 ± 0.0	85.7 ± 0.20
				81.70 ± 2.70	6.0 ± 0.0	8.0 ± 0.7	5.0 ± 0.0	81.7 ± 21.9	7.8 ± 0.9	2.5 ± 0.0	7.5 ± 0.0	21.5 ± 0.0	19.0 ± 0.0	93.2 ± 0.50
				98.00 ± 0.70	8.0 ± 0.0	7.0 ± 0.2	3.0 ± 0.0	131.2 ± 22.7	7.8 ± 0.9	1.5 ± 0.0	9.5 ± 0.0	26.5 ± 0.0	25.0 ± 0.0	92.1 ± 0.50
				100.40 ± 1.10	13.0 ± 0.0	4.6 ± 0.3	4.0 ± 0.0	146.1 ± 40.5	7.5 ± 0.0	2.8 ± 0.9	11.5 ± 0.0	25.5 ± 2.8	22.7 ± 2.9	84.5 ± 1.10
15	20	41,072	0,8332	65.30 ± 0.40	9.7 ± 0.9	6.6 ± 0.4	8.0 ± 0.0	69.3 ± 1.5	6.5 ± 0.0	5.5 ± 0.0	7.5 ± 0.0	20.5 ± 0.0	15.0 ± 0.0	88.7 ± 1.60
				72.70 ± 0.70	10.0 ± 0.0	6.3 ± 0.7	9.0 ± 0.0	90.4 ± 3.7	8.2 ± 0.9	6.5 ± 0.0	10.5 ± 0.0	23.8 ± 0.9	17.3 ± 0.9	79.8 ± 0.50
				76.70 ± 0.50	13.0 ± 0.0	4.5 ± 0.5	8.0 ± 0.0	109.1 ± 20.7	10.8 ± 0.9	5.5 ± 0.0	11.5 ± 0.0	28.5 ± 0.0	23.0 ± 0.0	83.8 ± 0.30
				73.40 ± 0.30	8.0 ± 0.0	6.3 ± 0.4	7.0 ± 0.0	81.0 ± 3.7	6.5 ± 0.0	4.5 ± 0.0	8.5 ± 0.0	21.5 ± 0.0	17.0 ± 0.0	92.2 ± 1.00
				85.90 ± 0.60	10.0 ± 0.0	7.0 ± 0.4	6.0 ± 0.0	97.6 ± 5.2	9.5 ± 0.0	3.5 ± 0.0	11.2 ± 0.9	25.8 ± 0.9	22.3 ± 0.9	86.7 ± 0.60
				87.70 ± 0.70	14.0 ± 0.0	6.4 ± 0.3	6.7 ± 0.9	106.4 ± 3.8	7.8 ± 0.9	4.5 ± 0.0	11.8 ± 0.9	26.5 ± 0.0	22.0 ± 0.0	86.9 ± 1.60
				81.70 ± 0.30	7.0 ± 0.0	7.6 ± 0.2	5.0 ± 0.0	90.7 ± 8.5	7.8 ± 0.9	2.5 ± 0.0	7.5 ± 0.0	22.5 ± 0.0	20.0 ± 0.0	94.5 ± 0.70
				94.30 ± 0.50	9.0 ± 0.0	6.0 ± 0.3	4.0 ± 0.0	138.1 ± 9.6	8.5 ± 0.0	2.2 ± 0.9	9.8 ± 0.9	23.8 ± 0.9	21.6 ± 1.3	89.0 ± 0.70
				96.30 ± 0.80	14.0 ± 0.0	5.3 ± 0.2	5.0 ± 0.0	167.3 ± 36.7	7.5 ± 0.0	3.5 ± 0.0	12.5 ± 0.0	25.5 ± 0.0	22.0 ± 0.0	87.0 ± 0.40
7	0	45,125	0,8395	66.80 ± 0.20	5.0 ± 0.0	6.5 ± 0.1	4.0 ± 0.0	76.7 ± 22.9	8.2 ± 0.9	1.5 ± 0.0	6.5 ± 0.0	21.5 ± 0.0	20.0 ± 0.0	82.7 ± 0.89
				73.80 ± 0.20	10.0 ± 0.0	6.3 ± 0.1	4.0 ± 0.0	83.8 ± 4.2	9.5 ± 0.0	2.5 ± 0.0	8.5 ± 0.0	26.5 ± 0.0	24.0 ± 0.0	81.0 ± 1.40
				84.80 ± 0.50	12.0 ± 0.0	4.9 ± 0.1	3.0 ± 0.0	125.0 ± 47.0	9.5 ± 0.0	2.5 ± 0.0	10.5 ± 0.0	27.5 ± 0.0	25.0 ± 0.0	81.0 ± 0.80
				95.80 ± 0.10	13.0 ± 0.0	3.0 ± 0.0	2.0 ± 0.0	140.2 ± 3.6	8.5 ± 0.0	2.5 ± 0.0	11.5 ± 0.0	31.5 ± 0.0	29.0 ± 0.0	80.5 ± 1.00
				76.30 ± 0.30	6.0 ± 0.0	7.6 ± 0.2	2.0 ± 0.0	100.9 ± 56.5	7.5 ± 0.0	-0.5 ± 0.0	4.5 ± 0.0	21.2 ± 1.9	21.7 ± 1.9	87.3 ± 0.70
				92.00 ± 0.10	9.0 ± 0.0	5.4 ± 0.2	1.0 ± 0.0	144.6 ± 90.7	7.5 ± 0.0	-0.5 ± 0.0	7.5 ± 0.0	24.5 ± 0.0	25.0 ± 0.0	85.2 ± 0.30
				105.90 ± 0.30	11.0 ± 0.0	3.9 ± 0.2	1.0 ± 0.0	158.9 ± 1.1	7.5 ± 0.0	0.5 ± 0.0	10.5 ± 0.0	28.2 ± 1.8	27.7 ± 1.8	86.4 ± 1.40
				120.20 ± 0.60	13.0 ± 0.0	3.2 ± 0.2	4.0 ± 0.0	213.0 ± 13.2	7.5 ± 0.0	2.2 ± 0.9	11.8 ± 0.9	33.8 ± 0.9	31.6 ± 1.3	85.6 ± 1.70
				83.60 ± 0.20	6.0 ± 0.0	7.6 ± 0.2	1.0 ± 0.0	68.6 ± 3.9	6.5 ± 0.0	-0.8 ± 0.9	4.5 ± 0.0	21.5 ± 0.0	22.3 ± 0.9	92.4 ± 1.40
				100.10 ± 0.30	9.0 ± 0.0	4.7 ± 0.1	0.0 ± 0.0	127.0 ± 18.6	6.5 ± 0.0	-0.5 ± 0.0	7.5 ± 0.0	23.5 ± 0.0	24.0 ± 0.0	89.9 ± 0.90
				116.80 ± 0.60	11.0 ± 0.0	4.2 ± 0.3	3.0 ± 0.0	167.4 ± 16.2	6.5 ± 0.0	-0.5 ± 0.0	9.5 ± 0.0	26.5 ± 0.0	27.0 ± 0.0	88.5 ± 1.20
				130.20 ± 0.40	10.0 ± 0.0	4.4 ± 0.1	2.0 ± 0.0	214.2 ± 8.9	5.5 ± 0.0	0.5 ± 0.0	10.5 ± 0.0	30.8 ± 0.9	30.3 ± 0.9	86.7 ± 0.60

PUC-Rio - Certificação Digital Nº 1312923/CA

Table H1: Experimental results of engine tests for each blend (Part 8 of 8).

Biodiesel content (%)	Ethanol content (%)	Lower Heating Value (kJ/kg)	Specific gravity (kg/m³)	Compression polytropic coefficient (-)	Expansion polytropic coefficient (-)	Injected energy (kJ)	Injected volume (µL)
15	10	42,736	0,8384	1.347 ± 0.001	1.421 ± 0.002	1.853 ± 0.025	51.7 ± 0.7
				1.351 ± 0.001	1.366 ± 0.002	3.121 ± 0.030	87.1 ± 0.8
				1.349 ± 0.001	1.346 ± 0.001	4.212 ± 0.017	117.6 ± 0.5
				1.354 ± 0.001	1.404 ± 0.001	2.180 ± 0.014	60.8 ± 0.4
				1.340 ± 0.001	1.357 ± 0.001	3.688 ± 0.012	102.9 ± 0.3
				1.346 ± 0.001	1.344 ± 0.007	5.014 ± 0.029	139.9 ± 0.8
				1.323 ± 0.002	1.398 ± 0.004	2.298 ± 0.014	64.1 ± 0.4
				1.333 ± 0.001	1.372 ± 0.002	3.697 ± 0.006	103.2 ± 0.2
				1.331 ± 0.002	1.349 ± 0.004	5.184 ± 0.007	144.7 ± 0.2
15	15	41,906	0,8358	1.339 ± 0.001	1.422 ± 0.001	1.855 ± 0.004	53.0 ± 0.1
				1.349 ± 0.001	1.374 ± 0.002	3.109 ± 0.010	88.8 ± 0.3
				1.347 ± 0.000	1.348 ± 0.002	4.043 ± 0.024	115.4 ± 0.7
				1.349 ± 0.007	1.401 ± 0.006	2.220 ± 0.022	63.4 ± 0.6
				1.352 ± 0.003	1.365 ± 0.001	3.737 ± 0.005	106.7 ± 0.1
				1.344 ± 0.003	1.351 ± 0.003	4.259 ± 0.005	121.6 ± 0.1
				1.334 ± 0.002	1.398 ± 0.002	2.262 ± 0.004	64.6 ± 0.1
				1.314 ± 0.001	1.347 ± 0.002	3.723 ± 0.007	106.3 ± 0.2
				1.335 ± 0.004	1.358 ± 0.001	4.721 ± 0.006	134.8 ± 0.2
15	20	41,072	0,8332	1.341 ± 0.000	1.419 ± 0.003	1.867 ± 0.011	54.6 ± 0.3
				1.348 ± 0.001	1.380 ± 0.004	3.140 ± 0.008	91.8 ± 0.2
				1.347 ± 0.000	1.353 ± 0.002	3.790 ± 0.021	110.8 ± 0.6
				1.343 ± 0.001	1.398 ± 0.001	2.200 ± 0.006	64.3 ± 0.2
				1.345 ± 0.001	1.365 ± 0.001	3.695 ± 0.010	108.0 ± 0.3
				1.344 ± 0.000	1.358 ± 0.001	4.029 ± 0.012	117.7 ± 0.3
				1.324 ± 0.002	1.386 ± 0.001	2.284 ± 0.004	66.7 ± 0.1
				1.336 ± 0.000	1.368 ± 0.003	3.749 ± 0.006	109.5 ± 0.2
				1.336 ± 0.000	1.363 ± 0.003	4.401 ± 0.014	128.6 ± 0.4
7	0	45,125	0,8395	1.343 ± 0.001	1.423 ± 0.001	1.900 ± 0.003	50.2 ± 0.1
				1.345 ± 0.001	1.373 ± 0.002	3.092 ± 0.008	81.6 ± 0.2
				1.350 ± 0.001	1.342 ± 0.002	4.345 ± 0.013	114.7 ± 0.3
				1.352 ± 0.003	1.305 ± 0.002	5.701 ± 0.030	150.5 ± 0.8
				1.349 ± 0.002	1.399 ± 0.002	2.213 ± 0.007	58.4 ± 0.2
				1.347 ± 0.001	1.360 ± 0.001	3.629 ± 0.002	95.8 ± 0.1
				1.346 ± 0.001	1.330 ± 0.001	5.154 ± 0.004	136.0 ± 0.1
				1.345 ± 0.001	1.298 ± 0.001	6.640 ± 0.052	175.3 ± 1.4
				1.334 ± 0.000	1.397 ± 0.001	2.299 ± 0.009	60.7 ± 0.2
				1.333 ± 0.001	1.364 ± 0.003	3.694 ± 0.002	97.5 ± 0.1
				1.333 ± 0.003	1.341 ± 0.003	5.134 ± 0.003	135.5 ± 0.1
				1.338 ± 0.005	1.311 ± 0.000	6.485 ± 0.006	171.2 ± 0.1